MDOT RC-1629

Remote Monitoring of Fatigue-sensitive Details on Bridges

MARCH 2015

Research

Department of Civil & Construction Engineering
College of Engineering and Applied Sciences
Western Michigan University

Intentionally left blank

1. Report No. RC-1629	**2. Government Accession No.** N/A	**3. MDOT Project Manager** Steve Kahl, P.E.
4. Title and Subtitle Remote Monitoring of Fatigue-sensitive Details on Bridges		**5. Report Date** 03/30/2015
		6. Performing Organization Code N/A
7. Author(s) Upul Attanayake, Ph.D., P.E. and Haluk Aktan, Ph.D., P.E., Western Michigan University. Robert Hay, Ph.D., TISEC Inc. Necati Catbas, Ph.D., P.E., Transtek International Group LLC.		**8. Performing Org. Report No.** N/A
9. Performing Organization Name and Address Western Michigan University 1903 West Michigan Avenue Kalamazoo, Michigan 49008		**10. Work Unit No. (TRAIS)** N/A
		11. Contract No. 2010-0297
		11(a). Authorization No. Z7
12. Sponsoring Agency Name and Address Michigan Department of Transportation Research Administration 8885 Ricks Road P.O. Box 30049 Lansing, MI 48909		**13. Type of Report & Period Covered** Final Report 10/01/2012 - 03/30/2015
		14. Sponsoring Agency Code N/A
15. Supplementary Notes		

16. Abstract

Fatigue is one of the most critical problems for steel bridges as well as for any steel structures that needs to be considered during design and operation. The objectives of this study are to explore monitoring technologies, and to develop effective structural and data analysis strategies as well as implementation recommendations for evaluating performance of fatigue-sensitive details and retrofits in steel bridges. Acoustic emission (AE) was selected as a candidate inspection technology, and a monitoring system was installed on a bridge. In general, the performance of the monitoring system and associated software is satisfactory. The majority of AE monitoring challenges are associated with AE data analysis and interpretation of results. In this study, cluster analysis and non-linear mapping signal analysis techniques are used to group AE data with similar waveform characteristics. The presence of the signals that resemble the characteristics of crack opening signals, noise, and structural resonance is identified through waveform analysis. Once the presence of crack opening signals is confirmed, the source location plots are utilized to assess the concentration and the level of activity at the locations of interest.

A significant difference is observed in the fatigue life calculated using measured stress, and the stresses calculated using finite element models loaded with a fatigue truck. Hence, a two-tier implementation process is recommended. Tier I process includes the assessment of bridges with repaired details. Tier II process recommends evaluating the entire bridge population with fatigue-sensitive details. Additional recommendations include implementing AE data interpretation capability in an on-line system to provide reliable input with minimal interpretation requirements for inspection-based maintenance management.

17. Key Words Acoustic emission, bridge, fatigue, fatigue life, hot spot stress, monitoring	**18. Distribution Statement** No restrictions. This document is available to the public through the Michigan Department of Transportation.		
19. Security Classification - report Unclassified	**20. Security Classification - page** Unclassified	**21. No. of Pages** 179 (excluding appendices)	**22. Price** N/A

Intentionally left blank

Remote Monitoring of Fatigue-sensitive Details on Bridges

Project Manager: Steve Kahl, P.E.

Submitted to:

MDOT

Submitted by

Upul Attanayake, Ph.D., P.E.
Associate Professor
Western Michigan University
(269) 276 – 3217
upul.attanayake@wmich.edu

Haluk Aktan, Ph.D., P.E.
Professor
Western Michigan University
(269) 276 – 3206
haluk.aktan@wmich.edu

Robert Hay, Ph.D.
TISEC Inc.
Morin Heights, QC, Canada
(450) 226 - 6804
bobhay@structuralinsights.com

Necati Catbas, Ph.D., P.E.
Transtek International Group LLC
fncatbas@gmail.com
(321) 945-1786

Western Michigan University
Department of Civil & Construction Engineering
College of Engineering and Applied Sciences
Kalamazoo, MI 49008-5316
Fax: (269) 276 – 3211

Intentionally left blank

DISCLAIMER

"This publication is disseminated in the interest of information exchange. The Michigan Department of Transportation (hereinafter referred to as MDOT) expressly disclaims any liability, of any kind, or for any reason, that might otherwise arise out of any use of this publication or the information or data provided in the publication. MDOT further disclaims any responsibility for typographical errors or accuracy of the information provided or contained within this information. MDOT makes no warranties or representations whatsoever regarding the quality, content, completeness, suitability, adequacy, sequence, accuracy or timeliness of the information and data provided, or that the contents represent standards, specifications, or regulations."

Intentionally left blank

ACKNOWLEDGEMENTS

This project was funded by the Michigan Department of Transportation. The authors would like to acknowledge the support and effort of Mr. Steve Kahl for initiating this research. The authors also wish to acknowledge the continuing assistance of the Research Advisory Panel (RAP) members in contributing to the advancement of this study. Continuous technical support provided by Mr. Juan Mejia, Vice President, Engineering & Inspections, TISEC Inc., is greatly appreciated. Support and efforts of graduate research assistant Lizmert Lopez and undergraduate research assistants, Timothy Schnell and Simon Matar, are acknowledged. Authors also would like to acknowledge the support of Dr. Diana Prieto. Last but not least, the support of the department technician, John Cernius, is greatly appreciated.

Intentionally left blank

EXECUTIVE SUMMARY

INTRODUCTION

Fatigue is one of the most critical problems for steel bridges as well as for any steel structures that needs to be considered during design and operation. The objectives of this study are to explore monitoring technologies, and to develop effective structural and data analysis strategies as well as implementation recommendations for evaluating performance of fatigue-sensitive details and retrofits in steel bridges.

Fatigue cracking is developed at certain steel bridge details due to a direct result of the loads (load-induced fatigue) or a deformation that is not accounted for during design (distortion-induced fatigue). The details that are prone to load-induced fatigue can be identified using the detail categories presented in the American Association of State Highway Officials (AASHTO) Load and Resistance Factor Design (LRFD) Bridge Design Specifications Table 6.6.1.2.3-1. The secondary and/or distortion-induced stresses that are not typically used in design are the most common reasons for fatigue cracking developed in bridges. The existence and the need to evaluate distortion-induced fatigue are acknowledged in the Manual for Bridge Evaluation (MBE) as well as in the National Cooperative Highway Research Program (NCHRP) Project 12-81 proposed revisions; yet, the scope of the manual as well as the proposed revisions are limited to assessing the cumulative fatigue damage of uncracked members subjected to load-induced stresses. Therefore, identifying the details that are prone to distortion-induced fatigue cracking requires utilizing information in bridge files, refined analysis capabilities, and experience. Developing high-fidelity analysis models and/or effective monitoring systems is vital to evaluate the causes of cracking or potential for cracking as well as to estimate remaining fatigue life, especially when evaluating complicated details or the effect of secondary stresses. A majority of the fatigue problems are associated with weld terminations and weld defects. The hot spot stress (HSS) method is widely used in other disciplines such as ship building and offshore structures for the assessment of weldments. However, the HSS method applications in bridge engineering are rarely documented.

The Michigan Department of Transportation (MDOT) performs inspections of over 200 bridges with fatigue-sensitive details. MDOT is interested in identifying technology that can be implemented on bridges with fatigue-sensitive details as well as to learn the recent advances in

fatigue-sensitive detail assessment and retrofits. Hence, this study is completed with five tasks: (1) review the state-of-the-art and practice literature to identify technologies for a structural health monitoring (SHM) system, (2) select a bridge and perform structural analysis to identify details for monitoring, (3) procure an SHM system, (4) install and calibrate the system, and analyze data, and (5) develop recommendations for technology integration into MDOT practice.

LITERATURE REVIEW

Fatigue-sensitive detail assessment methods, technology for fatigue-sensitive detail monitoring, technology implementation considerations, and retrofit methods for fatigue-sensitive details were reviewed within the scope of this project. A summary of the key findings from the literature review is given below:

- The AASHTO MBE Section 7 presents a procedure to assess the cumulative fatigue damage of uncracked members subjected to load-induced stresses. The outcome of this process has been in much debate because the calculation process, in many cases, resulted in a negative remaining fatigue life indicating that the detail had expired several years before the assessment was undertaken even when the in-service bridge in good condition. Hence, the NCHRP Project 12-81 proposed revisions to Section 7 and presented a process to calculate a non-dimensional parameter (the fatigue serviceability index - Q), fatigue rating, and guidance for using the fatigue serviceability index in bridge management decision-making.
- A combined effort of utilizing information in bridge files, refined analysis capabilities, and experience is needed to identify the details that are prone to distortion-induced fatigue cracking. The HSS method is widely used for the assessment of weldments. The International Institute of Welding (IIW) presents guidelines for HSS calculation as well as for using S-N curves to assess weldments.
- The fracture mechanics approach with an assumed initial crack size can be used to estimate crack growth rate; thus, to determine the inspection frequency. When such an approach is implemented, an accurate estimation of the initial crack size is important. The suggested approach is inspecting the detail using a nondestructive testing technique and selecting the largest non-detectable crack as the initial crack size.
- When a large number of bridges with fatigue-sensitive details or fracture-critical members (FCM) are present, bridges that require detailed evaluation and implementation of structural

health monitoring systems can be identified by grouping the bridges based on inventory data and performing detailed structural analysis of representative bridges from each group.

- An acoustic emission (AE) monitoring system with strain gages is one of the most effective technologies for fatigue event detection (i.e., crack initiation or crack growth monitoring). AE has been successfully implemented in the field and evaluated for continuous monitoring of fatigue-sensitive details. At this time, AE is the only technology that is capable of real-time monitoring of fatigue events and providing data for damage location detection. In addition to the AE sensors, strain gauges are required to evaluate the stress state to calculate remaining fatigue life, and to support AE data analysis by developing a load matrix.

- An extensive list of AE technology implementation challenges is prepared within the scope of this project. The majority of the challenges are associated with noise elimination, AE signal analysis, and interpretation of the results.

- AE technology can be implemented for global, semi-global, or local monitoring. Global monitoring is to identify potential source locations for planning or asset management purposes. Semi-global monitoring is implemented to identify individual source locations to assess, evaluate, and rank. The ranking is based on the source characteristics and number of emissions. The ranking system is used for planning detailed investigations through local monitoring. The local monitoring is implemented to identify the source location and to characterize the AE events. The sensor array for local monitoring is designed based on (a) the classification of the detail to be monitored, (b) prior experience with similar details, (c) inspection and maintenance records, (d) an attenuation survey, and (e) finite element analysis or a combination thereof.

- Monitoring duration is defined as short-term, loading pattern dependent, and long-term or continuous. Short-term monitoring is suitable when the causes and damage mechanisms are well understood. Short-term monitoring is also used as a means of repair/retrofit quality control. The duration for short-term as well as loading pattern dependent monitoring needs to be selected based on the traffic patterns. Long-term or continuous monitoring is primarily implemented when fatigue-sensitive or fracture-critical details are present, and the bridge is a critical node of a road network.

- Several repair and retrofit methods are presented in the report. The fatigue resistance of welds can be enhanced with the ultrasonic impact treatment (UIT). This method is relatively new,

and following manufacturer specifications is recommended. Repair or retrofit methods for out-of-plane distortion are presented. A majority of these methods requires evaluating alternatives through refined structural analysis and developing implementation recommendations.

STRUCTURAL MODELING AND HOT SPOT STRESS ANALYSIS

The bridge (S16 of 11015) that carries I-94 EB over Puetz Road, located in Stevensville, Michigan was selected for monitoring system implementation and performance evaluation. The bridge consists of category C' fatigue-sensitive partial depth diaphragm details and category E fatigue-sensitive welded cover plate detail. In addition to having fatigue-sensitive details, the other reasons for selecting the bridge include heavy truck traffic and easy access to the bridge for instrumentation and system maintenance. The primary objective of this study was to evaluate the state-of-the-art technology; hence, bridge access was an important parameter when selecting the site.

A 3D finite element (FE) model of the bridge was developed, and a submodeling concept was implemented to calculate hot spot stresses using the quadratic extrapolation equation recommended by the International Institute of Welding. The permanent stresses developed at the weld toe were calculated using deck dead load as a construction load. The fatigue truck given in AASHTO LRFD is a notional truck. Hence, Michigan legal load configurations were used to evaluate the stress state at the weld toe, representing more realistic loads on the bridge. Based on the analysis results, two web gap details located underneath the truck lane were selected for instrumentation.

STRUCTURAL HEALTH MONITORING (SHM) SYSTEM IMPLEMENTATION

The SABRE^{TM} (Structural Acoustics for Bridge Reliability Evaluation) with monitoring and interpretation capabilities was developed by TISEC Inc. as a result of over two decades of collaboration and inspection of over 500 bridges with the railroad industry. As a commercially available implementation-ready SHM system, the SABRE^{TM} system comprising the Mistras Group Inc. Sensor Highway^{TM} II System instrumentation and a set of TISEC software post processing modules were selected as the basic AE system. One web gap detail was instrumented with 4 AE sensors and a strain gage. The other detail was instrumented with 3 strain gages to calculate hot spot stress. As per the International Institute of Welding recommendations, strain

gages were mounted at 0.4t, 0.9t, and 1.4t distance from the weld toe; where *t* is the web thickness. As per the American Society for Testing and Materials (ASTM) E976-10, pencil lead breaks (PLB) were performed, the system was calibrated, and a region was demarcated for monitoring.

AE Win was the primary software used to set up the data acquisition system and parameters, and acquire and present AE and strain data. *Omega USB* was used to configure the temperature sensor and data logger. *LogMe In* was used for remote access and data transfer. Also, *Remote Desktop Connection* was used to access the remote computer in the SHM system. In addition, the *MS View* software program that was provided with the SunSaver MPPT charge controller was used to program the charge controller and record solar power system parameters.

DATA ANALYSIS AND SYSTEM PERFORMANCE

The sub-tasks performed include (a) analysis of a set of acoustic emission (AE) data recorded by the monitoring system using ICEPAK™ (Intelligent Classifier Engineering Package), (b) calculation of effective stress at a web gap using a refined finite element model loaded with a fatigue truck, (c) calculation of effective stress at a web gap using strain data from field monitoring, and (d) documenting monitoring system performance. A summary of key findings of AE data analysis is given below:

- ICEPAK™ can perform cluster analysis and non-linear mapping (NLM) of data in the time, power, phase, cepstral and auto-correlation domains independently. The AE data collected from the bridge was examined directly to identify any significant similar AE activity formations. NLM with the spectral power domain produced three significant concentrations. Clustering was performed using the same spectral power domain features, and the clusters were well aligned with the visual presentation of the NLM result. NLM and cluster analysis demonstrated the usefulness of such techniques for understanding the AE data.
- PLB data and the AE data in three clusters were evaluated. Waveform characteristics were evaluated using PRISM™ software developed by TISEC Inc. The dominant frequency ranges of each cluster were calculated. The results were used to identify the relationship of each cluster to the characteristics of crack opening signals, background noise, and structural resonance.

- When waveform characteristics in any of the signal clusters resemble the crack opening signal characteristics, location plots can be reviewed to verify the presence of sources within the zone of interest.

The MBE procedure was used to assess fatigue performance. The findings are given below:

- Weigh-in-motion data yielded the gross fatigue truck weight of 57 kips.
- The maximum stress range calculated using refined FE models loaded with a fatigue truck can be as high as 10.88 ksi. When combined with the effects of other loads, the stress range well exceeded the constant-amplitude fatigue threshold (CAFT) indicating a finite fatigue life for the detail.
- The detail was instrumented with strain gages, and hot spot stress was calculated. The maximum stress range of 1.6 ksi was calculated using the measured strain under ambient traffic. When combined with the effects of other loads, the maximum stress range barely reaches the CAFT indicating an infinite fatigue life.

The monitoring system's ruggedness and reliability was evaluated by installing it on a bridge with fatigue-sensitive details and subjecting it to an outdoor environment. A summary of key findings is given below:

- One of the AE board channels malfunctioned and needed to be repaired. This highlights the need of using rugged electronics to develop reliable monitoring systems for outdoor applications. System reliability and ruggedness are very important for monitoring critical bridge details or hard to reach details.
- When dealing with software from different vendors, compatibility issues are common. However, within the data acquisition, interpretation, and presentation stream, these issues were resolved for this application by using the integrated SABRE^{TM} system.
- A standalone solar power system is ideal for short-term or as needed monitoring. However, the system needs to be designed by considering the monitoring system power requirement, solar irradiance at the site, type and quality of the solar array and the charge controller, along with the required power storage (battery bank capacity).
- In general, the performance of the monitoring system and associated software can be considered as satisfactory.

IMPLEMENTATION RECOMMENDATIONS

A two-tier implementation process is recommended. Tier I includes assessment of bridges with repaired details. Tier II includes grouping bridges with fatigue-sensitive details based on a defined set of attributes, and selecting a representative bridge from each group for further analysis and assessment. Additional recommendations to enhance the two-tier implementation process as well as for future research are listed below:

1. Implement AE data interpretation capability demonstrated in this study with an on-line system to provide reliable input with minimal interpretation requirements for inspection-based maintenance management.
2. Develop a fatigue cracking signal characteristic database using typical steel and welds used in Michigan bridges. This database would allow further refining of the AE data interpretation and more accurately detecting the critical events.
3. Install the AE monitoring system with the on-line signal classification system at a half dozen sites to gather data from typical fatigue-sensitive details to identify optimal settings and to optimize other deployment issues.

Intentionally left blank

TABLE OF CONTENTS

Intentionally left blank

LIST OF TABLES

Intentionally left blank

LIST OF FIGURES

1 INTRODUCTION

1.1 OVERVIEW

Fatigue is one of the most critical problems for steel bridges as well as for any steel structures that needs to be considered during design and operation. Fatigue cracking is developed at certain steel bridge details due to a direct result of the loads (load-induced fatigue) or a deformation that is not accounted for during design (distortion-induced fatigue). The details that are prone to load-induced fatigue can be identified using the detail categories presented in the AASHTO LRFD (2013) specifications Table 6.6.1.2.3-1. These details are grouped into 8 different categories such as A, B, B', C, C', D, E, and E'. Of these categories, Category A has the greatest fatigue resistance while Category E' has the least. According to the AASHTO Manual for Bridge Evaluation (MBE 2011) a majority of the fatigue problems are associated with weld terminations and weld defects. In addition to weld locations, fatigue cracks can initiate at a material flaw, changes in member cross-sections, or some combinations thereof. The MBE (2011) section 7 presents a procedure to assess the cumulative fatigue damage of uncracked members subjected to load-induced stresses. Recently, Bowman et al. (2012) proposed revisions to MBE (2011) section 7.

The secondary and/or distortion-induced stresses that are not typically used in design are the most common reasons for fatigue cracking developed in bridges (Fisher 1984). The existence and the need for evaluating distortion-induced fatigue are acknowledged in the MBE (2011) as well as in the proposed revisions by Bowman et al. (2012). However, the scope of the MBE (2011) section 7 as well as the proposed revisions is limited to the load-induced fatigue evaluation. Therefore, identifying the details that are prone to distortion-induced fatigue cracking requires a combined effort of utilizing information in bridge files, refined analysis, and experience. Developing high fidelity analysis models and effective monitoring systems is vital to evaluate the causes of cracking or potential for cracking as well as to estimate remaining fatigue life, especially when evaluating weldments, complicated details, or the effect of secondary stresses. According to the MBE (2011), a majority of the fatigue problems are associated with weld terminations and weld defects. The hot spot stress (HSS) method is widely used in other disciplines such as ship building and offshore structures for the assessment of weldments (Fricke and Kahl 2005; Chakaray et al. 2008; Fricke et al. 1998; Nguyen et al. 2012).

However, the HSS method applications in bridge engineering are rarely documented (Alemdar et al. 2014b, Hassel et al. 2010; Akhlaghi et al. 2009).

MDOT performs inspections of over 200 bridges with fatigue-sensitive details. Once the fatigue-sensitive details are identified, a structural health monitoring (SHM) system can be implemented to achieve the following objectives:

- Alert bridge managers when a crack initiates so that the crack growth is monitored to schedule retrofits.
- Identify details with active cracks so that the growth is monitored to schedule retrofits.
- Evaluate effectiveness of repairs or retrofits.
- Evaluate the response of a detail under permit loads.
- Evaluate the response of a detail due to change in service conditions.
- Monitor stress flow to calculate remaining fatigue life (or the fatigue serviceability index) to support bridge management decisions.

The development of a reliable SHM system requires implementing technologies with proven records of field performance. Further, the system needs to be robust and portable enough to be used at multiple sites as needed.

1.2 OBJECTIVES AND TASKS

As presented in the overview, fatigue is one of the most critical problems for steel bridges as well as for any steel structures that needs to be considered during design and operation. The objectives of this study are to explore fatigue monitoring technologies, and to develop effective structural and data analysis strategies as well as implementation recommendations for bridge engineering. The scope of this study is to:

1. Prepare a synthesized report from a literature search and provide recommendations for the appropriate technology to use for remote monitoring steel bridges having fatigue-sensitive details.
2. Select an appropriate SHM system using commercially available equipment to the extent possible, and perform an installation on a selected bridge with fatigue-sensitive details.
3. Conduct field monitoring to validate the system's accuracy and robustness.
4. Provide recommendations for implementation of the SHM system and further research.

To achieve the project objectives with the given scope, this project is organized into five tasks: (1) review the state-of-the-art and practice literature to identify technologies for a SHM system and to develop implementation recommendations, (2) select a bridge and perform structural analysis to identify details for monitoring, (3) procure an SHM system, (4) install and calibrate the system, and analyze data, and (5) develop recommendations for technology integration into MDOT practice and further research.

1.3 REPORT ORGANIZATION

The report is organized into 7 chapters.

Chapter 1, (this chapter) includes the introduction and overview of the study.

Chapter 2, literature review, presents the fatigue-sensitive detail categories, methodologies to establish the needs for monitoring fatigue-sensitive details, technology for fatigue-sensitive detail monitoring, and technology implementation considerations. In addition, retrofit methods for fatigue-sensitive details are also presented.

Chapter 3 provides a description of the bridge with partial depth diaphragms and welded details. Evaluation of the welded details requires calculating hot spot stresses. Hot spot stress calculation requires selecting appropriate element types, mesh parameters, and reference points for stress calculation. Therefore, this chapter also presents (a) element types and mesh parameters for hot spot stress calculation, and (b) bridge structural analysis results and recommended details for instrumentation and monitoring.

Chapter 4 provides information related to field implementation, SHM system calibration, and power supply. This chapter also presents the system components and software used for system configuration, along with data acquisition, data display, remote access, and data transfer.

Chapter 5 presents (a) a set of acoustic emission (AE) data recorded by the monitoring system and data analysis using ICEPAK^{TM}, pattern classifiers for use in real-time structural health and reliability monitoring, (b) calculation of effective stress at a web gap detail using WIM data and refined finite element analysis, (c) calculation of effective stress at a web gap detail using strain data from field monitoring, and (d) findings from the monitoring system performance evaluation.

Chapter 6 provides a summary, along with the conclusions, and recommendations.

Chapter 7 includes the list of cited references.

Intentionally left blank

2 STATE-OF-THE-ART AND PRACTICE REVIEW

2.1 OVERVIEW

To develop a successful program for monitoring fatigue-sensitive detail, it is required to (i) identify fatigue-sensitive details, (ii) establish monitoring objectives, (iii) select technology suitable for achieving the monitoring objectives, and (iv) decide on the level and duration of monitoring.

The following sections of this chapter present fatigue-sensitive detail categories, methodologies to establish the needs for monitoring the fatigue-sensitive details, technology for monitoring the fatigue-sensitive detail, and technology implementation considerations. In addition, retrofit methods for the fatigue-sensitive details are also presented.

2.2 FATIGUE-SENSITIVE DETAIL CATEGORIES

The AASHTO LRFD Bridge Design Specifications (2013), Table 6.6.1.2.3-1, present detail categories for load-induced fatigue. These details are grouped into 8 different categories such as A, B, B', C, C', D, E, and E'. Of these categories, Category A has the greatest fatigue resistance while Category E' has the least. Figure 2-1 is a graphical representation of the nominal fatigue resistance for these details. The horizontal broken lines represent the constant amplitude fatigue threshold (CAFT). According to Section 7 of the Manual for Bridge Evaluation (MBE 2011), fatigue life of the load-induced fatigue-sensitive details is evaluated when two times the effective stress is greater than the CAFT.

The secondary and/or distortion-induced stresses that are not typically used in design are the most common reasons for fatigue cracking developed in bridges (Fisher 1984). The existence and the need of evaluating distortion-induced fatigue are acknowledged in the MBE (2011); yet, the scope of the Section 7 of the MBE is limited to the load-induced fatigue evaluation. Therefore, the details prone to distortion-induced fatigue cracking need to be identified with prior experience with similar details, by reviewing inspection and maintenance records, and through refined analysis. Also, the assessment procedures of such details need to be identified and documented from literature.

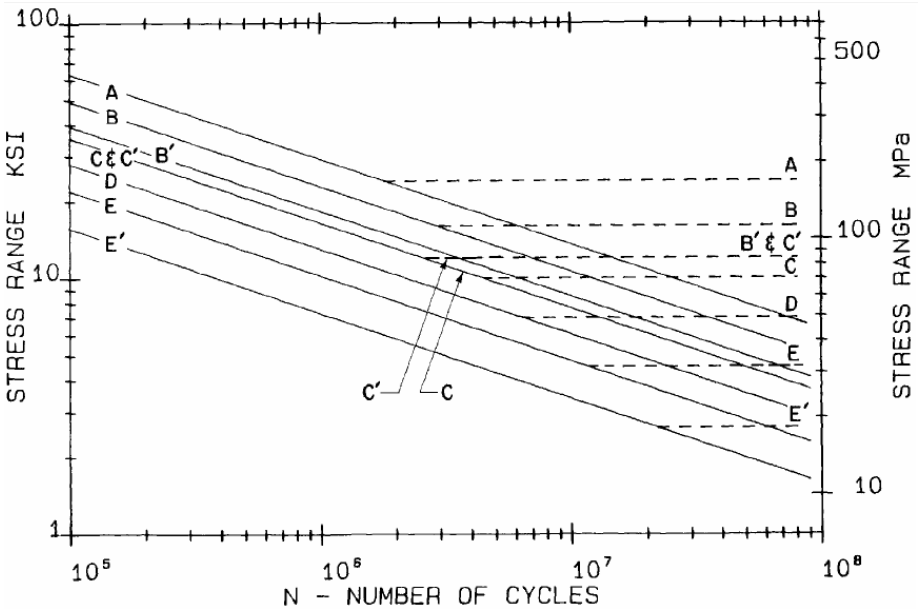

Figure 2-1. Stress range (S) versus number of cycles (N) (AASHTO LRFD 2013)

2.3 EVALUATION OF FATIGUE-SENSITIVE DETAILS

Kühn et al. (2008) provide a technical background for further development of the Eurocode for assessing existing steel structures and estimating remaining fatigue life through a four-phase process to estimate the remaining fatigue life of existing steel structures. These phases include (i) a preliminary evaluation by an engineer in accordance with the current codes, (ii) detailed investigation by an engineer with the help of an expert and supported with data collected using low-tech nondestructive testing (NDT) methods, (iii) expert investigations that may be supported with data collected using high tech NDT, and (iv) evaluation of fatigue performance after developing remedial measures, such as enforcing load restrictions, or performing repairs or retrofits. This monitoring is used to support detailed investigation by experts. Another aspect of monitoring is to evaluate the effectiveness of remedial measures.

The key step in the evaluation of fatigue-sensitive details is the calculation of remaining fatigue life. Nominal stress, hot spot stress, effective notch stress, fracture mechanics, and component testing are the methods used for assessing fatigue life (Hobbacher 2008). The most common fatigue assessment method uses S-N curves (Figure 2-1). This approach is based on the nominal stress. In addition, hot spot and notch stresses are also used for fatigue assessment of welded details. The fracture mechanics based approach can be used irrespective of the detail configuration. Hobbacher (2008) developed a report, titled *Recommendations for Fatigue*

Design of Welded Joints and Components, for the International Institute of Welding (IIW). The guidelines presented in this report are commonly cited in literature as IIW guidelines. Hobbacher (2008) defines the nominal stress, hot spot stress, and notch stress as follows:

- Nominal stress – *stress calculated in the sectional area under consideration.*
- Hot spot stress – *also known as the structural or geometric stress at the hot spot includes all the stress raising effects of a structural detail excluding that due to the local weld profile itself.*
- Notch stress – *total stress at the root of a notch taking into account the stress concentration caused by the local notch, consisting of the sum of structural stress and nonlinear stress peak.*

A graphical representation of the above definitions are shown in Figure 2-2.

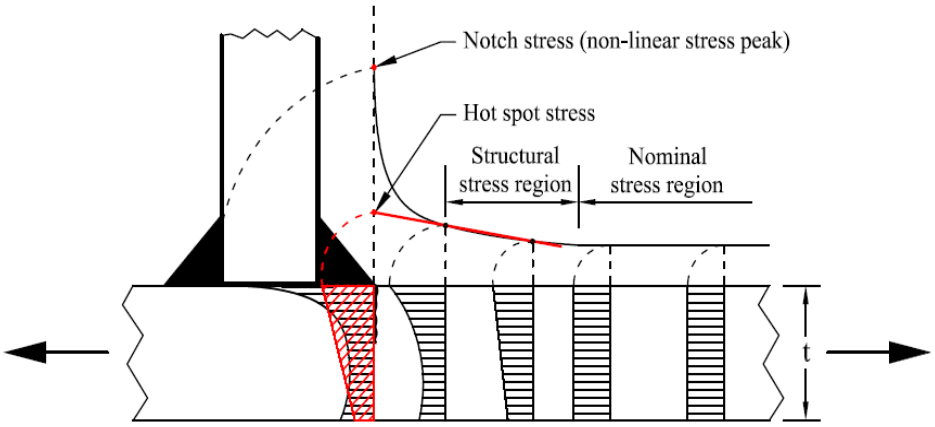

Figure 2-2. Nominal, hot spot, and notch stress definitions

Kühn et al. (2008) proposed using the linear Palmgren-Miner damage rule based approach. The fatigue assessment procedure for existing steel bridges proposed by Kühn et al. (2008) is presented in section 2.3.1.

At present, highway agencies in the U.S. follow the provisions of Article 7.2 of the AASHTO MBE (2011) to assess the cumulative fatigue damage of uncracked members subjected to load-induced stresses (See Section 2.3.2 for more details.) The NCHRP Project 12-81, "Evaluation of Fatigue on the Serviceability of Highway Bridges" was initiated to address the shortcomings in the MBE (2011) procedure (Bowman et al. 2012). Instead of calculating a remaining fatigue life, calculation of a nondimensional parameter (the fatigue serviceability index - Q) was presented by Bowman et al. (2012) to evaluate the condition and the assessment outcome with respect to

fatigue. Section 2.3.3 presents calculation process of the fatigue serviceability index (Q), fatigue rating, and guidance for using Q in bridge management decisions.

Hot spot stress is commonly used for fatigue life assessment of welded details. Hot spot stress is calculated by extrapolating structural stress using linear or cubic extrapolation equations. Structural stress for extrapolation equations is calculated using refined finite element models. Section 2.3.4 presents finite element guidelines, extrapolation equations, and the procedure for using hot spot stresses with a reference detail to calculate fatigue life.

The effective notch stress method has not been widely used in assessing bridges. Hence, that method is not discussed in this report. The fracture mechanics based approach is used to calculate the rate or duration of a crack growth under fatigue loading. This method has been used to formulate inspection frequency. Section 2.3.5 presents two case studies where the fracture mechanics based approach was used to assess fatigue-sensitive details or fracture-critical members, and to determine the inspection frequency.

2.3.1 Linear Palmgren-Miner Damage Rule

Kühn et al. (2008) presented a four-phase process to estimate the remaining fatigue life of existing steel structures. As per the phase I investigation, the preliminary assessment is carried out by an engineer to identify the presence of fatigue-sensitive details and critical members. This level of assessment is carried out by studying the documents in the bridge file (such as plans, design calculations, and inspection and maintenance reports) and data collected by performing an inspection of the bridge. In general, highway agencies have performed such investigations and have identified the need for detailed assessment.

Presence of fatigue-sensitive details and fracture-critical members can be identified using an agency database or, in the U.S., by using the National Bridge Inventory (NBI) database. Because of this reason, only phase II to IV presented by Kühn et al. (2008) are discussed here. The relation between three assessment phases and decision-making involved throughout the processes are depicted in Figure 2-3. The variables used in the figure are defined in Appendix B. As shown in Figure 2-3, phase II investigation is carried out by an engineer alone. The linear Palmgren-Miner damage rule (Eq. 2-1) is used to calculate the damage sum (D). If the calculation shows sufficient safety (i.e., $D < 1$), the remaining fatigue life (T_{fat}) is calculated. If

T_{fat} > 10 years, the standard inspection is performed. When $T_{fat} \leq 10$ years, phase IV activities are performed. Phase IV activities include intensified monitoring of the detail of concern and other decisions such as repair, rehabilitation, imposing load restrictions, or structure demolition. Once repair, rehabilitation, or load restriction decisions are implemented, new residual life is calculated, and the bridge file is updated.

$$D = \sum \frac{n_i}{N_i} \quad (2\text{-}1)$$

where, n_i is the actual number of cycles at stress range i, and N_i is the theoretical fatigue life at stress range i.

When D ≥ 1, the following steps can be used to update the calculations:

- Use site-specific traffic and material data, and an accurate estimation of the variable loads and dead or permanent loads.
- Use detail focused refined and advanced analysis techniques such as submodeling.
- Acquire real-time data such as stresses under service loads. The measured data can help improve understanding of the structure such as unintended composite behavior, unforeseen load distribution, effect of non-structural elements, and boundary condition effects (such as partial fixity, frozen bearings, and unintended continuity at intermediate supports). Hence, strain at the detail of interest can be measured to perform the rainflow counting as per the ASTM E1049-85. Once the rainflow counting is performed and the data is placed in bins to develop a stress histogram, Miner's rule can be applied to calculate an accurate damage sum.

When the refinements do not improve the calculations to yield D < 1, the consequences of failure and the cost of repair/retrofits need to be evaluated. If the consequences or the repair/retrofit costs justify, phase III investigations, with the help of a team of experts, are initiated. The phase III investigations include use of advanced monitoring, quantitative advanced NDT, material property evaluation, and fracture mechanics and/or probabilistic assessment methods. Based on the phase III outcome, remedial measures can be developed under phase IV. Monitoring technologies such as AE can be used to evaluate the effectiveness of the remedial measures.

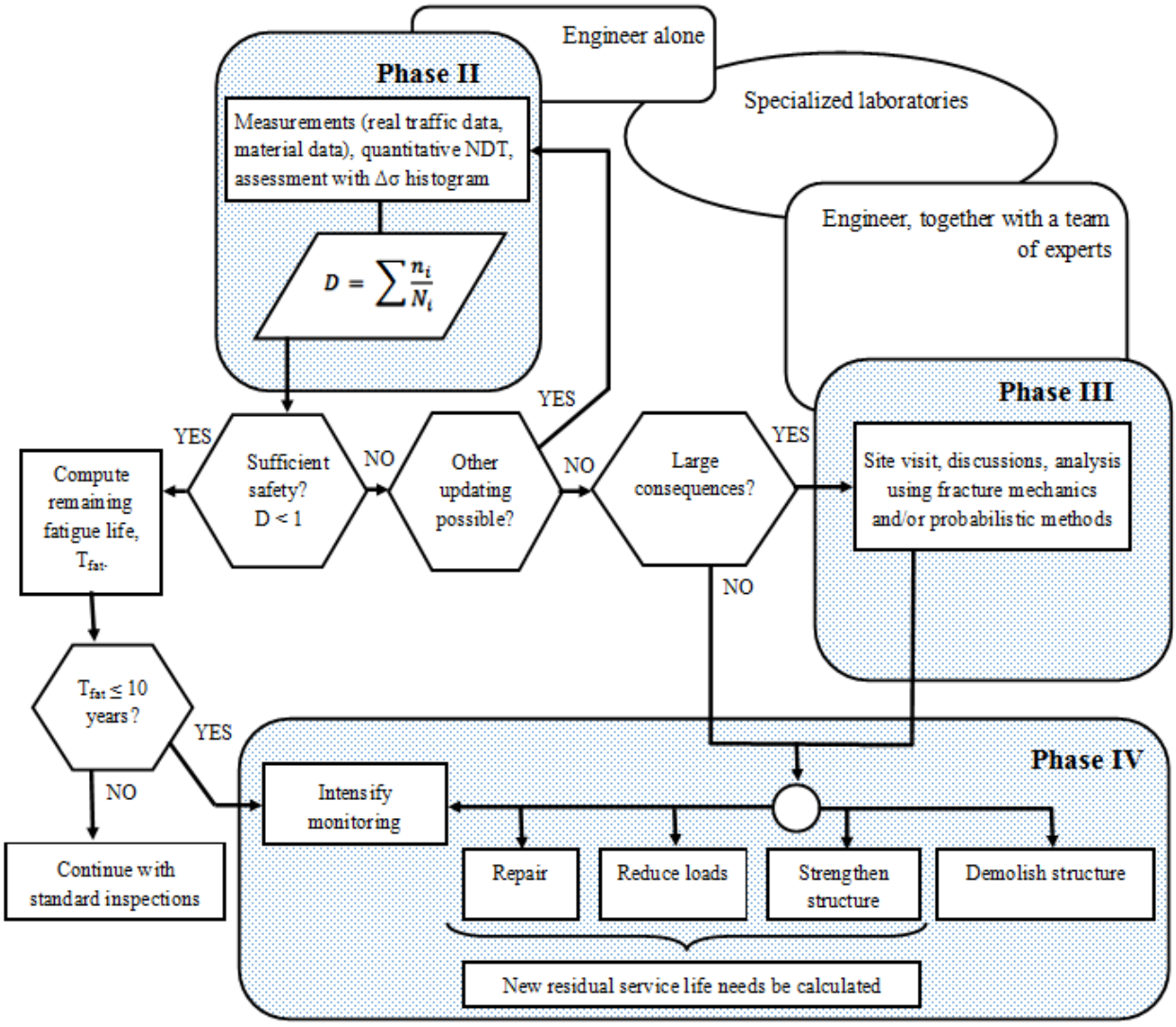

Figure 2-3. Fatigue assessment procedure for steel bridges (Kühn et al. 2008)

2.3.2 AASHTO MBE Procedure

Section 7 of the AASHTO Manual for Bridge Evaluation (MBE 2011) provides a procedure for evaluating load-induced fatigue. As depicted in Figure 2-4, the first step is to identify the fatigue-sensitive details. The next step is to evaluate the need for fatigue assessment. Once the need is identified, required data for an accurate assessment of a detail such as traffic data and strain is acquired. The variables used in the figure are defined in Appendix B. The process depicted in Figure 2-4 is based on measured strains. Hence, strain at the detail of interest is measured, and the rainflow counting is performed as per the ASTM E1049-85. Once the rainflow counting is performed and the data is placed in bins to develop a stress histogram, the effective stress is calculated. As the first step in evaluation, an infinite-life check is performed.

The AASHTO LRFD Bridge Design Specifications (2013) in Table 6.6.1.2.3-1 provide the threshold values, $(\Delta f)_{TH}$. In general, the maximum effective stress, $(\Delta f)_{max}$, is taken as twice the effective stress, $(\Delta f)_{eff}$. If the check fails, finite fatigue life (Y) is calculated. Once the present age of the detail (A) is subtracted from the finite fatigue life, the remaining fatigue life can be calculated. Remedial measures are suggested in the MBE (2011) when an inadequate or negative remaining life is yielded through this process.

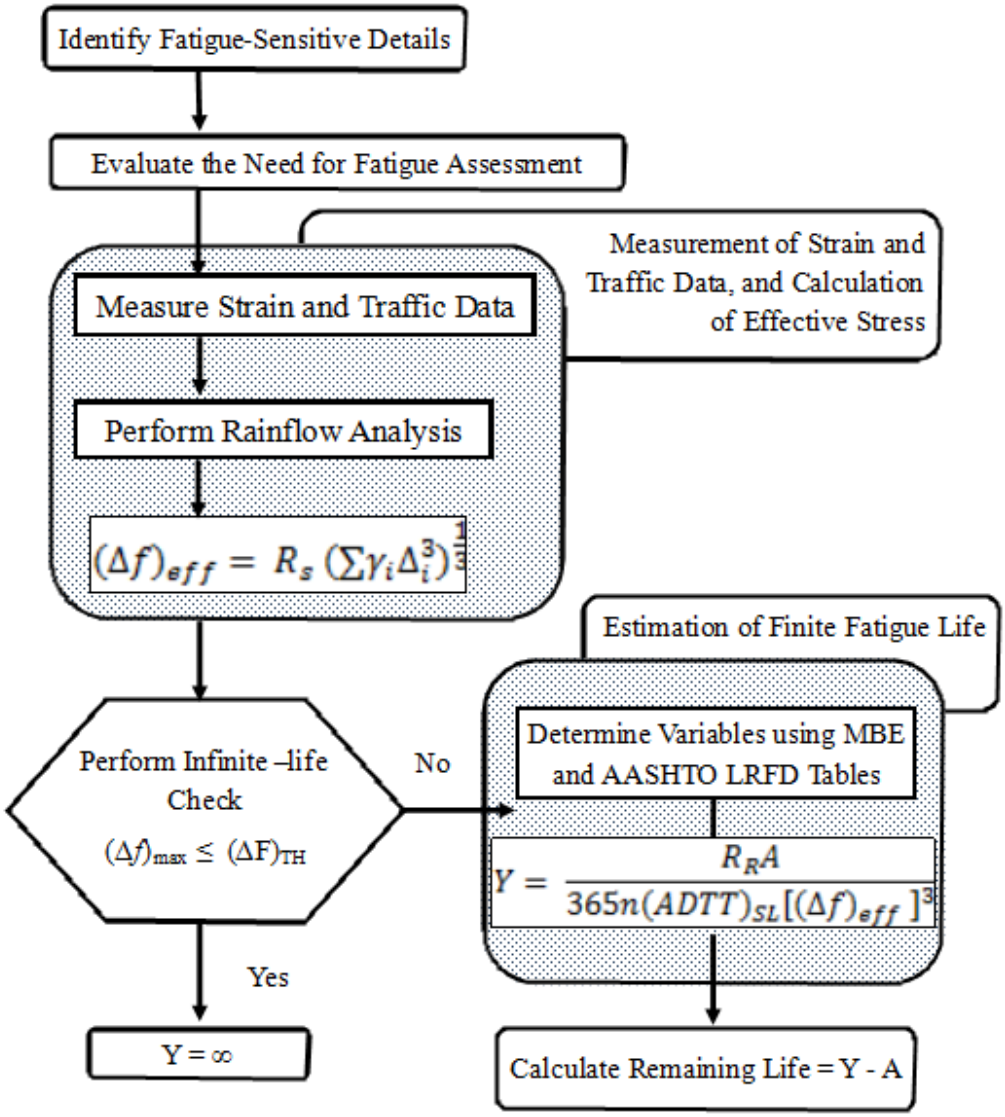

Figure 2-4. AASHTO Manual for Bridge Evaluation – Fatigue life calculation procedure

2.3.3 NCHRP 271 Procedure

As depicted in Figure 2-5, the process up to performing the infinite-life check is the same as the process presented in section 2.3.2. If the infinite-life check fails, finite life is calculated using a

much more elaborate equation than the equation presented in Figure 2-4. The variables used in Figure 2-5 are defined in Appendix B. Using the finite fatigue life and the current age of the detail, fatigue serviceability index (Q) is calculated. Revisions to the calculation of Q are needed when the values are negative. If the revised calculation yields a negative value for Q, the fatigue rating of the detail is determined as "critical" fatigue rating (Table 2-1). This requires considering retrofit, replacement, or reassessing the detail. When Q is equal or greater than zero, the detail is assigned a fatigue rating and corresponding management decisions are taken. When the fatigue rating of a detail is determined as either Fair or Poor, the detail needs to be assessed frequently (Table 2-1).

Table 2-1. Fatigue Rating and Assessment Outcomes (Bowman et al. 2012)

Fatigue Serviceability Index, Q	Fatigue Rating	Assessment Outcome
1.00 to 0.50	Excellent	Continue Regular Inspection
0.50 to 0.35	Good	Continue Regular Inspection
0.35 to 0.20	Moderate	Continue Regular Inspection
0.20 to 0.10	Fair	Increase Inspection Frequency
0.10 to 0.00	Poor	Assess Frequently
< 0.00	Critical	Consider Retrofit, Replacement or Reassessment

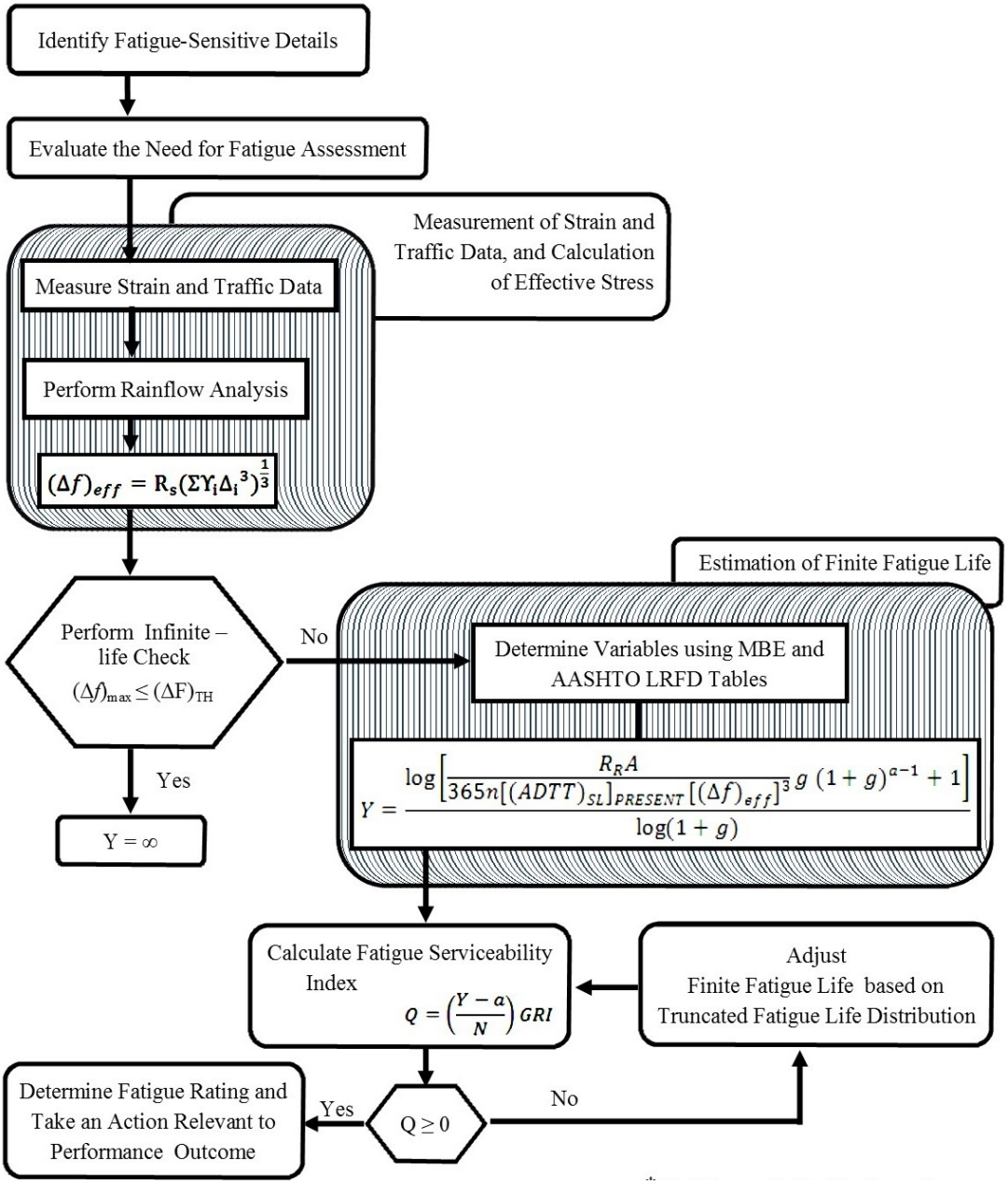

Figure 2-5. NCHRP 721 – Fatigue life and serviceability index calculation procedure

2.3.4 Hot Spot Stress Method

2.3.4.1 Hot Spot Stress Analysis

The hot spot stress (HSS) method is widely used for the assessment of weldments. Causes of cracking or potential for cracking is investigated through analysis with the support of experimental data. Developing high fidelity analysis models is vital to understand the behavior of fatigue-sensitive details in bridges for estimating remaining fatigue life, especially when evaluating complicated details or secondary stresses (Alemdar et al. 2014a; Aygul et al. 2012; Lee et al. 2010; Bhargava 2010; Akhlaghi et al. 2009; Hobbacher 2008). Even though the use of the HSS method for calculating secondary stresses is briefly discussed in design specifications, manuals, and many publications such as the AASHTO LRFD Bridge Design Specifications (AASHTO LRFD 2013) and the AASHTO Manual for Bridge Evaluations (MBE 2011), there are no clear guidelines provided in those documents for selecting model parameters and interpretation of results. Also, the recently proposed updates to the Manual for Bridge Evaluation Section 7 by Bowman et al. (2012) do not include guidelines for hot spot stress analysis.

Fatigue cracks initiate at weld toes; thus, it is critical to quantify stresses due to load effects at such a location (Hobbacher 2008). According to Lee et al. (2010) the HSS method is also useful for fatigue resistant design. The HSS method has been extensively used in other disciplines such as ship building and offshore structures (Fricke and Kahl 2005; Chakaray et al. 2008; Fricke et al. 1998; Nguyen et al. 2012). More recently, the HSS method is used in investigating bridge details (Alemdar et al. 2014b, Hassel et al. 2010; Akhlaghi et al. 2009).

Linear elastic theory or numerical methods (e.g., FE) can be used in conjunction with S-N curve classification to estimate the fatigue life (Aygul 2012). State-of-the-art technology allows accurate representation of geometries and complex details using refined FE models. However, calculating HSS using FE is a challenge due to the sensitivity of analysis results to element types and mesh discretization within the region of high strain gradient. FE analysis results depend on (1) element type, (2) mesh discretization parameters such as size, Jacobian, skew, and aspect ratio, (3) boundary conditions, (4) loads and load application procedures, and (5) postprocessor capabilities. Therefore, various guidelines and recommendations for calculating HSS using FE

are presented in literature (Bhargava 2010; Hobbacher 2008; Aygul 2012; Niemi 1993; Niemi et al. 2006). This section of the report presents a comprehensive summary of FE modeling, analysis, and results interpretation guidelines for the HSS method documented in literature.

HSS is a combined effect of membrane and bending stresses, and follows a linear stress distribution in steel welded structures along the surface. Analysis results are expected to be 'mesh size insensitive' (Akhlaghi et al. 2009). Hence, an expert panel led by Hobbacher representing the International Institute of Welding Commissions XIII and XV developed recommendations for fatigue design of welded joints and components (Hobbacher 2008); this document is commonly stated in literature as the IIW guidelines. The recommendations are for element types and sizes as well as type of extrapolation and location of extrapolation points. According to Hobbacher (2008), there are two types of hot spots, Type A and Type B, based on their location on the plate and orientation with respect to the weld toe (Figure 2-6a).

When calculating Type A HSS, reference points are defined at specific distances from the weld toe based on the plate thickness. The reference point stresses are calculated from the plate surface. For Type B HSS, the reference points are defined at absolute distances from the weld toe, regardless of plate thickness. Then, the stresses at the weld toe are calculated by extrapolating the reference point stresses. According to Hobbacher (2008), reference points are located within the structural stress region (Figure 2-6b). With the above stated process, nonlinear stress peak at the weld toe due to notch effect is excluded from calculation. Hence, HSS is dependent on global geometry and loading parameters, and quantified using HSS equations presented in Table 2-2. Columns 1 and 2 of Table 2-2 list hot spot (HS) type and mesh type, respectively. Columns 3 and 4 list the element length and the location of reference points, respectively. Column 5 shows the order of the stress extrapolation equation as well as the extrapolation equations.

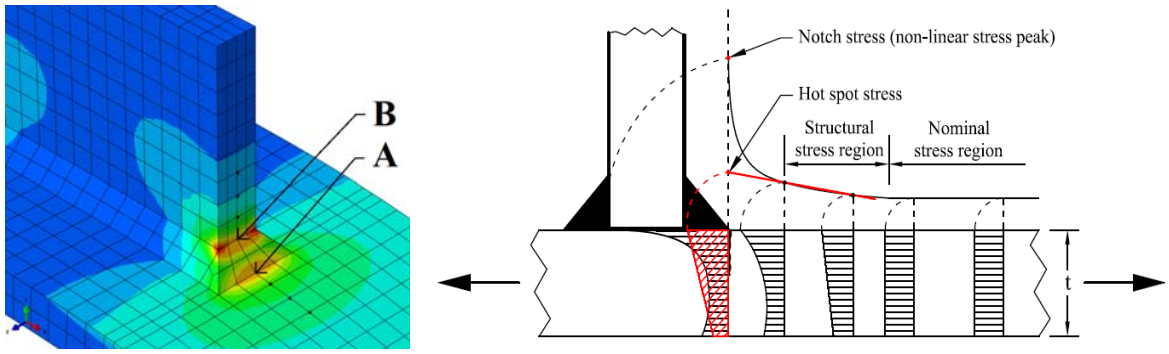

(a) Type A and B hot spots (b) Stress distribution along the surface and through thickness

Figure 2-6. (a) Type A and B HS locations and (b) cross-section of specimen showing stress distribution through plate thickness and along the surface close to the weld (Hobbacher 2008).

Figure 2-6a shows a finite element model of a welded steel plate assembly using solid elements. The recommended extrapolation path is shown along the plate surface for Type A and along the edge for Type B HSS calculation methods. Probing HSS from the FE model at the weld toe is misleading, because nodal stresses at the weld toe include non-linear notch stress developed due to weld geometry. Notch stress is included in S-N design curves based on experimental results (Lee et al. 2010). Hence, the elements that are located in front of the weld toe and within the structural stress region are of interest. In order to eliminate the influence of notch stress on HSS calculation, Hobbacher (2008) recommended using an extrapolation technique with the stresses calculated at least at 0.4t away from weld toe for Type A detail. Hobbacher (2008) presented two extrapolation equations to calculate HSS for Type A and B locations when a weld detail is modeled with solid elements: linear with 2 reference points and quadratic with 3 reference points (Table 2-2). With the recent advances in FE pre- and post-processing capabilities, stress at specified reference points can be probed and used with the equations presented in Table 2-2 to calculate HSS.

Table 2-2. Extrapolation Methods for HSS Calculation using Solid Element FE Models (Hobbacher 2008)

HSS Type	Mesh Type	Element length at HS		Reference points		Extrapolation Method and Equation
A	Fine	Based on Plate Thickness	≤ 0.4 t × t* or ≤ 0.4 t × w/2	Located at Plate Surface	0.4 t and 1.0 t Nodal Points	Linear $1.67\ \sigma_{0.4t} - 0.67\ \sigma_{1.0t}$
					0.4 t, 0.9 t and 1.4 t Nodal Points	Quadratic** $2.52\ \sigma_{0.4t} - 2.24\ \sigma_{0.9t} + 0.72\ \sigma_{1.4t}$
	Coarse		t × t or Max t × w*** (Use higher-order elements)		0.5 t and 1.5 t Surface Center	Linear $1.50\ \sigma_{0.5t} - 0.50\ \sigma_{1.5t}$
B	Fine	Based on Absolute Distance	≤ 4 × 4 mm	Located at Plate Edge Surface	4, 8 and 12 mm Nodal Points	Quadratic* $3\ \sigma_{4mm} - 3\ \sigma_{8mm} + \sigma_{12mm}$
	Coarse		10 × 10 mm		5 and 15 mm Surface Center	Linear $1.5\ \sigma_{5mm} - 0.5\ \sigma_{15mm}$

* t = plate thickness
** Quadratic extrapolation is recommended when non-linear structural stress increase is expected towards the hot spot.
*** w = longitudinal attachment thickness + 2* weld leg length
Note: 1 in. = 25.4 mm

Different FE modeling guidelines and recommendations for welded details are presented in literature. Table 2-3 summarizes FE pre/post processing and HSS calculation guidelines from literature and available specifications since 1992 to 2012. Typical guidelines include model type, mesh, element size, element shape, HHS calculation method, distance to reference points from weld toe, type of stress used for calculating HSS, and inclusions/exclusions of the model. The majority of sources listed in Table 2-3 has followed the guidelines and recommendation presented by Hobbacher (2008).

When preprocessing a FE model, in order to have nodes at each reference point, it is prudent to define element length near a weld toe based on the distance to the reference points measured from the weld toe. As an example, if the quadratic extrapolation recommended by Hobbacher (2008) is used to calculate HSS at Type A detail, sizes of the first three elements located in front of the weld toe need to be defined as shown in Table 2-4c and e. The other option is to use higher order elements and the stress values calculated at the center of the element top surface with the extrapolation equations to calculate HSS (Table 2-4a and d).

Table 2-3. FE Pre/Post-Processing and HSS Calculation Guidelines

Year	Reference	FE Pre/Post-Processing and HSS Calculation Guidelines
1992	ABS (1992)	• Model with solid elements: 20-node solid elements • Model with shell elements: 8-node thick shell elements • Element size: t × t • HSS calculation method: Linear extrapolation • Distance to reference points from weld toe: 0.5t and 1.5t • Stress used for HSS calculation: Maximum Principal Stress
1998	Fricke et al. (1998)	• Model with solid elements: 20-node solid elements • Element size: t × t • Mesh guidelines: Use at least three elements of equal length within the area of high stress gradient • HSS calculation method: Quadratic extrapolation from the 3 equal length elements. • Recommendation: Include weld in model
1998	Eurocode 9 (1998)	• Model with shell or solid elements • Element size: Increase fineness till stress converge 0.25 (t × t) • Stress used for HSS calculation: Structural stress is defined as the greatest value of the component stress extrapolated in the normal direction to the weld
2002	Reijmers (2002)	• Model with solid elements: 8 or 20 node with element size: t/2 × t/2 × t/2 • Model with shell elements: 4 or 8 node with element size t × t • Recommendation: Increase the number of solid elements through plate thickness until solution converges.
2008	Hobbacher (2008)	• Refer to Table 2-2 and Table 2-3 • Include weld in solid element models • Do not include weld in shell element models
2010	Lee et al. (2010)	• Tension: No significant differences between linear and quadratic extrapolation presented in Hobbacher (2008) • Bending: The effect of higher order elements and number of node may be sufficiently small to ensure convergence. • Solid elements is recommended when dominant loading pattern is out-of-plane bending. • Recommend quadratic extrapolation for calculating stress under bending.
2010	Bhargava (2010)	• Model with solid elements: 8 or 20-node solid elements with element size 0.25 (t×t) 20-node reduced integration solid element with element size t×t • Model with shell elements: 4-node thick shell elements • HSS calculation method: Linear extrapolation (Note: same as Hobbacher 2008) • Recommendation: Include weld in model • Stress used for HSS calculation: Maximum Principal Stress
2010	ABS (2010)	• Model with solid (Quadrilateral shape element) • Mesh guidelines: element size t×t • Aspect Ratio: 1:1 near HS, 1:3 to 1:5 away from HS • HSS calculation method: Linear extrapolation (Note: same as Hobbacher 2008) • Stress used for HSS calculation: Maximum Principal Stress
2011	DNV (2011)	• Model with solid elements: 20-node solid elements with element size: *t*/2 × *t*/2 • Model with shell elements: 8-node shell elements with a size of *t* × *t* • HSS calculation method: Linear extrapolation 0.5t and 1.5t (Note: same as Hobbacher 2008) • Stress used for HSS calculation: Maximum Principal Stress
2012	Aygul (2012)	• Model with solid elements: 20-node solid element • Element size: 1 mm^3 (note: 1 in. = 25.4 mm) • Mesh guidelines: Fine (1mm, 2mm, 4mm), and Coarse (10mm) • HSS calculation method: Use quadratic extrapolation for Type B HSS (Note: same as Hobbacher 2008) • Recommendation: Include weld in model

Table 2-3. FE Pre/Post-Processing and HSS Calculation Guidelines (Contd.)

Year	Reference	FE Pre/Post Processing and HSS Calculation Guidelines
2012	Aygul (2012)	• Model with shell elements: 8-node shell element (Quadrilateral element) • Element size: 1 mm (note: 1 in. = 25.4 mm) • Mesh guidelines: Fine (1mm, 2mm, 4mm), and Coarse (10mm) • Mesh guidelines: Fine or Coarse (Note: same as Hobbacher 2008) • Recommendation: Do not include weld in model
2012	Aygul (2012)	• Model with shell elements: 8-node thick shell elements • Element size: ≤ 4mm (quadratic), ≤ 10mm (linear) (Note: extrapolation equations are same as in Hobbacher (2008); 1 in. = 25.4 mm) • HSS calculation method: Use linear or quadratic extrapolation for Type B • Distance to reference points from weld toe: 4, 8, and 12 mm for quadratic 5 and 15mm for linear • Recommendation: Include weld in the model at 45º

Table 2-4. FE Discretization Guidelines (Hobbacher 2008)

Reference Point Locations with Respect to Weld Toe	HSS Type A		
	Coarse Mesh	Fine Mesh	
	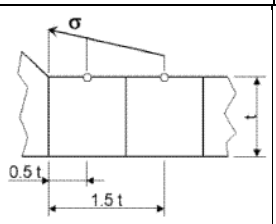	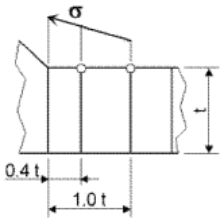	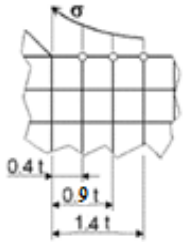
	(a) Linear	(b) Linear	(c) Quadratic
	HSS Type B		
	Coarse Mesh	Fine Mesh	
	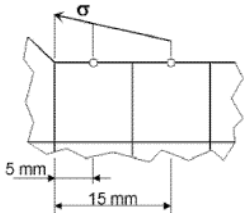	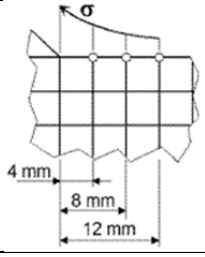	
	(d) Linear	(e) Quadratic	

2.3.4.2 Submodeling

Berglund and Schultz (2006) used linear finite element (FE) models to understand the behavior of web gap distortion and correlate the fatigue stresses in the web gap region to differential vertical deflection between girders for skewed multi-girder steel bridges. However, the global structural FE models are not effective in accurately predicting the local behavior of the fatigue-sensitive detail or the web gap distortion. Also, use of a densely meshed model representing the entire bridge is not justifiable. Hence, the submodeling approach is widely used to understand the local behavior and to quantify the strains developed at critical details (Shifferaw and Fanous 2013; Bowman et al. 2012; Bhargava 2010; Ju and Tateishi 2012; Hassel 2011). The

submodeling approach reduces the time and effort required for refined FE analysis of such details.

A recent study conducted by Shifferaw and Fanous (2013), through field testing and FE analysis of a multi-girder steel bridge with web gap fatigue-sensitive detail, demonstrated the use of the submodeling approach with refined FE models to simulate out-of-plane displacement or distortion and the strains induced in the web gap region. Also, Bhargava and Roddis (2007) used a refined finite element analysis and field investigation to identify the source of distortion induced fatigue cracking at a cross-frame to girder connection. The state-of-the-art research performed on fatigue-sensitive details shows the usefulness of refined FE modeling and submodeling approaches for evaluating distortion induced fatigue details.

2.3.4.3 Fatigue Resistance Using a Reference Detail

Hobbacher (2008) presents structural details and detail specific S-N curves for fatigue assessment using hot spot stresses. When the detail to be assessed does not exactly represent the reference detail for a given S-N curve, Hobbacher (2008) recommends implementing the following steps for fatigue assessment using hot spot stresses:

i. Select a reference detail with known fatigue resistance. The reference detail should represent the detail to be assessed as closely as possible in terms of geometry and loading.
ii. Identify the type of stress used in the S-N curve for the reference detail. In a majority of the guides or specifications, S-N curves are presented in terms of nominal stress.
iii. Develop finite element models of both details using the same element type and mesh discretization parameters.
iv. Load both models to yield the stress identified in step (ii).
v. Calculate hot spot stresses for both details. Label hot spot stress of reference detail and the detail to be assessed as $\boldsymbol{\sigma_{hs,\,ref}}$ and $\boldsymbol{\sigma_{hs,\,assess}}$, respectively.
vi. Use Eq. 2-2 to calculate the constant amplitude fatigue threshold of the detail to be assessed: $\mathbf{CAFT_{assess}}$. $\mathbf{CAFT_{ref}}$ is the constant amplitude fatigue threshold of the reference detail.

$$CAFT_{assess} = k \cdot CAFT_{ref} \qquad (2\text{-}2)$$

where, $k = (\sigma_{hs,ref})/ (\sigma_{hs,assess})$

Figure 2-7 shows the positions of reference S-N curve and the S-N curves used for assessment depending on the k value. As per Eq. 2-2, the $CAFT_{ref}$ value is adjusted using the hot spot stress ratio (k). When k > 1, the $CAFT_{ref}$ value is increased, and the $CAFT_{assess}$ and S-N $curve_{assess}$ are located above the references. Similarly, when k < 1, the $CAFT_{ref}$ value is decreased, and the $CAFT_{assess}$ and S-N $curve_{assess}$ are located below the references. Hence, depending on the hot spot stress ratio, the adjusted $CAFT_{ref}$ and S-N $curve_{ref}$ can be used to assess fatigue-sensitive details using hot spot stresses.

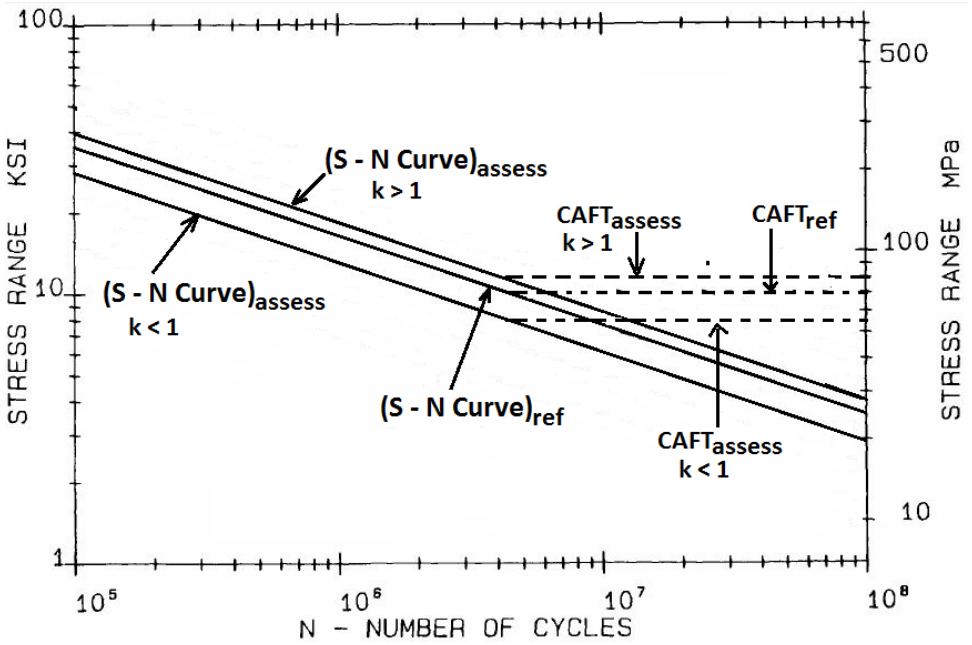

Figure 2-7. S-N curve definitions for fatigue assessment using hot spot stresses

2.3.5 Fracture Mechanics Based Assessment

The fracture mechanics approach with an assumed initial crack size can be used to estimate crack growth rate (Kühn et al. 2008; Lovejoy 2003). Once the crack growth rate is calculated, inspection frequency can be determined. As an example, Kühn et al. (2008) presented a case study for a railway bridge. In this example, a 0.2 in. (5 mm) visible crack at a rivet hole was considered, and the remaining fatigue life was calculated as 3.6 years (Figure 2-8). If the bridge owner decides to make three inspections, the detail needs to be inspected at least every 1.2 years. Using the inspection data, the calculated fatigue life can be revised, and the inspection or repair/retrofit/maintenance decisions can be taken accordingly. Even if no cracks are identified, the process can be implemented with an assumed crack size. Later, the inspection frequency can be revised based on the findings from the subsequent inspections.

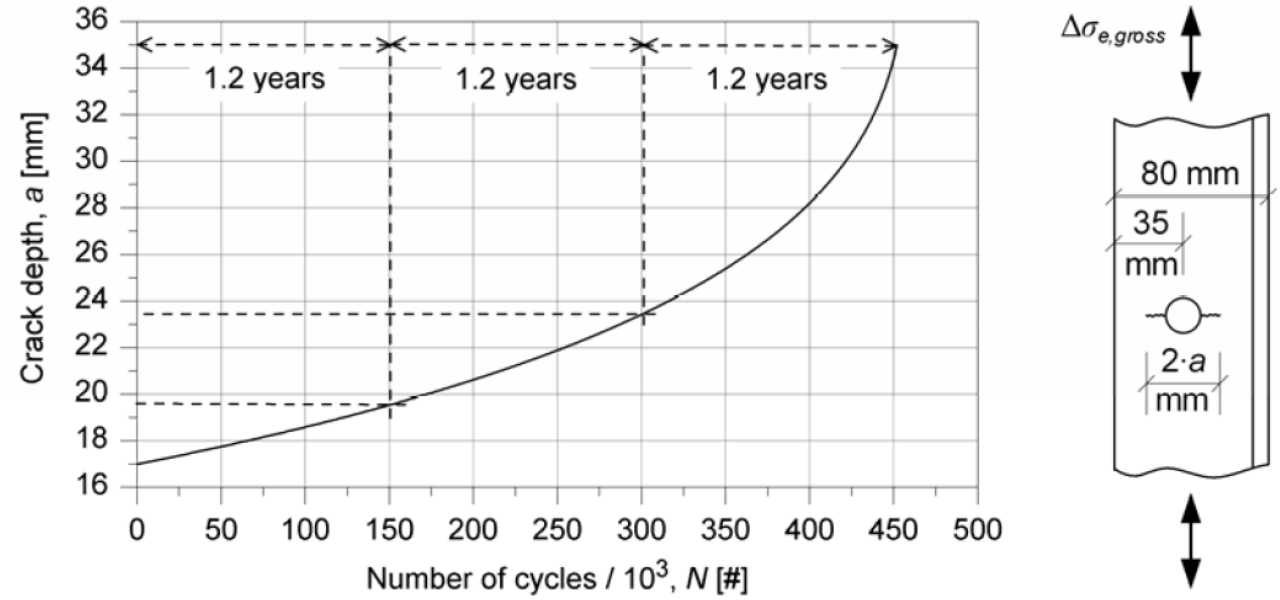

Figure 2-8. Fracture mechanics based fatigue life calculation for a riveted detail (Kühn et al. 2008)

A linear elastic fracture mechanics (LEFM) based inspection decision-making process was developed for Montana DOT fracture-critical bridges (Lovejoy 2003). This process was presented to the Federal Highway Administration (FHWA) and received the approval to be executed to assure safety of nonredundant bridges in lieu of implementing procedures given in the FHWA publication ‘‘Inspection of Fracture-critical Bridge Members’’. With the ODOT process, a bridge specific inspection program was developed and, at that time, the expected cost saving from 1995 to 2005 was over $6 million. An example fatigue inspection frequency decision-making diagram that was developed for a specific bridge in Oregon is shown in Figure 2-9. The figure was developed with an assumed initial crack size of ($2a_i$ = 38 mm), a critical crack length of 6 in. ($2a_{crit}$ = 150 mm), and the maximum allowable final crack length of 2 in. ($2a_f$ = 50mm). A safety margin of 3.5 has been achieved by setting the number of stress cycles between inspections to 500,000. Further, by knowing the number of cycles to grow a crack from a_i to a_f, the number of significant stress cycles per truck, and the ADTT at the site, a family of curves can be developed to help bridge managers schedule inspection intervals (Figure 2-10). By the year 2003, Oregon DOT has calculated the fracture-critical inspection period of 76 bridges in their inventory. The inspection periods of 76 bridges ranged from 2 to 10 years with an average of 8.4 years and a standard deviation of 2.7 years.

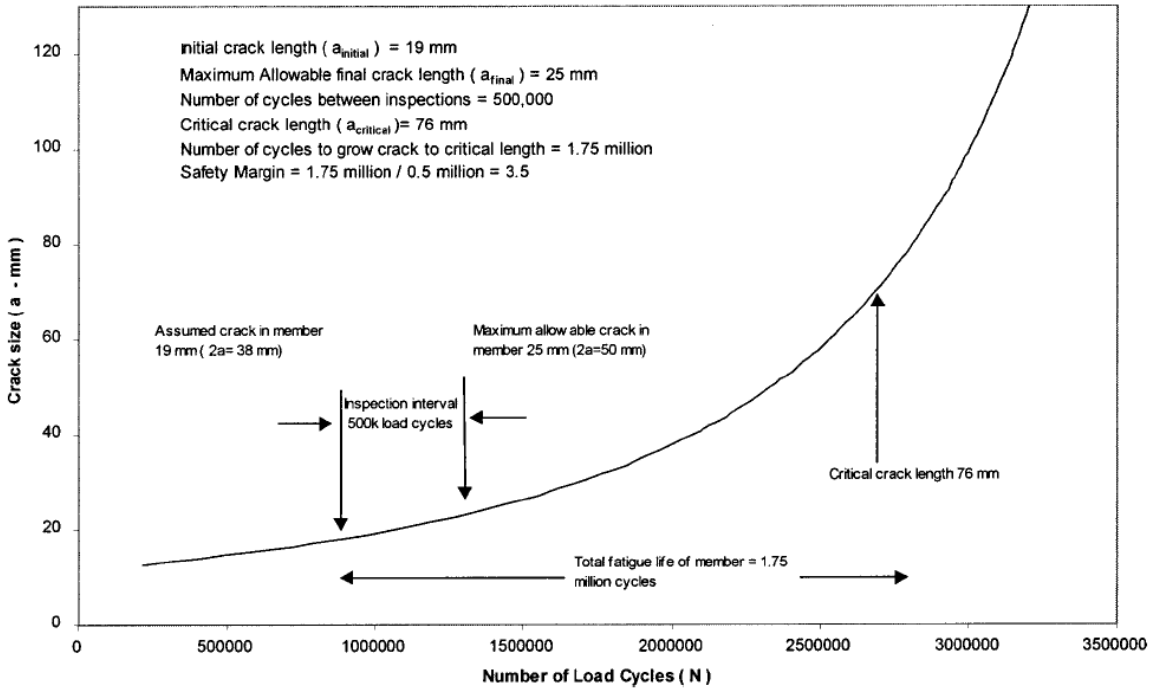

Figure 2-9. Details of an example fatigue inspection cycle (Lovejoy 2003)

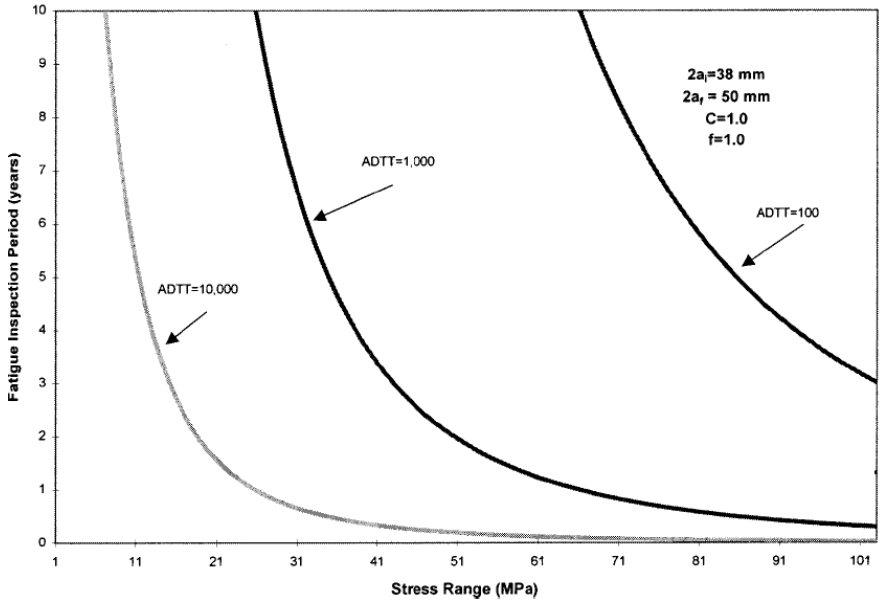

Figure 2-10. Fatigue inspection periods for a riveted section crack model at various stress ranges and traffic volumes (Lovejoy 2003)

When fracture mechanics analysis is implemented, establishing an accurate initial crack size is important. Åkesson (2010) suggests inspecting the detail using a nondestructive testing technique and selecting the largest non-detectable crack as the initial crack size. As an example, when inspected using ultrasonic testing, the largest non-detectable crack at a rivet hole is 0.08 in. (2 mm) and can be taken as the initial crack size (Åkesson 2010). However, if a crack is

detected, the practice is to immediately stop the growth (Åkesson 2010). In addition to visual inspection, ultrasonic testing and acoustic emission can be used to determine the presence of fatigue cracks. Ultrasonic testing is more suitable for rivet connections because of the challenges in identifying AE signals that arise from friction slip and crack propagation. AE is a more suitable method for welded structures to monitor crack growth (Åkesson 2010).

2.4 FATIGUE-SENSITIVE DETAIL MONITORING

Kühn et al. (2008) presented a four phase process to assess a structure and to develop remedial measures. These phases include (i) a preliminary evaluation by an engineer in accordance with the current codes, (ii) detailed investigation by an engineer with the help of an expert and supported with data collected using low tech NDT methods, (iii) expert investigations that may be supported with data collected using high tech NDT, and (iv) development of remedial measures such as structural response monitoring, enforcing load restrictions, or performing strengthening, repair or rehabilitation. Monitoring is used to support detailed investigation by experts as well as to evaluate the effectiveness of remedial measures.

When a large number of bridges with fatigue-sensitive details or fracture-critical members (FCM) are present, it is very difficult to evaluate fatigue performance of each and every detail of every bridge. Hence, Fu et al. (2003) suggested clustering bridges with fatigue-sensitive details (both load-induced as well as distortion-induced) based on the following attributes:

- Jurisdiction (state vs. local agency)
- Functional class of the roadway
- Type of construction (plate girders, rolled beams, trusses, etc.)
- Type of span (simple or continuous)
- Span length
- The year of original construction
- Any other parameter deemed necessary.

Once the clustering is completed, the presence of targeted fatigue-sensitive details, as well as the condition, can be verified by reviewing bridge plans, inspection records, and maintenance records. After that, a representative bridge from each cluster is selected to calculate remaining fatigue life or fatigue serviceability index. If the analysis results call for additional

investigations, the bridge can be monitored to evaluate stresses under ambient loads as well as to verify the presence of active cracking.

2.5 TECHNOLOGY FOR FATIGUE-SENSITIVE DETAIL MONITORING

2.5.1 Overview and Technology Selection

The mature as well as emerging technologies for fatigue-sensitive detail monitoring were synthesized and presented in Appendix C. The nondestructive evaluation (NDE) technology, which is currently integrated into the visual inspection for crack detection and characterization, was not included in the review. Table 2-5 lists the sensor types and implementation objectives. The information presented in Appendix C was used to develop Table 2-6 to Table 2-11 that list the implementation objective, technology, and technology ranking based on their capabilities and status (i.e., their ability to address the implementation objective and readiness for field implementation). The tables also include a few remarks to explain the ranking decisions. The technologies listed in the tables are: AE- acoustic emission, DIC- digital image correlation, EFS- electrochemical fatigue sensor, FD - Fatigue damage sensor, FF - fatigue fuse, PE- photoelasticity, RFID- radio frequency identification, SG- strain gauges, TS- temperature sensor, USGW- ultrasonic guided wave, and XRD- X-ray diffraction. The rank 1 to 4 indicates the most to least appropriate technology for achieving the implementation objectives.

Table 2-5. Sensor Types and Implementation Objectives

Sensor Type	Implementation Objectives
Fatigue event detection and characterization of cracks	
Acoustic emission (AE) sensors	detect crack initiation detect crack growth or the status of a crack (i.e., an active or a dormant crack) detect potential for cracking (material plasticity)
Electrochemical fatigue sensors (EFS)	detect crack growth or the status of a crack detect potential for cracking (monitoring strain localization and/or micro plasticity)
Fatigue damage (FD) sensor and fatigue fuse (FF)	measure crack growth rate predict remaining fatigue life
Radiofrequency identification (RFID) chips	measure strain detect crack initiation detect crack growth
Ultrasonic guided wave (USGW) sensors	detect presence of a crack detect crack growth
Complementary technologies	
Accelerometers	measure dynamic response
Displacement transducers, laser distance measurement sensors	measure differential deflection measure component deformation
Digital image correlation (DIC)	measure displacement and strain
Strain gages (SG) and strain transducers (ST)	measure strain (with many objectives including fatigue life calculation, crack growth potential evaluation, and development of a load matrix for evaluating AE data)
Thermocouples (TC)	measure temperature
Laser point tracking	measure displacement
Photoelastic (PE) imaging	measure strain
X-ray diffraction (XRD)	measure strain (to determine in-service dead load, load path determination, crack-stop hole validation by checking the stresses around it, baseline stress measurement for enhanced structural monitoring, and residual stress measurement before and after a retrofit).

Table 2-6. Crack Initiation Detection Technology

Objective	Tech	Rank	Remarks
Crack initiation detection	AE	1	This technology has been widely implemented in the field. It can detect crack initiation based on the energy release from the source. Also, the technology is capable of detecting material plasticity by monitoring burst signals that arise due to dislocation or slipping of portions of the crystal over on another near the yield stress. However, when the signal strength is weak, it requires implementation of filtering techniques and advanced analysis tools to differentiate between crack-relevant emissions from ambient noise. The rank is assigned considering its extensive use in the field, suitability for long-term as well as short-term monitoring, capability to identify early signs to crack initiation, capability to identify the crack location, and mainly not requiring mounting the sensors over a potential crack location.
	EFS	3	Limited use under field conditions. Sensors can be used only for short-term monitoring due to evaporation of the electrolyte. Primarily one group has been involved in technology implementation so far; hence, limited experience is documented. Technology has the capability to capture early signs to crack initiation and growth in sensitive regions. It is required to mount the sensor over or very close to a crack tip to monitor growth. The ranking is assigned because there are limited field implementations; as well it requires identifying potential crack initiation locations. Also, the technology, at the current state, is not suitable for long-term monitoring due to the need of refilling electrolyte.
	RFID	4	RFID tags are like EFS that need to be placed on top of the potential crack location. However, technology is still under development.
Rank 1 to 4 defines most to least appropriateness of the technology for the stated purpose			
Abbreviations: AE- Acoustic emission, EFS- Electrochemical fatigue sensor, RFID- Radio frequency identification.			

Table 2-7. Crack Location Detection Technology

Objective	Tech	Rank	Remarks
Crack location detection	AE	1	Crack source location can be detected in real-time with the use of sensor arrays mounted around the area of concern and the time of arrival of the emissions at sensors within the array. The theory behind crack location measurement is well developed. The rank is assigned because of availability of successful implementation records and well developed procedures in establishing crack location.
	USGW	3	Sensor data need to be transferred from the field and need to be mapped using tomography approach to locate the cracks. The rank is assigned because it is an active sensor system and requires triggering to detect crack growth. Very limited use in bridges and details with multiple plates and welds. Also, pulsers and receivers need to be mounted on either side of a potential crack growth location or an existing crack to detect the crack location.
	DIC	4	These technologies are only evaluated under laboratory conditions. Sensitivity of the technology is not evaluated under laboratory and field conditions. The noise levels of DIC and PE methods are around +/-150 με and +/- 50 με, respectively, and may lead to greater inaccuracies under outdoor conditions. Technology is expensive and not suitable to monitor hidden cracks. However, they have the potential of monitoring crack growth over a large area within the camera range.
	PE	4	
Rank: 1 to 4 defines most to least appropriateness of the technology for the stated purpose			
Abbreviations: AE- Acoustic emission, DIC- Digital image correlation, PE- Photo elastic, USGW- Ultrasonic guided wave.			

Table 2-8. Crack Growth Monitoring Technology

Objective	Tech	Rank	Remarks
Crack growth monitoring	AE	1	AE is capable of providing indication of crack growth activity. When a senor array is used, the instantaneous location of the crack activities can be continuously recorded to give the crack growth path. AE can detect material plasticity by monitoring burst signals that arise due to dislocation or slipping of portions of the crystal over on another near the yield stress. However, the signal strength is weak and requires implementation of filtering techniques and advanced analysis tools. AE can detect and monitor internal cracks that are not visible on the surface. The rank is assigned because the technology is good for long-term monitoring, capable of identifying early signs to crack growth, supported with advanced data analysis tools, and has a long history of field implementation. Also, the sensors can be mounted in different configurations based on the monitoring objectives.
	EFS	2	The crack sensor needs to be mounted on top of an existing crack tip and also along the predicted crack growing path to monitor the crack growth. It requires mounting a reference sensor in a place with similar stress intensity. A rapidly growing crack may grow beyond the sensors. Rank is assigned because the technology, at the current state, is not suitable for long-term monitoring due to the need of refilling electrolyte as well the need for mounting the sensor over the identified crack tip. However, EFS are capable of identifying early signs to crack growth. After identifying an existing crack, growth can be monitored.
	USGW	2	USGW sensors need to be mounted in an array such that the detectable path of the actuators and sensors is intercepted by the growing crack. The rank is assigned because the sensors can be triggered automatically at regular intervals or when a crack activity is detected by other sensors such as AE. However, the sensors need to be mounted around an existing crack or a potential crack location. Further, the technology is still under evaluation stages for fatigue crack monitoring of multi girder bridges.
	FD and FF	3	Technology is still under development with limited applications. Data interpretation is simple; however, sensor calibration can be a challenge depending on the complexity of the detail configuration, boundary conditions, and loading. Crack growth can be determined based on the number of fuses broken.
	DIC	4	These technologies are only used under laboratory conditions. Sensitivity of the technology is not evaluated under laboratory and field conditions. The noise levels of DIC and PE methods are around +/-150 με and +/- 50 με, respectively, and may lead to greater inaccuracies under outdoor conditions. Technology is expensive. It may not be suitable for monitoring internal cracks. However, the technology has the potential for monitoring crack growth over a large area within the camera ranges.
	PE	4	
	SG	3	Technology is primarily used for developing a load matrix rather than crack growth monitoring. However, multiple strain gages can be placed across the potential crack growth path to detect crack growth similar to FD or FF.
	RFID	4	RFID tags are like EFS that need to be placed on top of the growing crack. However, technology is still under development.
Rank: 1 to 4 defines most to least appropriateness of the technology for the stated purpose			
Abbreviations: AE- Acoustic emission, EFS- Electrochemical fatigue sensor, FD- Fatigue damage sensor, FF – Fatigue fuse, PE- Photo elastic, SG- Strain gauges, RFID- Radio frequency identification, USGW- Ultrasonic guided wave.			

Table 2-9. Technology for Fatigue Crack Characterization

Objective	Tech	Rank	Remarks
Crack characterization	AE	2	AE can be used to characterize cracks; however, it requires access to a database of signals with characteristics specific to the detail being investigated. Hence, the signal characteristics need to be specific to the material, component thickness, surface finish, temperature, etc. Further, having access to an advanced data analysis tool is important to evaluate signal characteristics.
	EFS	2	The crack sensor needs to be mounted on top of the existing crack tip and also along the predicted crack growing path to monitor the crack growth. The system requires mounting the reference sensor in a place with comparable stress intensity. A rapidly growing crack may grow beyond the sensors. The technology, at the current state, is not suitable for long-term monitoring due to the need of refilling electrolyte.
	USGW	2	Sensors need to be mounted around an existing crack or in an array with enough sensors to capture sufficient wave propagation data around the potential damage area. Data can be analyzed and interpreted for crack characterization using tomography approach. Technology is not widely used and needs additional research to integrate this technology in bridge monitoring.
Rank: 1 to 4 defines most to least appropriateness of the technology for the stated purpose			
Abbreviations: AE- Acoustic emission, EFS- Electrochemical fatigue sensor, USGW- Ultrasonic guided wave.			

Table 2-10. Strain Measurement Technology

Objective	Tech	Rank	Remarks
Strain measurement	SG	1	Strain gauges are a proven technology for strain measurement. Real-time strain measurement data can be obtained. Single or multiple gauges can be used to measure the strain field distribution of a global structure or local component. However, the measurements are made at discrete locations.
	FD and FF	2	Technology is still under development with limited applications. Strain is recorded with the aim of calculating remaining fatigue life. Hence, the technology is more suitable for remaining fatigue life calculation rather than just the strain monitoring. Data interpretation is simple; however, sensor calibration can be a challenge depending on the complexity of the detail configuration, boundary conditions, and loading. Ranking is primarily assigned due to lack of implementation records in the field of bridge engineering.
	DIC	4	These technologies are mainly used under laboratory conditions. Very limited field applications for displacement and strain measurement of highway bridges. Suitable for measuring strain field distribution of a larger area within the range of the camera. Measurement accuracy depends on many factors including exposure and ambient conditions. Ranking is primarily assigned due to lack of implementation records in the field of bridge engineering.
	PE	4	
	XRD	4	A newly developed technology to measure in-service strain using x-ray diffraction method. It requires point to point measurement. It is not suitable for continuous monitoring at multiple locations simultaneously. Technology has been use in very limited highway bridge applications. Ranking is assigned considering the inability to incorporate into remote monitoring at the current state of technology.
Rank: 1 to 4 defines most to least appropriateness of the technology for the stated purpose			
Abbreviations: DIC- Digital image correlation, FD- Fatigue damage sensor, FF – Fatigue fuse, PE- Photo elastic, SG- Strain gauges, XRD- X-ray diffraction.			

Table 2-11. Technology for Measuring Residual Stress and Temperature

Objective	Tech	Rank	Remarks
Residual stress measurement	XRD	1	The only technology currently implemented in the field. Uses x-ray diffraction for measuring residual stress of a component. The technology has been used at a few bridge sites. Ranking is assigned considering the state-of-the art. Further, measuring residual stress is required only at discrete times, mainly to calculate remaining fatigue life.
Temperature	TS	1	Continuous measurement can be recorded for parametric input required for other technologies such as AE and strain measurement.
Rank: 1 to 4 defines most to least appropriateness of the technology for the stated purpose			
Abbreviations: TS- Temperature sensor, XRD- X-ray diffraction.			

Section 1.1 lists the SHM system implementation objectives. As per the listed objectives, technology for detecting crack initiation and growth needs to be a major component in any fatigue-sensitive detail monitoring system. AE is the most effective technology for fatigue event detection (i.e., crack initiation or crack growth monitoring). AE has been successfully implemented in the field and evaluated for continuous monitoring of fatigue-sensitive details. At this time, AE is the only technology that is capable of real-time monitoring of fatigue events and providing data for damage location detection. In addition, strain gauges are required to validate FE models, evaluate stress state to calculate remaining fatigue life, and support AE data analysis by developing the load matrix. Even though Table 2-6 to Table 2-9 list capabilities of AE justifying the selection of technology, reasons for widespread use of the technology is listed below;

- AE can be used as a local as well as global crack growth monitoring tool (FHWA 2012; DFT UK 2006; Nair and Cai 2010).
- Very minimal surface preparation is required to mount AE sensors (FHWA 2012).
- Frequent access to a detail is not required once the sensors are installed (FHWA 2012; DFT UK 2006).
- Portable systems with permanently attached transducers to bridge structures offer cost effective means of as-needed remote monitoring (McCrea et al. 2002; DFT UK 2006).
- AE is capable of locating the source of failure (McCrea et al. 2002; DFT UK 2006).
- AE is capable of detecting and locating defects in areas obscured from view or in areas that are difficult to inspect (e.g. weld defects, material imperfections, etc.) (Kaphle et al. 2012; DFT UK 2006).

- The data from an AE monitoring system can be used to track the history of crack growth activity (FHWA 2012).
- Parametric data (strain, displacement, temperature, etc.) can be used to correlate AE events to improve the accuracy of data analysis results (DFT UK 2006).
- Real-time data display tools are available (Wang et al. 2012).
- AE signal characteristics and source location plots can be used to help with management decisions (DFT UK 2006).
- Technology has been used for decades in many disciplines and the experience is well documented.

With any technology there are advantages as well as implementation challenges. This is no different to AE technology implementation and data interpretation. Table 2-12 lists the challenges and potential solutions.

Table 2-12. AE Implementation Challenges and Mitigation Strategies

AE Implementation Challenges	Mitigation Strategies
In many instances, AE can only qualitatively gauge the extent of damage.	In order to obtain quantitative results about size, depth, and overall acceptability of a part, other NDT methods are necessary. Source: FHWA 2012; DFT UK 2006; Huang et al. 1998; Nair and Cai 2010.
Extensive expertise is required to plan, set up the sensors, test, and interpret results (McCrea et al. 2002)	
Standardized procedures are not available for all types of bridges, as most recommendations cater for bridges under unique conditions of loading, materials, etc. (Nair and Cai 2010)	Volume 3 section 1 of the Design Manual for Roads and Bridges (DMRB), Department for Transport, UK, Advice Notes on the Non-Destructive Testing of Highway Structures, provides guidelines up to a certain extent to help the technology implementation. Source: DFT UK 2006
Impact of the service environments which contribute extraneous noise to the signals. (FHWA 2012; DFT UK 2006; Huang et al. 1998)	• In order to eliminate receiving background noise in AE data acquisition, a lower bound threshold can be defined. Any signal below a user defined signal voltage or signal in the frequency range will be ignored by the AE sensor. • Parametric data (e.g., strain) can be used to distinguish crack related AE from noise that occurred from mechanical rubbing and crack closure. • Waveforms and their characteristics obtained from Pencil Lead Break (PLB) tests are used as a frame of reference to indicate genuine hits. Typical parameters of AE waveforms include peak amplitude, rise time, duration and emission counts. The waveforms caused by 'false' hits generally have long rise time, high counts, and poorly defined peak amplitudes. In PLB tests, the signal rapidly attains the peak amplitude and then fades gradually. The shorter rise time, lower counts, and higher peak amplitude are indicative of genuine AE, as is the clean front-end of the waveform. Source: Yu et al. 2011; Shield and McKeefry 1999; Schultz and Thompson 2010; Wang et al. 2012.
Background noise due to fretting bolts (Shield and McKeefry 1999)	• A method for eliminating this type of background noise is placing an AE sensor local to the fretting bolt, and then all AE signals this sensor receives will be ignored by sensors located at other areas of interest. • The noise generated from fretting of bolted connections can be filtered by selecting a lower bound threshold value. Source: Schultz and Thompson 2010
Background noise from grating	AE from grating can be minimized by collecting and analyzing signals in the vicinity of the peak load. Source: Yu et al. 2011
Acoustic coupling requires clean smooth flat surface and the removal of thick coating (McCrea et al. 2002)	

Table 2-12. AE Implementation Challenges and Mitigation Strategies (Contd.)

AE Implementation Challenges	Mitigation Strategies
Transducer arrangement is critical to the results (McCrea et al. 2002)	• The effect of geometric dispersion of signals can be limited by an understanding of the structure e.g. the hidden structure of box girders, and by placing AE sensors accordingly. When high accuracy is required for complex structures the number of sensors is generally increased. • Attenuation survey is performed to identify the optimal sensor placement. • Resonant AE transducers are used in linear or planar arrays to detect the presence and the location of defects and to monitor their activity under normal service loads • Areas of interest, such as long welds, can be monitored using linear arrays. Source: DFT UK 2006; Hay et al. 2009.
Lack of possibilities to intensify the elastic waves field (McCrea et al. 2002)	• Perform attenuation survey to identify the optimal sensor placement. Source: DFT UK 2006
Measurements cannot be repeated (McCrea et al. 2002)	• The data from an AE monitoring system can be continuously recorded and used to track the history of crack growth activity. • Data replay tools can be used to backtrack the activities. Source: FHWA 2012
Signals are transient and random in time (standard noise reduction methods cannot be used) (McCrea et al. 2002)	• Perform attenuation survey to identify the optimal sensor placement. • Implement advanced analysis techniques such as supervised and un-supervised learning techniques and pattern recognition classification. Source: DFT UK 2006; ICEPak® 2014
Several simultaneous measurements are required for verification and orientation and determination (McCrea et al. 2002)	Pencil lead break should be conducted before each fatigue test to check the condition of each sensor and the location capability of the sensor arrangement. Source: Wang et al. 2012
It does not detect defects that are either no longer propagating or not growing during the monitoring period (e.g., dormant cracks) (DFT UK 2006)	Structure should be monitored under representative peak loading Source: DFT UK 2006
It may not be applicable where the critical crack size is very small and failure is sudden (DFT UK 2006)	
Generation of large amount of data during the testing; hence an effective data analysis and management is necessary, especially for long term monitoring (Kaphle et al. 2012)	Use of pencil lead break calibration and setting up the thresholds and gains will help eliminate most of the noises; thus, reducing the amount of data collected by the system.
Quantifying the level of damage to assess severity of source (Kaphle et al. 2012)	Develop a database of signals through laboratory studies to correlate.

Table 2-12. AE Implementation Challenges and Mitigation Strategies (Contd.)

AE Implementation Challenges	Mitigation Strategies
AE monitoring of bridges has generally been limited to short-term tests contingent on either fair weather or availability of some shelter on site.	A weatherproof enclosure could be developed to protect the AE hardware and connect it to a rugged laptop computer and a battery-backed power supply. This enclosure could be clamped to the bridge near the area of interest making long noise-prone cable runs unnecessary. To reduce electrical noise and spurious AE hits from the enclosure itself, the enclosure could be mounted on rubber feet and placed well outside the AE arrays so any events would be rejected by the AE processing filters Source: Kosnik 2008
The noise levels are greater than the threshold	In order to filter out the noises, the following approaches can be implemented. • The first-hit channel (FHC) analysis. • Use average frequency spectrums of triggered signals from multiple (e.g., three) AE sensors. • Use a guard sensor. • Use a band-pass filter. Source: Kosnik 2008; Zhang et al. *2013*; Schultz and Thompson 2010
Complicated geometry and low strength signals make tasks unattainable.	• Implement advanced signal enhancing and processing techniques to minimize the noise effects. • Monitor the structure for an adequately long duration to identify the noise sources and establish thresholds to capture fatigue events. • Use wave form parameters such as amplitude, energy, signal count, signal rise time, and signal duration for event characterization. • Use Artificial Intelligence Software such as ICEPAK™ for development and implementation of pattern classifiers. Source: Kosnik 2008; Schultz and Thompson 2010; Hay et al. 2000.

2.6 TECHNOLOGY IMPLEMENTATION CONSIDERATIONS

Kühn et al. (2008) presented a four-phase process to assess a structure. According to the four-phase procedure, AE is implemented during the 3rd and 4th phases. Fu et al. (2003) conducted a study to evaluate the effect of truck weight on bridge network cost. As part of the study, a methodology was developed to calculate the network level maintenance, repair, and replacement costs due to fatigue damage. The first step in the evaluation starts with clustering bridges based on the jurisdiction, functional class, type of construction, type of span, span length, and the year of construction. Then the fatigue life of selected bridge details is calculated to make repair, retrofit, or replacement decisions. A similar bridge clustering approach as well as the DOT experience with specific structures in the inventory can be used to identify bridges and/or details for monitoring stress state and AE events.

Implementation of structural response or health monitoring systems requires a thorough understanding of the structure, careful planning, development of strategies based on the level of

monitoring and the duration of monitoring, access to advanced data analysis tools, and experience in understanding data and results interpretation (DFT UK 2006).

2.6.1 Level of Monitoring

Global, semi-global, and local monitoring are the three levels (DFT UK 2006). The purpose of global monitoring is to identify potential source locations for planning or asset management purposes. Semi-global monitoring is implemented to identify individual source locations to assess, evaluate, and rank. The ranking is based on the source characteristics and number of emissions. The ranking system is used for planning detailed investigations through local monitoring. The local monitoring is implemented to identify the source location and to characterize the AE events. The AE event characteristics help to identify if the events are due to fatigue crack growth or due to fretting, crack opening or closure, or grinding of debris between cracked surfaces. The local monitoring can also be implemented as a means of quality control. As an example, a retrofit can be monitored using AE to evaluate if the defect's growth has been arrested. Local monitoring can be planned based on global/semi-global monitoring results, inspection records, or prior experience with similar details. The sensor array for local monitoring is designed based on (a) the classification of the detail to be monitored, (b) prior experience with similar details, (c) inspection and maintenance records, (d) an attenuation survey, (e) the finite element (FE) analysis, or a combination thereof.

2.6.2 Monitoring Duration

When an AE monitoring system is installed, it is crucial that the correct monitoring duration is selected so that active defects may be detected. The key to successful implementation of an AE monitoring system is an understanding of the causes and damage mechanisms. Knowing the stimulus of cracking, the monitoring duration can be selected. Otherwise, a short monitoring duration may miss defects that are inactive under prevalent conditions; whereas an extended monitoring may provide no further new information while being carried out at an unnecessary cost. Volume 3 section 1 of the Design Manual for Roads and Bridges, Department for Transport, UK, Advice Notes on the Non-Destructive Testing of Highway Structures, defines monitoring duration as short-term, loading pattern dependent, and permanent (DFT UK 2006).

2.6.2.1 Short-Term Monitoring

Short-term monitoring is suitable when the causes and damage mechanisms are well understood. The monitoring duration should be sufficiently long to acquire a representative amount of AE data to locate the sources and characterize the cracks. Short-term monitoring is also used as a means of quality control, such as an evaluation of effectiveness of a retrofit (i.e., use of crack stop hole). Even though it is not related to AE monitoring, Zhou (2005) suggested monitoring a structure for at least seven continuous days to capture the structural response to a representative unit of vehicle patterns. Monitoring duration is primarily based on the traffic patterns. On certain roads, a uniform traffic volume can be observed. Different monitoring durations and use of data for fatigue evaluation are documented by Li et al. (2001), Leander et al. (2009), and Fasl et al. (2013).

2.6.2.2 Loading Pattern Dependent Monitoring

When AE monitoring is used as a means of quality control, such as an evaluation of effectiveness of a retrofit (i.e., use of crack stop hole), loading pattern dependent monitoring is more effective than short-term monitoring. When loading pattern dependent monitoring is implemented, the monitoring duration decision needs to be made with a clear understanding of the traffic patterns. In such cases, it is vital to have access to weigh-in-motion (WIM) data or information about a passage of a permit load (a large load). According to DFT UK (2006), monitoring AE activities should take place for one day on a heavily travelled road bridge with uniform traffic patterns and for two or more days for less frequently trafficked bridges.

2.6.2.3 Long-Term or Continuous Monitoring

Long-term or continuous monitoring is primarily recommended when fatigue-sensitive or fracture-critical details are present, and the bridge is a critical node of a road network. Even if data is collected sporadically, it is cost effective to have the sensors and the cables mounted on a bridge when it is challenging to access the bridge due to traffic or site conditions.

2.6.3 Inspection Frequency

Stresses calculated using refined models and accurate traffic data can be used as the first step to make a decision on the level of inspection or monitoring. Kühn et al. (2008) recommended using

Miner's rule to calculate fatigue life. As the initial step, it is recommended to calculate stresses using codified loads, if possible, using more realistic loads calculated from WIM data. As shown in Figure 2-3, when the remaining fatigue life is greater than 10 years, performing biennial inspection is adequate.

If the calculation yields a negative life, it is recommended to inspect the detail for presence of cracking. Cracks can be present in two forms: active and dormant. If the detail is accessible for close inspection, traditional NDE can be used to locate cracks and measure crack size. If no cracks are identified using traditional NDE or all the surfaces are not accessible for inspection, short-term or loading pattern dependent monitoring can be performed using a system with AE and strain sensors. Strain data can be used to recalculate the fatigue life and provide parametric input for AE data analysis while AE data can be used to identify the presence of active cracking.

If no cracks are found, the inspection frequency is normally decided based on the codes and/or experience. However, inspection frequency can be determined based on an estimated crack growth rate. The fracture mechanics approach with an assumed initial crack size can be used to estimate crack growth rate (Kühn et al. 2008; Lovejoy 2003). Once the crack growth rate is calculated, inspection frequency can be determined. Two such examples are presented in section 2.3.5. Establishing an accurate initial crack size is very important when the fracture mechanics based approach is used to determine inspection frequency. As suggested by Åkesson (2010), the largest non-detectable crack size, determined by applicable nondestructive testing techniques, can be used as the initial crack size. However, if a crack is detected, the practice is to immediately stop the growth (Åkesson 2010). The AE system can be used to monitor crack growth or effectiveness of a repair.

2.7 REPAIR AND RETROFIT METHODS

Repair of a fatigue-sensitive detail is performed to arrest the propagation of a crack, while retrofitting is primarily meant to upgrade the fatigue resistance of a detail with the goal of prevention of cracks (Dexter and Ocel 2013). According to Dexter and Ocel (2013), the repair and retrofit methods can be broadly grouped into surface treatments, repair of through-thickness cracks, modification of connections or the global structure to reduce the cracking potential and repair of out-of-plane distortion (Figure 2-11). Repair methods for out-of-plane distortion can be

grouped into hole drilling, diaphragm or cross-frame removal, diaphragm repositioning, bolt loosening, web-gap stiffening and web-gap softening (Figure 2-12). In addition to using doubler plates, several methods that are listed in Figure 2-12 such as diaphragm or cross-frame removal, diaphragm repositioning, and bolt loosening methods can be used to modify the global structure response. Also, a connection can be modified by loosening the bolts.

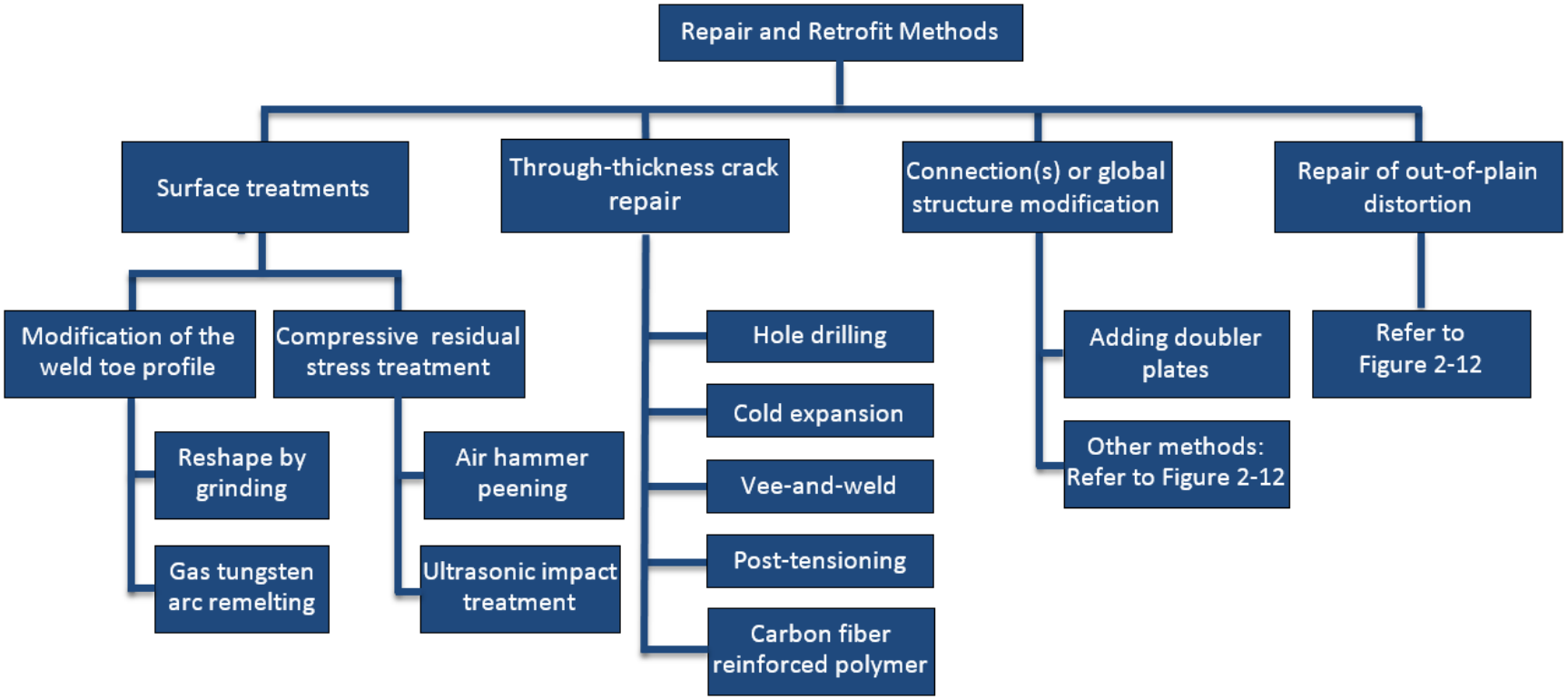

Figure 2-11. Repair and retrofit methods

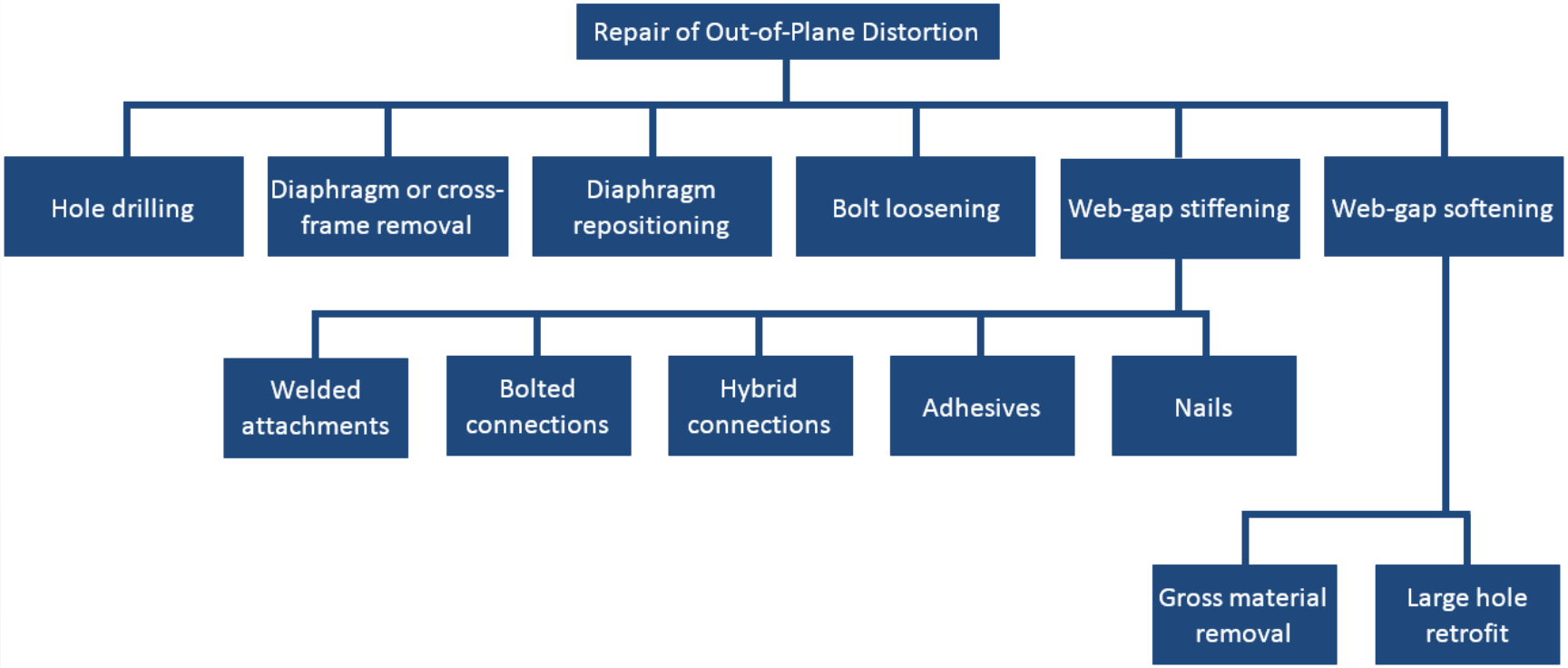

Figure 2-12. Repair of out-of-plain distortion

2.7.1 Surface Treatments

The weld toe surface treatment methods can be divided into two major groups: modification of the weld toe profile and compressive residual stress treatments. These methods can be used as retrofit techniques to enhance fatigue durability of uncracked welds (Dexter and Ocel 2013).

2.7.1.1 Modification of a Weld Toe Profile

The objective of modifying a weld toe profile is to remove the intrusions at the weld and obtain a continuous connection between the weld and the plate. This can be achieved by reshaping a weld toe using a grinder or remelting a weld using gas tungsten arc welding equipment.

2.7.1.1.1 Reshape by Grinding

Disc and burr grinders can be used to reshape a weld toe (Figure 2-13, Figure 2-14, and Figure 2-16). Small cracks at the edges of flanges or other plate like components can be effectively removed by grinding. However, grinding is not an effective or an economical method for removing microcracks in welds; it is also not the best on-site process for reshaping welds at bridge details. Grinders are commonly used in the field as finishing tools during repair or retrofit of bridge details (as an example, burr removal during hole drilling or toe finishing during welding).

Only the required amount of material is removed by grinding. If extra material is lost, the surface may be gouged (Dexter and Ocel 2013). To control the amount of material removed, the angle that the equipment must be held is important. When a disc is utilized, the disc must be held at an angle between 30° to 45° to the material being ground (Figure 2-13). When a burr is preferred, it must be held only at 45° as shown in Figure 2-15. In more confined regions, a burr is recommended over a grinding disc (Gregory et al. 1989).

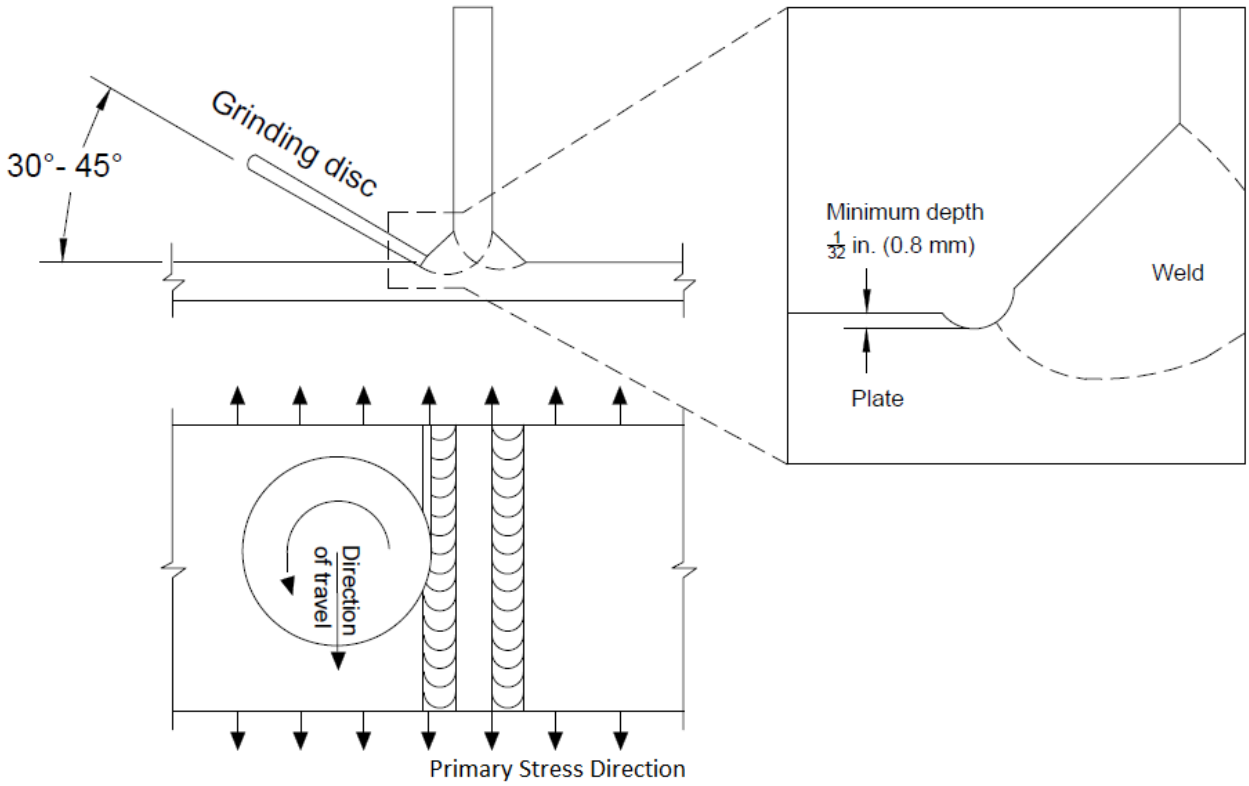

Figure 2-13. Position of the grinding disk with respect to the material surface (Gregory et al. 1989)

Figure 2-14. Typical disc grinders (Dexter and Ocel 2013)

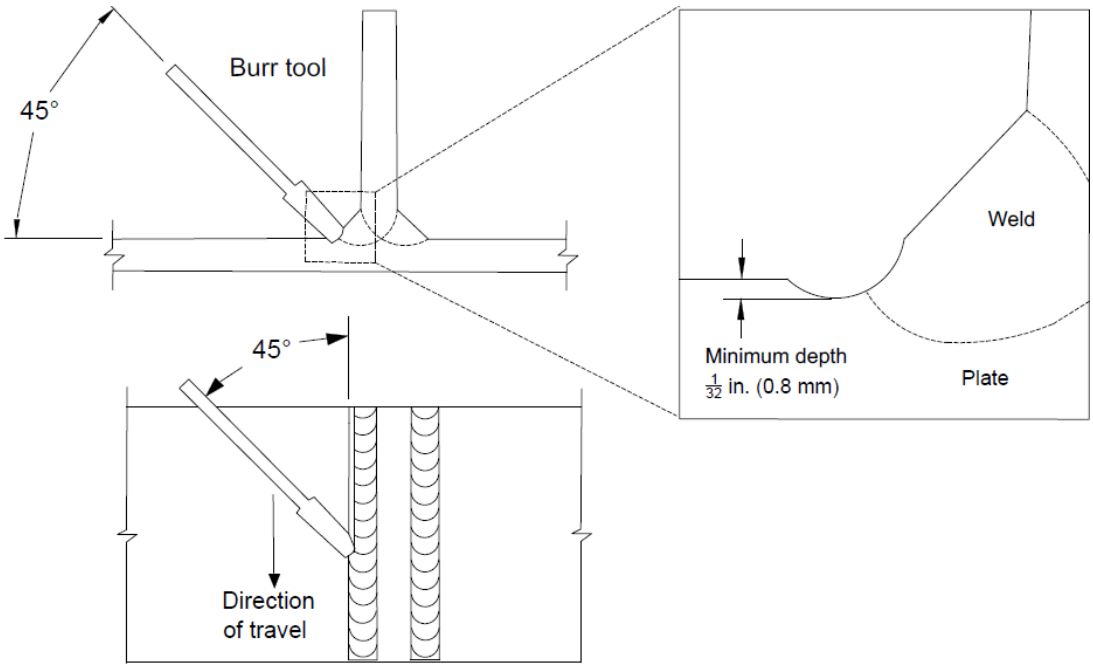

Figure 2-15. Position of the burr tip relative to material surface (Gregory et al. 1989)

Figure 2-16. Burr grinder and carbide burr tips (Dexter and Ocel 2013)

2.7.1.1.2 Gas Tungsten Arc (GTA) Remelting

GTA remelting helps reducing stress concentration at the weld toe. The GTA remelting is used for removing slag intrusions as well as to repair cracks up to approximately 3/16 in. deep (Dexter and Ocel 2013). During the process, a gas shielded tungsten electrode is moved along the weld toe at a steady speed in order to melt the targeted area of the weld without adding a new filler material. This retrofit technique requires highly skilled operators; hence, it is challenging and cost prohibitive to implement in the field.

2.7.1.2 Compressive Residual Stress Treatment

Impact treatment methods can be used to induce compressive residual stresses near a weld toe. Induced residual stresses are most effective when a weld toe is treated under dead load. Air hammer peening and ultrasonic impact treatment are the two methods that are currently used in the industry (Dexter and Ocel 2013).

2.7.1.2.1 Air Hammer Peening

In addition to treating weld toes, air hammer peening can be used to repair up to 1/8 in. deep surface cracks (Hausammann et al. 1983; Dexter and Ocel 2003). Figure 2-17 shows the positioning of the hammer for weld toe treatment and penetration depth range. Figure 2-18 shows a pneumatic hammer and a close-up view of the peening tip.

The recommended pressure for air hammer peening is 40 psi, and the number of passes is up to 6. The depth of penetration may range from 0.03 in. to 0.06 in. (Figure 2-17), where thinner sections may require less penetration. Light surface grinding to remove lap-type defects (that are introduced by the air hammer peening operation) is required for enhancing the performance of treated welds. Maintaining quality (or consistency of the depth of penetration), requires several passes to achieve the required penetration depth; while the noise produced by the hammer is one of a few concerns (Hacini et al. 2008).

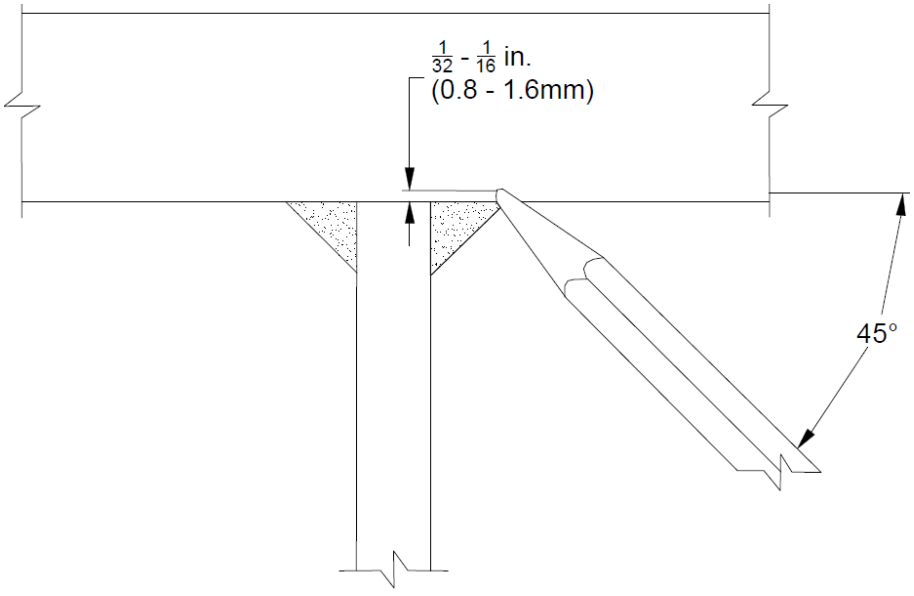

Figure 2-17. Hammer positioning and the depth of penetration (Hausammann et al. 1983)

(a) Pneumatic hammer/chisel

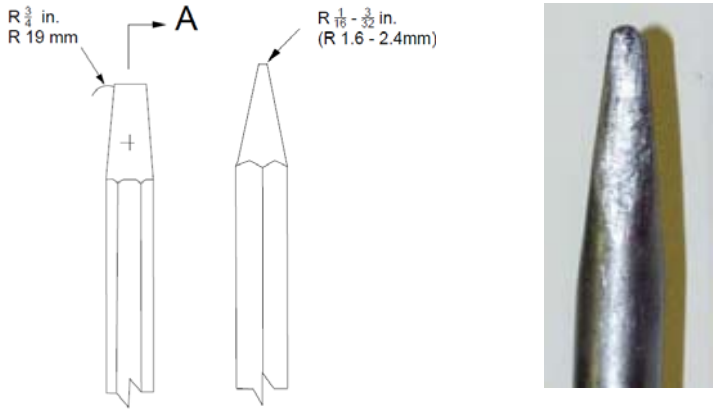

(b) Close-up view of the peening tip

Figure 2-18. (a) Pneumatic hammer/chisel and (b) close-up view of the peening tip (Hausammann et al. 1983)

2.7.1.2.2 Ultrasonic Impact Treatment (UIT)

Another method to induce compressive stresses by improving the weld toe profile is known as Ultrasonic Impact Treatment (UIT). It is commonly used as an alternative to hammer peening. According to several recent studies, this method is more effective, relatively quiet, and easier to handle (Fisher et al. 2001; Roy et al. 2003; GÜNTHER et al. 2005). Roy et al. (2003) show that the UIT can increase the fatigue strength of cover plate details and transverse stiffeners by at least one detail category. After compiling available test results, Yildirim and Marquis (2011) concluded that the welds treated with high frequency treatment methods (such as UIT) have slightly improved performance compared to the welds treated with traditional hammer peening. A detailed study conducted by Yekta et al. (2013) shows that the fatigue life of treated welds is improved regardless of under- or over-treating as per the current guidelines. The 2008 interim of AASHTO LRFD Construction Specifications (AASHTO 2008) section 11.9 included a detailed UIT procedure for weld toe treatment. UIT is a proprietary method; hence, it is prudent to follow manufacturer recommendations during special provisions development. Further, the UIT application will be more expensive compared to traditional methods, and may require a licensing agreement (Dexter and Ocel 2013).

Figure 2-19. UIT equipment (GÜNTHER et al. 2005)

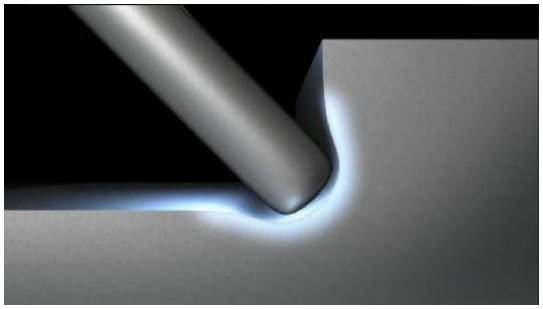

(a) Deformed shape of a treated surface

(b) Application at a weld

Figure 2-20. UIT (a) deformed shape of a treated surface and (b) application at a weld (Applied Ultrasonics 2014)

2.7.2 Repair of Through-Thickness Cracks

Through-thickness crack repair methods include hole drilling, cold expansion, vee-and-weld, post-tensioning and use of carbon fiber reinforced polymers.

2.7.2.1 Hole Drilling

The objective is to remove the sharp notch at a crack tip by placing a hole as shown in Figure 2-21; thus, it removes the stress concentration points. Effective implementation requires complete removal of a crack tip. The major challenge in successful implementation of this method is identifying the correct location of the crack tip prior to drilling (Li and Schultz 2005).

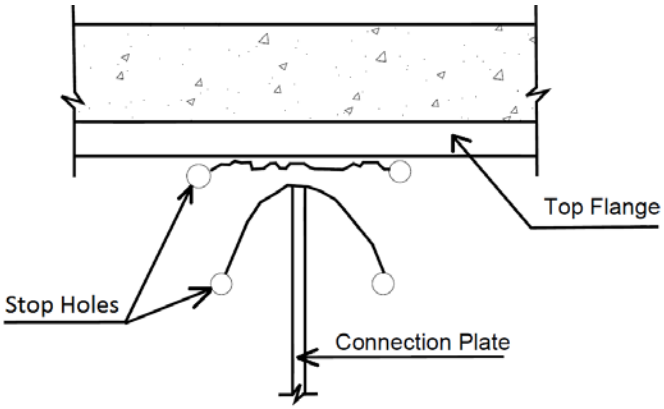

Figure 2-21. Crack arrest holes drilled at crack tips (Roddis et al. 2001)

Fisher et al. (1990) recommended the following equations for calculating crack-stop hole diameters (2ρ) using the stress intensity factor range (ΔK) and the yield strength (σ_y).

$$\frac{\Delta K}{\sqrt{\rho}} < 10.5\sqrt{\sigma_y} \qquad \text{(for } \sigma_y \text{ in MPa)} \qquad \text{(Eq. 1)}$$

$$\frac{\Delta K}{\sqrt{\rho}} < 4\sqrt{\sigma_y} \qquad \text{(for } \sigma_y \text{ in ksi)}$$

For certain details, Eq. 1 may yield a hole diameter less than 1 in. In such cases, Dexter and Ocel (2013) recommend increasing the diameter by 25%. However, according to Gregory et al. (1989) the hole diameter depends on the plate thickness (Table 2-13). Satisfactory performance of hole diameters ranging from of 2 to 4 in. (50.8 to 101.6 mm) has been recorded (Dexter and Ocel 2013). For a hole size ranging from 1 to 1.5 in., the performance can be improved by introducing compressive stresses around the crack stop hole. This can be accomplished by placing a fully-tensioned, high strength bolt with hardened washers on both sides (Figure 2-22). Bolts and nuts are also used for aesthetics purposes. However, the use of bolts and nuts might hinder the crack growth inspection using traditional methods. In such instances, acoustic emission (AE) technology can be an alternative for monitoring performance of the repair. When bolts and nuts are not used, plugging crack stop holes is also recommended to avoid fecal or nesting material left from birds as well as to avoid unwarranted public attention to perforated bridge details. It is advised to drill crack stop holes and never to flame-cut (Dexter and Ocel 2013).

As an alternative to using bolts and nuts, a tapered mandrel that is slightly larger than a crack stop hole diameter can be forced through to develop residual stresses around the hole. This process is known as the cold expansion of a drilled hole and will be discussed in section 2.7.2.2.

Table 2-13. Crack Stop Hole Diameter Recommendation Based on Plate Thickness (Gregory et al. 1989)

Plate Thickness (in.)	Hole Diameter (in.)
up to $\frac{3}{8}$	$\frac{5}{8}$
$> \frac{3}{8}$ - $\frac{3}{4}$	$\frac{3}{4}$
$> \frac{3}{4}$	$1\frac{3}{4}$

Figure 2-22. Drilled holes covered by bolts and nuts (Courtesy: Michigan DOT)

2.7.2.2 Cold Expansion

The standard procedure includes either pushing or pulling hardened components (e.g., mandrels, bearings, etc.,) through a drilled hole (Leon 1998). The procedure initiates with an expansion of an undersized hole generating a radial plastic flow of material that introduces residual compressive stresses around the hole (Ozelton and Coyle 1986; Adams 2010; Stefanescu et al. 2004). The induced compressive stresses retard crack initiation and growth. Cold expansion is used as a complement with hole drilling to undersize hole diameter when a sufficient diameter cannot be achieved due to space limitations (Adams 2010).

2.7.2.3 Vee-and-Weld

The objective is to remove the entire crack and provide continuity using a weld. The procedure is presented in Figure 2-23.

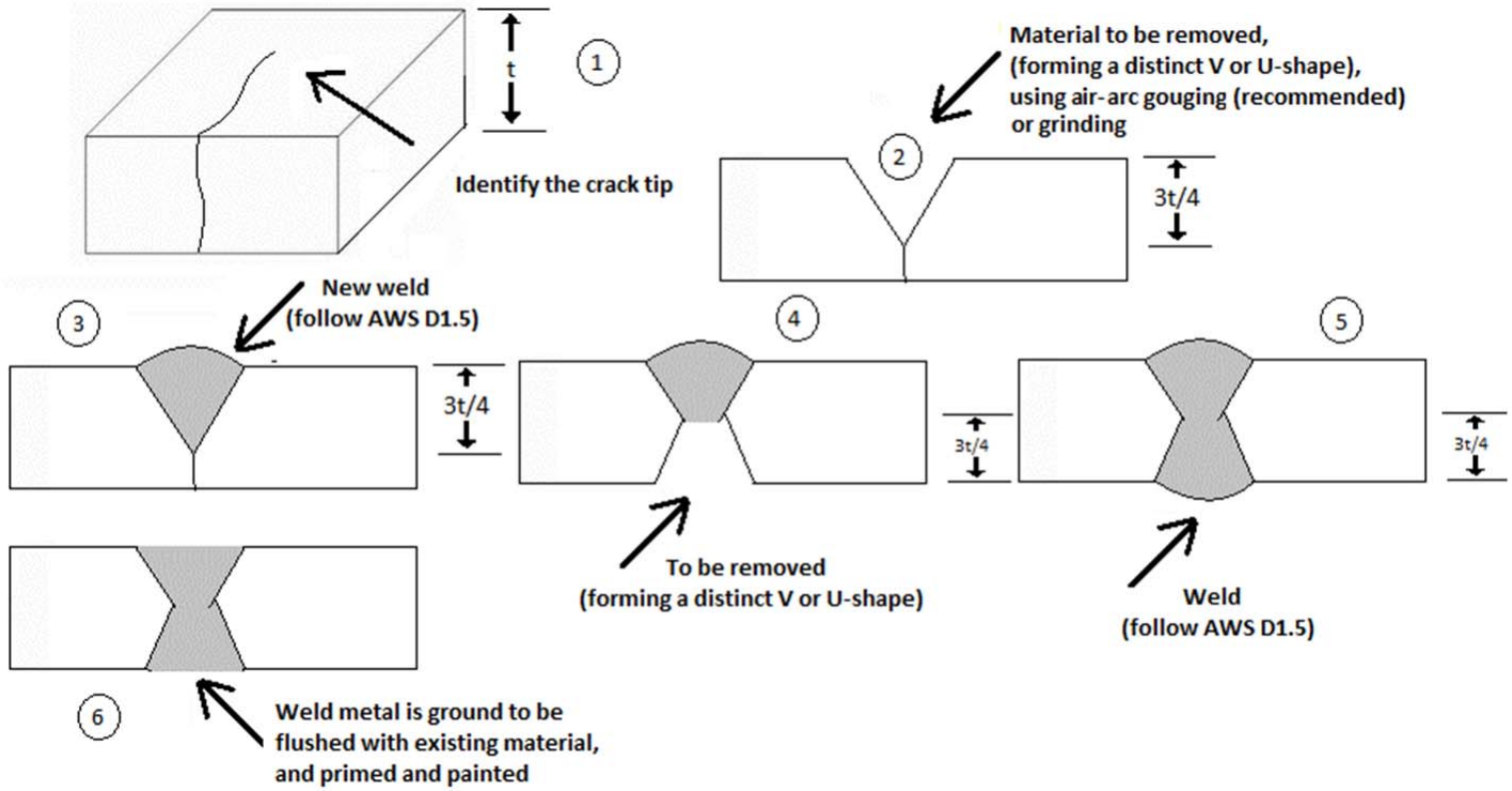

Figure 2-23. Vee-and-weld repair process

2.7.2.4 Post-tensioning

The objective is to keep the cracks closed while inducing compressive stress to abate fatigue crack growth. However, this method is not widely used and needs additional research.

2.7.2.5 Carbon Fiber Reinforced Polymer Application

The application of Carbon Fiber Reinforced Polymer (CFRP) patches for improving fatigue performance is new to the steel bridge industry (Bassetti et al. 2000). Research has shown that the CFRP patches can be used over existing cracks to reduce crack growth rate (Bassetti et al. 2000). The effectiveness of this retrofit method greatly depends on the quality and strength of the bond between patch and steel substrate. According to recent research, an adequate bond was developed by attaching the patch using a layer of epoxy with embedded breather cloth with a thickness of 1/8 in. (Alemdar et al. 2011). However, this method is not widely used and needs additional research.

2.7.3 Connection(s) or Global Structure Modification

The objective is to reduce the effective stress range in order to minimize the potential for fatigue cracking. This is achieved by adding doubler plates, smoothing out sharp corners, or modifying selected details such as diaphragm or cross-frame removal, diaphragm repositioning, and bolt loosening. A connection also can be modified by loosening the bolts. These modifications can decrease the stress ranges, but the connection or structural detail modification decision has to be well supported by structural analysis. Only the use of doubler/splice plates is discussed in this section. The other methods are discussed in section 2.7.4.

2.7.3.1 Adding Doubler/Splice Plates

The objective is to increase the cross-section in order to reduce stresses, provide continuity across a crack, or a combination thereof. It is often used as a complement to other repair methods to ensure adequate fatigue resistance to the stresses that contributed to the original cracking. Doublers can be attached by welding or using high-strength bolts. Use of bolted doublers, as shown in Figure 2-24, is recommended to enhance fatigue resistance. When the doublers are used to provide continuity across a crack, crack tips need to be removed by drilling holes – consider the information provided in section 2.7.2.1 on sizing a hole, protecting, and

monitoring performance. When welded doublers are used, a challenge often observed is to maintain the alignment of the cracked section before welding the plates. Another application of doublers is to restore the properties of a severely corroded section (Dexter and Ocel 2013).

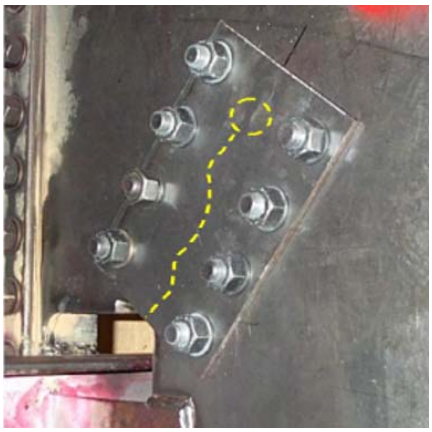

Figure 2-24. Bolted doubler plate retrofit (the dashed line and the circle represent a crack and a drilled hole to remove the crack tip) (Dexter and Ocel 2013)

2.7.4 Repair Methods to Eliminate Out-of-Plain Distortion

Out-of-plane distortion at web gaps has led to fatigue cracking in steel bridges. The web gap is the unstiffened portion between the girder flange and the end of the stiffener that is connected to a cross-frame or a beam-type diaphragm. Design codes and specifications provide assumptions and do not describe the real behavior of the bridge or its components. The secondary stresses that are developed within the web gap due to out-of-plane distortion are often not accounted for during analysis and design. These secondary stresses are the primary cause of fatigue cracking. Hole drilling, diaphragm or cross-frame removal, diaphragm repositioning, bolt loosening, and web gap stiffening are the documented approaches for repair or retrofit of details that are susceptible to fatigue due to out-of-plane distortion.

2.7.4.1 Hole Drilling

The objective is to remove the crack tip; thus to eliminate or lower the crack propagation potential. A detailed discussion on hole drilling is presented in section 2.7.2.1. In a straight bridge, hole drilling is sufficient when the following conditions are satisfied (Li and Schultz 2005; Fisher et al. 1990);

- In-plane bending stress < 6 ksi (42 MPa)
- Out-of-plane stress range < 15 ksi (105 MPa)

At certain details, even if the aforementioned criterion is met, drilled holes alone are inadequate to arrest crack propagation. Hence, other retrofit methods need to be implemented in conjunction with the crack stop holes (Dexter and Ocel 2013).

Cracks due to out-of-plane distortion initiate from the welds. However, quantifying stress range at the weld toe has been a challenge. Section 2.3.4 presents a detailed discussion as well recommendations for calculating weld toe stress range due to out-of-plane distortion.

2.7.4.2 Diaphragm or Cross-Frame Removal

The objective is to remove or minimize the out-of-plane bending stress. The decision to remove diaphragms or cross-frames needs to be supported by detailed analyses to evaluate girder capacities, adequacy of alternate load paths, structural redundancy, and girder stability under all applicable loads such as live, wind, temperature gradient, and potential constraints to bridge expansion and contraction under uniform thermal loads. In addition, the effects of member removal on lateral-torsional buckling of compression flanges, girder stability during deck replacement, the additional cost to provide temporary bracings, and load distribution during a high load hit need to be evaluated. Further, it is vital to maintain an accurate record of any modification to the original as-built details within the current bridge management system.

2.7.4.3 Diaphragm Repositioning

The objective is to increase the flexibility of the detail. Limited applications of this approach are documented in literature. The diaphragm repositioning design needs to be adequately supported by detailed analyses. Any modification to the original as-built details needs to be accurately documented within the current bridge management system.

2.7.4.4 Bolt Loosening

Bolt loosening is a retrofit method that can be implemented as a stand-alone method or in conjunction with other methods. It is performed on the bolts that connect the bracing elements to the connection plates in the negative moment area. The method has been implemented on bridges with I-beam diaphragms, channel-type diaphragms, X-type cross-frames, and K-type cross-frames. The implementation records indicate a reduction of strain in or around the web gap by approximately 30-80% (Dexter and Ocel 2013; Tarries et al. 2002; Wipf et al. 2003).

However, the results depend on the bracing configuration, the number of loosened bolts, and the degree of restraint provided by each bolt. Hence, the decision needs to be supported by detailed analyses. A few recommendations are as follows:

- Evaluate bridge structural stability. When needed, provide bracings to prevent lateral torsional buckling (Tarries et al. 2002).
- Loosen the bolts sequentially until the desired strain reduction is obtained (Dexter and Ocel 2013).
- Consider lateral load distribution (Tarries et al. 2002).
- Secure bolts in place using lock nuts or double nuts to prevent from fall out due to vibration (Tarries et al. 2002; Dexter and Ocel 2013).

As documented in Dexter and Ocel (2013), the relative displacement between a girder flange and a connecting plate is small and ranges between 0.001 - 0.03 in. The bolt or rivet holes can be drilled to a size larger than the fasteners to be inserted in order to provide adequate flexibility to the web gap region; thus, leading to lower stresses.

2.7.4.5 Web-Gap Stiffening

The objective is to minimize the relative displacement between the connection plate and the girder flange in order to lower the secondary stresses due to out-of-plane distortion. Web-gap stiffening retrofit uses positive attachments (plates, angles or tee sections) connected by welds, bolts, a combination of welds and bolts (i.e., hybrid connection), adhesives or nails.

2.7.4.5.1 Welded Attachment

Connection plates that are welded to the top and bottom flanges are used to stop out-of-plane distortion between the girder flange and connection plate. The AASHTO LRFD section 6.6.1.3.1 recommends providing transverse welds on both the tension and compression flanges to mitigate out-of-plane distortion (AASHTO LRFD 2013). However, fatigue cracks have been developed at the new field welds leading to greater challenges in preventing fatigue cracks. This is mainly due to the challenges associated with maintaining weld quality in the field while providing an overhead weld at the plate to the top flange connection. The additional challenges to maintain field weld quality as well as to execute this retrofit method are listed below:

- High-strength steel is difficult to weld. If the girder flanges are made from A514 or T1 steel, welding is a challenge and this retrofit approach is undesirable.
- When the web gap is at the top girder flange that is embedded in a concrete deck, this retrofit method is undesirable because the concrete deck works as a heat sink making it difficult to maintain the proper preheat and interpass temperatures.
- Due to impact of live traffic on weld integrity, especially at the root, closure of lanes over and adjacent to the girder for root pass must be considered.
- The effect of heating girder flanges that are carrying deck dead load needs to be evaluated.

A few recommendations related to this retrofit method are listed below:

- Remove all contaminants and paint from the area before welding.
- If the dead load is considerably large, temporary shoring is needed to maintain bridge stability with the soften girder flanges under high temperatures.
- Welds need to be designed as per the current specifications. Also, the interaction of new welds with the existing welds needs to be avoided.
- Welds should have the same length as the length of the plate-flange connection. However, the weld should not wrap around the connection plate, nor intersect the longitudinal flange-web weld.
- In the case where there is a slide gap between the connection plate and flange, additional plates or spaces will be needed. The width of the spacer block should not be wider than 1.5 in. (38.1 mm).

2.7.4.5.2 Bolted Connection

Angles or tee sections are used for bolted connections between girder flanges and connection plates. This method is only applicable if the net section fracture does not control the strength of the member (Dexter and Ocel 2013). A bolted connection does not provide the same stiffness as a welded connection. The following minimum requirements must be met when bolted connections are established:

- A total of four bolts must be utilized across the flange when connecting angles or tee sections. Bolts need to be placed in two rows and two columns. The minimum thickness of the angles or tees needs to be 0.75 in. (19.1 mm).

- Tees need to be rolled sections because built-up sections have a tendency to crack.
- The haunch or a portion of the deck needs to be removed for bolting tees or angles to the flange when it is embedded into a concrete deck.
- Partial deck removal requires maintenance of traffic. Use of tapped holes into the girder flange is an option to prevent traffic disruption. However, it is recommended to give at least 1 in. embedment length to the bolt or stud in a tapped hole. Hence, this is only possible in girders with a thick flange.

2.7.4.5.3 Hybrid Connection

Hybrid connection, as the name implies, utilizes both welding and bolting to establish the connection. It includes bolting a thick plate to the girder flange and welding the connection plate to the already bolted thick plate (Figure 2-25). The plate must be bolted as specified in section 2.7.4.5.2 and have a minimum thickness of 0.875 in. (22.2 mm). The connection plate welding to the thick plate needs to be performed as specified in section 2.7.4.5.1.

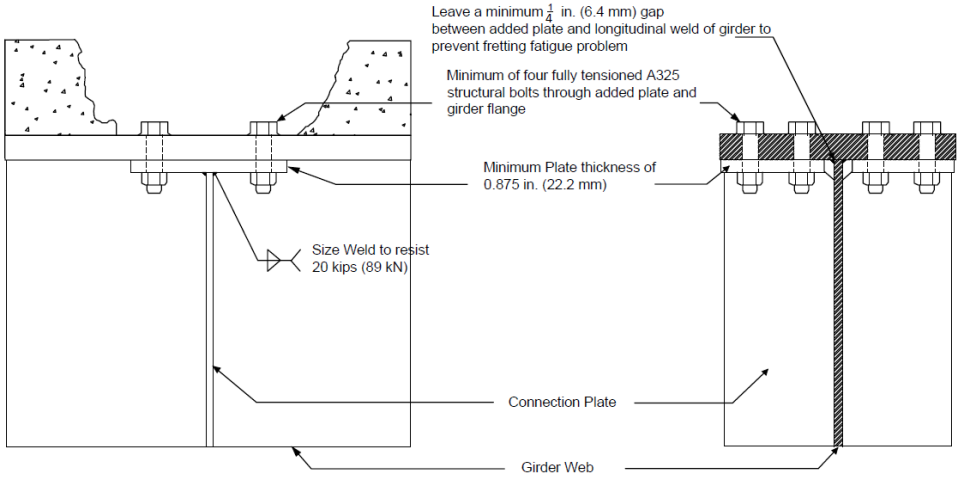

Figure 2-25. A typical hybrid connection detail (Dexter and Ocel 2013)

2.7.4.5.4 Adhesives

The use of adhesives is an option when partial deck removal or access to haunch is limited. Use of adhesives is currently at the experimental level. Hence, this method is not recommended as a long-term solution. Service life of an adhesive connection may be adequate for a year (Dexter and Ocel 2013). This method can be implemented as a temporary fix for a bridge with a deteriorated deck which is already in a program to be replaced. The adhesives used in such applications need to be suitable for field application, compatible with the substrate, and durable

under the specific exposure conditions. Further, small bolts can be used to prevent the angles or tees falling onto traffic, and also to hold the angles or tees at the final position until the adhesives are hardened (See Figure 2-26).

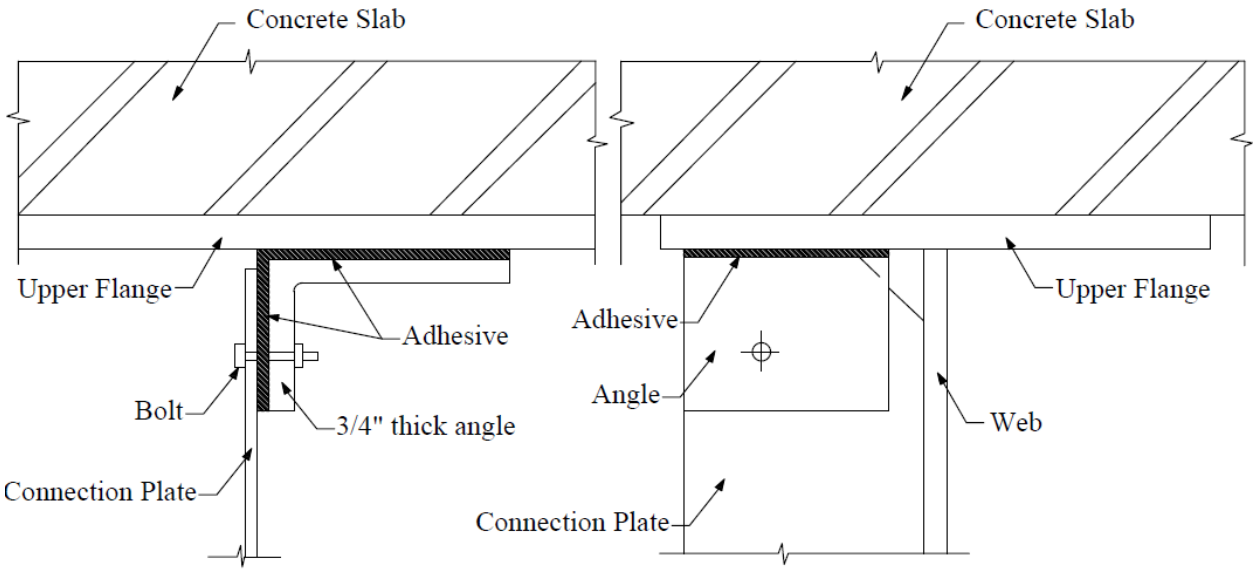

Figure 2-26. Proposed retrofit scheme with adhesives (Hu et al. 2006)

2.7.4.5.5 Nails

Use of nailed connections is also a new retrofit technique that requires additional investigations. The use of nails for this purpose has been experimentally tested, but not to failure (Dexter and Ocel 2013). It can be performed under traffic and does not require deck concrete removal. Further, this technique allows developing permanent connections. However, the use of nails with tee connections is recommended, but not with angles because of a possible misalignment on the opposite side (Dexter and Ocel 2013).

2.7.4.6 Web-Gap Softening

The objective is to increase flexibility at the web gap. This retrofit method includes removal of a connection plate section (which is stated in literature as gross material removal) or drilling large diameter holes.

2.7.4.6.1 Gross Material Removal

The process involves removal of a portion of the connection plate by flame cutting or any other means to increase web gap in order to reduce secondary stresses. All residual weld material from the girder web must be removed, ground smooth, and painted. It is recommended to limit

the new web gap dimension to the smallest of 15 in. or 1/6th of the web depth. A limited number of applications, with inconsistent performance records, are documented in literature.

2.7.4.6.2 Large Hole Retrofit

This method includes drilling large diameter holes close to the web-gap area. The diameter equal to or greater than 3 in. (76 mm) is defined as a large hole. An example is shown in Figure 2-27. A few implementation examples are documented in literature. The effect of such a retrofit method on secondary stress reduction needs to be evaluated through refined analysis before implementation.

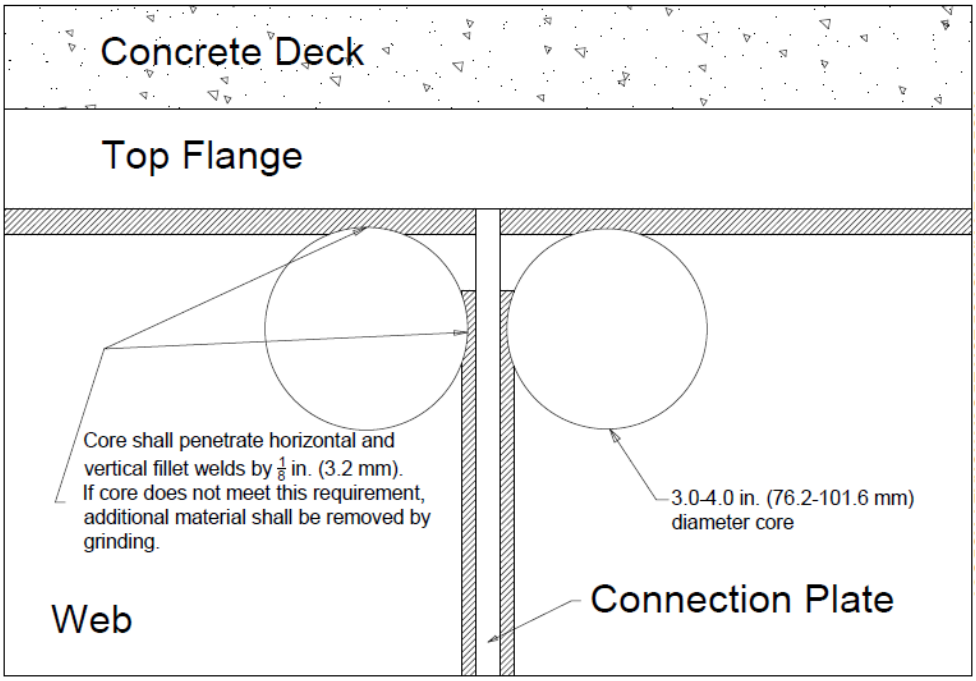

Figure 2-27. A large hole retrofit example (Dexter and Ocel 2013)

2.8 SUMMARY

To develop a successful program for monitoring the fatigue-sensitive detail, it is required to (i) accurately identify the fatigue-sensitive details, (ii) establish monitoring objectives, (iii) select technology suitable for achieving the monitoring objectives, and (iv) decide on the level and the monitoring duration. This chapter presents the fatigue-sensitive detail categories, methodologies to establish the needs for monitoring fatigue-sensitive details, technology for monitoring the fatigue-sensitive detail, and technology implementation considerations. A good understanding of the retrofit methods for fatigue-sensitive details is required to develop an appropriate monitoring

program for evaluating the effectiveness of the retrofits. Hence, retrofit methods for fatigue-sensitive details are also presented in this chapter.

An acoustic emission (AE) monitoring system with strain gages was recommended as one of the most effective technology for monitoring fatigue-sensitive details. AE has been successfully implemented in the field and evaluated for continuous monitoring of fatigue-sensitive details. At this time, AE is the only technology that is capable of real-time monitoring of fatigue events and providing data for damage location detection. In addition to the AE sensors, strain gauges are required to evaluate the stress state to calculate remaining fatigue life. Strain data is also needed to support AE data analysis by developing the load matrix.

This chapter presents a cluster analysis approach for developing a monitoring program for bridges with fatigue-sensitive details. Fatigue-sensitive details can be identified using the detail categories presented in the AASHTO LRFD Bridge Design Specifications (2013) Table 6.6.1.2.3-1 or through a combined effort of utilizing information in bridge files, refined analysis, and experience. The weld toe stresses are calculated using the hot spot stress (HSS) method. Structural modeling and HSS calculation guidelines are presented in this chapter to help evaluating the fatigue-sensitive welded details. Finally, the technology implementation considerations such as level of monitoring, duration of monitoring, and inspection frequency are presented.

3 STRUCTURAL MODELING AND HOT SPOT STRESS ANALYSIS

3.1 OVERVIEW

The scope of the work documented in this chapter includes selecting a bridge with fatigue-sensitive details, documenting as-built details to develop analysis models, evaluating the structural behavior and girder and diaphragm deformation under specific loads and load patterns, and selecting details for instrumentation and monitoring.

The bridge selected for this study contained partial depth diaphragms with welded details. Hot spot stresses were calculated in order to identify the critical details for monitoring. Hot spot stress calculation requires selecting appropriate element types, mesh parameters, and reference points for stress calculation. Therefore, this chapter presents information on (a) element types and mesh parameters for hot spot stress calculation, and (b) bridge structural analysis for identification of details for instrumentation and monitoring.

3.2 BRIDGE LOCATION AND DETAILS

The bridge (S16 of 11015) is located in Stevensville, Michigan, and carries I-94 over Puetz Road (Figure 3-1). The bridge was built in 1961. In 1997, MDOT performed girder end retrofits. There are two parallel bridges to carry westbound (WB) and eastbound (EB) traffic on I-94. After reviewing MDOT biennial inspection reports and conducting a field visit to document the bridge superstructure and substructure condition, the I-94 EB bridge was selected. The longest span (span 3) of the EB Bridge is 56 ft - 6 in. and has a 54.5^{o} skew (Figure 3-2). The span is supported on an integral abutment and a pier with expansion bearings (Figure 3-3). The superstructure consists of 12 steel I-girders (10-W30×108 and 2-W30×99) and a 9 in. thick cast-in-place concrete deck. The girders are connected transversely using intermediate and end diaphragms (Figure 3-4). The partial depth diaphragm connection detail is classified as a category C' fatigue-sensitive detail (AASHTO LRFD 2013). As shown in Figure 3-3, partial length welded cover plates are attached to girder bottom flanges. This detail is classified as a category E fatigue-sensitive detail because the girder flange width is less than 0.8 in. (AASHTO LRFD 2013).

The bridge has been designed following the 1958 Edition of the Specifications for Design of Highway Bridges, Michigan State Highway Department (MDOT 1958). This is several years earlier than the first fatigue design provisions of the AASHTO Standard Specifications for Highway Bridges appeared; that is in 1965. At that time, details were not specifically designed for fatigue. However, Article 8.02h of MDOT (1958), acknowledges developing alternating stress due to the combined effect of dead, live, impact, and centrifugal stresses. In order to accommodate the effect of cyclic nature of stresses, the specifications states "*If alternating stresses occur in succession during one passage of the live load, each shall be increased by 50% of the smaller*."

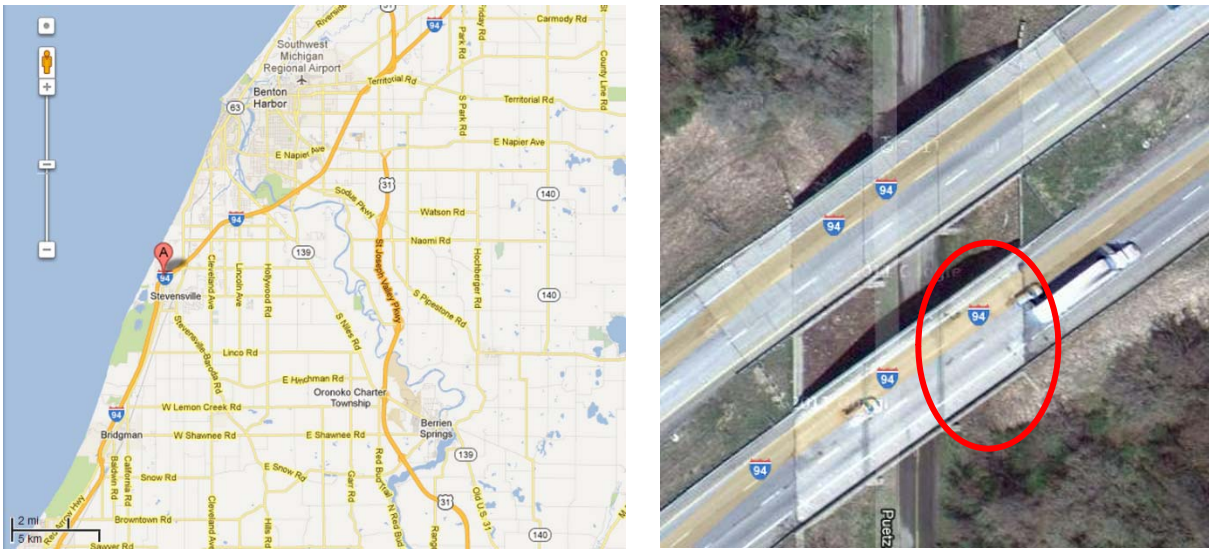

(a) (b)

Figure 3-1. (a) Bridge location and (b) aerial view of the EB and WB bridges (Google)

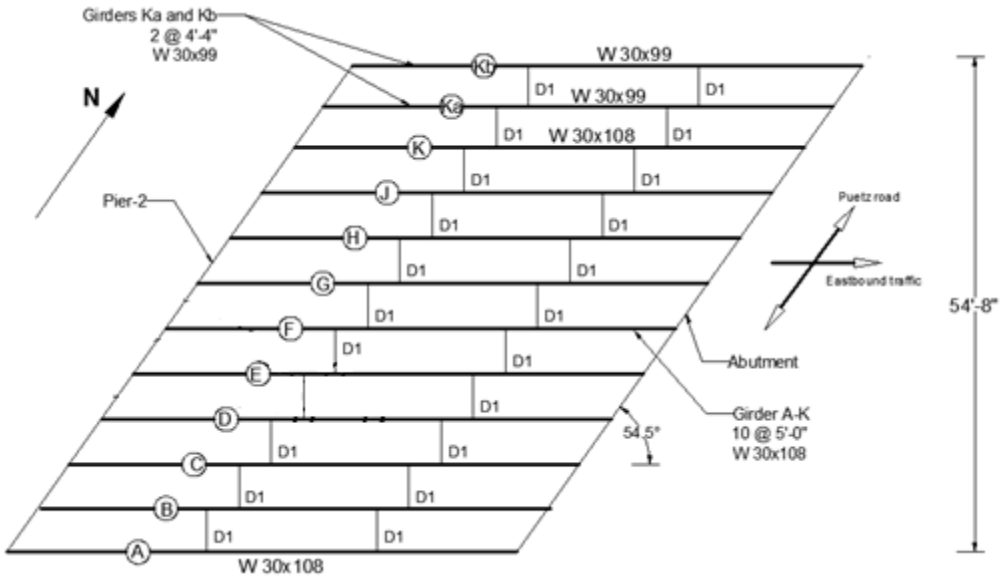

Figure 3-2. Girder and diaphragm layout of the EB bridge span 3

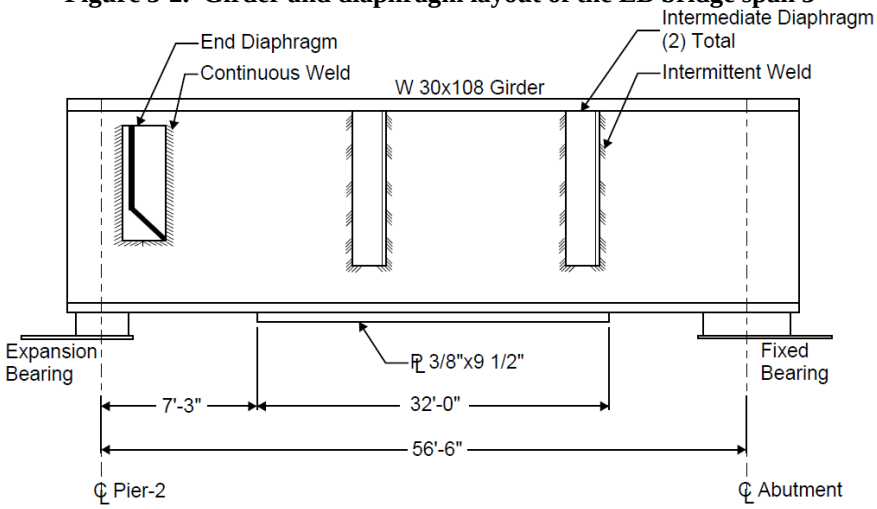

Figure 3-3. Typical girder elevation showing the partial depth diaphragms

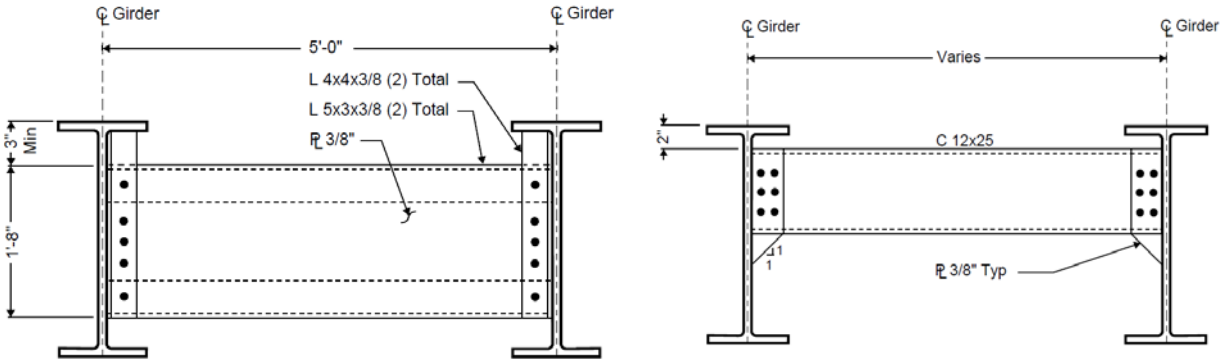

(a) Intermediate diaphragm (D1) (b) End diaphragm (D2)

Figure 3-4. Typical diaphragm detail

3.3 SITE SELECTION

This I-94 EB bridge was selected for structural health monitoring (SHM) system installation. In addition to having fatigue-sensitive details and staggered diaphragms, the other reasons for selecting the bridge include heavy truck traffic and easy access to the bridge for instrumentation and system maintenance. Since the primary objective of this research project is to evaluate technology for fatigue-sensitive detail monitoring, and this is the first time such a monitoring system is implemented in Michigan and powered by solar panels, bridge access was a major consideration when selecting the bridge.

3.4 AS-BUILT DETAIL DOCUMENTATION

The EB and WB bridges were labeled as *South Bridge* and *North Bridge*, respectively. After reviewing maintenance records, *span 3* of the I-94 EB bridge was selected for documentation of as-built details and in-service condition using Leica C-10 laser scanner. Figure 3-5 shows an aerial view and a snap shot of *span 3*. Visual inspection was performed, and digital images were also taken. The information collected through visual inspection and digital images was necessary for the reverse engineering process of the bridge details. Figure 3-6 shows the reverse engineered model.

(a) Aerial view of I-94 over Puetz Road in Stevensville, Michigan

(b) Span 3 of I-94 EB over Puetz Road

Figure 3-5. (a) Aerial view and (b) span 3 of the I-94 EB bridge

(a) Digital image

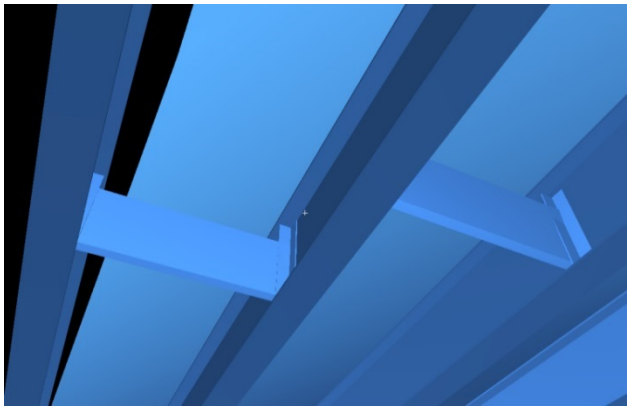

(b) Modeled geometry

Figure 3-6. Girders and intermediate diaphragms

3.4.1 Comparison of As-Built and As-Designed Details

One of the primary objectives of this work was to compare the as-built details with the as-built plan dimensions. The girder and diaphragm spacing were calculated from the modeled bridge geometry and compared to the plan dimensions. Also, web gap dimensions were calculated from the model.

3.4.1.1 Girder Spacing

The bridge was originally constructed with only 10 girders at 5 ft spacing and was later widened by adding two girders with a spacing of 4 ft 4 in. (Figure 3-2). Using the scanned geometry and *Measurement* tool in *Cyclone*, as-built spacing of the girders was calculated. Table 3-1 lists the as-designed and as-built spacing dimensions. As shown in Table 3-1, girder spacing matches with as-designed spacing except at one location where a maximum of 0.6 in. deviation was observed.

Table 3-1. As-Designed and As-Built Girder Spacing

Girder Spacing	As-Design Spacing (ft:in)	As-Built Spacing (ft:in)
G1	4 ft 4 in	4 ft 3.8 in
G2	4 ft 4 in	4 ft 4.0 in
G3	5 ft 0 in	4 ft 11.9 in
G4	5 ft 0 in	4 ft 11.9 in
G5	5 ft 0 in	4 ft 11.8 in
G6	5 ft 0 in	4 ft 11.6 in
G7	5 ft 0 in	4 ft 11.9 in
G8	5 ft 0 in	4 ft 11.8 in
G9	5 ft 0 in	5 ft 0.0 in
G10	5 ft 0 in	5 ft 0.1 in
G11	5 ft 0 in	4 ft 11.4 in

3.4.1.2 Intermediate Diaphragm Spacing

The intermediate diaphragm spacing calculated from the model was 18 ft 3.8 in. (Figure 3-7). The diaphragm spacing from the design plans were not specified, but the plans stated that the diaphragm spacing is $^1/_3$ the span length. The span was given as 55 ft $4^5/_8$ in., which gives a diaphragm spacing of 18 ft. 5.5 in. Hence, the difference between as-designed and as-built diaphragm spacing is 1.7 in.

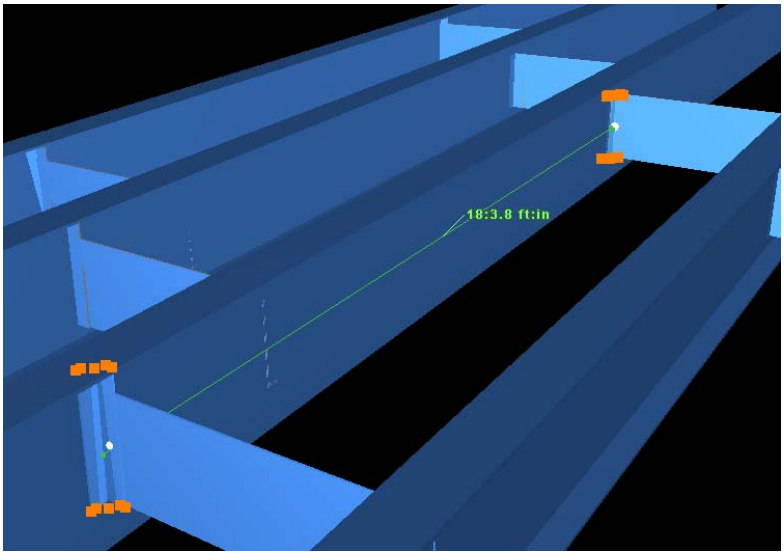

Figure 3-7. Diaphragm spacing calculated from the model

3.4.1.3 Diaphragm Elevation

As per the bridge plans, diaphragms were supposed to be located at a minimum of 3 in. below the girder top flange (Figure 3-8a). Knowing exact dimensions at the web gaps is important for structural modeling and analysis. Hence, the diaphragm elevations, with respect to the bottom surface of girder bottom flange, were measured. As shown in Figure 3-8c, the diaphragm is located 2.5 in. and 4.1 in. from girder 6 and 7 bottom surfaces, respectively. The bottom flange thickness of girders A to K (W30×108) is 0.76 in. In addition, these girders have 3/8 in. cover plates. Hence, the web gap was calculated by subtracting 1.135 in. from the distances calculated using the point cloud data (Table 3-2). Girders K_a and K_b are W30×99. Hence, appropriate flange thicknesses and cover plate thicknesses were considered in calculating the web gap.

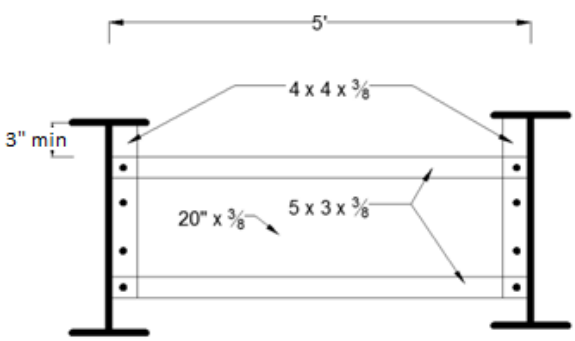

(a) Intermediate Diaphragm Detail

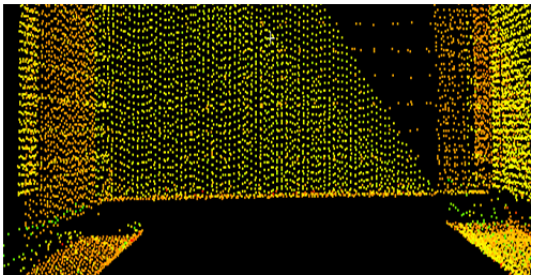

(b)) Intermediate diaphragm point cloud

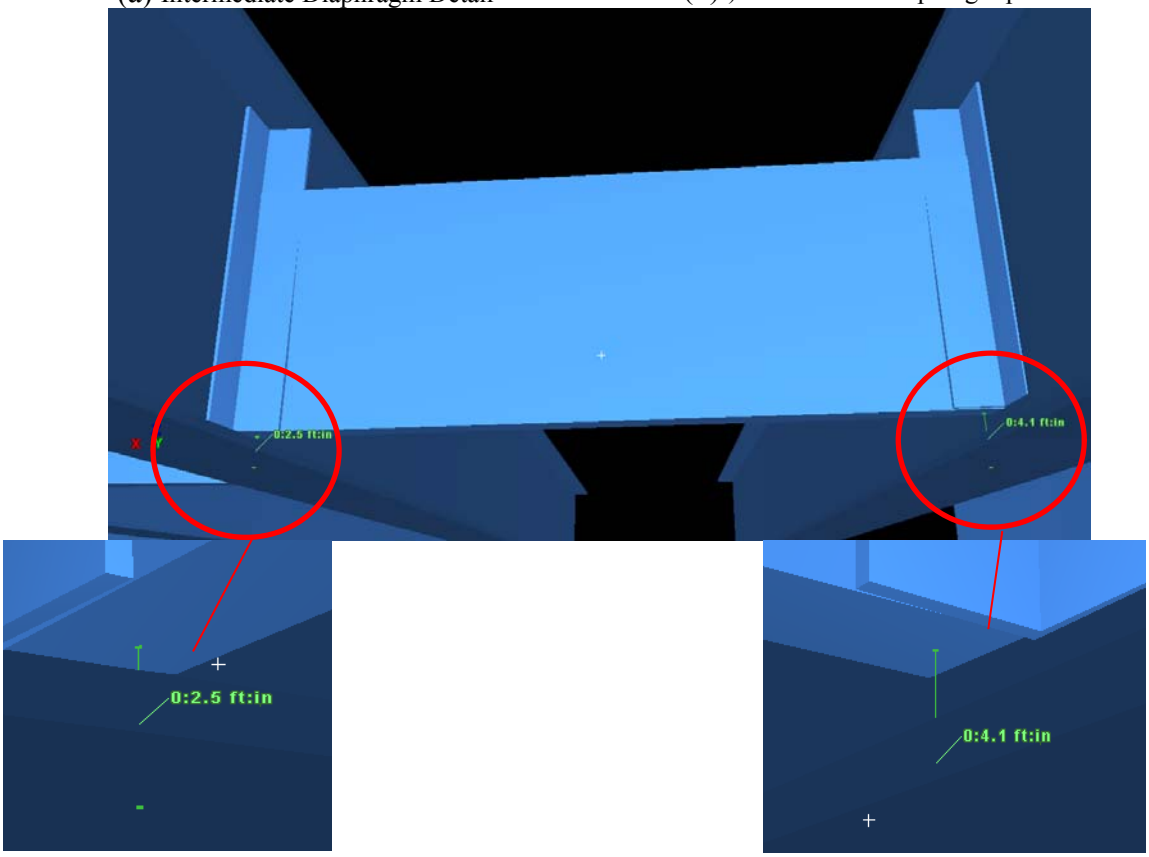

(c) Diaphragm elevation measured from girder bottom flange

Figure 3-8. Intermediate diaphragm detail and elevations at girder F and G

Table 3-2. Web Gap Dimensions

Diaphragm	Girder	Web gap (in.)	
		Diaphragm closer to the abutment	Diaphragm closer to the pier
1	A	3.065	3.765
	B	1.065	1.865
2	B	3.065	3.765
	C	0.565	1.165
3	C	3.065	3.665
	D	0.465	1.265
4	D	3.165	3.765
	E	0.465	1.665
5	E	3.065	3.665
	F	1.165	1.165
6	F	2.965	3.565
	G	1.365	2.065
7	G	3.265	3.565
	H	2.065	2.765
8	H	2.865	3.465
	J	2.665	3.165
9	J	3.165	3.465
	K	2.665	3.265
10	K	2.865	3.465
	K_a	3.290	3.490
11	K_a	3.390	3.090
	K_b	3.390	3.490

3.5 ELEMENT TYPES AND MESH PARAMETERS FOR HOT SPOT STRESS CALCULATION

Section 2.3.4 presents finite element modeling guidelines and hot spot stress calculation methods. This section details the evaluation process and results of those guidelines as well as the recommendations for modeling, analysis, and results interpretation with regards to hot spot stress calculation.

Lee et al. (2010) used two specimens to perform tension and flexural tests. Bhargava (2010) also performed a tension test evaluating various parameters such as weld geometries and longitudinal length of gusset plates. The specimen geometry, loading, boundary conditions, and experimental results presented in Lee et al. (2010) were used to evaluate the guidelines and recommendations given in literature for FE modeling, analysis, and calculation of HSS at a weld toe. In this evaluation, Abaqus CAE was used as the pre- and post-processor while Abaqus standard was the FE solver. 3D FE models of both specimens were developed using solid elements.

Figure 3-9 shows the specimen geometry. Both specimens represent two welded plates. The Type 2 detail represents a typical partial depth diaphragm. Plates were made from ship structural steel grade A with a modulus of elasticity of 29,000 ksi (200 GPa) and Poisson's ratio of 0.3. Plate thickness is 0.4 in. (10 mm). A forty five (45) degree fillet weld with a leg length of 0.2 in. (5 mm) is used in the model. Plate length and width are 11.8 in. (300 mm) and 2.8 in. (70 mm), respectively. Specimen grip width is 3.5 in. (90 mm). Plate height is 2 in. (50 mm). Figure 3-10 shows the loading and boundary conditions. Figure 3-10a and b show the boundary conditions and loads applied on specimen types 1 and 2 during the tension test. Figure 3-10c and d show the boundary conditions and loads applied on specimen types 1 and 2 during flexure test.

Specimens with fine and coarse meshes were used. Lee et al. (2010) used an element size of 0.5t as a fine mesh and *t* as a coarse mesh; where *t* is the plate thickness. According to Hobbacher (2008), 0.4t is considered as a fine mesh while 0.5t and larger are considered as coarse meshes. As stated in Section 2.3.4, FE analysis results are sensitive to element types and mesh discretization within regions of high strain gradient. Element type and mesh recommendations in Lee et al. (2010) and Bhargava (2010) were evaluated because these two references encompass most of the recommendations given in literature for HSS analysis (refer to Table 2-3 in chapter 2).

Lee et al. (2010) suggested element types of C3D8 and C3D20 (Abaqus 2014) and mesh configurations with 0.5(t×t) and t×t element sizes. Following the recommendations by Bhargava (2010), C3D20R was also used with an element size of (t×t). Linear and quadratic extrapolation techniques were utilized following the guidelines for the Type A HSS method presented in Table 2-2. The maximum principal stress was probed from nodes at exact reference points. The maximum principal stress contours and deformed shapes of the specimen type 1 and 2 are shown in Figure 3-11a-d.

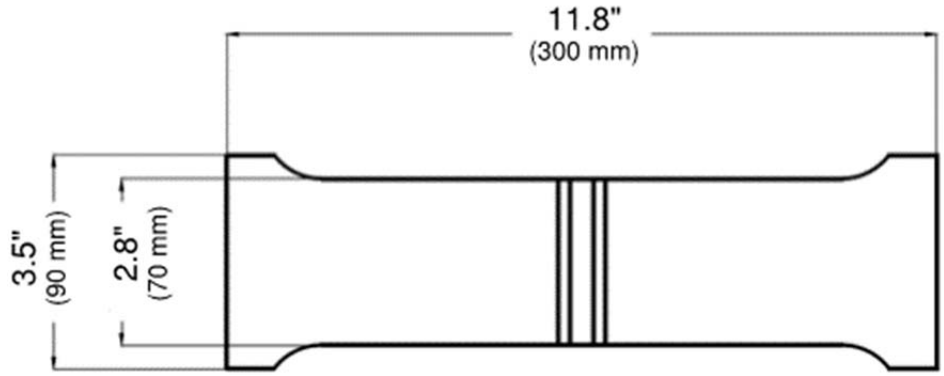

(a) Type 1 specimen - plan

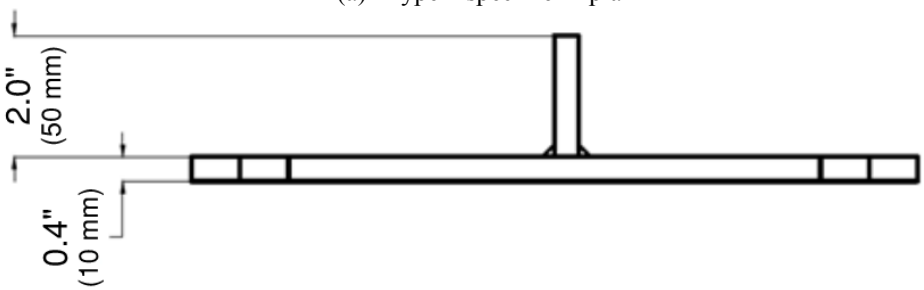

(b) Type 1 specimen - elevation

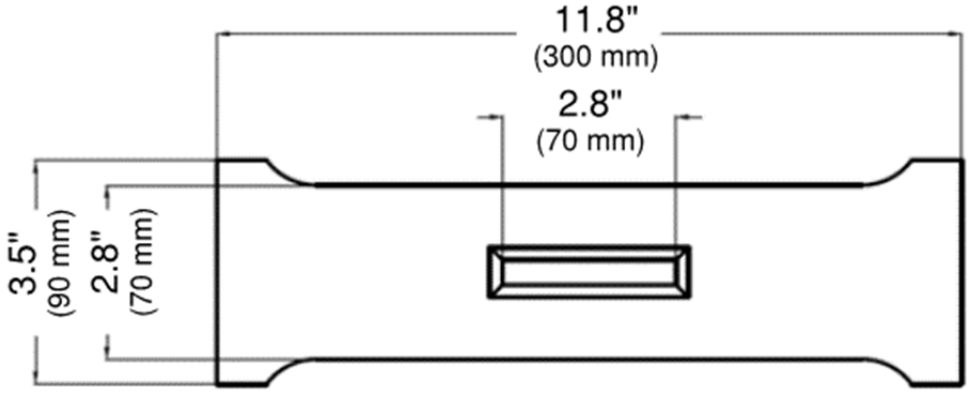

(c) Type 2 specimen - plan

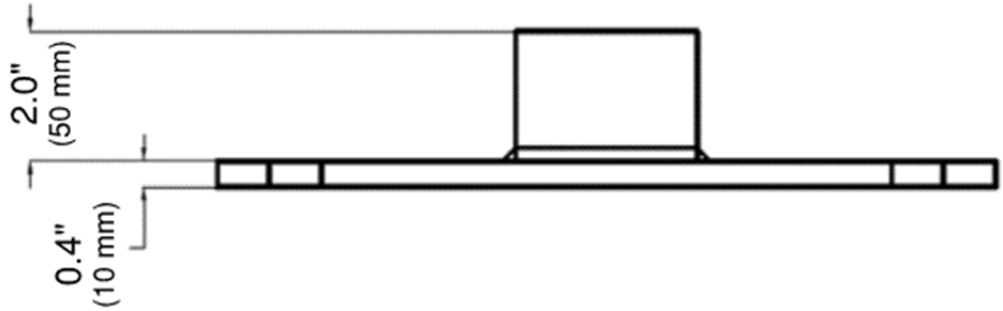

(d) Type 2 specimen - elevation

Figure 3-9. Specimen 1 and 2 geometry

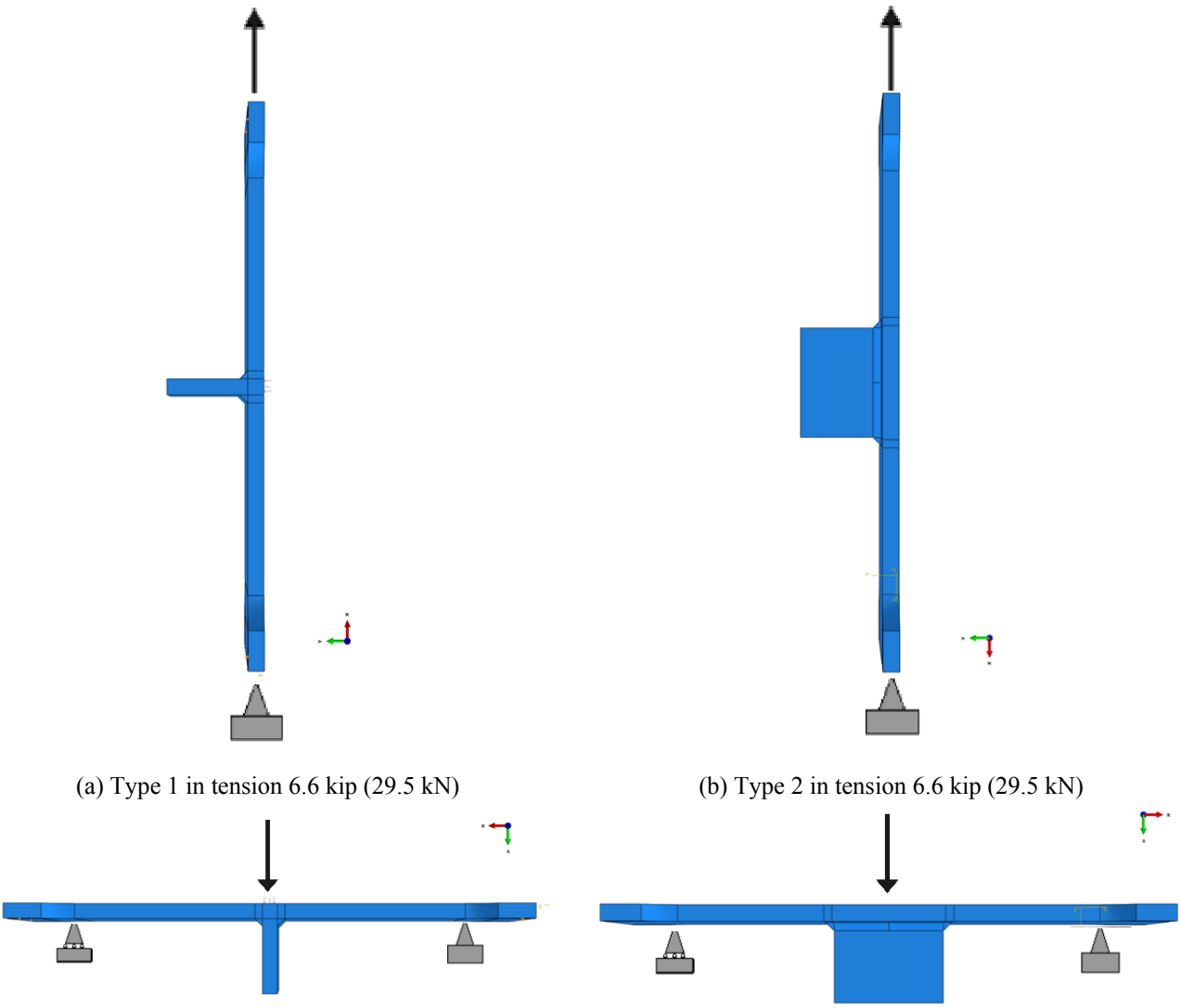

(a) Type 1 in tension 6.6 kip (29.5 kN)

(b) Type 2 in tension 6.6 kip (29.5 kN)

(c) Type 1 in flexure 1.54 kip (6.86 kN)

(d) Type 2 in flexure 1.54 kip (6.86 kN)

Figure 3-10. Specimen loading and boundary conditions

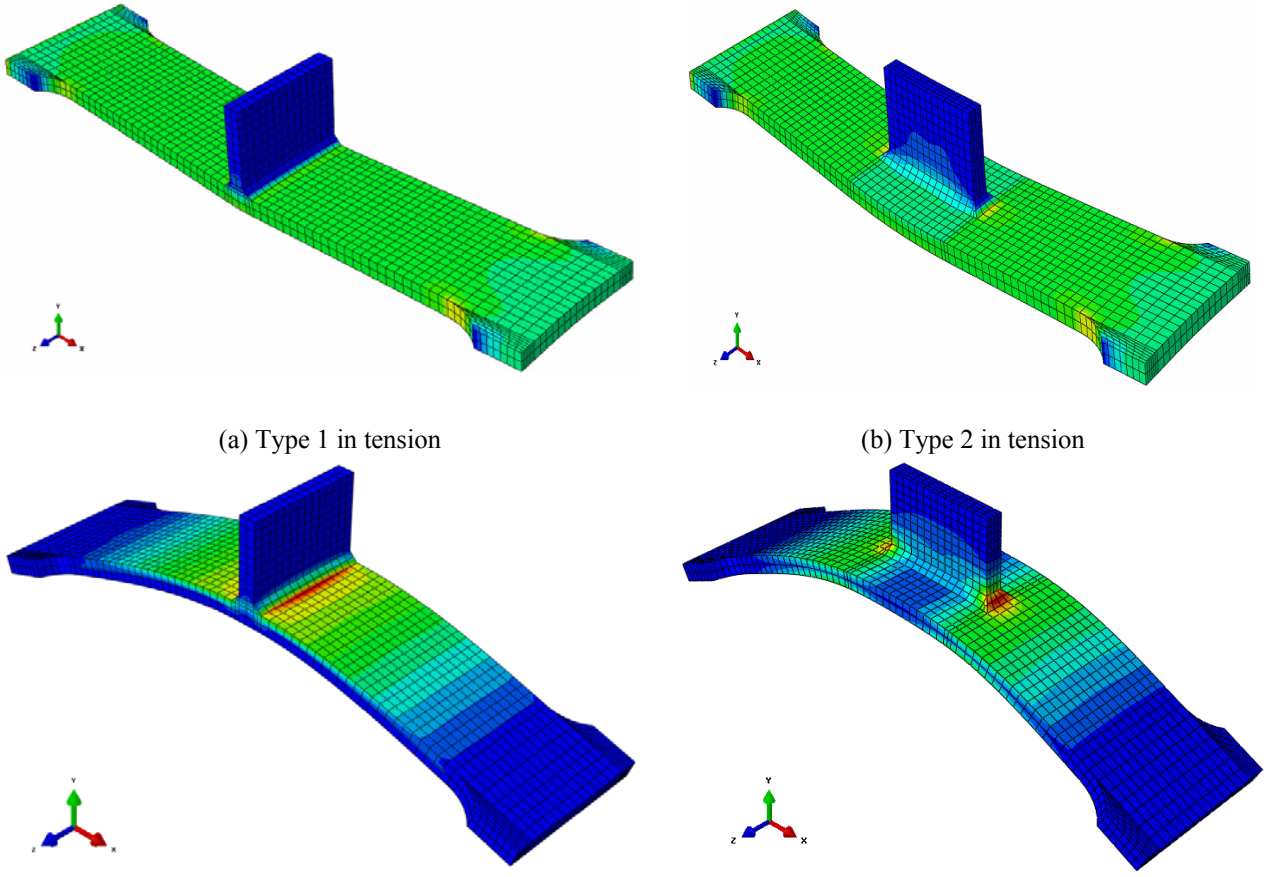

(a) Type 1 in tension

(b) Type 2 in tension

(c) Type 1 flexure

(d) Type 2 flexure

Figure 3-11. The maximum principal stress contours under tension and flexure

Hot spot stress (HSS) calculated from FE analysis was compared with experimental and other published results in literature (Table 3-3). The first column of the table specifies the specimen type. Column 2 presents FE model parameters such as mesh (F-fine or C-coarse), nodes per element, and element size as a fraction of plate thickness (*t*). The next two columns include HSS calculated using linear and quadratic equations presented in Hobbacher (2008) (Refer to Table 2-2 for details.) as well as the experimental results documented in Lee et al. (2010). The last column shows percentage difference between experimental and FE analysis results. The comparison was made using only the linear extrapolation results because the quadratic extrapolation results of experimental data were not available in Lee et al. (2010).

Bhargava (2010) recommended FE modeling, analysis, and results interpretation guidelines based on experimental and finite element analysis results of specimens that were subjected to axial tension. These recommendations were evaluated using the specimen geometry, loads,

boundary conditions, and the experimental results presented in Lee et al. (2010). Table 3-4 presents an evaluation of both specimens in tension. The load applied on the specimen is 6.6 kips (29.4 kN). The first column shows the specimen type while the second column shows mesh refinement, number of nodes per element and the element size. The third, fourth, and fifth columns show the FE analysis results, experimental results, and the percent difference between FE and experimental results, respectively. As per the results shown in Table 3-3 and Table 3-4, the following conclusions can be derived;

1) Use of finer mesh, 0.25(t×t), compared to 0.5(t×t) mesh with 8-node linear brick elements and linear extrapolation to calculate HSS does not increase the accuracy of the analysis results of Type 1 and 2 details under tension.

2) When Type 1 and 2 details are simulated under tension, the use of 0.25(t×t) mesh with 20-node quadratic brick elements and linear extrapolation to calculate HSS increases error by at least 10% compared to the results obtained from a 0.5(t×t) mesh.

3) When the Type 1 detail is simulated under tension, use of a 0.25(t×t) mesh with 8-node linear brick, 20-node quadratic brick, or a t×t mesh with 20-node quadratic brick reduced integration elements and linear extrapolation to calculate HSS leads to about a 20% error compared to the experimental results.

4) When Type 2 detail is simulated under tension, the use of a 0.25(t×t) mesh with 8-node linear brick, a 20-node quadratic brick, or a t×t mesh with 20-node quadratic brick reduced integration elements and linear extrapolation to calculate HSS leads to an about 12% error compared to the experimental results.

5) When Type 1 and 2 details are simulated under tension, the use of a 0.5(t×t) mesh with 20-node quadratic brick elements gives the least amount of errors (about 12% and 2%, respectively) compared to other mesh configurations and element types. Hence, the use of a 0.5(t×t) mesh with 20-node quadratic brick elements is recommended for simulating Type 1 and 2 details under tension.

6) When Type 1 detail is simulated under flexure, the use of a t×t mesh with 20-node quadratic brick elements or a 0.5(t×t) mesh with 20-node quadratic brick elements leads to almost identical error percentages (i.e., about 2% and 3%, respectively). However, the stress

calculated with a 0.5(t×t) mesh with 20-node quadratic brick elements is 3% greater than the experimental results, and it is recommended for fatigue life calculation.

7) When Type 2 detail is simulated under flexure, the use of a t×t mesh with 20-node quadratic brick elements or a 0.5(t×t) mesh with 20-node quadratic brick elements leads to identical results (i.e., about 0% and 1% error, respectively). Both approaches give higher stresses than the experimental values. Comparing simulation results of Type 1 and 2 details, use of a 0.5(t×t) mesh with 20-node quadratic brick elements is recommended for fatigue life calculation.

8) As shown in Table 3-3, the use of 0.5 (t×t) mesh with 20-node quadratic brick elements and quadratic extrapolation to calculate HSS yields about 10 to 15% greater stresses at the hot spot compared to using the linear extrapolation function. These estimates are conservative for fatigue evaluation and recommended to use until additional experimental data proves otherwise.

Table 3-3. HSS Calculated Using FE Models of Type 1 and 2 Specimens

Specimen Type	FE Model - Solid Element			HSS, ksi (MPa)			Percent Difference $\lvert(b-a_1)/b \times 100\rvert$
				Extrapolated Analysis Results (a)		Extrapolated Experimental Results (b)	
	Mesh	Nodes	Size	Linear (a_1)	Quad. (a_2)	Linear	
Tension Test with a 6.6 kip (29.4 kN) Force							
1	F	8	0.5(t×t×t)	6.3 (44)	6.5 (45)	7.6 (52)	17%
	F	20	0.5(t×t×t)	6.7 (46)	7.1 (49)		12%
	C	20	t×t×t	6.5 (45)	-		15%
2	F	8	0.5(t×t×t)	7.9 (54)	8.3 (57)	8.8 (60)	10%
	F	20	0.5(t×t×t)	8.6 (59)	9.3 (64)		2%
	C	20	t×t×t	8.1 (56)	-		8%
3-Point Bending with a 1.54 kip (6.86 kN) Force							
1	F	8	0.5(t×t×t)	45.0 (310)	47.4 (327)	59.5 (411)	24%
	F	20	0.5(t×t×t)	61.2 (422)	69.9 (482)		3%
	C	20	t×t×t	58.5 (403)	-		2%
2	F	8	0.5(t×t×t)	50.3 (347)	56.1 (387)	63.1 (435)	20%
	F	20	0.5(t×t×t)	63.4(437)	70.9 (489)		0%
	C	20	t×t×t	63.7 (439)	-		1%

Table 3-4. HSS Calculated Using Bhargava (2010) Recommendations - Type 1 and 2 Specimens under Tension

Specimen Type	FE Model - Solid Element			HSS, ksi (MPa)		Percent Difference |(b-a)/b × 100|
				Extrapolated Analysis Results (a)	Extrapolated Experimental Results (b)	
	Mesh	Nodes	Size	Linear	Linear	
1	F	8	0.25(t×t)	6.2 (43)	7.6 (52)	18%
	F	20	0.25(t×t)	5.9 (41)		22%
	C	20R	t×t	6.1 (42)		20%
2	F	8	0.25(t×t)	7.7 (53)	8.8 (60)	12%
	F	20	0.25(t×t)	7.5 (52)		14%
	C	20R	t×t	7.8 (54)		11%

3.6 BRIDGE STRUCTURAL MODELING AND HOT SPOT STRESS ANALYSIS

The girder and diaphragm layout, a girder geometry, and diaphragm configurations are shown in section 3.2. The objective of this section is to identify a few critical details for instrumentation. This was accomplished by evaluating stresses at cover plate ends and partial depth diaphragms. A finite element model of the bridge was developed using the dimensions documented in section 3.2 and 3.3 and the as-built plans.

3.6.1 Material Properties

Table 3-5 shows the material properties used in the finite element model. The bridge deck concrete modulus was reduced to account the current deck condition.

Table 3-5. Bridge Material Properties

Material	Material Property		
	Unit Weight (lbs/ft^3)	Modulus of Elasticity (ksi)	Poisson's Ratio
Concrete	150	4,000	0.2
Steel	490	29,000	0.3

3.6.2 Loads

Analysis was performed under deck and barrier self weight and live loads. The fatigue truck given in the MBE (2011) is a notional configuration. It was decided to use more realistic loads and vehicle configurations for the analysis to identify the fatigue-sensitive details for instrumentation. Hence, Michigan Legal Vehicle configurations with designated loads and an impact factor of 0.3 were used as live loads. These vehicle configurations are provided in the

Michigan Bridge Analysis Guide (MDOT 2009) and represent the typical trucks travelling over the bridge. The bridge carries 48,500 vehicles daily, with 30% of the vehicles being trucks. Of the trucks, 84.6% travel in the outer lane daily (Figure 3-12). Therefore, preliminary analysis was performed by placing the legal loads on the outer lane (Figure 3-13). After the preliminary analysis, truck number 17 (Figure 3-14) was identified as the critical load for HSS at the web gap welds.

Figure 3-12. Typical truck traffic on the bridge

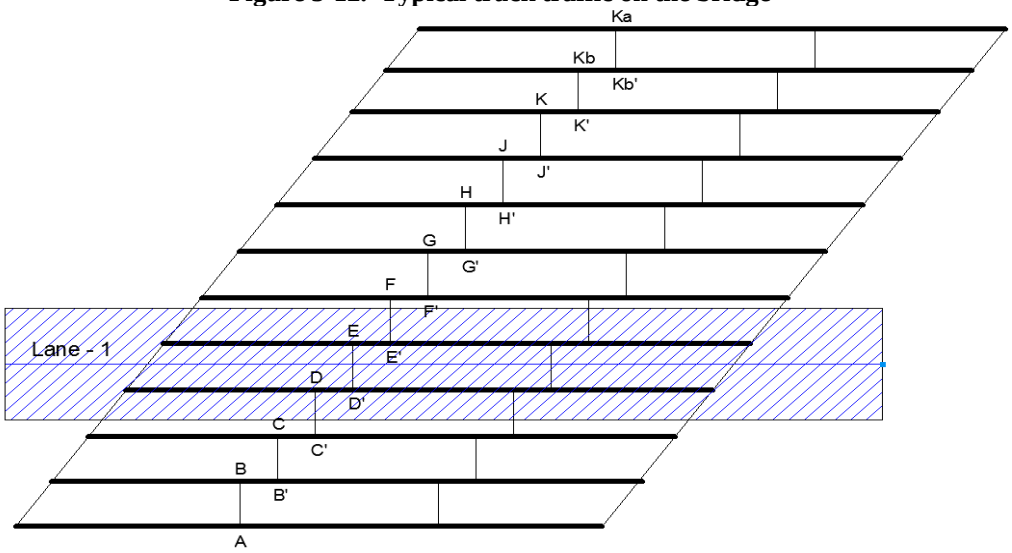

Figure 3-13. Girder layout and outer lane position

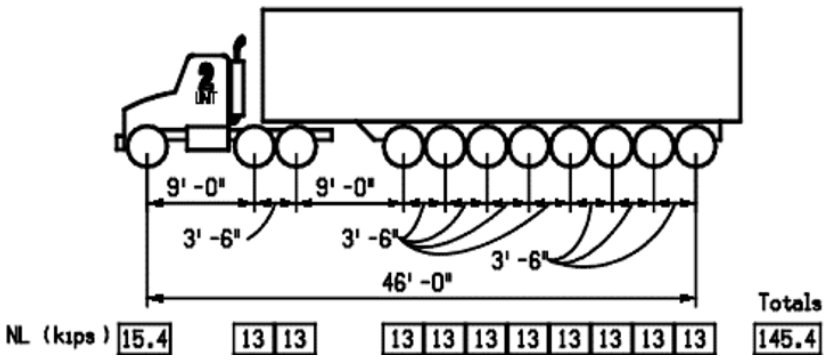

Figure 3-14. Michigan legal load: truck no. 17 configuration with normal axle loads

3.6.3 Boundary Conditions

Girder ends over the pier are supported on expansion bearings. Hence, roller boundary conditions were used over the pier. The bridge has an integral abutment where the girder ends are embedded in the backwall. Girder end fixity over the abutment is not easy to quantify. Hence, weld toe stresses were calculated using pin and fixed support conditions to develop a stress envelope. Since the girder end is embedded into the backwall, girder ends were restrained for torsion.

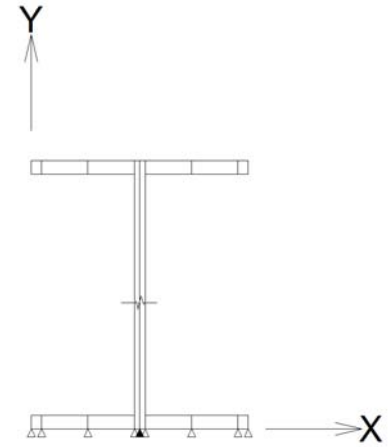

(a) Pin or roller boundary conditions

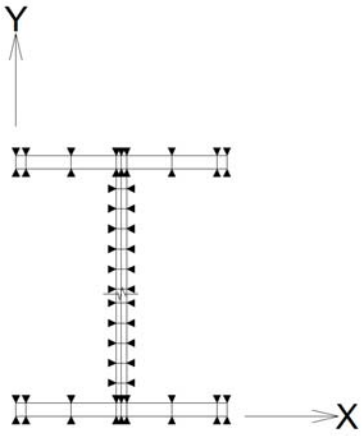

(b) Fixed boundary conditions

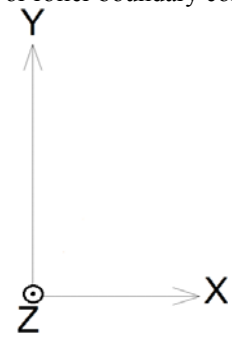

(c) Coordinate system

	Roller			Pin			Fixed		
Node	X	Y	Z	X	Y	Z	X	Y	Z
▲	R	R	NR	R	R	R	R	R	R
△	NR	R	NR	NR	R	R	-	-	-

R: Restrained; NR: Not Restrained

(d) Definitions of restrained conditions

Figure 3-15. Girder end boundary conditions

3.6.4 Finite Element Representation of the Bridge

The reverse engineered model using point cloud data from the laser scanner was instrumental in measuring diaphragm positions and web gap space as well as verifying dimensions of the rest of the bridge components. The information collected through field measurements (such as weld length), laser scanning, and bridge plans was used to develop a 3D finite element model of the bridge. The welds, at web gap and coverplate ends, were identified as fatigue-sensitive details. Preliminary analysis under Michigan legal loads indicated that stresses at partial depth

diaphragms located below the outer lane are the greatest. Based on the outer lane position, three web gap locations were identified for detailed investigation of the weld toe stresses and labeled as L_1, L_2, and L_3 (Figure 3-16 and Figure 3-17). The web gap dimensions of L_1, L_2, and L_3 are 3.765 in., 1.665in., and 3.665 in., respectively. According to Zhou (2005), three conditions must be simultaneously present for the development of weld toe cracking due to out-of-plane deformation at a web gap. These conditions are (1) an unstiffened web gap, (2) out-of-plane deformation, and (3) constraint at the web gap boundaries. Even though the web gaps are located above the girder bottom flange, which provides less restraint than the top flange with a deck, large skew and staggered diaphragm positions are other reasons for the large stresses observed. Hence, a detailed analysis was performed using truck #17, the most critical legal load, to calculate stresses at L_1, L_2, and L_3 locations.

The entire bridge superstructure was modeled using solid elements (Figure 3-18). Figure 3-19 shows a close up view of the web gaps. A submodeling approach was implemented to develop refined FE models for weld toe stress calculation (Figure 3-20). Section 3.5 presents recommendations for element types, mesh configuration, and stress extrapolation methods for HSS calculation. As per the recommendations, C3D20 elements with an average element size of 0.5t were selected for the submodels. Mesh size close to the weld toe was modified based on the stress extrapolation technique to define reference points for stress calculation.

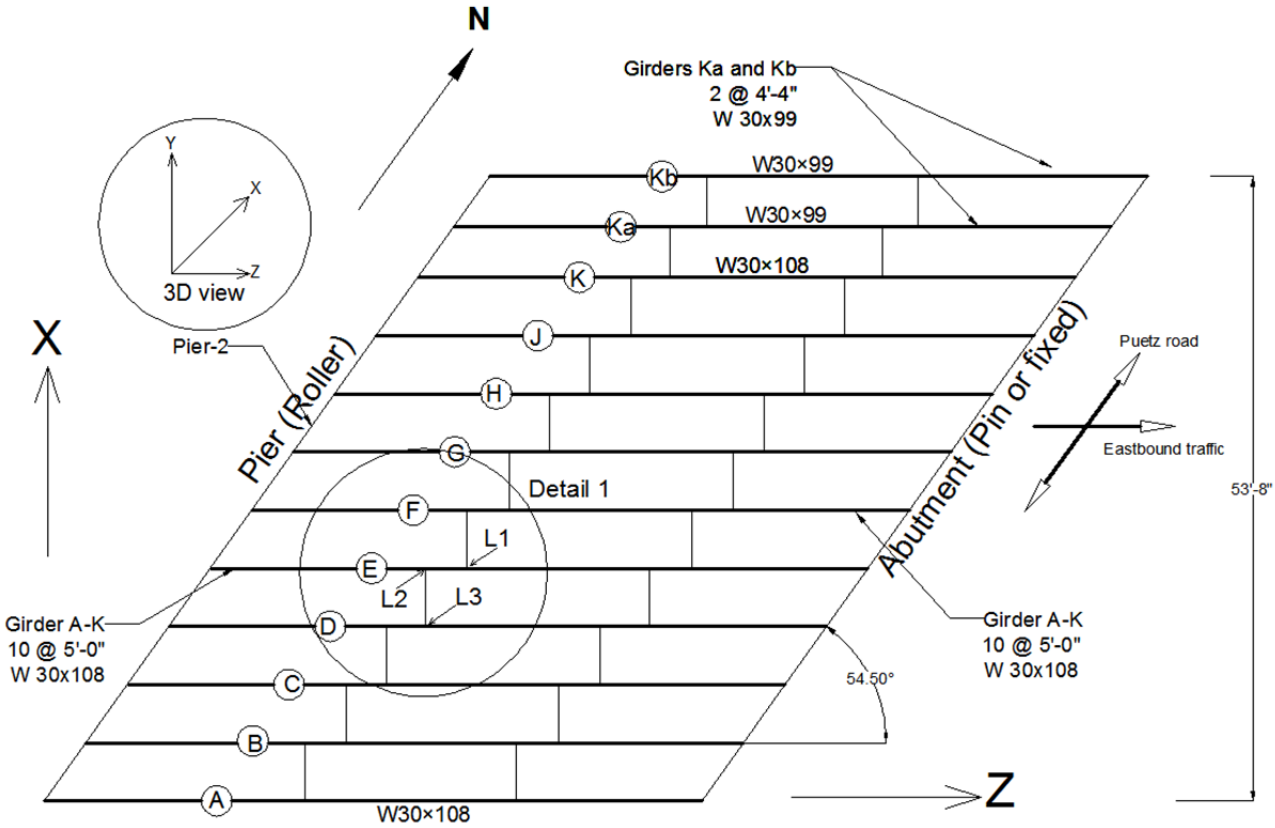

Figure 3-16. Girder and diaphragm layout, and the three web gap locations selected for detailed stress analysis

(a) Back side of the connection (view from abutment towards pier)

(b) Front side of the connection (view from pier towards abutment)

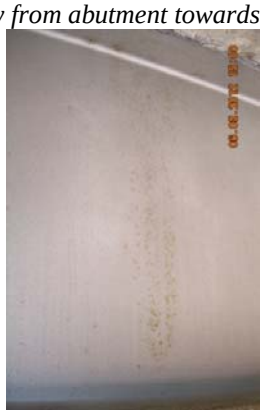

(c) Opposite face of the connection

(d) Close-up view of the web gap

Figure 3-17. A typical web gap fatigue-sensitive detail

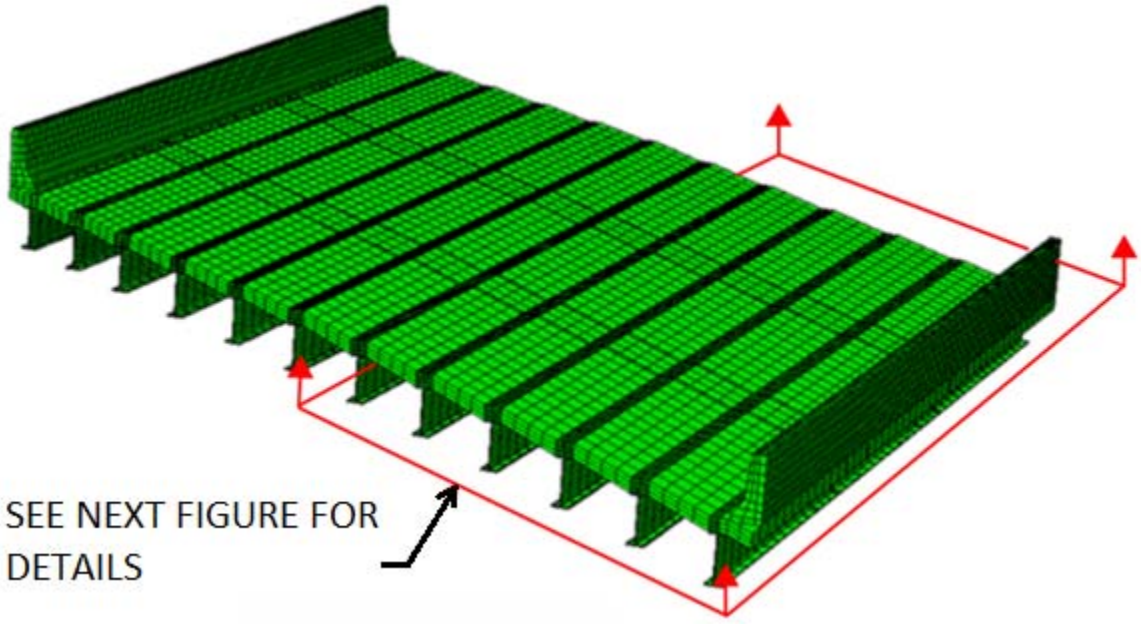

Figure 3-18. 3D view of the bridge model

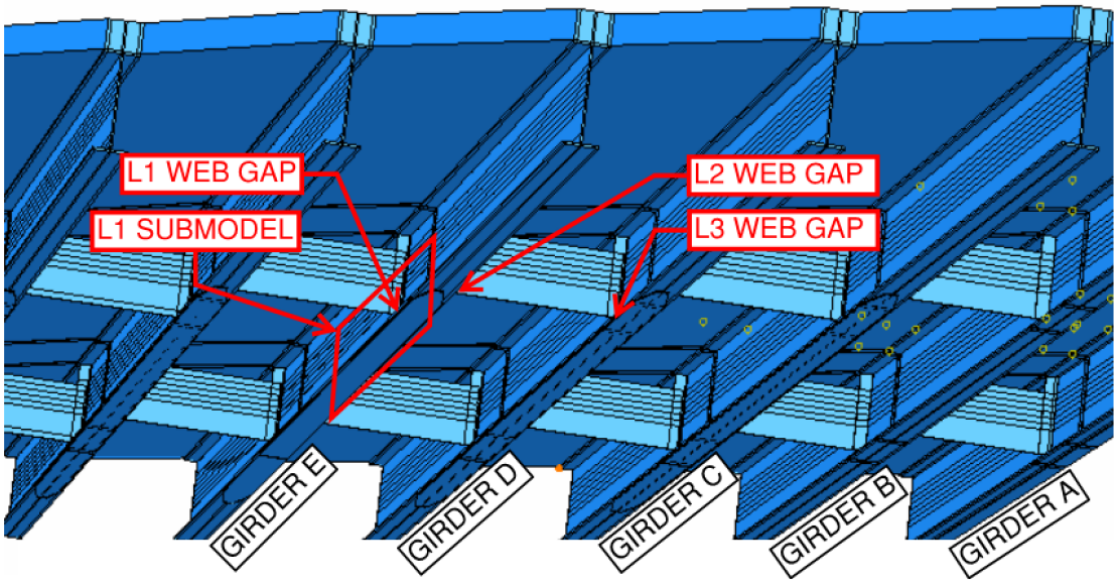

Figure 3-19. Detailed view of web gaps

(a) Webgap at L_1 (Bridge)

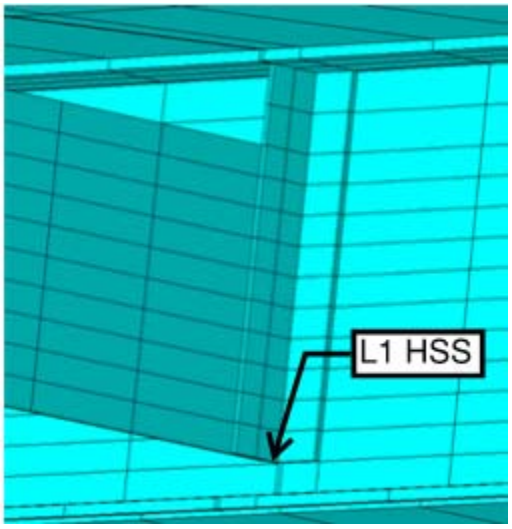

(b) Webgap at L_1 (FE Model)

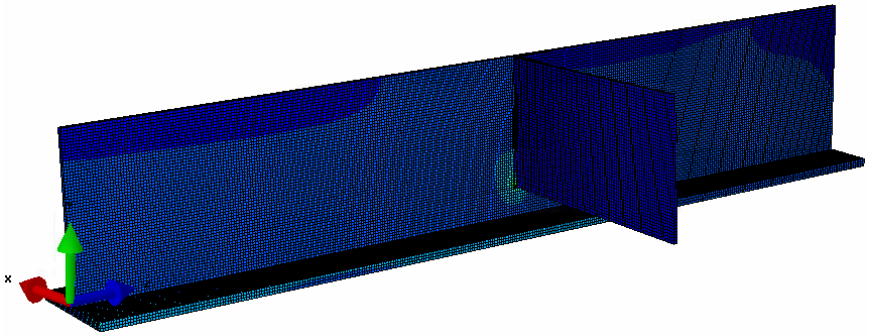

(c) Submodel L_1

Figure 3-20. Web gap at L_1 and the FE representation using a submodel

3.6.5 Analysis Results

3.6.5.1 Hot Spot Stresses under Michigan Legal Loads

Abaqus CAE (Abaqus 2014) was used as the pre/post-processor. Analysis was performed using the Abaqus standard solver. Based on the recommendations presented in section 3.5, the HSS calculation method recommended by Hobbacher (2008), also known as the International Institute of Welding (IIW) guidelines, was utilized. Note that the cracks at the transverse connection plate weld toe develop parallel to the girder flange or the primary bending stresses in the web plate (Fisher et al. 1990). Hence, instead of using principal stresses, the stresses perpendicular to cracking (S_{YY}) were calculated at reference points and presented in Table 3-6. Then, the HSS at L_1 and L_3 was calculated using Eq. 4-1 (Table 3-6). The quadratic extrapolation equation (Eq. 4-1) is not applicable for the L_2 web gap because the stress pattern around the weld toe does not represent the experimental stress pattern that was used to derive the equation. The web gap space (1.665in.) is smaller than the gaps at other two locations. Also, the stresses below the weld changes from compression to tension under truck #17 load. Linear extrapolation uses two reference points that are located at 0.5t and 1.5t from the weld toe. However, this method is also not applicable because the reference points are located within tension and compression zones. Further investigations of weld toe stresses at L_2 were not conducted because the stresses at this location are much smaller compared to the stresses at L_1 and L_3. Hence, location L_1 and L_3 were selected for instrumentation. Additional details related to instrumentation are provided in chapter 4. Figure 3-25 shows the girder and diaphragm deformation under truck #17. Figure 3-26 and Figure 3-27 show girder and web gap deformation under truck # 17. According to Figure 3-26 and Figure 3-27, the web gap deformation under truck # 17, with fixed or pinned abutment conditions, shows a single curvature. This deformation validates the application of liner or quadratic stress extrapolation methods to calculate HSS at L_1 and L_3 weld toes.

$$\mathbf{HSS} = 2.52\,\sigma_{0.4t} - 2.24\,\sigma_{0.9t} + 0.72\,\sigma_{1.4t} \qquad (4\text{-}1)$$

Table 3-6. HSS at L_1 and L_3 Web Gap Weld Toe Due to Truck #17

Reference point location from weld toe	Distance from weld toe with t = 0.545 in. (in.)	Stress in Y-direction (S_{YY}), (ksi)			
		Fixed support over the abutment		Pinned support over the abutment	
		L_1	L_3	L_1	L_3
1.4t*	0.218	1.96	2.90	4.40	2.90
0.9t	0.491	3.31	3.90	5.46	3.86
0.4t	0.763	5.12	5.70	8.14	5.71
*t = web thickness	**Hot Spot Stress, (ksi)**	**6.90**	**7.72**	**11.45**	**7.83**

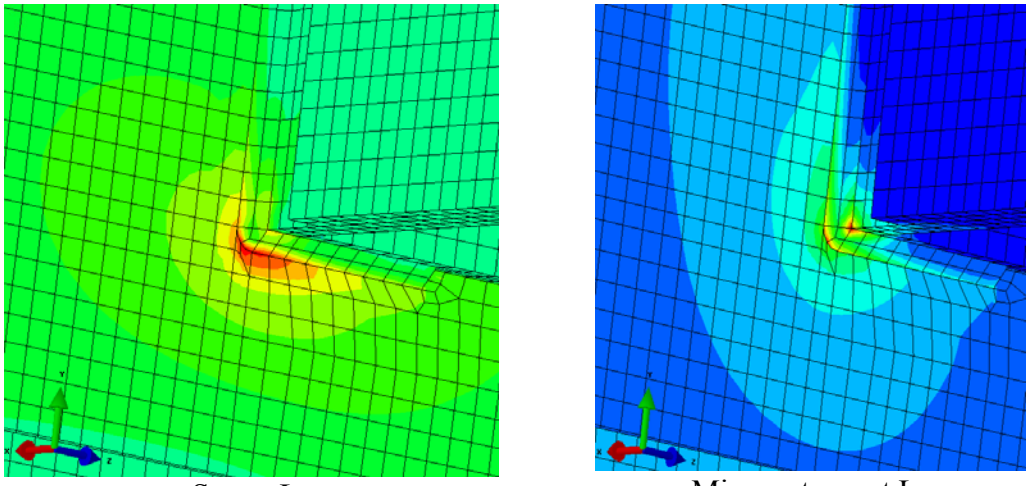

S_{YY} at L_1 Misses stress at L_1

Figure 3-21. Web gap at L_1 and stresses around weld toe due to truck #17

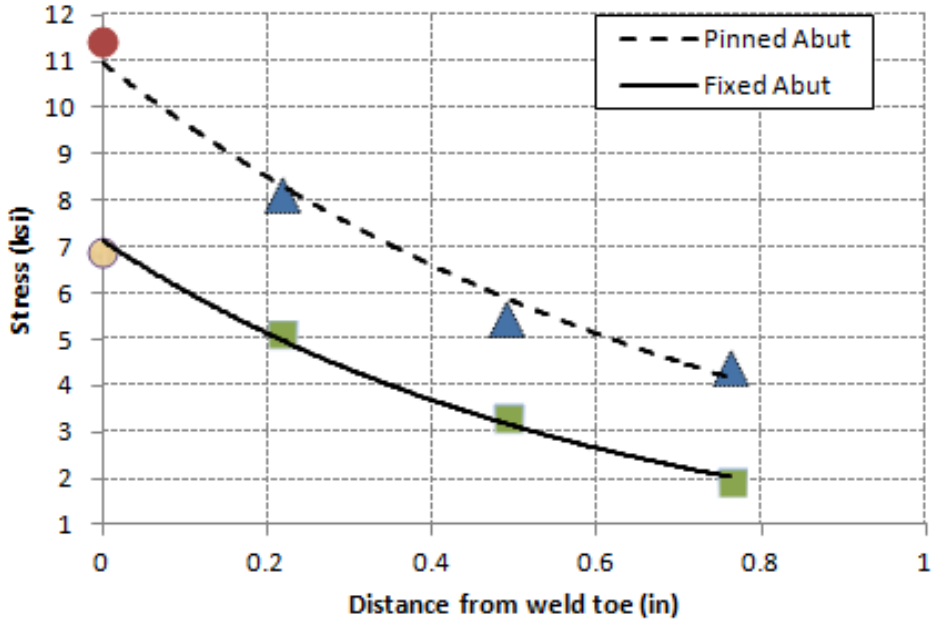

Figure 3-22. Hot spot stress (S_{YY}) at L_1 using quadratic extrapolation

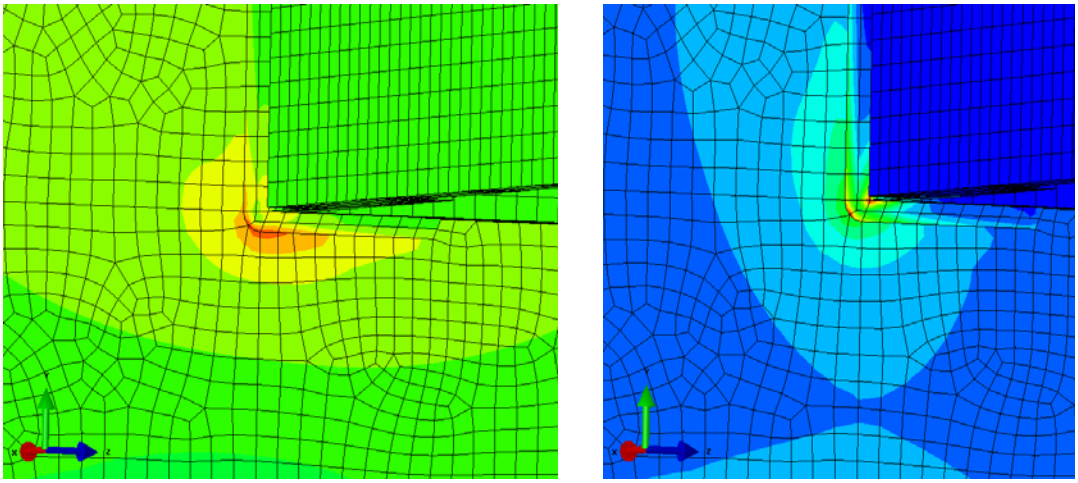

S_{YY} at L_3 Misses stress at L_3

Figure 3-23. Web gap at L_3 and stresses around weld toe due to truck #17

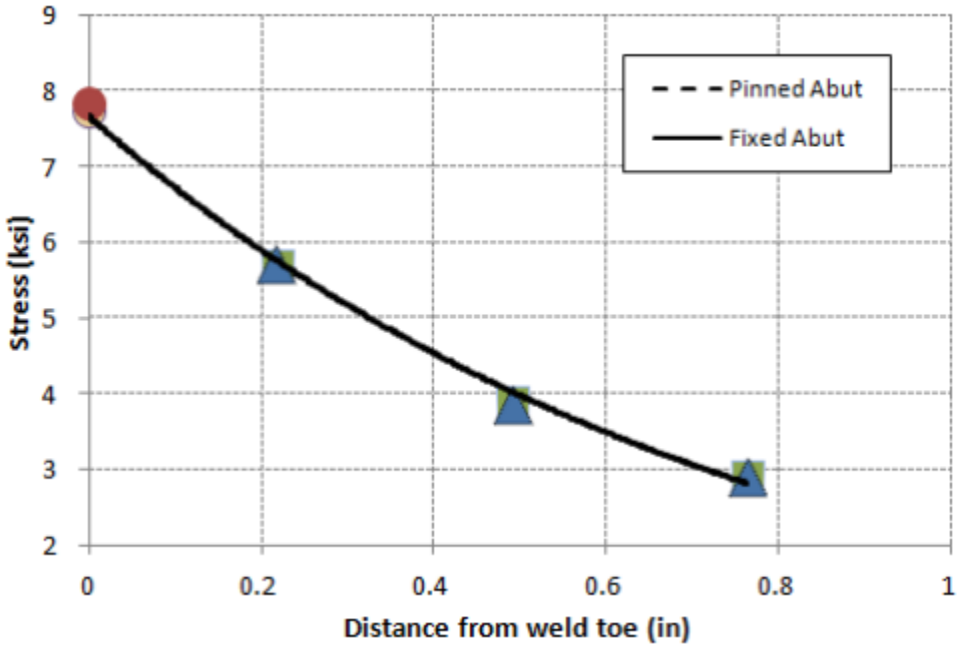

Figure 3-24. Hot spot stress (S_{YY}) at L_3 using quadratic extrapolation

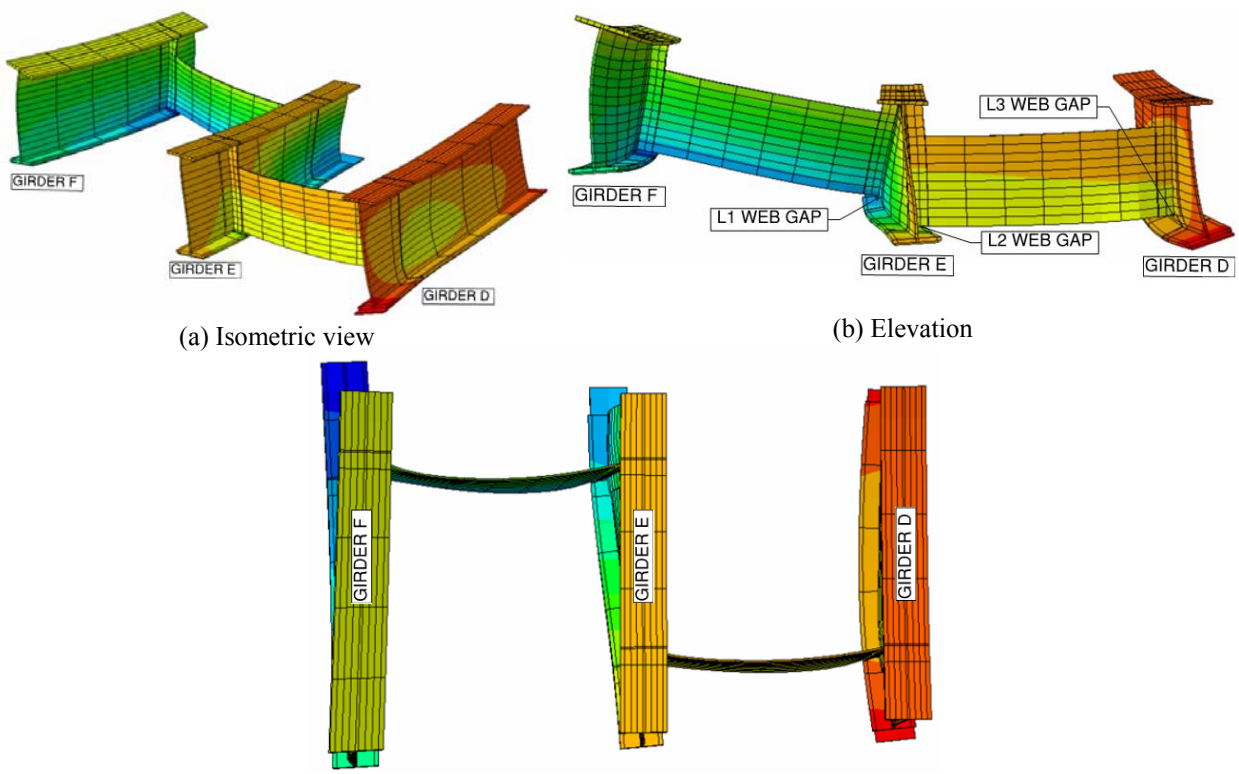

(a) Isometric view (b) Elevation

(c) Plan

Figure 3-25. Girder and diaphragm deformation under truck #17

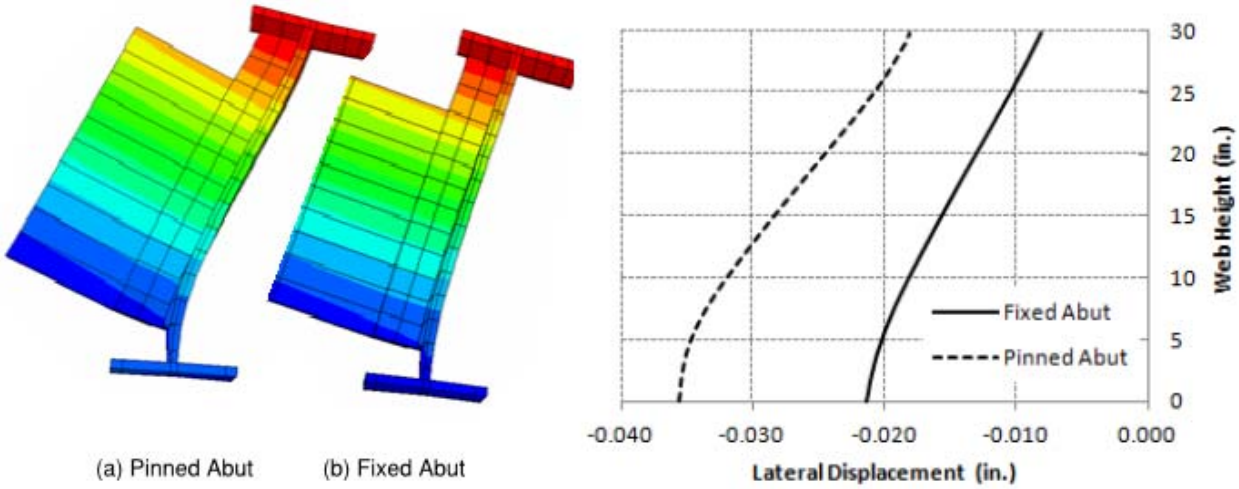

(a) Pinned Abut (b) Fixed Abut

Figure 3-26. Deformation of girder E and the web gap (L_1) due to truck # 17

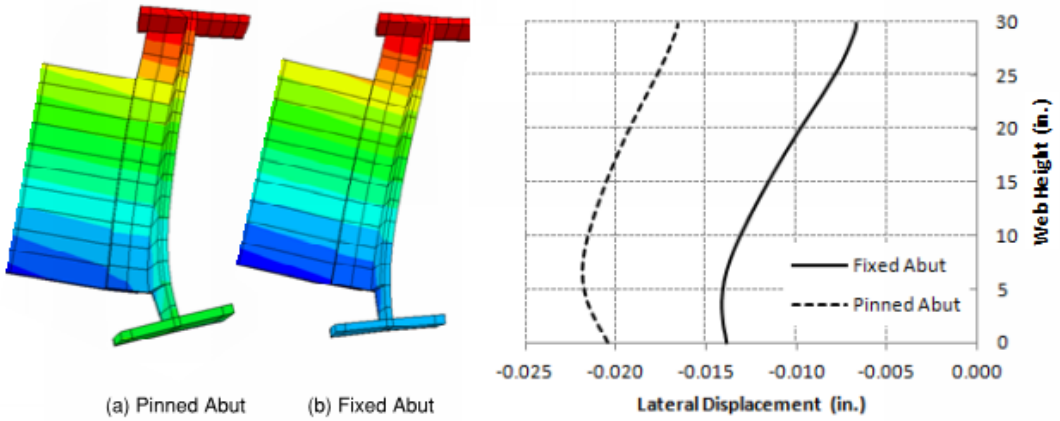

Figure 3-27. Deformation of girder D and the web gap (L_3) due to truck # 17

3.6.5.2 Hot Spot Stresses under Deck Dead Load

Plastic concrete weight during bridge deck placement is carried by the girder-diaphragm assembly. Considering this scenario, analysis was performed to calculate weld toe stresses due to the weight of plastic concrete. In order to establish a stress envelope with lower and upper bound values, two different boundary conditions were considered over the abutment: fixed and pinned. Table 3-7 presents hot spot stresses. Figure 3-28 and Figure 3-29 show stresses at reference points and weld toe. According to the Figure 3-30 and Figure 3-31, web gap deformation under deck weight with fixed or pinned abutment condition shows a single curvature. This deformation validates the application of liner or quadratic stress extrapolation methods to calculate HSS at L_1 and L_3 weld toes.

Table 3-7. HSS at L_1 and L_3 Web Gap Weld Toe Due to Deck Weight

Reference point location from weld toe	Distance from weld toe with t = 0.545 in. (in.)	Stress in Y-direction (S_{YY}), (ksi)			
		Fixed support over the abutment		Pinned support over the abutment	
		L_1	L_3	L_1	L_3
1.4t*	0.218	2.41	0.99	3.35	2.42
0.9t	0.491	3.05	2.41	4.24	3.19
0.4t	0.763	4.63	3.55	6.44	4.68
*t = web thickness	**Hot Spot Stress, (ksi)**	**6.57**	**4.26**	**9.14**	**6.39**

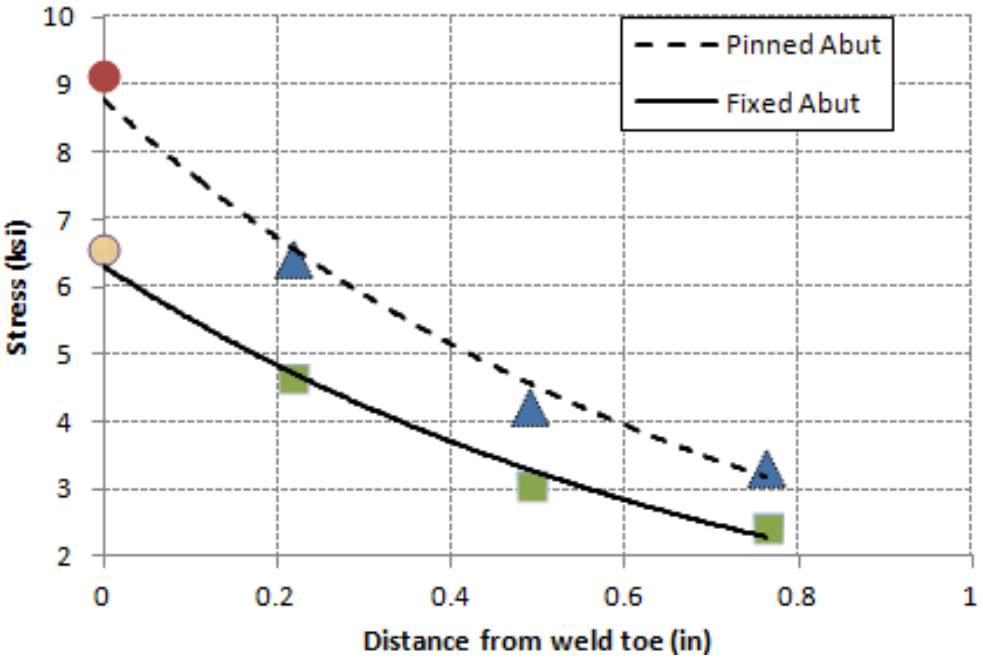

Figure 3-28. Hot spot stress (S_{YY}) at L_1 using quadratic extrapolation (deck dead load)

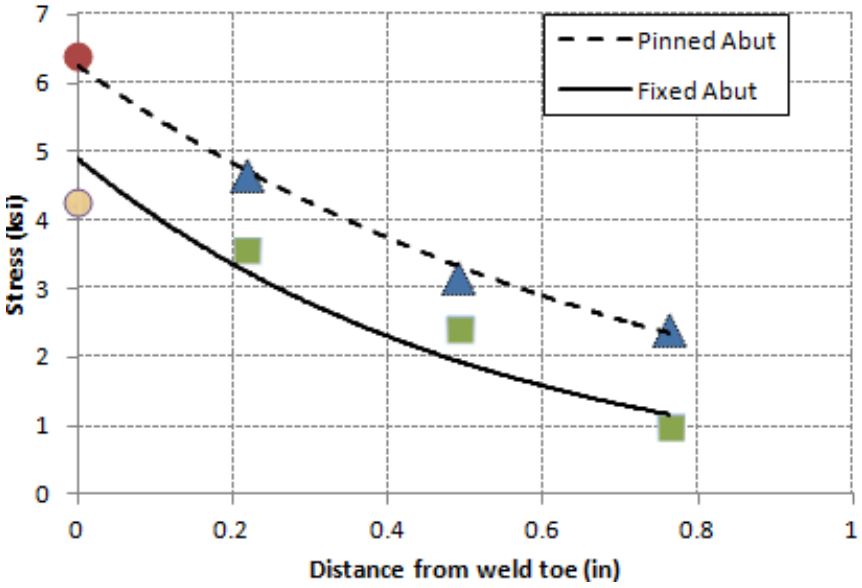

Figure 3-29. Hot spot stress (S_{YY}) at L_3 using quadratic extrapolation (deck dead load)

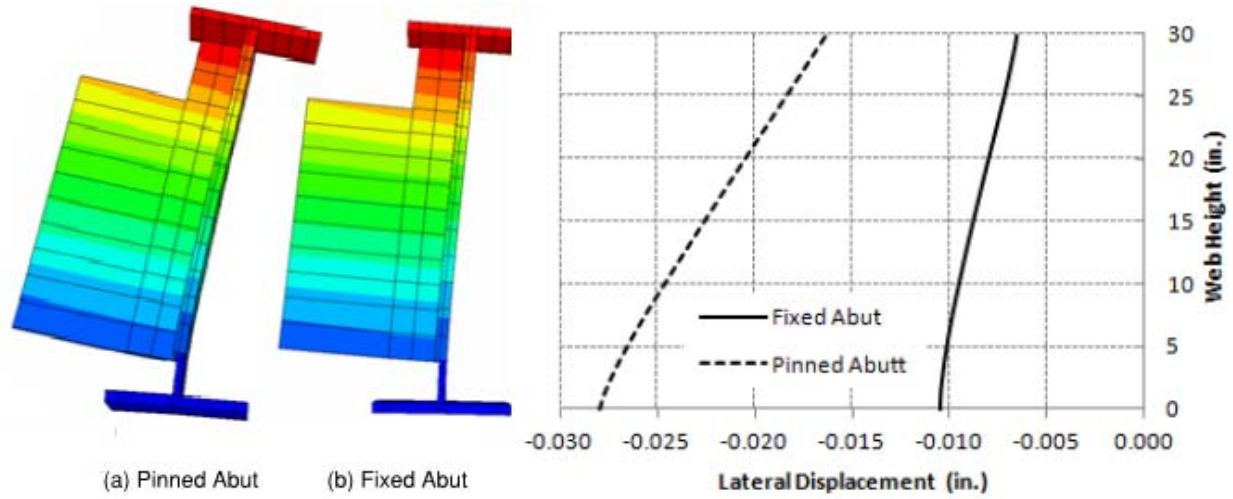

Figure 3-30. Deformation of girder E and the web gap (L_1) due to deck weight

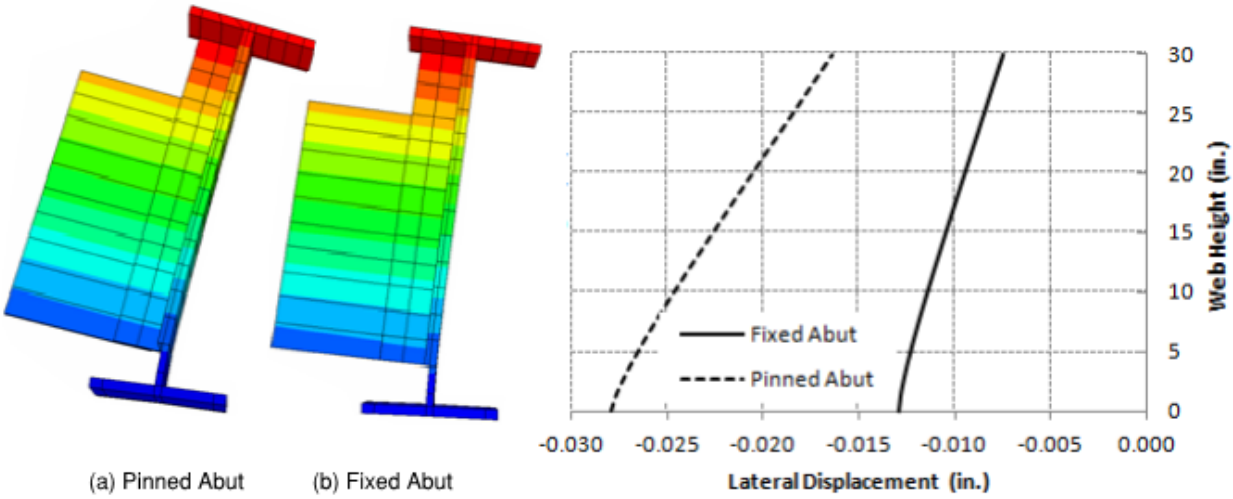

Figure 3-31. Deformation of girder D and the web gap (L_3) due to deck weight

A New Jersey Type-4 safety barrier weight was applied on the deck-girder assembly. Barrier weight develops very small compressive stresses (< 0.9 ksi) at the weld toes. According to Hobbacher (2008) stresses developed from all the loads, including transient temperature changes, need to be considered. Residual stresses due to welding and manufacturing need to be considered as the tensile residual stresses decrease the fatigue resistance. However, fatigue data that is commonly presented in S-N curve format includes the effect of residual stresses. Following a conservative approach, the stresses developed under barrier weight were neglected; only truck #17 and the deck dead load were considered. Table 3-8 shows hot spot stress at weld toes due to the deck dead load and Truck #17. As discussed previously, girder end fixity over the abutment is not easy to quantify. Hence, weld toe stresses were calculated using pin and

fixed support conditions to develop a stress envelope. Since the girder end is embedded into the backwall, girder ends were restrained for torsion when the pinned supports were used for analysis. Yield strength of steel girders (f_y) is 36 ksi. Hence, the hot spot stress at L_1 and L_3 weld toes ranges from $0.37f_y - 0.57f_y$ and $0.33f_y - 0.40f_y$, respectively. Due to these very high stresses, the details were selected for instrumentation and monitoring. Further, the analysis results show the importance of quantifying residual stresses and the stresses due to permanent loads using technologies such as XRD.

Table 3-8. HSS at L_1 and L_3 Web Gap Weld Toe Due to Deck Weight and Truck #17

Reference point location from weld toe	Distance from weld toe with t = 0.545 in. (in.)	Stress in Y-direction (S_{YY}), (ksi)			
		Fixed support over the abutment		Pinned support over the abutment	
		L_1	L_3	L_1	L_3
1.4t*	0.218	9.75	9.25	14.58	10.39
0.9t	0.491	6.36	6.31	9.70	7.05
0.4t	0.763	4.37	3.89	7.75	5.32
*t = web thickness	**Hot Spot Stress, (ksi)**	**13.47**	**11.98**	**20.59**	**14.22**

3.7 SUMMARY

A bridge with fatigue-sensitive details was selected, and as-built details and in-service condition were documented. A three-dimensional (3D) finite element model of the bridge was developed and used to evaluate the structural behavior and girder and diaphragm deformation under specific loads and load patterns. Finally, two details were selected for instrumentation and monitoring.

The bridge selected for this study contained partial depth diaphragms with welded details. Evaluation of the fatigue-sensitive welded details requires calculating hot spot stress (HSS). HSS calculation requires selecting appropriate element types, mesh parameters, and stress extrapolation methods. The finite element modeling guidelines and HSS calculation methods presented in Section 2.3.4 were evaluated by simulating tension and flexure tests conducted by Lee et al. (2010). These simulations were helpful in selecting C3D20 elements with an average element size of 0.5t for the submodels used in the subsequent analysis. The quadratic extrapolation technique was recommended to calculate HSS.

Based on the recommendations, a 3D finite element model of the bridge was developed and HSS were calculated under Michigan legal loads and deck dead load. In order to develop a stress

envelope for each weld, girder end boundary conditions over the abutment were considered as fixed and pin. The HSS at two web gap weld toes (L_1 and L_3) ranged from $0.37f_y$ – $0.57f_y$ and $0.33f_y$ – $0.40f_y$, respectively. Due to these very high stresses, the details were selected for instrumentation and monitoring. Furthermore, the analysis results show the importance of quantifying residual stresses and the stresses developed under permanent loads for accurate evaluation of the fatigue-sensitive details.

4 STRUCTURAL HEALTH MONITORING (SHM) SYSTEM IMPLEMENTATION

As presented in Chapter 2, after an extensive review of successes and challenges of implementing technologies for fatigue event detection and crack growth monitoring, a monitoring system with acoustic emission (AE) sensors was selected. Chapter 3 presents the process that was followed for selecting bridge details for instrumentation and monitoring. This chapter presents information related to field implementation, calibration of the SHM system, and power supply. In addition, a brief description of the system components and software used for system configuration, data acquisition, data display, remote access, and data transfer is presented.

4.1 IMPLEMENTATION AND CALIBRATION

4.1.1 Monitoring System Components

The Sensor Highway™ II System selected for this project has a low-power computer. The operating system and essential software are installed in a 2 GB hard drive. The supplemental software and sensor data are stored in a 110 GB drive. The system for bridge monitoring was integrated for deployment by TISEC Inc. in its SABRE™ system to best suit it for the specific application. The monitoring system components are shown in Figure 4-1.

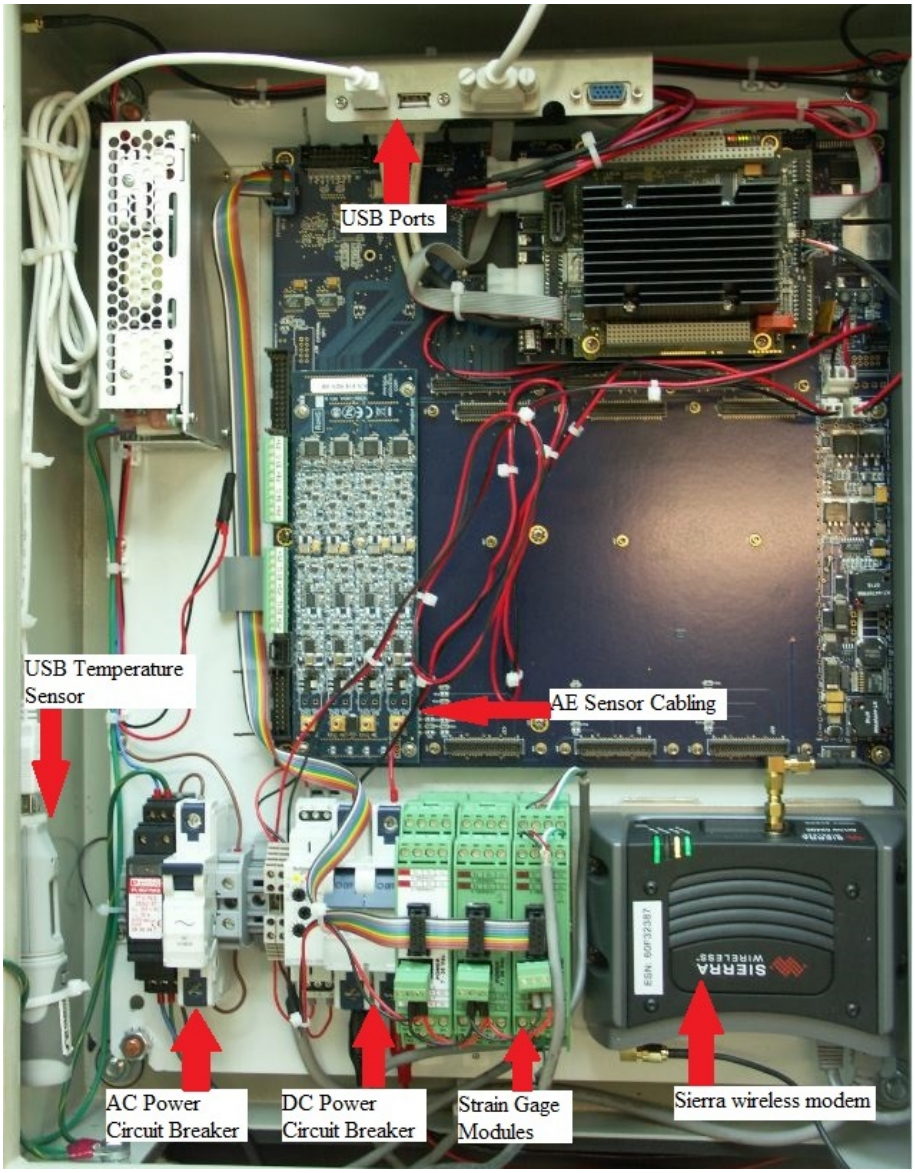

Figure 4-1. Monitoring system components in the enclosure

As shown in Figure 4-1, the monitoring system used in the project consists of only one Mistras AE board (PCI/DSP-4) with four-channels. The system capability can be extended to accommodate 3 AE boards with a total of 12 AE sensors. The monitoring system included Mistras 4 PK30I narrow band sensors (Figure 4-2a). The sensor has an integral, ultra-low noise, low power preamplifier. The frequency range of the sensor is 200 – 450 kHz with a resonance frequency of 300 kHz. Advice issued by the Department for Transport, the United Kingdom, recommends using a magnetic clamp to hold an AE sensor in place on steel structures (Figure 4-2b) (DFT UK 2006). The clamp design should include a spring to exert an adequate force on the sensor. The spring should be carefully selected not to deform the piezoelectric sensor

permanently but to ensure a constant contact pressure between the sensor and the structure. Magnetic holders, which comply with the requirements, were used to mount the AE sensors (Figure 4-2c). One of the objectives of the project was to identify a monitoring system that could be moved from site to site, as needed. Hence, using magnetic holders allows removing and remounting the sensors. Two handles, located at the top of the holder, help remove the strong magnets from the mounting surface. The holders are made of an electrical insulating material with a high acoustic attenuation.

(a) An acoustic emission sensor

(b) A spring-loaded magnetic holder

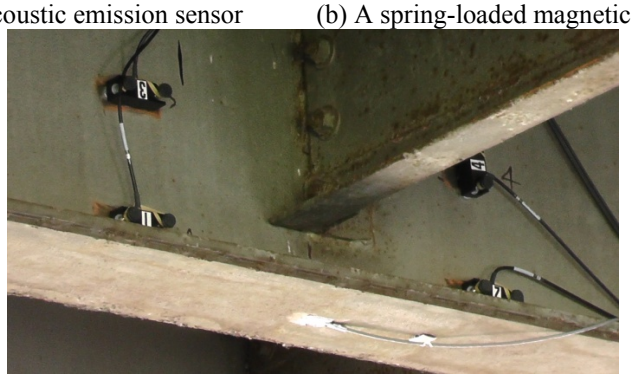

(c) AE sensors mounted on a steel girder

Figure 4-2. (a) An acoustic emission sensor, (b) a spring –loaded magnetic holder, and (c) AE sensors mounted on a steel girder

4.1.2 Instrumentation

Partial depth diaphragm connections at L_1 and L_3 locations, shown in Figure 3-16, were selected for instrumentation. Figure 3-17 shows the web gap detail at L_3. Four AE sensors were mounted around the web gap, and a strain gauge was mounted at the bottom flange of Girder D to establish the load matrix (Figure 4-3 and Figure 4-4). In general, an attenuation survey needs to be performed to determine the optimum sensor spacing and arrangement. Data from the survey helps in setting up the signal threshold so that signals arising from fatigue cracks do not fall below the threshold before arriving at a sensor. Prior experience with similar details can play a significant role when designing sensor configurations and setting up signal thresholds. During this project, the sensor configuration was developed based on prior experience. The process that

was followed for sensor calibration and setting up of signal thresholds is discussed in Section 4.1.4. Three metal foil strain gauges were mounted at the web gap of the connection detail at Girder E (L_1) to calculate hot spot stresses under ambient traffic. Following the recommendations given in Hobbacher (2008) for calculating hot spot stress, three strain gages were mounted at 0.4t, 0.9t, and 1.4t distances from the weld toe; where *t* is the web thickness. Figure 4-5 shows the strain gages mounted at the web gap.

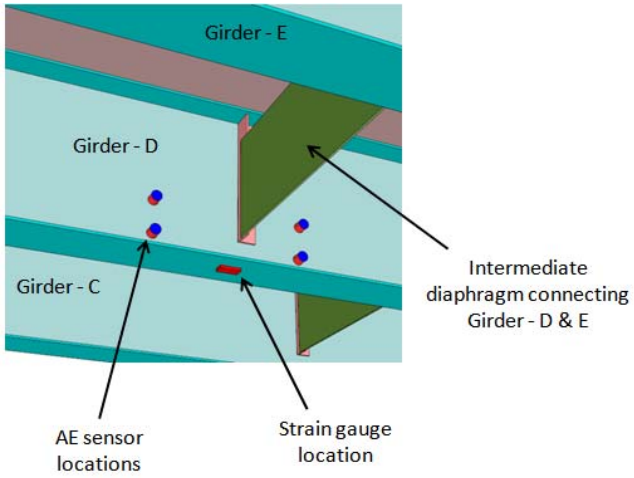

Figure 4-3. AE sensors and a strain gauge at the partial depth diaphragm connection, L_3

(a) AE sensors are mounted using magnet holders

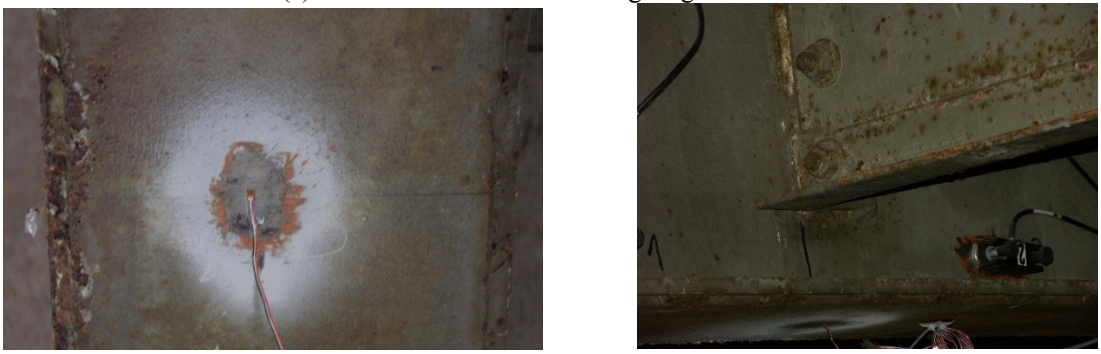

(b) a strain gage at girder bottom flange

Figure 4-4. AE sensors around the web gap and a strain gage at girder bottom flange

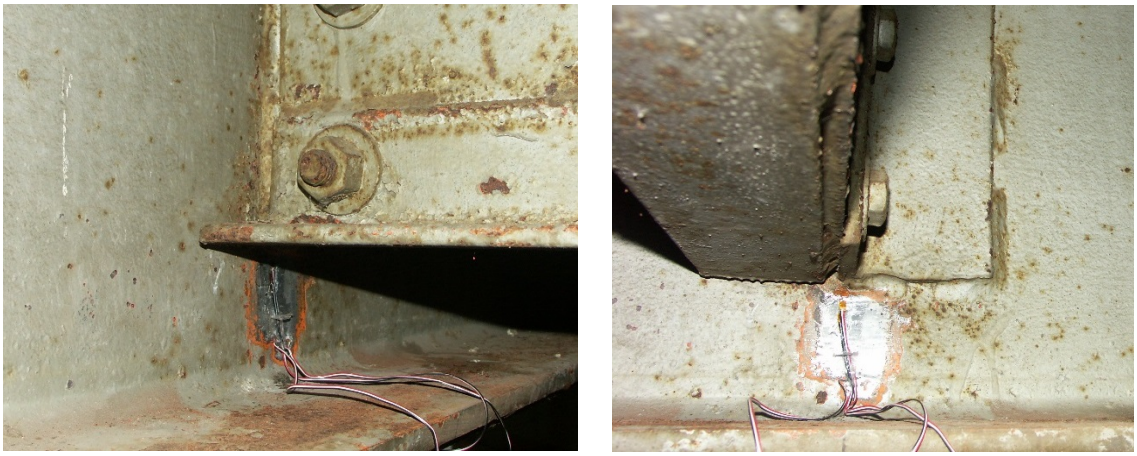

(a) (b)

Figure 4-5. Strain gages at the webgap

4.1.3 Power Management for Filed Monitoring

One of the single most important factors in regard to as-needed or short-term monitoring is a reliable and cost-effective power supply. Grid power, while being extremely reliable and low cost for long-term monitoring, is not always readily accessible or economical for as-needed or short-term monitoring. Most power companies throughout the United States are willing to drop and run a line up to 300 ft for little to no cost; however, the costs of additional materials required for system operation including the transformer and power meter, often are in the $3,000 to $5,000 range. Because these associated costs are high, and such materials cannot be easily transferred to new locations, grid power is not feasible for short-term monitoring. The most significant obstacle is that the power supply from the grid will not be available when needed.

The use of energy harvested from sources such solar, structural vibration, sound, wind or a combination thereof is one of the fastest growing areas in the field of remote monitoring and sensing (Shirahata et al. 2014). Solar power systems or photovoltaic (PV) systems are devices that use sunlight to generate electricity (Ramchandra and Boucar 2011). Sunlight provides energy in the form of radiation. The amount of solar irradiance directly corresponds to the amount of energy that can be produced from a solar panel, and is the single largest factor effecting the production of electricity. Solar irradiance is the term used to denote the amount of solar radiation that reaches a surface or an area over a certain period of time, and it is often expressed in units of Langley (Ly) or kilowatts per square meter per day ($kW/m^2/day$). Due to the extreme importance of solar insolation in the production of reliable power, it is important to

determine the solar insolation instead of the number of sunshine hours. This is because the sunshine hours provide only the number of hours that sunlight is available at a site, but not the intensity of sunlight (Shirahata et al. 2014). Solar insolation data can be obtained from the *Atmospheric Science Data Center* at the *NASA Langley Research Center* (NASA 2014).

In addition to solar insolation, exposure conditions and type of solar photovoltaic affect the solar power system performance. Cloud cover, temperature, humidity, wind, and dust effect the production of solar power from a panel. Cloud cover affects energy production by way of reducing the amount of solar irradiance that comes into contact with the panel. Similarly, dust particles and shadows from nearby structures or trees can have a large impact on the electricity generation. Higher temperature also reduces the amount of energy being produced by a solar panel. In addition, humidity levels in excess of 75% can lead to a decrease in solar panel efficiency (Ettah et al. 2012; Kazem et al. 2012). Kazem et al. (2012) studied the effect of humidity on the performance of three types of solar photovoltaic: Monocrystalline, Polycrystalline and Amorphous silicon. Results show that the reduction in relative humidity increases the voltage, current and efficiency. Further, the Monocrystalline panel has the highest efficiency when relative humidity is decreased with respect to other technologies.

4.1.3.1 A Standalone Solar Power System

The standalone, hybrid, and grid tie systems are the three basic solar power systems (Hee and Isa 2009). Three main components of a standalone solar power system are (a) a solar panel (or an array), (b) a power control equipment such as a charge controller, and (c) batteries or other forms of energy storage devices (Figure 4-6 and Figure 4-7) (Tianze et al. 2011). A standalone system is ideal for short-term or as needed monitoring.

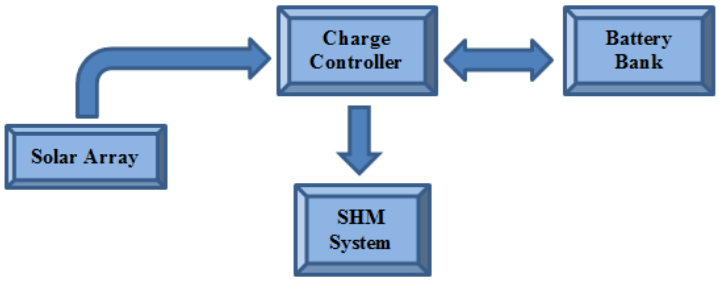

Figure 4-6. Basic components of a solar powered monitoring system

(a) A solar panel

(b) The MPPT charge control

(c) A deep-cycle marine battery

Figure 4-7. Basic components of a solar power system

As shown in Figure 4-6, an advanced charge controller can manage the entire solar power system. It has the ability to manage the power to equipment, and to protect the battery bank from overcharging and over-discharging and the solar array from reverse current (Hee and Isa 2009). Where needed, inverters can be used to convert direct current (DC) power into alternating current (AC) power. However, additional losses due to an inverter need to be considered when sizing the solar array and the storage. Some charge controllers have load control options for the purpose of setting up timers as well as advanced programming to improve charging efficiency. One such example is the Maximum Power Point Tracking (MPPT) charge controller. The MPPT charge controller uses DC to DC conversion to convert the array's operational voltage to the battery charging voltage. The conversion works on the principle that power into the MPPT is equal to the power out of the MPPT (i.e. Volts In × Amps In = Volts Out × Amps Out). The efficiency of the power conversion ranges from 92% to 95% (Sunsaver 2014). With the power conversion algorithm used in the MPPT controller, the charge (amperage) supplied to the battery can be increased by about 10% to 35% (Sunsaver 2014). The advantage of using an MPPT charge controller is that it allows the solar array to operate at its maximum power point voltage (V_{mp}); whereas, a typical charge controller supplies a charge to the battery in proportion to the power produced by the array.

The battery provides needed energy storage. Deep discharge lead-acid batteries are good for storing solar energy that can later be delivered with minimal damage to the battery cells. Battery storage or capacity is often expressed in amp-hours. The capacity stated on the battery is the total amount of energy that can be withdrawn from the battery before complete discharge. However, the total capacity of a battery can be affected by the rate of discharge and operating environment conditions (e.g., battery capacity drops to about 60% under below freezing

temperatures). This effect on the battery's capacity can be determined by using Peukert's equation or through C-rate tables available on most battery datasheets from the manufacturer of the battery. Inefficiency also exists in the process of discharging and recharging a battery; for a typical lead-acid battery, this loss can be in the range of 10%-30% (Shirahata et al. 2014). Batteries have a cycle life, or an estimated number of times that they can be discharged and recharged before the battery begins to lose its ability to maintain a charge. A cycle is the period over which the battery is discharged and recharged once; thus in a solar system a cycle would occur every day. The depth of discharge (DoD) is a term that refers to the amount of energy discharged from a battery, before it begins a new cycle. The DoD can affect the life of a battery, the majority of battery manufacturers recommend not exceeding 50%-60% discharge.

4.1.3.2 Solar Power System Implementation

The monitoring system was configured to run on either AC or DC by providing two circuit breakers (Figure 4-1). Also, the system can be connected simultaneously to an AC as well as a DC power source. This feature allows uninterrupted operation of the system by switching between the power sources seamlessly. Nevertheless, the monitoring system was powered by only a solar power system that comprised of a solar panel, a Maximum Power Point Tracking (MPPT) charge controller, and a battery bank with deep cycle marine batteries (Figure 4-7). The solar panel was rated at 140 W, with a peak production of 8.1 A and 17.2 V. The battery bank included two deep discharge lead-acid, marine batteries connected in parallel: one providing 140 Ah capacity and the other 160 Ah capacity, providing a total of 300 Ah. The monitoring system draws about 40 W. With a 12V battery bank, about 3.33 A current was required to operate the monitoring system.

The monitoring system power requirement, system losses, and solar insolation need to be considered for solar power system design. It is typical to select the month with the lowest amount of solar insolation as the 'design month.' However, with access to adequate historical data, the system can be configured for the specific month(s) that the monitoring system will be operated. Nevertheless, the solar array used in this study was undersized. This required using advanced programming features in the MPPT charge controller to operate the monitoring system based on the availability of adequate charge from the battery bank. To control power supply to a load, the MPPT charge controller has an option to define voltage thresholds: low voltage

disconnect (LVD) and low voltage reconnect (LVR). This is mainly to control the depth of discharge (DoD) to prevent battery damage as well as to maintain the longest possible SHM system operation duration. Considering the fluctuations in battery voltage at the start and end of a battery charge cycle, LVR and LVD thresholds were set to 13.6 V and 11 V, respectively. The targeted maximum battery voltage was set to 14 V.

4.1.4 Data Acquisition and AE Sensor Calibration

After AE sensors are mounted and the data acquisition system and data processing software are ready, AE signals generated by pencil lead breaks (PLB) are used to evaluate the sensitivity of sensors. The AE signals generated by PLB represent the AE signals from fracture events (ASTM E976-10, Standard Guide for Determining the Reproducibility of Acoustic Emission Sensor Response). A well-mounted sensor is expected to record a signal between 95 and 97 dB when a PLB is performed at a distance of 2 in. from the sensor (DFT UK 2006). Source location calculation requires knowing wave velocity through the material. Wave velocity can be calculated by performing PLB outside the sensor array and recording the arrival times at two sensors. The wave velocity is calculated using the distance between two sensors and the difference in the signal arrival times. Also, the noise sources are identified prior to monitoring in order to set up appropriate thresholds and determine the need for guard sensors.

The AE monitoring system implementation discussed in this study did not require using guard sensors. Wave velocity was determined knowing the girder material, A36 structural steel. Wave velocity and the signal arrival time are used to calculate the distance to an AE signal source location from an AE sensor. At least three AE sensors are needed to accurately locate the source of an AE signal on a plane. The other settings of an AE data acquisition system are signal threshold, preamplifier gain, analog filter range, and waveform parameters. The PK 301 AE sensor used in this study has an integral preamplifier with a 26 dB voltage gain. In addition, the data acquisition settings included a 40 dB preamplifier voltage gain, 45 dB threshold, 1 kHz to 1 MHz analog filter range, and waveform settings of 1MSPS sample rate, 256 μs pre-trigger, and 1k waveform length.

Once the AE sensors were mounted and the data acquisition started, AE source locations appeared on the *AE Win* source location page (Figure 4-8). The numbers 1 to 4 in blue show the

AE sensor positions while the red dots indicate the source locations. PLB signals are used to demarcate the area of interest as well as to fine-tune the data acquisition settings: preamplifier voltage gain and the signal threshold. Pencil lead breaks were performed and the waveforms were recorded. Figure 4-9 shows the source locations calculated based on the PLB signal arrival time. These source locations mark the boundaries of the area of interest for continuous monitoring. If AE activities are documented within this region, advanced AE data analysis techniques could be implemented to understand the signal characteristics to evaluate the potential signal sources. The findings can be confirmed by conducting a detailed inspection of the detail using traditional NDE techniques. This process will verify the system performance and help fine-tune the data acquisition system variables for the specific detail.

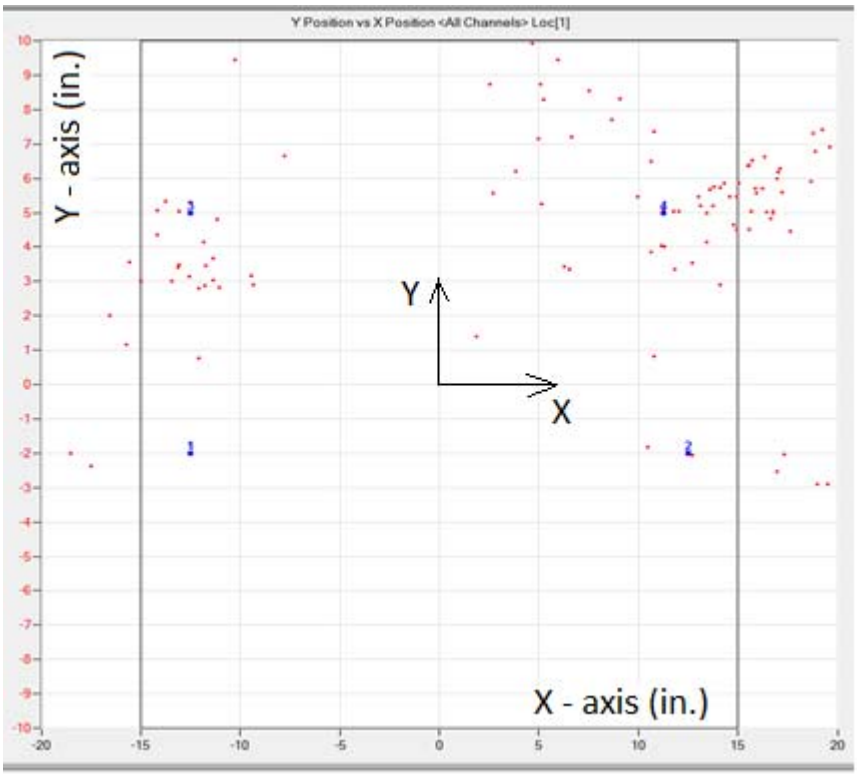

Figure 4-8. The source location page in *AE Win* showing several AE source locations

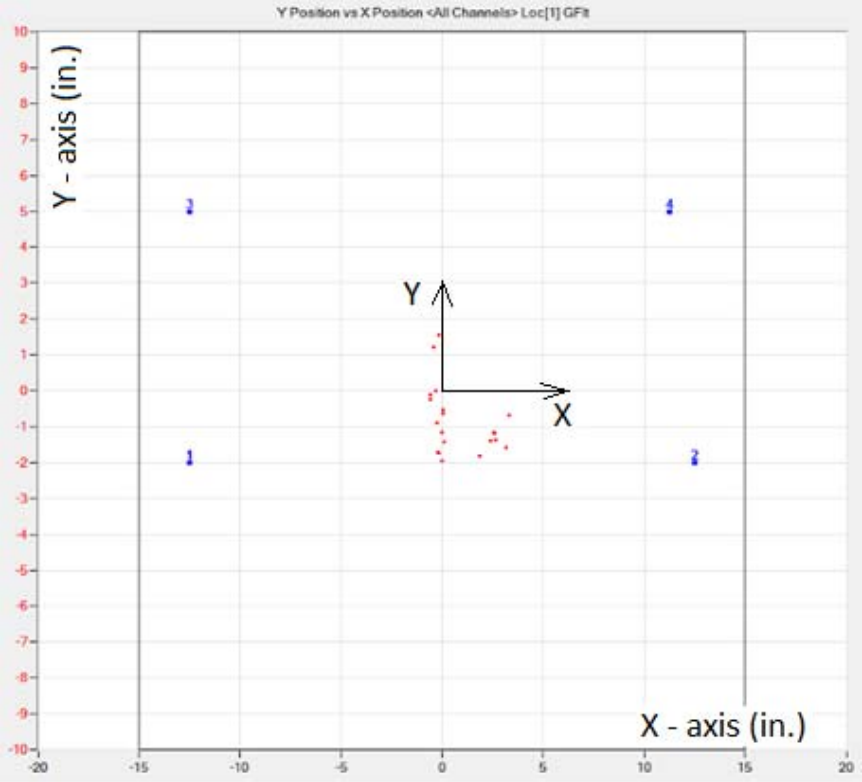

Figure 4-9. AE source locations generated through pencil lead breaks

4.1.5 Software for System Configuration, Data Acquisition, Data Display, Remote Access, and Data Transfer

AE Win is the primary software used to set up the data acquisition layout and parameters, and acquire and present AE and strain data. *Omega USB* is used to configure the temperature sensor and record data. *LogMe In* allows remote access and data transfer. Also, the *Remote Desktop Connection* can be used to access the remote computer in the SHM system. In addition, the *MS View* software program provides the SunSaver MPPT charge controller to program the charge controller and record solar power system parameters.

4.1.5.1 AE Win

AE Win allows system configuration, data acquisition, and real-time data display or data replay. A data acquisition setup layout was developed for the monitoring system based on the sensor layout that was designed based on the fatigue-sensitive detail configuration. A typical layout includes a source location display, an activity screen, and parametric data display (Figure 4-8, Figure 4-10, and Figure 4-11). *AE Win* can be used to replay recorded data. The process is depicted in Figure 4-12 and Figure 4-13.

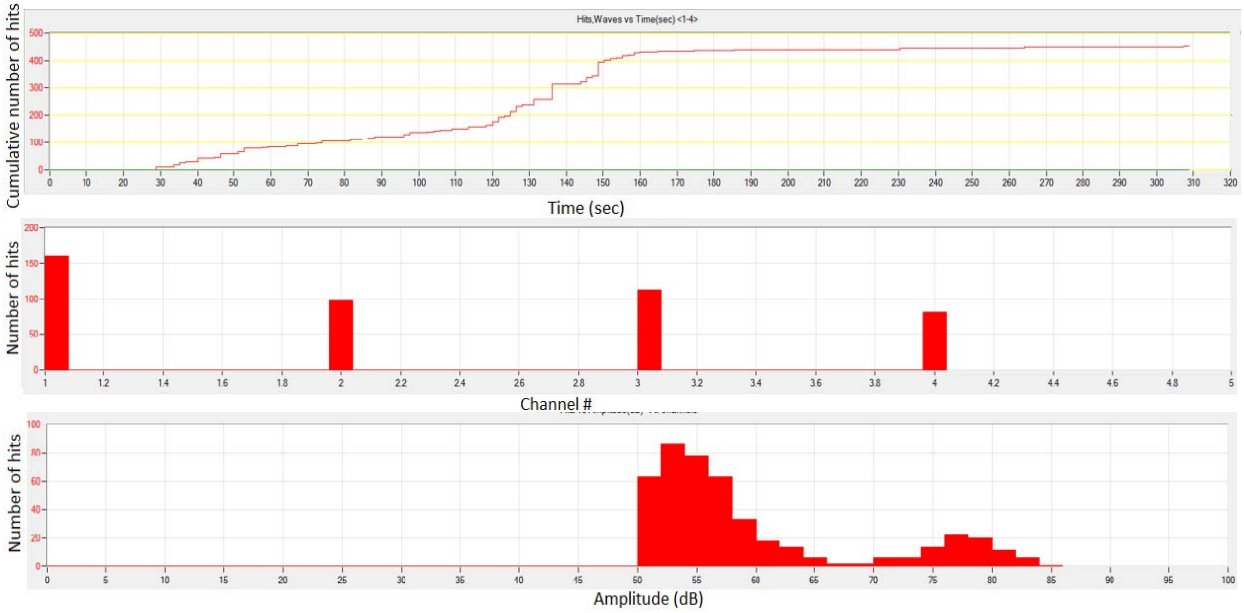

Figure 4-10. Activity screens

Figure 4-11. Parametric data display (microstrain vs. time in seconds)

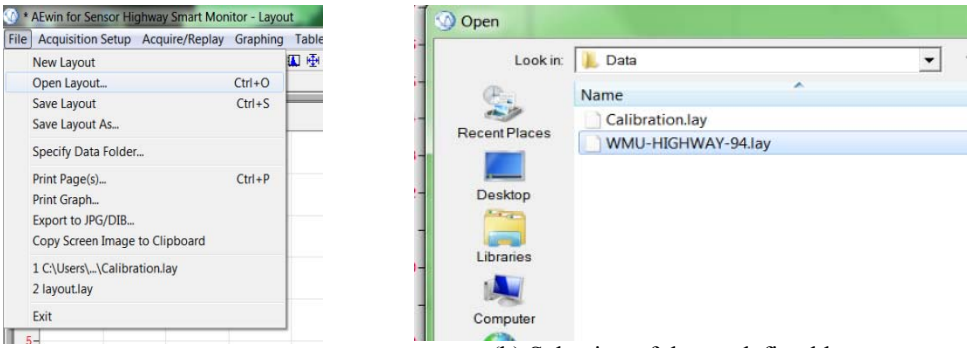

(a) Open an existing layout (b) Selection of the predefined layout

Figure 4-12. Opening an existing sensor layout

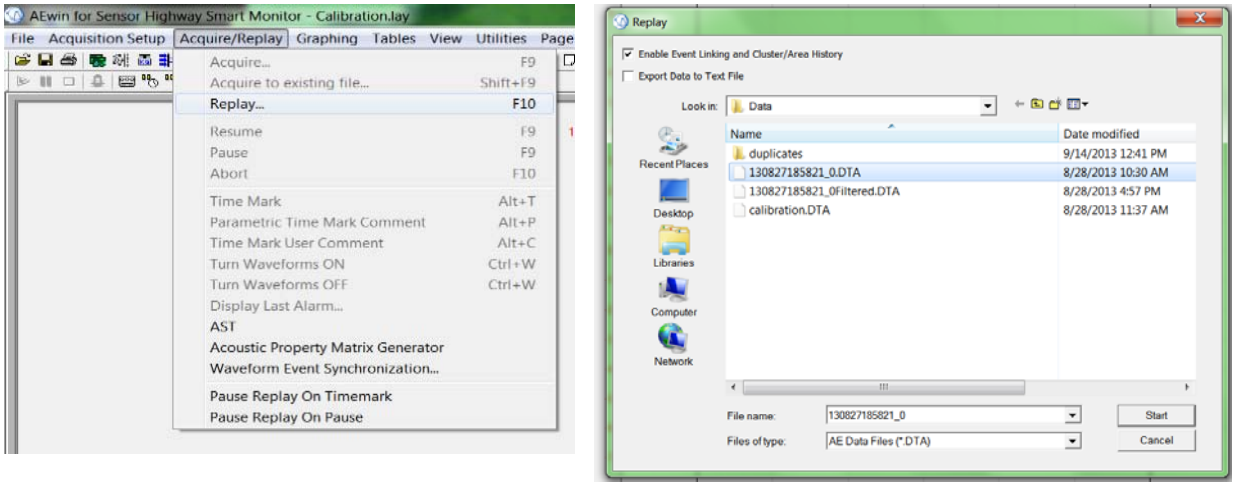

(a) Selection of replay command (b) Selection of an existing data file

Figure 4-13. Accessing an existing data file for replaying

4.1.5.2 LogMe In

LogMe In is used to access a remote computer and transfer data using a web browser (Figure 4-14).

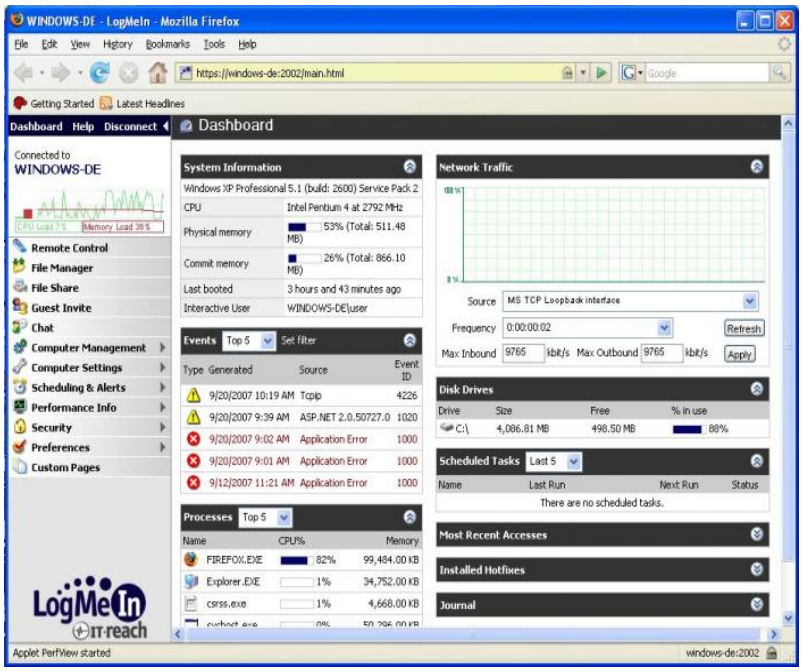

Figure 4-14. *LogMe In* interface

In addition, there is a mobile application that allows remote access and data visualization (Figure 4-15).

LogMe In logo

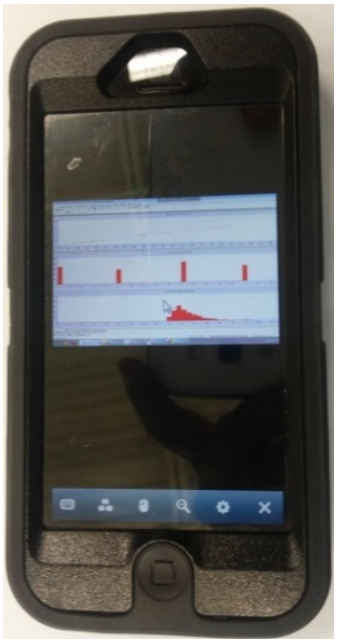

(a) Application on a mobile device (b) AE activity screen on a mobile device

Figure 4-15. Accessing the SHM system using a mobile device

4.1.5.3 MS View

The MS View software program allows users to program the charge controller and record solar power system parameters such as battery voltage, array voltage, charge current, load voltage,

load current, etc. A SunSaver MPPT can be connected to a computer in the SHM system using a PC MeterBus Adapter, RJ-11-6P6C and RS-232 cables. Using MS View software, the low-voltage disconnect (LVD) and low-voltage reconnect (LVR) thresholds can be specified, and several timers can be added to control system operation duration.

4.2 SUMMARY

A monitoring system with acoustic emission (AE) sensors was selected. Moreover, the SHM system components, field implementation, power management for field monitoring, AE monitoring system calibration, and software used for system configuration, data acquisition, data display, remote access, and data transfer were presented for an integrated implementation with most relevant considerations.

MDOT RC-1629

Remote Monitoring of Fatigue-sensitive Details on Bridges (Part II)

MARCH 2015

Research

Department of Civil & Construction Engineering
College of Engineering and Applied Sciences
Western Michigan University

Remote Monitoring of Fatigue-sensitive Details on Bridges

Project Manager: Steve Kahl, P.E.

Submitted to:

MDOT

Submitted by

Upul Attanayake, Ph.D., P.E.
Associate Professor
Western Michigan University
(269) 276 – 3217
upul.attanayake@wmich.edu

Haluk Aktan, Ph.D., P.E.
Professor
Western Michigan University
(269) 276 – 3206
haluk.aktan@wmich.edu

Robert Hay, Ph.D.
TISEC Inc.
Morin Heights, QC, Canada
(450) 226 - 6804
bobhay@structuralinsights.com

Necati Catbas, Ph.D., P.E.
Transtek International Group LLC
fncatbas@gmail.com
(321) 945-1786

Western Michigan University
Department of Civil & Construction Engineering
College of Engineering and Applied Sciences
Kalamazoo, MI 49008-5316
Fax: (269) 276 – 3211

5 DATA ANALYSIS AND SYSTEM PERFORMANCE

This chapter presents (a) a set of acoustic emission (AE) data recorded by the monitoring system and data analysis using ICEPAK™, a pattern classifier for use in real-time structural health and reliability monitoring, (b) calculation of effective stress at a web gap detail using weigh-in-motion (WIM) data and refined finite element analysis, (c) calculation of effective stress at a web gap detail using strain data from field monitoring, (d) findings related to monitoring system performance, and (d) a summary.

5.1 ACOUSTIC EMISSION DATA ANALYSIS

The goal was to examine the types of AE signals detected from fatigue-sensitive details to determine, among the different AE signals generated during normal traffic conditions, how to use these signals to assess the performance of the bridge detail.

5.1.1 Data Acquisition

AE data was recorded using four sensors arranged as shown in Figure 4-3 and Figure 4-4. Two sample data files that were recorded on July 09, 2014 and on July 11, 2014, respectively, were used in the data analysis presented in this section. The data represent AE signals captured on the bridge near the fatigue-sensitive detail under normal traffic conditions. PLB signals near the sensors were also recorded for reference.

5.1.2 Data Preprocessing

Data generated in the *AE Win* closed proprietary format (".dta") are not compatible with the ICEPAK™ software developed by TISEC Inc. The TISEC SABRE™ system components include a waveform extraction utility (WEU v 2.1) to convert *AE win* data in a format compatible with ICEPAK™. WEU v 2.1 was also used to convert to a second universal format (.wav) that is compatible with the waveform visualization software. The PRISM module enabled waveform visualization in both time and power spectral domains. ICEPAK™ was used to classify data via pre-trained classifiers designed by the ICEPAK software package.

5.1.3 Pencil Lead Break (PLB) Signals

The fracture-event representation signals generated by PLB serve as a reference to identify the presence of any significant fracture type signals within the ensemble of AE data collected under normal traffic conditions.

Typical signals present in a PLB data file are shown in Figure 5-1. The PRISM package can be used for visual inspection after converting the data to PRISM compatible .wav files. Visual inspection of signals is very important to identify the signals that are not suitable for further analysis. One such example is the presence of oversaturated signals. Use of such signals in analysis is known to produce skewed spectral characteristics that prevent reliable signal analysis.

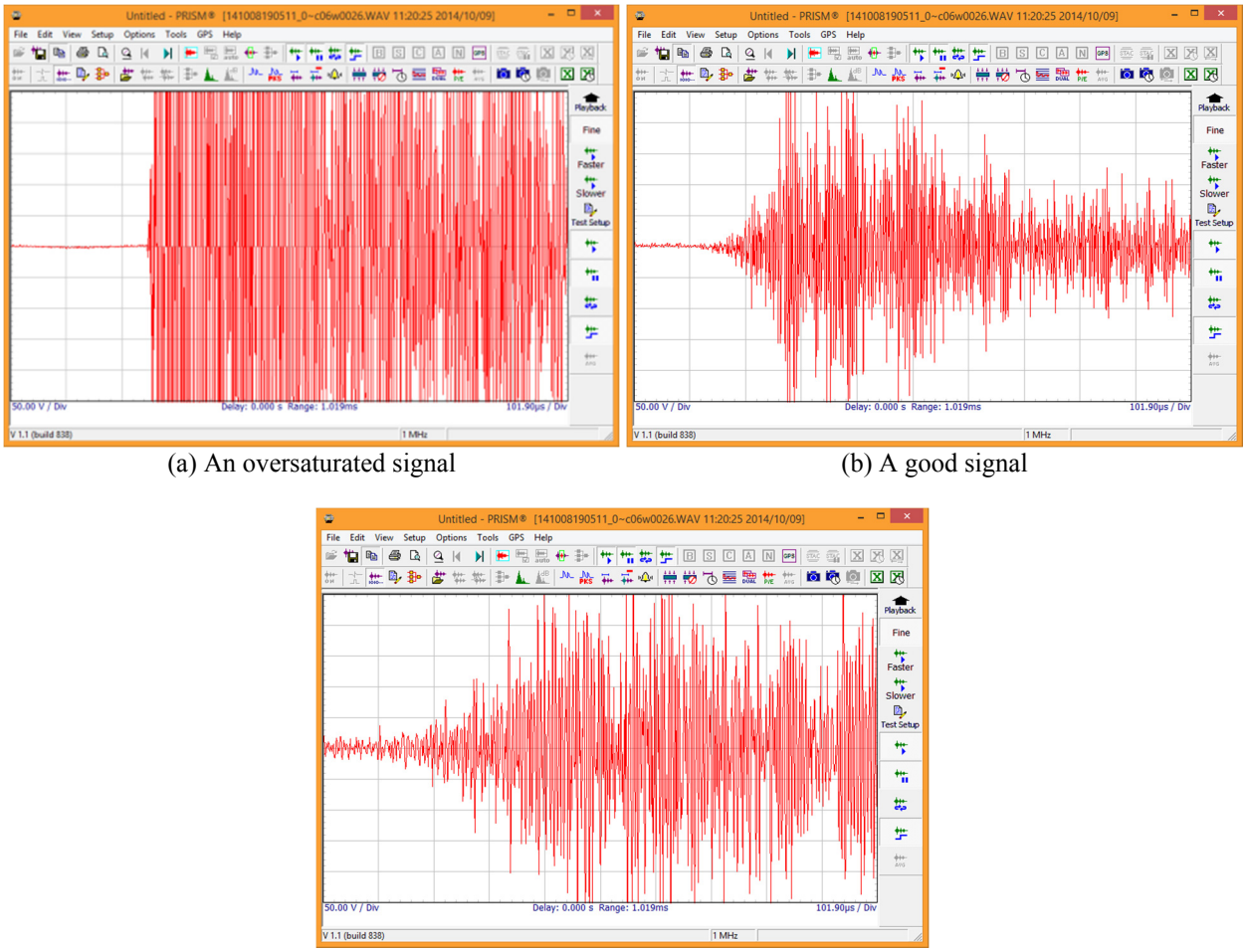

(a) An oversaturated signal

(b) A good signal

(c) A possible noise

Note: X-axis: Time (101.9 µs/Div); Y-axis: Voltage (50 V/Div)

Figure 5-1. Typical signals present in a data file

5.1.4 Unsupervised Learning via Clustering

The data collected from the bridge was examined directly to identify any significant similar AE activity formations using non-linear mapping (NLM) and clustering analysis available in ICEPAK™. NLM presents multi-dimensional data in a 2-D space and preserves the inter-data distance and directional information. If the data in the multi-dimensional space are very close to one another, the corresponding NLM should also render their closeness to one another but not their orientation.

NLM can be performed in time, power, phase, cepstral, and auto-correlation domains. The data set used for NLM and clustering analysis included little more than 11,000 AE signals that were above the set threshold of 45dB. NLM was performed using one feature domain at a time to visually detect significant naturally forming concentrations. These results are shown in Figure 5-2 to Figure 5-6. Out of the 5 domains, the spectral power domain produced three significant concentrations as shown in Figure 5-3. Clustering was performed using the same spectral power domain features, and produced three significant concentrations as presented in Figure 5-7. The clusters are aligned with the visual presentation of the NLM result. In order to make the side-by-side comparison easier, spectral power domain results from NLM and clustering are presented in Figure 5-8 and Figure 5-9. Later, as shown in Figure 5-10, the three clusters that were identified through the power domain analysis were separated for further analysis.

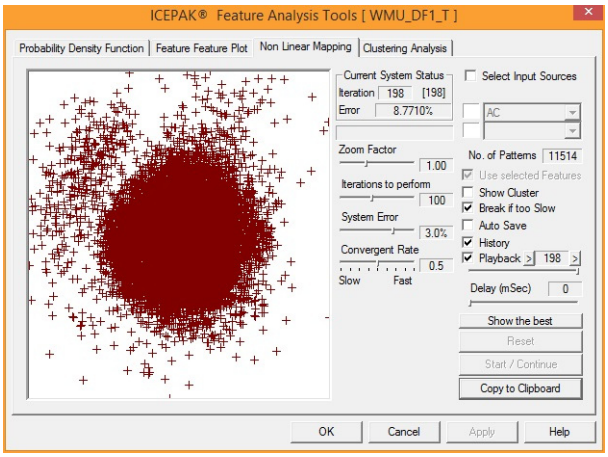

Figure 5-2. NLM Time Domain

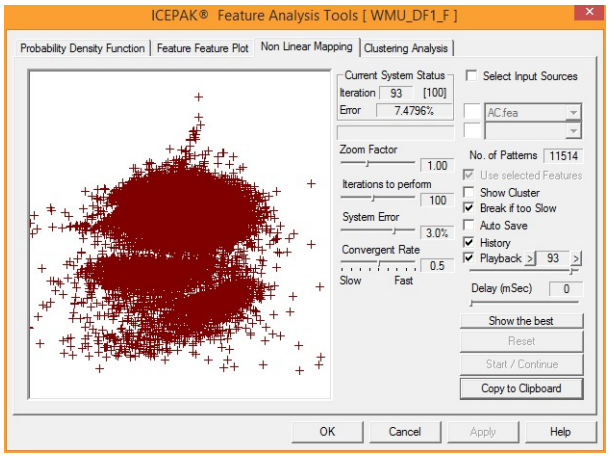

Figure 5-3. NLM Power Domain

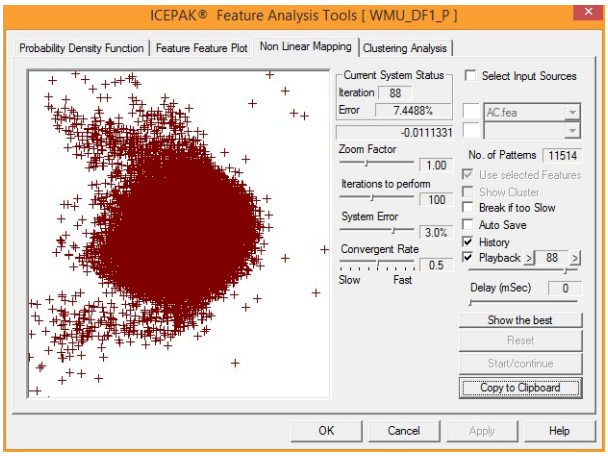

Figure 5-4. NLM Phase Domain

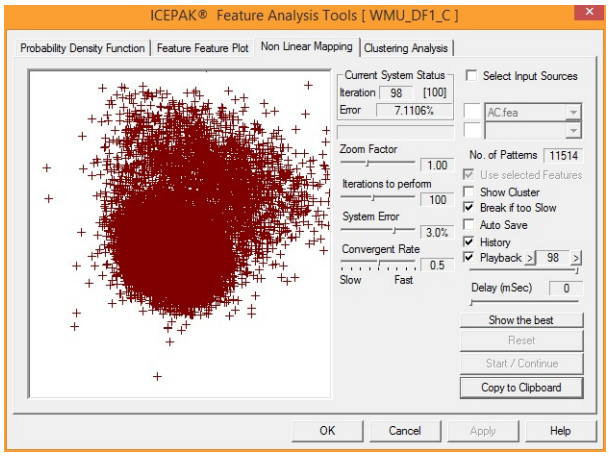

Figure 5-5. NLM Cepstral Domain

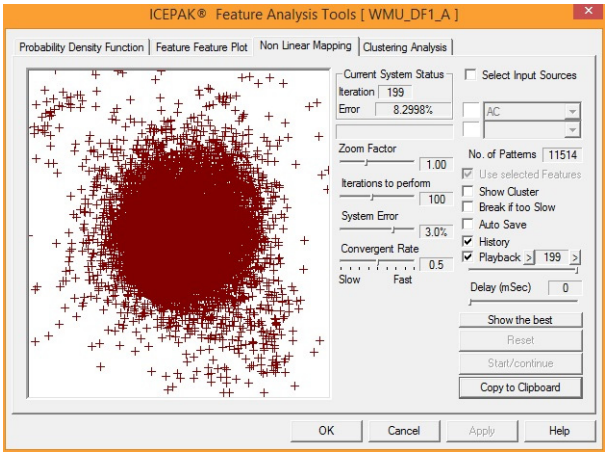

Figure 5-6. NLM Auto-Correlation Domain

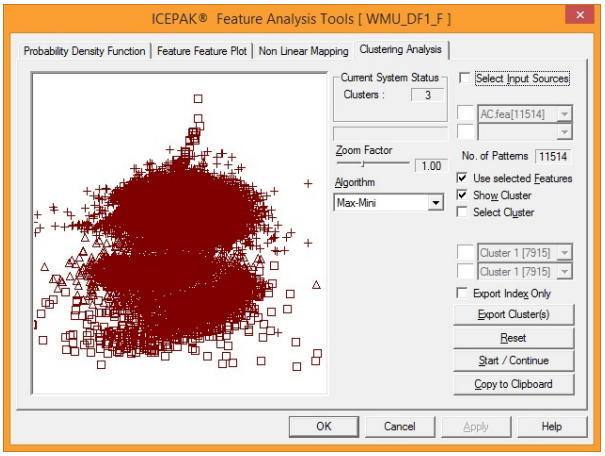

Figure 5-7. Clustering Power Domain

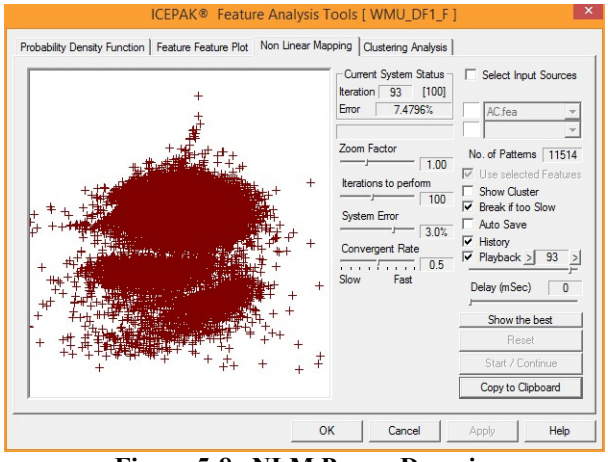

Figure 5-8. NLM Power Domain

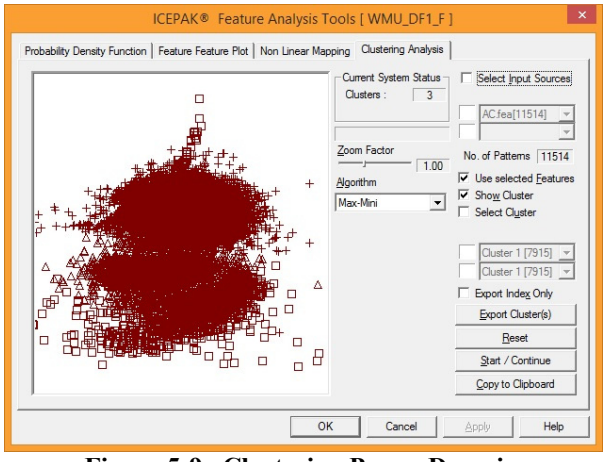

Figure 5-9. Clustering Power Domain

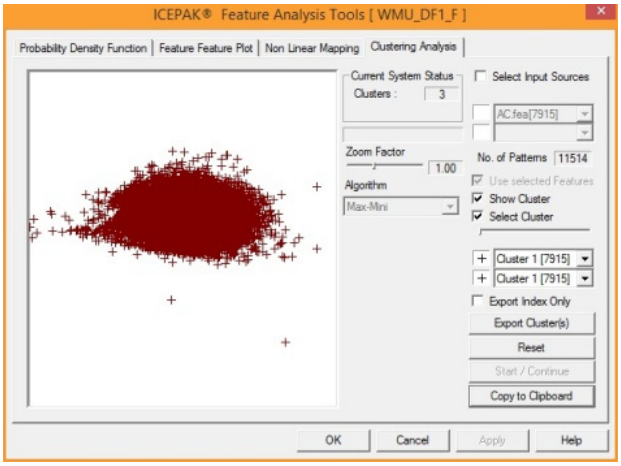

(a) Cluster 1

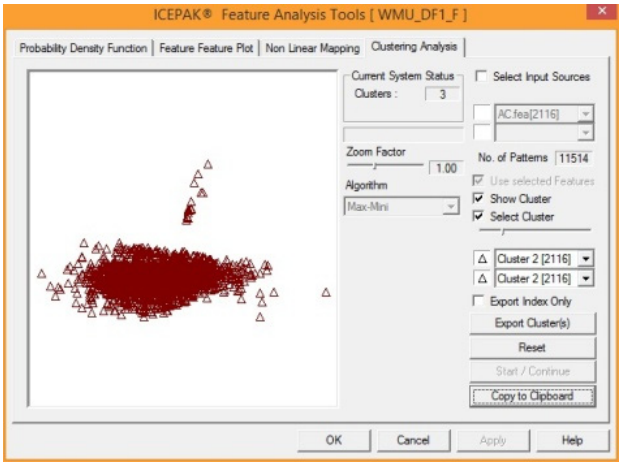

(b) Cluster 2

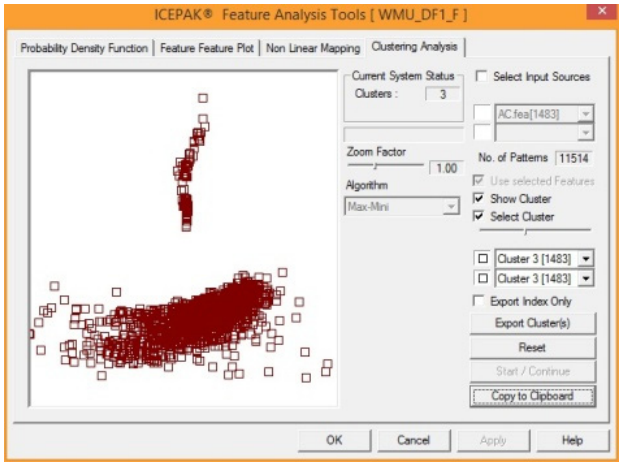

(c) Cluster 3

Figure 5-10. Individual data clusters

The individual data clusters were exported and labeled as [cl1], [cl2], and [cl3]. Then, each cluster was used to train a three-class classifier. Four statistical classifiers (i.e., linear discriminant, K-nearest neighbor, empirical Bayesian, and minimum distance classifiers) and a neural network classifier were tested. The design of the classifiers included optimizing the feature sets. The design procedure included separating available data into two groups; one was used to train the classifiers and the other to test the performance of the classifiers. The classification results are shown in Figure 5-11 to Figure 5-15. As an example, [cl1] had a total of 7,915 data points. This set was separated into two groups of 3,957 and 3,958 data points for training and testing, respectively. When the linear discriminant three-class classifier was trained with 3,957 data points, the data was classified into three classes with rejections. As shown in Figure 5-11, classes 1, 2, and 3 contain 3777, 2, and 0 data points with 178 rejections. The classification rate is 95.45%. In other words, 95.45% of the data in [cl1] falls into class 1 (i.e.,

3,777/3,957 × 100). A similar process was employed for [cl2] and [cl3] data sets, and yielded classification rates of 94.99% and 95.95%, respectively. When all three data sets were considered, the linear discriminant three-class classifier yielded a weighted average classification rate of 95.43% for training (Figure 5-11). Overall, all the classification methods yielded very high classification rates for training as well as for testing.

Linear Discriminant Classification Results

Class	1	2	3	Reject	Total	Percent
cl1.cxf	1 3777	2	0	178	3957	95.45%
cl2.cxf	2	0 1005	5	48	1058	94.99%
cl3.cxf	3	0	3 711	27	741	95.95%

Training : 95.43%

Class	1	2	3	Reject	Total	Percent
cl1.cxf	1 3822	2	0	134	3958	96.56%
cl2.cxf	2	0 995	6	57	1058	94.05%
cl3.cxf	3	0	7 715	20	742	96.36%

Testing : 96.08%

Figure 5-11. Linear Discriminant

K-Nearest Neighbors Classification Results

Class	1	2	3	Reject	Total	Percent
cl1.cxf	1 3827	2	0	128	3957	96.71%
cl2.cxf	2	98 900	23	37	1058	85.07%
cl3.cxf	3	1	48 678	14	741	91.50%

Training : 93.90%

Class	1	2	3	Reject	Total	Percent
cl1.cxf	1 3817	1	0	140	3958	96.44%
cl2.cxf	2	116 883	19	40	1058	83.46%
cl3.cxf	3	0	51 676	15	742	91.11%

Testing : 93.37%

Figure 5-12. K-Nearest Neighbors

Empirical Bayesian Classification Results

Class	1	2	3	Reject	Total	Percent
cl1.cxf	1 3758	11	0	188	3957	94.97%
cl2.cxf	2	12 971	49	26	1058	91.78%
cl3.cxf	3	0	6 702	33	741	94.74%

Training : 94.35%

Class	1	2	3	Reject	Total	Percent
cl1.cxf	1 3767	7	0	184	3958	95.17%
cl2.cxf	2	17 946	60	35	1058	89.41%
cl3.cxf	3	0	7 705	30	742	95.01%

Testing : 94.10%

Figure 5-13. Empirical Bayesian

Minimum Distance Classification Results

Class	1	2	3	Reject	Total	Percent
cl1.cxf	1 3879	0	0	78	3957	98.03%
cl2.cxf	2	2 1014	0	42	1058	95.84%
cl3.cxf	3	0	0 730	11	741	98.52%

Training : 97.69%

Class	1	2	3	Reject	Total	Percent
cl1.cxf	1 3887	0	0	71	3958	98.21%
cl2.cxf	2	2 1011	0	45	1058	95.56%
cl3.cxf	3	0	0 724	18	742	97.57%

Testing : 97.64%

Figure 5-14. Minimum Distance

Neural Network Classification Results

Class	1	2	3	Reject	Total	Percent
cl1.cxf	1 3846	0	0	111	3957	97.19%
cl2.cxf	2	0 976	0	82	1058	92.25%
cl3.cxf	3	0	48 667	26	741	90.01%

Training : 95.36%

Class	1	2	3	Reject	Total	Percent
cl1.cxf	1 3856	0	0	102	3958	97.42%
cl2.cxf	2	0 955	1	102	1058	90.26%
cl3.cxf	3	0	55 667	20	742	89.89%

Testing : 95.14%

Figure 5-15. Neural Network

Next, the PLB data was tested against this three-class classifier with a rejection option. The rejection option is triggered when an incoming signal cannot be classified with an acceptable level of confidence. The PLB data file contained 100 data points. The PLB data fell into class 1

and 2 but not class 3, with a lot of rejections. Nine data points were classified as class 1 and 8 as class 2. None was classified as class 3. There were 83 rejections.

Finally, the trained classifiers and the associated feature extraction engine were exported from the ICEPAK™ program. The AE data collected from the bridge and PLB data were also exported in the PRISM-compatible waveform format. The PRISM program waveform visualization and real time classification capability were used to identify the type of waveforms in the three classifications (i.e., in class 1, 2, and 3) along with the rejected ones. Figure 5-16 to Figure 5-18 show sample PLB signal waveforms in class 1, class 2, and the rejected group.

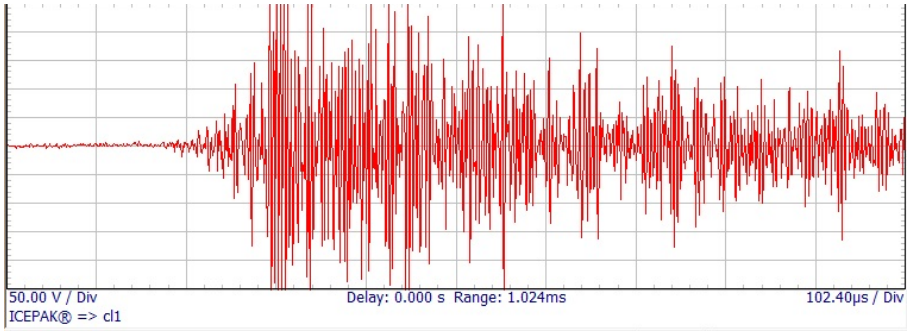

Note: X-axis: Time (102.4 µs/Div); Y-axis: Voltage (50 V/Div)

Figure 5-16. A sample PLB waveform in class 1

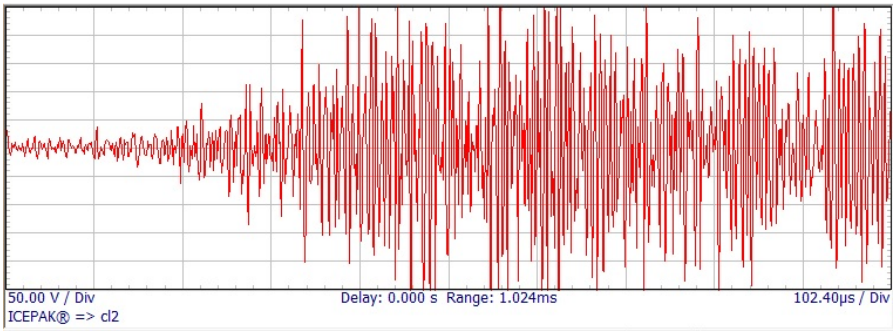

Note: X-axis: Time (102.4 µs/Div); Y-axis: Voltage (50 V/Div)

Figure 5-17. A sample PLB waveform in class 2

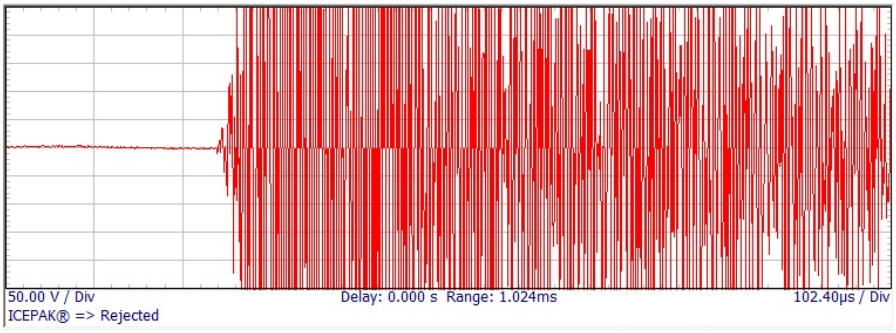

Note: X-axis: Time (102.4 µs/Div); Y-axis: Voltage (50 V/Div)

Figure 5-18. A sample rejected PLB waveform

The PRISM program was used to analyze the waveform characteristics of signals in each class and the rejected group, and yielded the following observations:

- The waveforms classified as class 1 usually have very fast rise times, relatively quiet pre-trigger portion, and a broad spectral content spanning from 100 to 400 kHz (Figure 5-19).
- The waveforms classified as class 2 usually have very fast rise times; however, the pre-trigger portion may show some small structure, and the main pocket contains multiple ringing peaks. The spectral content mainly centers around 150 kHz with very little or nothing above 250 kHz, and nothing below 100 kHz (Figure 5-20).
- The waveforms classified as class 3 usually have a slower rise time, and the spectral content is mainly located below 100 kHz and centered around 50 to 75 kHz. Moreover, there is absolutely nothing above 200 kHz (Figure 5-21).
- The waveforms classified as "rejected" are mostly associated with over-saturated clipped waveforms, and some have slow changing, somewhat smooth, waveform centered around 50 kHz (Figure 5-22).
- The number of waveforms being classified as class 1 is 4 to 6 times more than those of class 2 and class 3 while the sizes of class 2 and class 3 are relatively comparable. In general, there are about 5% of waveforms being rejected.

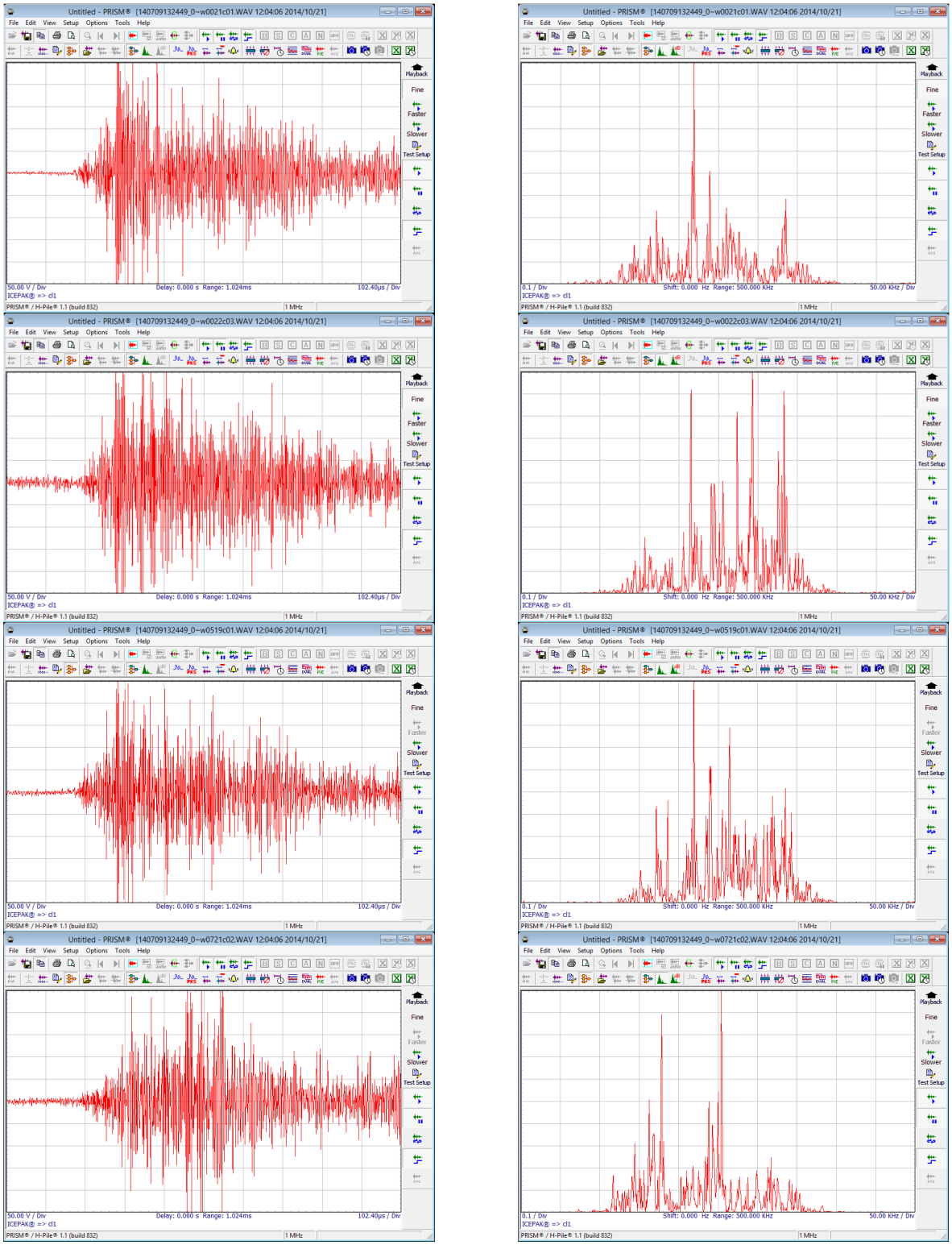

(a) Time domain

X-axis: Time (102.4 μs/Div)
Y-axis: Voltage (50 V/Div)

(b) Frequency domain

X-axis: Frequency (50 kHz/Div)
Y-axis: Amplitude (0.1/Div)

Figure 5-19. A sample class 1 waveform and its power spectrum

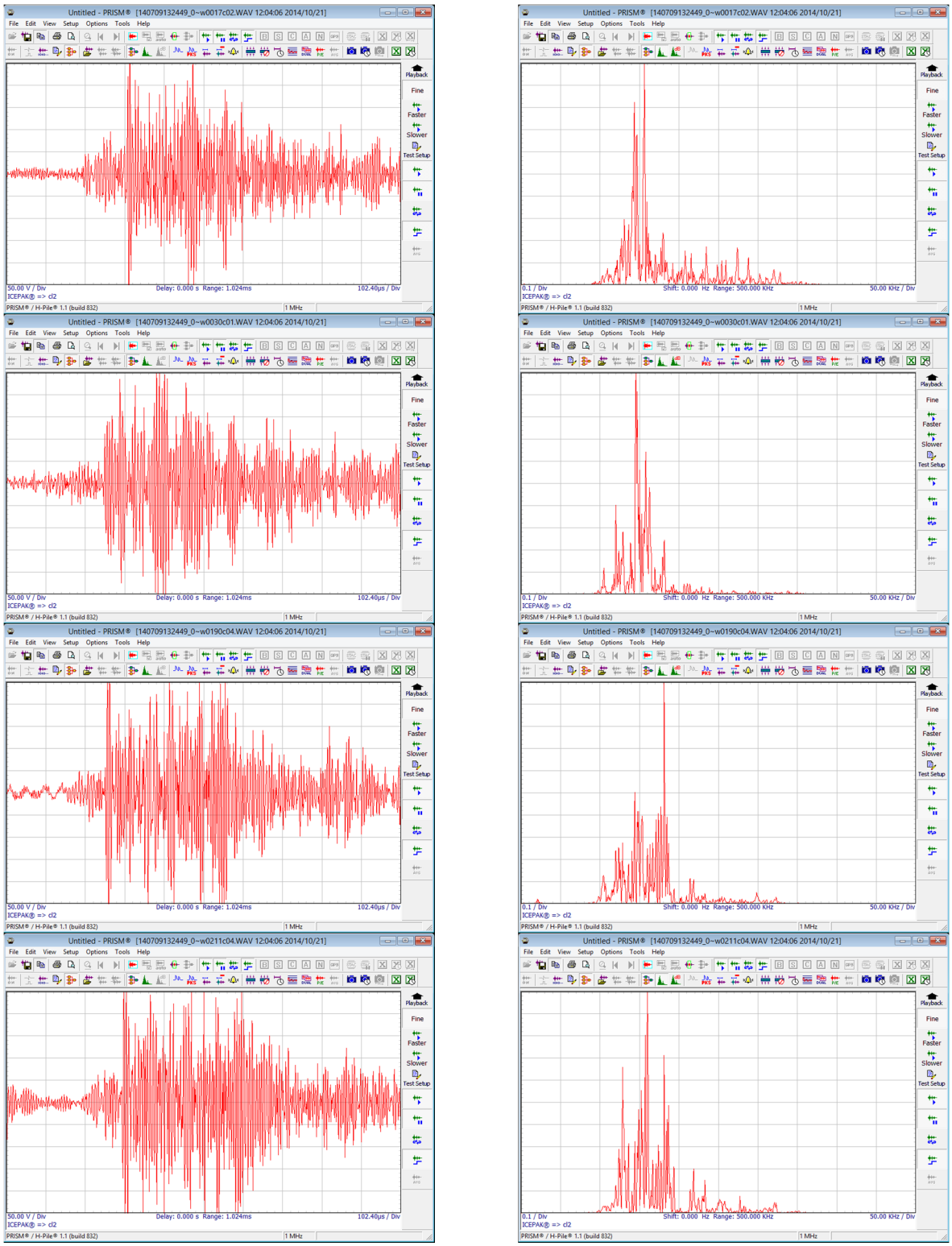

(a) Time domain

X-axis: Time (102.4 µs/Div)
Y-axis: Voltage (50 V/Div)

(b) Frequency domain

X-axis: Frequency (50 kHz/Div)
Y-axis: Amplitude (0.1/Div)

Figure 5-20. A sample class 2 waveform and its power spectrum

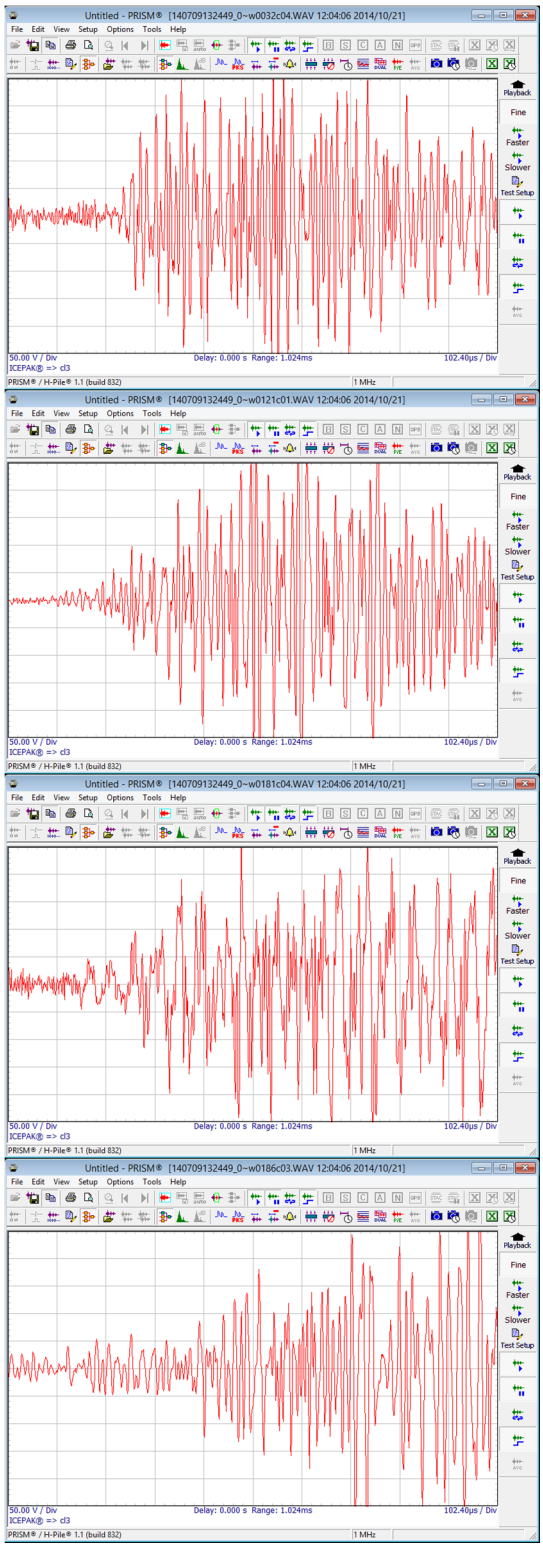

(a) Time domain

X-axis: Time (102.4 μs/Div)
Y-axis: Voltage (50 V/Div)

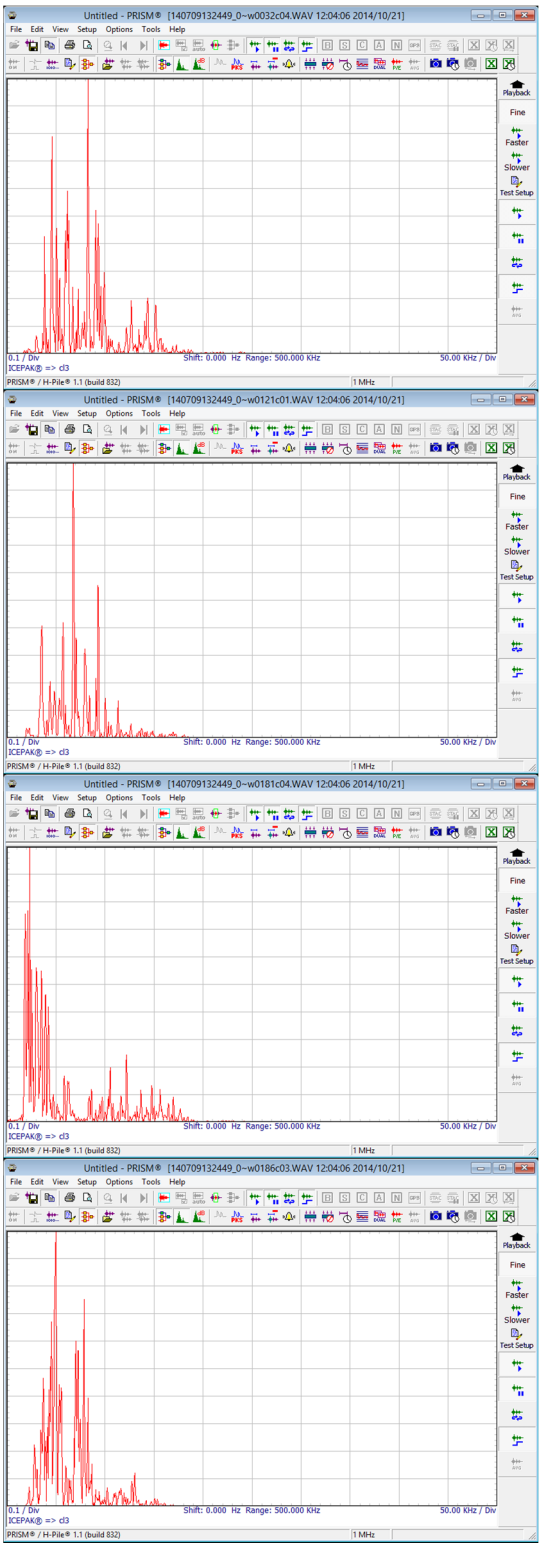

(b) Frequency domain

X-axis: Frequency (50 kHz/Div)
Y-axis: Amplitude (0.1/Div)

Figure 5-21. A sample class 3 waveform and its power spectrum

(a) Time domain

X-axis: Time (102.4 µs/Div)
Y-axis: Voltage (50 V/Div)

(b) Frequency domain

X-axis: Frequency (50 kHz/Div)
Y-axis: Amplitude (0.1/Div)

Figure 5-22. A sample "rejected" waveform and its power spectrum

5.1.5 AE Data Analysis Observations

There are two general types of fracture-related AE activities observed under cyclic loading conditions: crack tip opening during increased loading (upward load cycle) and crack face rubbing during decreasing load (downward cycle). This observation and correlation of the AE activities was derived largely based on past railroad bridge inspection experience of TISEC Inc.

The observations of sample data analysis show that both class 1 and class 2 waveforms are more structured with a faster rise time at the beginning of the waveform. Thus, they are associated with the AE signals from the crack opening. Even though class 1 and class 2 waveforms represent characteristics of crack opening signals, more accurate characterization requires having access to AE signals that represent properties of steel used in the bridge, component dimensions, exposure conditions, etc. Class 3 waveforms are more slowly rising, and their spectral content is more in line with common background transient noise. The rejected waveforms are more likely due to saturation and clipping of the signal, and the non-saturated ones, centered around 50 kHz are more likely results from structural resonance.

Since class 1 and 2 waveform characteristics closely represented AE signals from the crack opening, the source location plots were analyzed. As shown in Figure 5-23, there were no active sources documented within the zone of interest. Therefore, further analysis was not performed. When AE sources are located within the zone of interest, the following steps can be followed to validate the presence of potential cracking or crack opening events:

- Check the waveforms (Figure 5-24) to evaluate the resemblance of signals to the crack opening signals.
- Observe the source location plots for the formation of data clusters and the cluster growth direction.
- Correlate AE events with the strain data from the strain gage that is mounted to develop the load matrix. If AE events occur during increase in strain, there is a potential for the presence of a crack opening event.
- If the observations of the above steps require additional investigations, make a field visit and perform NDE to confirm the observations.
- If NDE fails to identify cracking, adjust signal thresholds and gains to calibrate the monitoring system for the specific detail.

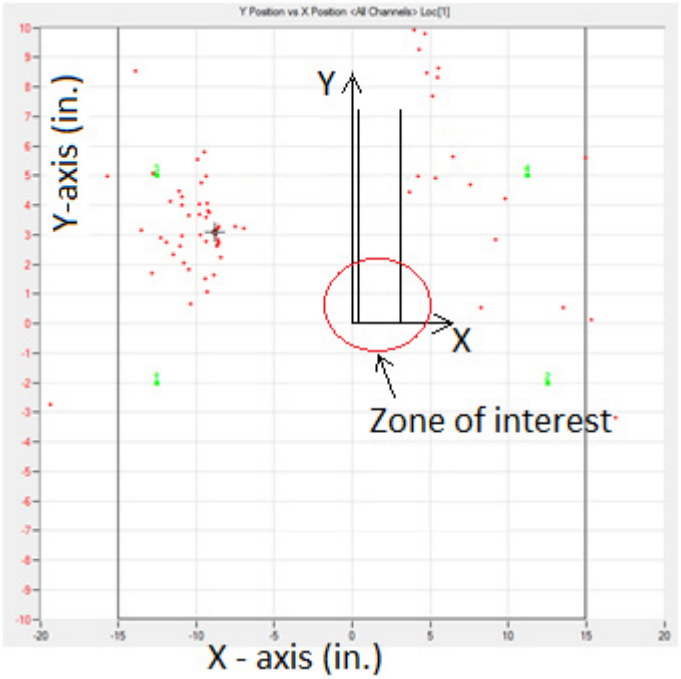

Figure 5-23. AE source location plot

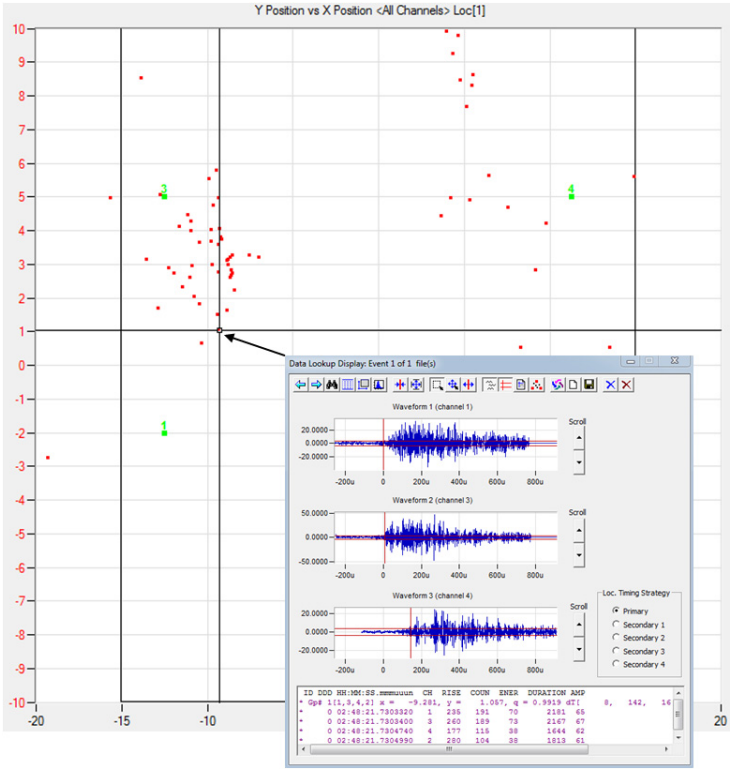

Figure 5-24. Waveform observation

5.2 FATIGUE PERFORMANCE EVALUATION

5.2.1 WIM Data and Hot Spot Stresses

WIM data was obtained for I-94 EB from a station located in Berrien County, City of New Buffalo. The station is located 22.5 miles west of the bridge site. The data covers 11 months of a year, except August due to a corrupted data file. According to the data, the bridge carries 48,500 vehicles daily, with 30% of the vehicles being trucks (i.e., ADTT of 14,550). Of the trucks, 84.6% travel in the outer lane (i.e., 12,309 trucks).

The gross weight of the fatigue truck was calculated following the Guide Specifications for Fatigue Evaluation of Existing Steel Bridges (AASHTO 1990), Section 2, Alternative 3, and weigh-in-motion data. Use of 11 month data yielded the gross weight of 57 kips. Following the AASHTO LRFD (2013) Article 3.6.1.4, an impact factor of 15% and a constant spacing of 30 ft between the main axles were used in analysis. As per the MBE (2011), 75 percent of the stress calculated using the fatigue truck with impact was used. Following the procedure discussed in section 3.6, fatigue truck load with impact was applied, and the weld toe stresses at L_1 web gap were calculated (Table 5-1). As per the MBE (2011) commentary C7.2.2.2, a multiplier less than two can be used to calculate the maximum stress range when the fatigue truck load is greater than 54 kips. However, a factor of two was considered to yield a conservative result. With the factor of two, the maximum stress range, $(\Delta f)_{max}$, ranges from 10.54 ksi to 10.88 ksi.

Table 5-1. HSS at L_1 Weld Toe due to Fatigue Truck Load

Reference point location from weld toe	Distance from weld toe with t = 0.545 in. (in.)	Stress in Y-direction (SYY) (ksi)	
		Fixed Abutment	Pinned Abutment
0.4t *	0.218	3.75	3.87
0.9t	0.491	2.52	2.60
1.4t	0.763	2.03	2.10
*t = web thickness	**Hot Spot Stress (ksi)**	5.27	5.44

According to Hobbacher (2008), all applicable load effects need to be superimposed. Pook (2007) indicated that the residual stresses affect fatigue performance in the same manner as the mean applied stress. As presented in section 3.6.5.2, depending on the girder end fixity over the abutment, hot spot stress at the L_1 web gap due to cast-in-place concrete deck weight ranges from 6.57 ksi to 9.14 ksi. According to the statements presented in Hobbacher (2008) and Pook (2007), the fatigue evaluation of L_1 detail requires combining deck weight effects and the fatigue truck induced stress. Following the procedure discussed in section 2.3.4, hot spot stress and S-N

curves can be used to evaluate fatigue performance. The L_1 web gap detail is a Category C' detail with a constant-amplitude fatigue threshold (CAFT) of 12 ksi. As discussed in section 2.3.4, the use of S-N curve with hot spot stress for fatigue performance evaluation requires modifying the values using a hot spot stress ratio between reference detail and the detail to be assessed. In order to simplify the calculation procedure presented herein, the S-N curve and the CAFT values were used without any modifications. When the combined effect of cast-in-place deck load and the fatigue truck is considered, the maximum effective stress, $(\Delta f)_{max}$, ranges from 17.11 ksi to 20.02 ksi. When compared with the CAFT of 12 ksi, the detail will have a finite fatigue life.

5.2.2 Hot Spot Stresses from Field Measured Strain Data

Three strain gages were mounted at the L_1 web gap to calculate weld toe stress (Figure 4-5). As per the hot spot stress calculation guidelines presented in Hobbacher (2008), the gages were mounted at a 0.4t, 0.9t, and 1.4t distance from the weld toe. In this particular instance, *t* is the thickness of the girder web. Figure 5-25, Figure 5-26, and Figure 5-27 show a set of sample strain data collected during the study. The strain data collected using each gage was multiplied by the steel modulus of elasticity, 29,000 ksi, to calculate the stresses at respective locations (i.e., $\sigma_{0.4t}$, $\sigma_{0.9t}$, and $\sigma_{1.4t}$). Then the hot spot stress (HSS) was calculated using Eq. 5-1 as a time series. The ASTM E1049-85 rainflow counting algorithm was used to calculate stress ranges and the respective number of stress cycles. Finally, the measured effective stress range, Δf, was calculated using Eq. 5-2.

$$2.52\,\sigma_{0.4t} - 2.24\,\sigma_{0.9t} + 0.72\,\sigma_{1.4t} \tag{5-1}$$

$$\Delta f = (\Sigma \gamma_i \Delta f_i^{\,3})^{\frac{1}{3}} \tag{5-2}$$

where, γ_i = fraction of cycles at a particular stress range and Δf_i = midwidth of the particular stress range.

According to the procedure given in MBE (2011), the effective stress is calculated using Eq. 5-3. When strain data is collected through field measurements and the mean fatigue life is to be calculated, the stress-range estimate partial load factor, R_s, is taken as 1.

$$(\Delta f)_{eff} = R_s(\Sigma \gamma_i \Delta f_i^{\,3})^{\frac{1}{3}} \tag{5-3}$$

Section 7 of MBE (2011) notes that field measurements are the most accurate way to estimate the stresses acting on a bridge of interest; however, the maximum stress range is unlikely to be observed by collecting data within a limited duration. As a result, the MBE (2011) recommends using the maximum stress range of twice the measured stress range, i.e., $(\Delta f)_{max} = 2(\Delta f)_{eff}$.

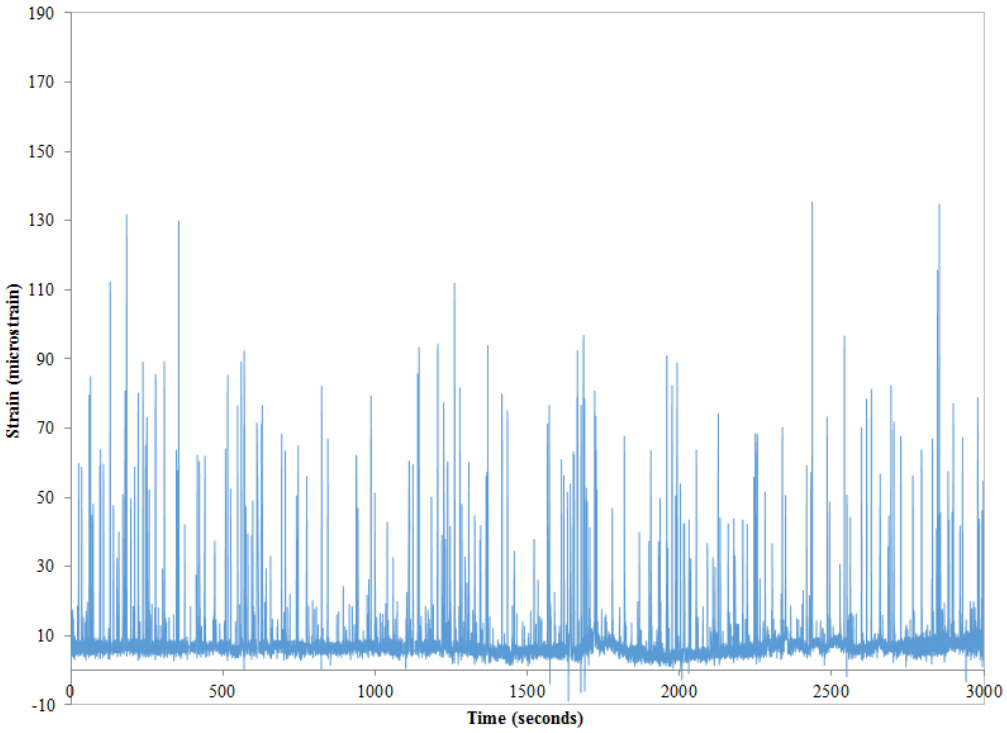

Figure 5-25. A sample strain profile collected at 0.4t

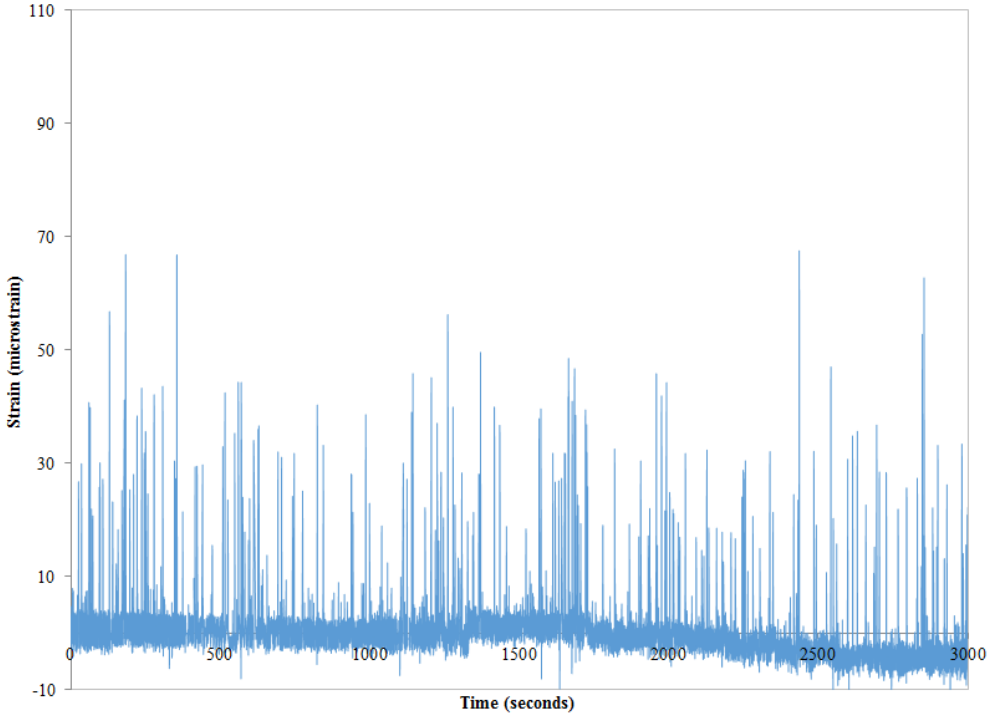

Figure 5-26. A sample strain profile collected at 0.9t

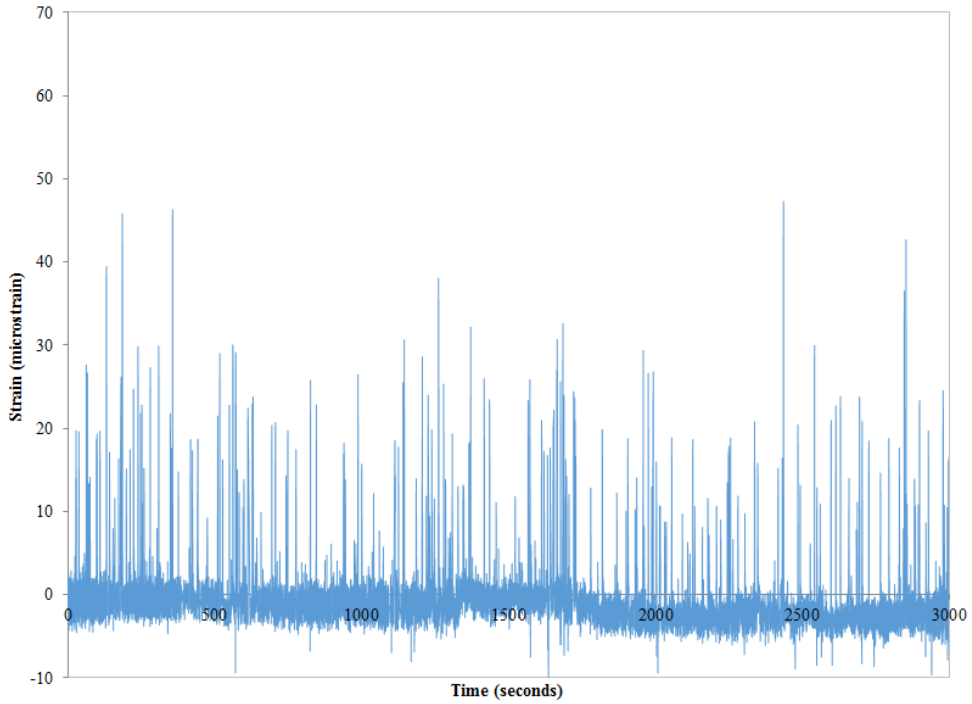

Figure 5-27. A sample strain profile collected at 1.4t

Hobbacher (2008) presented a procedure to use S-N curves with hot spot stresses (See Section 2.3.4 for details.) Even though hot spot stresses are used in this section for fatigue performance evaluation using measured strains, the S-N curve and the CAFT value of Category C' detail were

used without any modifications. Even if all the stress cycles are counted, the effective stress range, $(\Delta f)_{eff}$, calculated using strain data recorded at the web gap is only 0.8 ksi. As per the MBE (2011), the maximum stress range is1.6 ksi, which is twice the effective stress range [i.e., $(\Delta f)_{max} = 2(\Delta f)_{eff} = 1.6$ ksi]. When the stresses induced by the cast-in-place deck dead load is included, the $(\Delta f)_{max}$ ranges from 12.14 ksi to 12.48 ksi, which is slightly greater than the CAFT of 12 ksi, and it can be safely assumed to have an infinite fatigue life. However, the maximum stress ranges calculated using strain data are much smaller than the stresses calculated using fatigue truck loads based on WIM data. Above all, the cast-in-place concrete deck weight has generated very high stresses at the weld toe and requires further investigations.

5.3 RELIABILITY PERFORMANCE OF THE MONITORING SYSTEM

5.3.1 AE and Strain Data Acquisition

As presented in section 4.1.1, the monitoring system has a low power computer with a single AE board and 4 AE sensors. Channel 1 of the AE board malfunctioned after one year and two weeks from system installation on the bridge. The Mistras Inc. had a one-year warranty for the system, and the board was repaired and tested as per the warranty terms even though the warranty time had briefly expired. The diagnostic report stated "*the dual ADC IC at location U14A failed, the part number 13.04840 was replaced, and then retested channel 1 and the other three channels for signal amplitude and noise levels*." Other than the aforementioned channel 1 malfunction, the system was performing as expected.

The Mobile Broadband 5GB data plan from Verizon Wireless and Sierra Wireless – AirLink GX400 modem were used for communication and data transfer. The monitoring system is capable of acquiring strain data at a fast rate adequate to capture traffic-induced strain. However, real-time display of data from 12 strain gages and 4 AE data channels significantly slows down the display speed. The objective of this study was to monitor a targeted detail using a limited number of sensors. The real-time display of data from 4 AE sensors and the strain gage (for developing the load matrix) was satisfactory. Also, the delay in real-time display, wireless communication and data transfer speed is satisfactory.

5.3.2 Remote Access

LogMe In Pro software allows remote access and data transfer. Figure 5-28 shows a few menu options available in *LogMe In Pro*. *Remote Desktop Connection* can be used to access the remote computer in the SHM system. At several instances, operating *LogMe In Pro* features did not work due to an incompatibility between *LogMe In* and *Remote Desktop Connection*. When *LogMe In Pro* is activated following *Remote Desktop Connection*, the file transfer feature through *File Manager* becomes inactive. Further, once the *Remote Control* panel is accessed, a blank window opened and showed the message: "*Terminal Server Display is Inactive*." This problem was rectified after restarting the system using the *Reboot* option available under the *Computer Management* pulldown menu in *Log Me In Pro*. At one time, the system was in operation but could not access using *Log Me In Pro*. Hence, *Remote Desktop Connection* was used and gave access to *Log Me In* technical support using the logmein123.com website. Technical support provided a code over the phone to enable the web access. The Pro version of *Log Me In* was installed remotely, and the system was rebooted using the rebooting program available on the desktop.

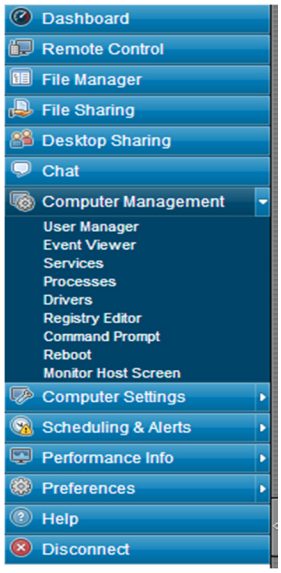

Figure 5-28. Menu options available in *LogMe In Pro*

5.3.3 Data Replay

AE Win can be used on a computer without an AE data acquisition board in the office to replay data downloaded from the remote monitoring system. When an AE board is not connected to the computer, the warning shown in Figure 5-29 appears. Once the "OK" button is selected, a

template file is loaded. If needed, the reasons for the warning can be viewed in the *error.log* file in the default folder. In order to replay data, a sensor layout file (**.lay*) that is developed for the particular bridge needs to be opened before replaying the data file. At several instances, the software crashed, and the message shown in Figure 5-30 appeared. Sometimes, this problem was rectified by opening a default layout file before opening the user generated bridge specific layout file.

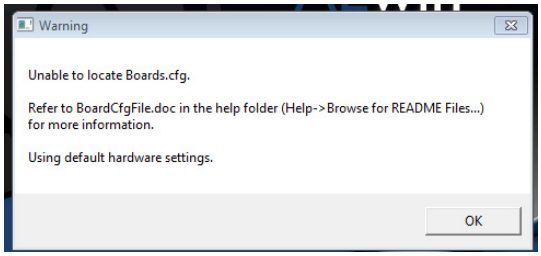

Figure 5-29. A warning message that appears when data replay program is opened

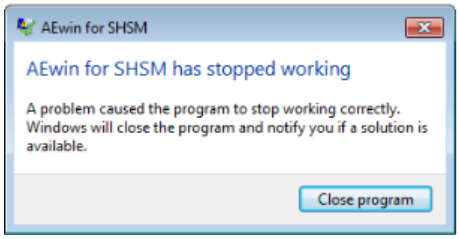

Figure 5-30. Program closure warning

5.3.4 System Reboot

As discussed in section 4.1.1, the computer should be rebooted using the rebooting program available on the desktop. It is very important to follow the rebooting sequence especially when the system is remotely located.

5.3.5 MS View

MS View program is used to display and record solar power system data (See section 4.1.5.3 for more details.) However, when the MPPT charge controller is programmed using *MS View*, it requires disconnecting and reconnecting the data cable manually from the computer in order to establish data communication. Otherwise, the MPPT charge controller is not identified by the *MS View* software. This requires programming the MPPT charge controller and evaluating the proper functioning of the device before incorporating the device in a remote monitoring system.

5.3.6 Solar Array

As the first step in solar power system performance evaluation, performance of the MPPT charge controller was evaluated under laboratory conditions using a constant voltage power supply. Figure 5-31 shows power supply (array) voltage, battery voltage, charge current, and load current. Initially, a load (other than the monitoring system) was connected and allowed to drain charge from the battery without supplying power from the array. As shown, the load drains a constant current of 1.70 A while the battery voltage drops steadily. When the battery voltage is about 11.8 V, array voltage was increased up to 17.4 V, and the charging cycle was started. As soon as the charging cycle started, there was an increase in battery voltage. The battery voltage was steadily increased to 14 V while the current drawn by the load was retained at 1.70 A. Once the battery voltage reached the preset maximum of 14 V, the absorption stage of the charging cycle began, and the battery voltage was maintained. When the battery voltage reached the maximum, there was an artificial increase in array voltage, but the charge current decreased. During the absorption duration, the charge current dropped gradually until it reached the load current of 1.70 A. The charge current and the load current remained at this value as long as the array voltage is maintained at a voltage above the battery voltage.

A typical discharge, charge, absorption, and float cycles are shown in Figure 5-32. During laboratory testing, the float cycle was not observed even after 5.5 hours. Also, when the power supply (array) voltage was disconnected, a sudden drop in battery voltage was observed (Figure 5-32).

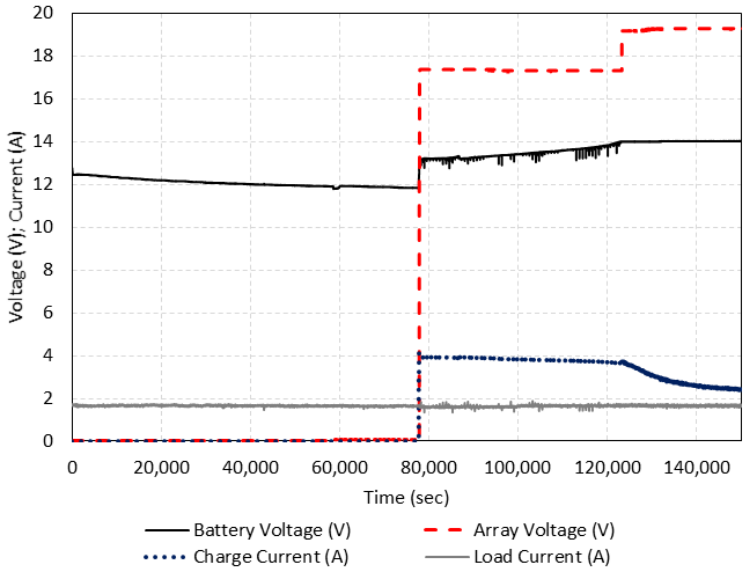

Figure 5-31. Battery charging and discharging evaluation under laboratory conditions

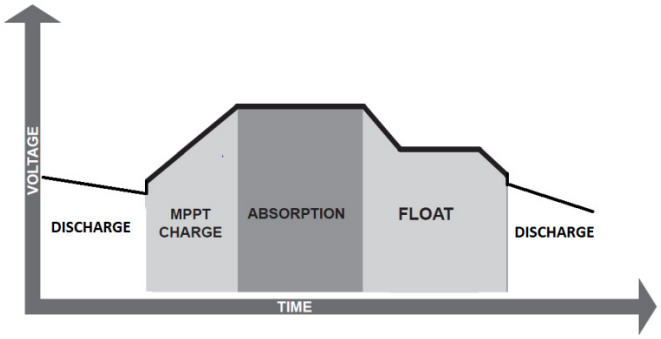

Figure 5-32. Theoretical battery discharge and recharge cycle

The solar array system performance was evaluated under field conditions. The data logging capability of the MPPT charge controller enabled the measurement of array voltage, array power, battery voltage, charge current, load current, exposure condition, and several other parameters. The solar power system performance was evaluated during the month of July, 2014. During the system evaluation period, the charge controller provided an average gain of 19% to the current produced by the solar panel, with peaks in current gain during peak sunshine hours of 34%. This average gain was lower than expected, but it was well within the range of 10% to 35% recorded in the operational manual. By knowing array power and voltage, the charge produced by the array was calculated (i.e., array power/array voltage). Experiments conducted under laboratory conditions showed negligible losses during power conversion (i.e., Power In ≅ Power Out). Hence, by knowing the charge current recorded by the software and the array power, charge voltage is calculated (i.e., array power/charge current). Figure 5-33 shows recorded array

voltage and charge current as well as the calculated charge voltage and array current. Figure 5-33 shows the ability of the MPPT charge controller to increase the charge current to yield a greater efficiency in charging a battery.

The MPPT LVR and LVD thresholds were set to 13.6 V and 11 V, respectively. The targeted maximum battery voltage was set to 14 V. During this evaluation, absorption period in the battery charging cycle was not included. Hence, as soon as the targeted voltage of 14V was reached, the charge current supply to the battery was automatically disconnected from the charge controller. The objective was to check if the power supply was going to resume once the battery voltage drops but before reaching the LVD. Figure 5-34 shows the variation of battery voltage (V) and array voltage (V) during a typical day. As shown in the figure, during the period A (2 hours) and B (5.5 hours), the battery bank was not efficiently charged even if the array voltage was higher than the battery voltage. Figure 5-35 shows a repeat of similar charge and discharge cycles during more than 4 consecutive days of operation. The performance could have increased by including absorption period in the charging cycle as long as the array voltage remained at a value greater than the battery voltage (Figure 5-31 and Figure 5-32).

As shown in Figure 5-35, the charge controller was not able to charge the battery bank to up to 14 V. The observed maximums were 13.78 V (July 1), 13.56 V (July 2), 13.59 V (July 3), and 13.33 V (July 4). The observed lower voltages were 11.61 V (July 1), 11.39 V (July 2), 11.27 V (July 3), and 11.16 V (July 4). Even though it is not documented in the user manual, the data recorded during this evaluation shows that there is a relation between LVD and the restart of the battery charging cycle. Because of these reasons, once the maximum battery voltage is reached, the charge controller does not charge batteries to keep at the maximum voltage even if adequate power is harvested by the panels.

According to the data collected under specific site conditions with an average solar insolation of 5.85 kWh/m^2 per day in the month of July, the total charge harvested by the 140 W array was 50.8 A-hrs/day. In addition to the solar array efficiency, the MPPT charge controller efficiency also contributed to yield a 50.8 A charge. During the same period that the array was harvesting solar energy and charging the batteries; the load consumed was 30 A-hrs. Hence, only 20 A-hrs were remaining to operate the load when the panel was not harvesting energy. During that time,

the monitoring system (the load) consumed an average charge of 2.35 A. Hence, without any losses, the maximum duration that the system can operate using the remaining 20 A-hrs is 8.5 hrs (20 A-hrs/2.35 A). Hence, in order to continuously operate a system that draws 2.35A under varying exposure conditions during summer requires a larger solar array, an extended battery bank, and exploring the optimum settings of the MPPT charge controller to use solar energy efficiently. In a nutshell, a solar power system needs to be designed based on the power demand, duration of monitoring, expected duration for power storage, time of the year, site location (latitude and longitude), and other site specific parameters that will reduce solar exposure on the panel. Therefore, the time of year and site location are two critical parameters in the design of a solar power system. As an example, the National Renewable Energy Laboratory (NREL 2014) presents the photovoltaic (PV) solar radiation data, and southwest Michigan receives solar radiation of about 2 $kWh/m^2/day$ during December and January while it is about 4.5 – 5.5 $kWh/m^2/day$ during July and August. Further, the ambient temperature during December/ January falls well below freezing. Under such exposure conditions, battery power output drops to about 60% of its capacity. Similarly, if the battery temperature is about 95^0F, battery service life is reduced by half. Therefore, solar array capacity needs to be sized based on the solar radiation while the battery bank needs to be sized by considering the exposure condition in addition to all other requirements.

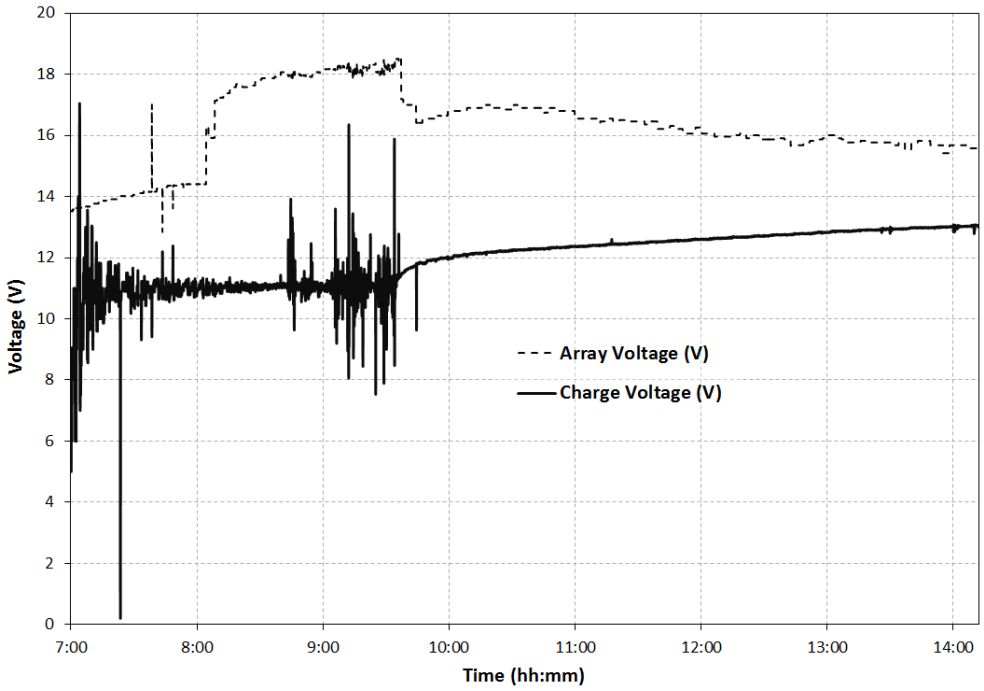

(a) Variation of array voltage and charge voltage during a charging period

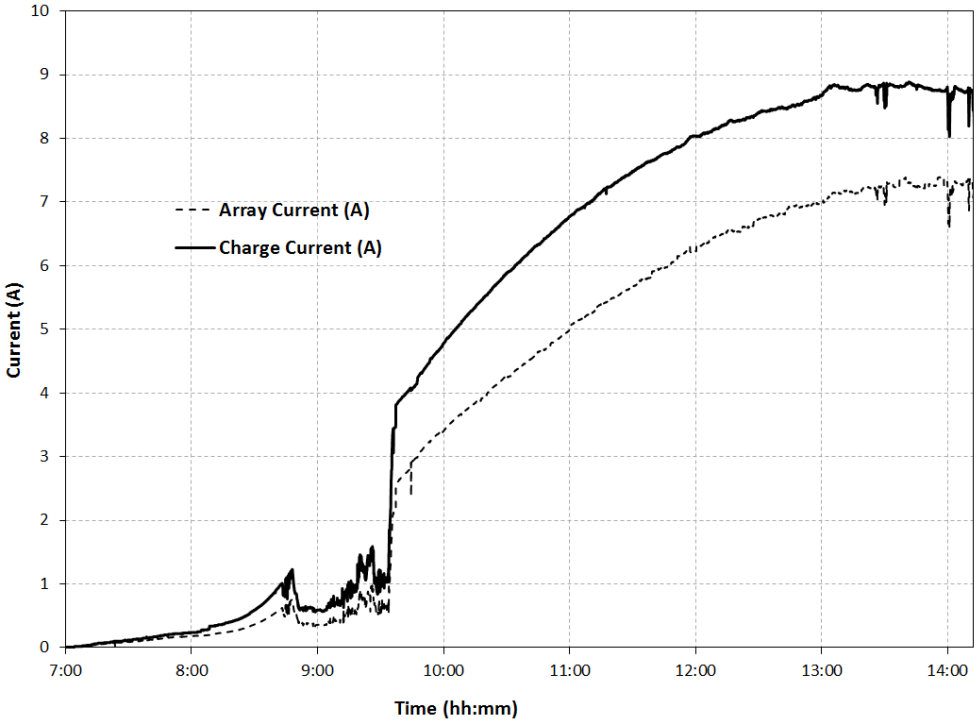

(b) Variation of array current and charge current during a charging period

Figure 5-33. Variation of array voltage, charge voltage, array current, and charge current during battery charging period

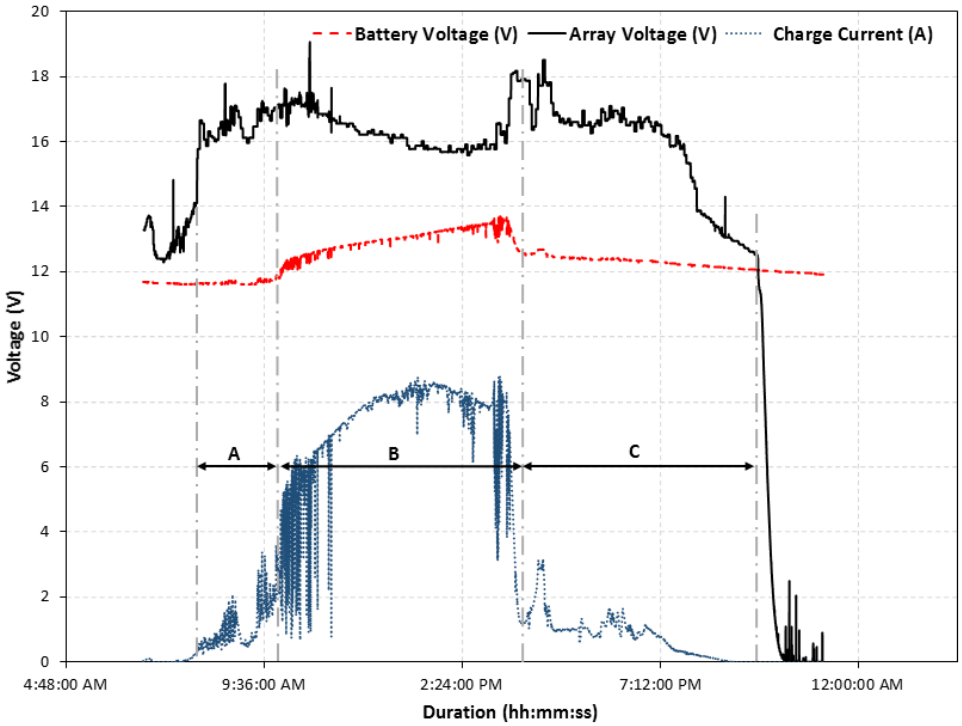

Figure 5-34. Variation of battery voltage and array voltage during a typical day

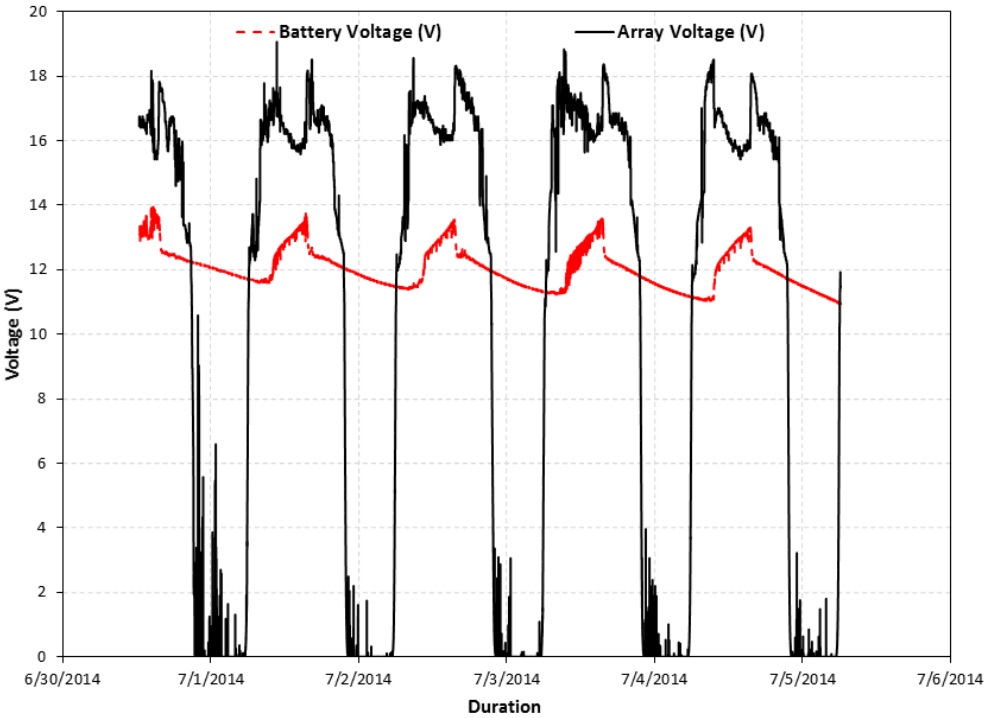

Figure 5-35. Variation of battery voltage and array voltage during continuous operation of a load from June 30 (12:21:38 hr) to July 5 (06:09:58 hr), 2014

5.4 SUMMARY

The following conclusions can be derived from the AE data analysis, fatigue performance evaluation, and monitoring system performance evaluation presented in this chapter:

- The data analysis methods presented in this section provides a sound basis for the use of acoustic emission (AE) for monitoring the condition of fatigue-sensitive details and/or retrofits. With a large database generated from operating traffic, tools for identifying and separating fracture events from traffic and ambient noise with a high recognition rate are provided. In addition, the associated theoretical basis is presented for providing the underlying concepts and assumptions.

- Examination of the overall AE data provides a basis for adjustment of the data acquisition parameters such as gain and threshold. While the PLB signals performed their role in confirming the source location capability, their oversaturation suggests that the gain can be reduced, and the threshold is adjusted accordingly to reduce the overall volume of the data.

- The effective stress that was calculated using the fatigue truck based on WIM data and field measured strains shows a significant difference. High stress ranges from the analytical calculations using the WIM data were obtained whereas the actual monitored stress ranges were much lower. This finding highlights the need of developing a comprehensive monitoring program for evaluating performance of fatigue-sensitive details especially when major decisions such as costly repairs, retrofits, and load postings are to be made.

- The monitoring system was subjected to outdoor environmental conditions during a period of more than a year. During this period, one of the AE channels was malfunctioned and repaired. A few software compatibility issues were encountered and resolved. In general, the performance of the monitoring system and associated software has been satisfactory.

6 SUMMARY, CONCLUSIONS, AND IMPLEMENTATION RECOMMENDATIONS

6.1 SUMMARY AND CONCLUSIONS

Fatigue is one of the most critical problems for steel bridges as well as for any steel structures that needs to be considered during design and operation. Fatigue cracking is developed at certain steel bridge details due to a direct result of the loads (load-induced fatigue) or a deformation that is not accounted for during design (distortion-induced fatigue). The details that are prone to load-induced fatigue can be identified using the detail categories presented in the AASHTO LRFD (2013) specifications, Table 6.6.1.2.3-1. Identifying the details that are prone to distortion-induced fatigue cracking requires a combined effort of utilizing information in bridge files, refined analysis, and experience. Developing high-fidelity analysis models is vital to identify details that are susceptible to distortion-induced fatigue, evaluate the causes of cracking or potential for cracking, estimate remaining life of details that are prone to distortion-induced fatigue, and to develop guidelines for instrumentation and monitoring.

MDOT performs inspections of over 200 bridges with fatigue-sensitive details, and was interested in identifying technology that can be implemented to evaluate performance of fatigue-sensitive details and retrofits. By considering MDOT monitoring needs and the vital role of refined analysis, this study was organized into five tasks. While the outcome of the fifth task is presented in Section 6.2, the other four tasks and the findings are described below.

(1) Review the state-of-the-art and practice literature to identify technologies for a structural health monitoring (SHM) system:

Technology for fatigue-sensitive detail monitoring, technology implementation considerations, and retrofit methods for fatigue-sensitive details were reviewed. After evaluating the needs and the state-of-the-art technology, an acoustic emission (AE) monitoring system with strain gages was recommended to be one of the most effective technology for fatigue event detection (i.e., crack initiation or crack growth monitoring). AE has been successfully implemented in the field and evaluated for continuous monitoring of fatigue-sensitive details. At this time, AE is the only technology that is capable of real-time monitoring of fatigue events and providing data for damage location detection. In addition to

the AE sensors, strain gauges are required to evaluate the stress state to calculate the remaining fatigue life, and to support AE data analysis by developing a load matrix.

(2) Select a bridge and perform structural analysis to identify details for monitoring:

The bridge (S16 of 11015) that carries I-94 EB over Puetz Road, located in Stevensville, Michigan, was selected for system implementation and performance evaluation. After reviewing MDOT biennial inspection reports and conducting a field visit to document bridge superstructure and substructure condition, the 54.5^{o} skew and 56 ft - 6 in. long span was selected. The span consists of category C' fatigue-sensitive partial depth diaphragm details and a category E fatigue-sensitive welded cover plate detail. A 3D finite element model of the bridge was developed, and hot spot stresses were calculated under Michigan legal loads and deck dead load. Based on the analysis results, two web gap details that are located underneath the tuck lane were selected for instrumentation.

(3) Procure an SHM system:

As a commercially available implementation-ready SHM system, the TISEC SABRE^{TM} system comprising the Mistras Group Inc. Sensor Highway^{TM} II System instrumentation and a set of TISEC software post processing modules were selected as the basic AE system. One web gap detail was instrumented with 4 AE sensors and a strain gage while the other detail was instrumented with strain gages to calculate hot spot stresses.

(4) Install and calibrate the system, and analyze data:

The SHM system was installed, calibrated using pencil lead break (PLB) signals, and operated by powering through a solar power system. Many challenges are documented in the literature regarding AE data analysis and results interpretation. The following steps were followed during this study to analyze and interpret the AE data collected by the monitoring system:

- Selected an AE data set with signals exceeding a set threshold.
- Performed nonlinear mapping (NLM) using one feature domain at a time in the time, power, phase, cepstral and auto-correlation domains to visually detect significant naturally forming data clusters. (*Note: During this study, out of the 5 domains, the spectral power domain produced three significant clusters.*)

- Performed clustering with the same spectral power domain features. (*Note: Observed formation of three distinct clusters. These clusters were well aligned with the visual presentation of the NLM result. These observations confirmed the observations of NLM results.*)
- Separated the AE data set into three distinct clusters based on NLM and clustering analysis results.
- Classified each cluster using statistical and neural network classification methods, and selected the data belonging to each class for further analysis. (*Note: Use half of each cluster for training and the other half for testing the classification algorithms. All the classifiers yielded very high classification rates.*)
- Observed waveform characteristics in time and frequency domains to identify the class of signals that resemble the characteristics of signals that emanate due to fatigue events (i.e., crack opening) as well as the signals due to structural resonance and background noise.
- Developed conclusions based on observed signal characteristics, data presented in the source location plots, and experience.

Even though a large number of AE data sets were recorded during monitoring, data analysis and interpretation process followed during this study confirmed the nonexistence of the fatigue cracks at the monitored detail. With a large volume of data generated from operating traffic, tools for identifying and separating fracture events from traffic and ambient noise with a high recognition rate are provided; and the associated theoretical basis is presented. The signal types belonging to each class can be identified by inspecting the waveform features. Therefore, the data analysis capabilities presented during this study provides a sound basis for the use of AE for monitoring the performance of fatigue-sensitive details and elements or sections with retrofits.

Fatigue performance of a welded web gap detail was evaluated using (a) hot spot stress calculated using a finite element model loaded with a fatigue truck and (b) strain data collected using instrumentation. The gross weight of the fatigue truck was calculated as 57 kips using WIM data. Hot spot stress was calculated using a refined finite element model as per the guidelines presented by the International Institute of Welding (IIW). The maximum stress range at the weld toe was as high as 10.88 ksi. When combined with the other load effects, the stress range well exceeded the constant-amplitude fatigue threshold (CAFT) indicating a finite fatigue

life for the detail. The detail was instrumented with strain gages, and hot spot stress was calculated. The maximum stress range of 1.6 ksi was calculated using measured strain under ambient traffic. When combined with the effects of other loads, the maximum stress range barely reaches the CAFT indicating infinite fatigue life for the detail.

The monitoring system's ruggedness and reliability was evaluated by installing it on a bridge and subjecting it to severe outdoor exposure during a period of more than a year. During this period, one of the channels in the AE board malfunctioned, and was repaired. Minor issues were experienced with the real-time data display and software compatibility. However, within the data acquisition, interpretation, and presentation stream, these issues were resolved for this application. In general, the performance of the monitoring system and associated software is satisfactory.

6.2 IMPLEMENTATION RECOMMENDATIONS

After carefully evaluating the outcome of the four tasks, a two-tier implementation process is recommended as shown in Figure 6-1. Tier I includes assessment of bridges with repaired details. The first step is to identify the causes of cracking at the fatigue sensitive details through analysis and monitoring. At the same time, the monitoring data and analysis techniques can be used to evaluate the performance of the repairs and to develop necessary modifications to the structure and the detail to enhance the fatigue performance. Finally, the best performing retrofits can be identified for implementation in similar structures.

Tier II includes grouping bridges with fatigue-sensitive details based on defined attributes, and selecting a representative bridge from each group. Then, the fatigue serviceability index (Q) is calculated using refined analysis and a fatigue truck load. If $Q > 0.2$, routine inspections is performed. Otherwise, strains and fatigue events are monitored with two objectives: (1) to determine the presence of active fatigue cracks, and (2) to calculate Q using measured strains. The monitoring results are used to make repair, retrofit, or inspection decisions.

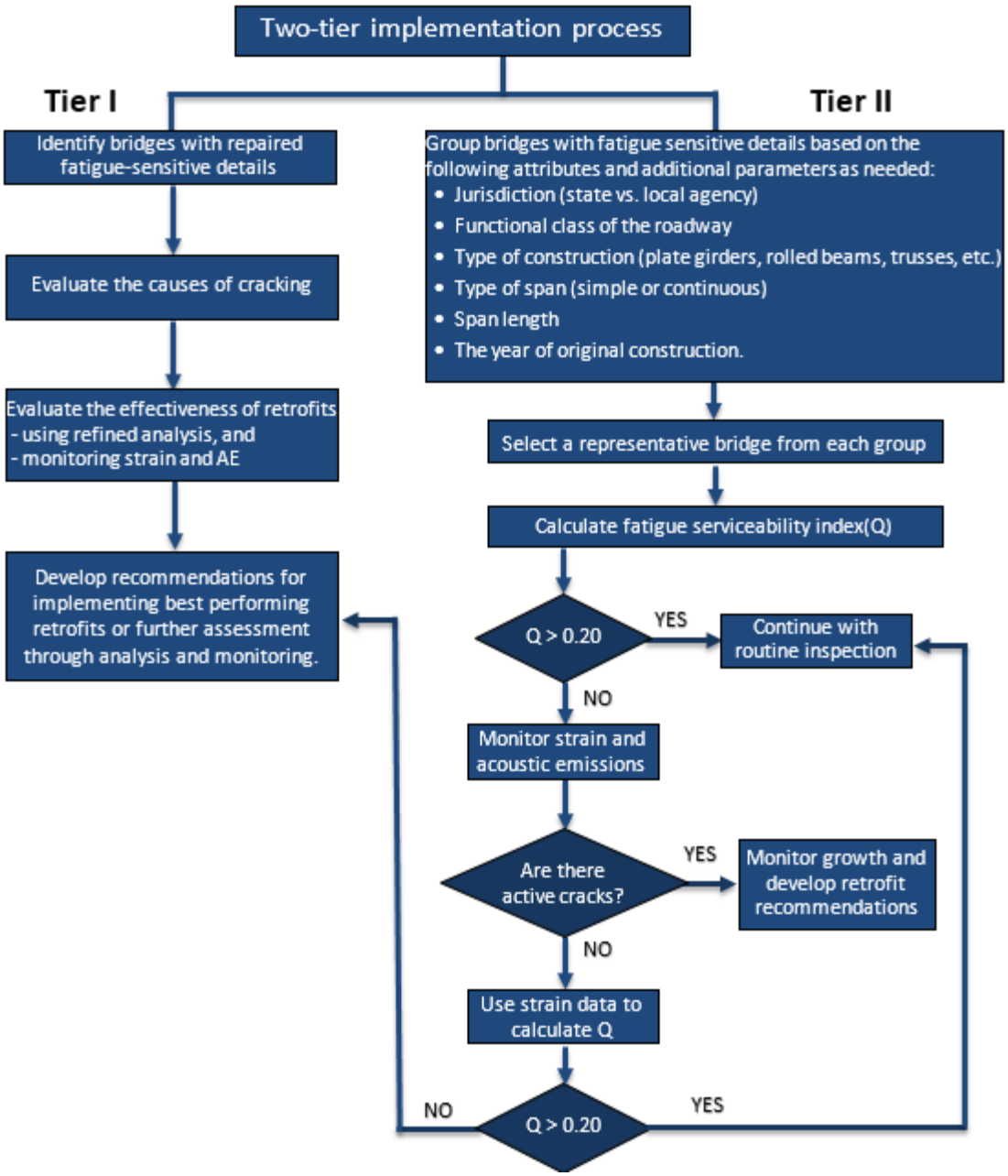

Figure 6-1. Two-tier implementation process

Additional recommendations to enhance the two-tier implementation process as well as for future research are listed below;

1. With ICEPACK, AE data interpretation capability was demonstrated. It is recommended that this interpretation capability be implemented in an on-line system with the real-time classifiers developed in this study in a prototype system using the remote communications capability deployed for this research project. Software for transforming proprietary data

formats from commercial AE instrumentation suppliers is available and pattern classifiers can be deployed in real-time versions. Such a system will provide reliable input with minimal interpretation requirements for inspection-based maintenance management.

2. The project has established that crack signals can be differentiated and separated from the substantial noise background using the artificial intelligence/pattern recognition methods described in the report. Hence, it is recommended to develop a fatigue cracking signal characteristic database using the typical steel and welds used in Michigan bridges. This database will help further refine the capability of the proposed automated system. Further, availability of signal characteristics to the AE monitoring system data analysts will help understanding the type of signals arise from the zones of interest.
3. Select representative bridges following the recommended process for Tier II implementation shown in Figure 6-1. Implement the AE monitoring system with the on-line signal classification system at a half dozen sites to gather data from typical fatigue-sensitive details to identify optimal settings and to optimize other deployment issues.

7 REFERENCES

AASHTO. (2008). AASHTO LRFD Bridge Construction Specifications, Second Edition with up to 2008 Interims, American Association of State Highway and Transportation Officials. Washington, D.C.

AASHTO LRFD. (2013). AASHTO LRFD Bridge Design Specifications, 6th Edition, the American Association of State Highway and Transportation Officials, Washington, DC 20001.

Abaqus (2012). Analysis User's manual, Volume 4, Section 25.1.4, Version 6.12, Three-Dimensional Solid Element Library. Dassault Systemes Simulia Corp.

ABS (2013). Guide for the Fatigue Assessment of Offshore Structures. American Bureau of Shipping, ABS Plaza, 16855 Northchase Drive, Houston, TX 77060

ABS (1992). Guide for fatigue strength assessment of tankers, Part 3 Steel Vessel Rules. American Bureau of Shipping (ABS), Houston, TX 77060, USA.

Adams, C. A. (2010). "Finite Element Study on Bridge Details Susceptible to Distortion-induced Fatigue." *Masters Thesis*, University of Kansas, Lawrence, KS 66045, USA.

Åkesson, B. (2010). *Fatigue life of riveted steel bridges*. Taylor & Francis Group, London, UK.

Akhlaghi, F. Z., Al-Emrani, M., Fryba, L., and Urushadze, S. (2009). "Fatigue testing and analysis of an orthotropic bridge welded detail using structural hot spot stress method," Fatigue Design 2009, Cetim - Technical Centre for Mechanical Industries, Senlis , France, November 25 – 26.

Alemdar, F., Nagati, D., Matamoros, A., Bennett, C., and Rolfe, S. (2014a). "Repairing distortion-induced fatigue cracks in steel bridge girders using angles-with-plate retrofit technique. I: Physical simulations." J. Bridge Eng., 10.1061/(ASCE)ST.1943-541X.0000876

Alemdar, F., Overman, T., Matamoros, A., Bennett, C., and Rolfe, S. (2014b). "Repairing distortion-induced fatigue cracks in steel bridge girders using angles-with-plate retrofit technique. II: Computer simulations." J. Struct. Eng., 10.1061/(ASCE)ST.1943-541X.0000874, 04014004.

Alemdar, F., Matamoros, A. B., Bennett, C. R., Barrett-Gonzalez, R., and Rolfe, S. T. (2011). "Improved Method for Bonding CFRP Overlays to Steel for Fatigue Repair" *42st Structures Congress Conference 2011*, ASCE, Las Vegas, NV, USA.

Applied Ultrasonics. (2014). http://www.appliedultrasonics.com/ (Last accessed: October 5, 2014).

ASTM E 976 (2010). "Standard Guide for Determining the Reproducibility of Acoustic Emission Sensor Response." ASTM International, 100 Barr Harbor Drive, PO Box C700, West Conshohocken, PA 19428-2959.

Aygul, M. (2012). Fatigue Analysis of Welded Structures Using the Finite Element Method. Thesis, Department of Civil and Environmental Engineering, Division of Structural Engineering, Steel and Timber Structures, Chalmers University of Technology, Gothenburg, Sweden.

Aygul, M., Al-Emrani, M., and Urushadze, S., (2012). "Modeling and Fatigue Life Assessment of Orthotropic Bridge Deck Details Using FEM." The International Journal of Fatigue, Vol. 40, p. 129-142.

Barut, S. (2006). "Use of piezoelectric films for NDT applications." The 9th European NDT Conference (ECNDT), Berlin, German, September 25 - 26.

Bassetti, A., Nussbaumer, A., and Hirt M. A. (2000). "Crack Repair and Fatigue Life Extension of Riveted Bridge Members Using Composite Materials." *Proceedings of Bridge Engineering Conference: The Egyptian Society of Engineers*, v 1, p 227-238.

Bell, E.S., Peddle, J.T., and Goudreau, A. (2012). "Bridge Condition Assessment using Digital Image Correlation and Structural Modeling." The 6th International Conference on Bridge Maintenance, Safety and Management, Stresa, Lake Maggiore, Italy, July 8-12, 2012.

Berglund, E. M., and Schultz, A. E. (2006). "Girder Differential Deflection and Distortion-Induced Fatigue in Skewed Steel bridges." *Journal of Bridge Engineering*. Vol. 11, pp. 169-177.

Bhargava, A. (2010). Fatigue Analysis of Steel Bridge Details: Hot Spot Stress Approach. Doctor of Philosophy Dissertation, the George Washington University, Washington, DC 20052.

Bhargava, A., and Roddis, W. M. K. (2007). *Finite Element Analysis of Fatigue Prone Details of the Tuttle Creek Bridge.* Report No. KS-07-5, Kansas Department of Transportation.

Bowman, M. D., Fu, G., Zhou, T. E., Connor, R. J., and Godbole, A. A. (2012). Fatigue Evaluation of Steel Bridges. NCHRP Report 721, Transportation Research Board of the National Academies, Washington, D.C.

Chakarav, K., Garbatov, Y., and Soares, C. G. (2008). "Fatigue analysis of ship deck structure accounting for imperfections," *International Journal of Fatigue*, Vol. 30, pp. 1881–1897.

Cintron, R., and Saouma, V. (2008). *Strain Measurements with the Digital Image Correlation System Vic-2D.* Center for Fast Hybrid Testing, Department of Civil and Environmental and Architectural Engineering, University of Colorado, UCB 428, Boulder, Colorado.

Det Norske Veritas (DNV) (2011). Fatigue Design of Offshore Steel Structures. Recommended Practice DNV-RP-C203, Det Norske Veritas.

Dexter, R. J., and Ocel, J. M. (2013). *Manual for Repair and Retrofit of Fatigue Cracks in Steel Bridges*. Technical Report FHWA-IF-13-020, Federal Highway Administration, McLean, VA 22101.

DFT UK (2006). Design Manual for roads and bridges. Report no. BA 86/06. Department for Transport, UK.

Ettah, E. B., Udoimuk, A. B., Obiefuna, J. N., and Opara, F. E. (2012). "The Effect of Relative Humidity on the Efficiency of Solar Panels in Calabar, Nigeria", Universal Journal of Management and Social Sciences, Vol. 2, No. 3, March 2012, pp. 8-11.

Eurocode 9, 1998. *Design of aluminum structures - Part 2: Structures susceptible to fatigue*. EN 1999-2:1998 E, British Standard, London.

Fasl, J. (2013). "Using NI WSN and LabVIEW to Wirelessly Monitor Fatigue Damage on Highway Bridges." The University of Texas at Austin.
<http://sine.ni.com/cs/app/doc/p/id/cs-15206> (Last accessed: March 29, 2013).

Fasl, J., Helwig, T., Wood, S.L., (2013) “Probabilistic method for estimating remaining fatigue life in steel bridges using measured strain data.” *Journal of Civil Structural Health Monitoring*. Vol. 3, Issue 4. pp. 317-324.

Fasl, J., Samaras, V., Reichenbach, M., Helwig, T., Wood, S.L., Potter, D., Lindenberg, R., and Frank, K. (2012). "Development of a Wireless Strain Node and the Software to Monitor Fracture-Critical Bridges." *Prc. SPIE 8347*, Nondestructive Characterization for Composite Materials, Aerospace Engineering, Civil Infrastructure, and Homeland Security 2012, 83471R (April 26, 2012).

FHWA (2012). *Feasibility of Nondestructive Crack Detection and Monitoring for Steel Bridges.* Report No. FHWA-HRT-12-060, Final Report, June 2006-March 2012, NDE Center, Federal Highway Administration, McLean, VA 22101.

Fisher, J.W., Statnikov, E., Tehini, L. (2001). “Fatigue Strength Enhancement by Means of Weld Design Change and the Application of Ultrasonic Impact treatment.” *Proceedings of the International Symposium on Steel Bridges*, Chicago.

Fisher, J. W., Jin, J., Wagner, D., and Yen, B. (1990). *Distortion Induced Fatigue Cracking in Steel Bridges*. NCHRP Report 336, Transportation Research Board, National Research Council. Washington D.C.

Fisher, J., Barthelemy, B., and Mertz, D. (1980). *Fatigue behavior of full-scale welded bridge attachments*. National Cooperative Highway Research Program (NCHRP) 227. Transportation Research Board. Washington, D.C.

Fisher, J. W. (1984). *Fatigue and fracture in steel bridges – Case studies*. John Wiley & Sons, New York.

Fricke, W. and Kahl, A. (2005). “Comparison of different structural stress approaches for fatigue assessment of welded ship structures,” *Marine Structures*, Vol. 18, pp. 473–488.

Fricke, W., Petershagen, H., and Paetzold, H. (1998). Fatigue Strength of Ship Structures-Example. GL-Tech.

http://www.gl-group.com/pdf/GL_Technology_Part_II_Examples.pdf (Last Accessed: 09/21/2014).

Fu, G., Feng, J., Dekelbab, W., Moses, F., Cohen, H., Mertz, D., and Thompson, P. (2003). *Effect of Truck Weight on Bridge Network Costs.* NCHRP Report 495, Transportation Research Board, Washington DC 20001.

Ghahremani, K., Sadhu, A., Walbridge, S., and Narasimhan, S. (2013). "Fatigue Testing and Structural Health Monitoring of Retrofitted Steel Highway Bridge Web Stiffeners." 92nd TRB Annual Meeting. Transportation Research Board, Washington DC 20001, January 13-17, 2013.

Gregory, E., Slater, G., and Woodley, C. (1989). *Welded repair of cracks in steel bridge members*. National Cooperative Highway Research Program (NCHRP) 321. Transportation Research Board. Washington, D.C.

Gunther, H. P., Kuhlmann, U., and Durr, A. (2005). "Rehabilitation of Welded Joints by Ultrasonic Impact Treatment (UIT)." *The International Association for Bridge and Structural Engineering (IABSE) Symposium,* Lisbon.

Hacini, L., Van Lê, N., and Bocher, P. (2008). "Effect of impact energy on residual stresses induced by hammer peening of 304L plates." *Journal of Materials Processing Technology*, v 208, n 1-3, p 542-548.

Hassel, H. L. (2011). "An Analytical Evaluation of Distortion-Induced Fatigue in Steel Bridges." Master's Thesis, University of Kansas.

Hassel, H. L., Hartman, A. S., Bennett, C. R., Matamoros, A. B., and Rolfe, S. T. (2010). "Distortion-Induced Fatigue in Steel Bridges: Causes, Parameters, and Fixes," Proceedings ASCE Structures Congress 2010, Orlando, Florida, May 12 – 15.

Hay, D.R. and Nyborg, E.O. (2000). *Acoustic emission handbook*, TISEC Inc. Morin Heights, Quebec, Canada J0R 1H0.

Hay, D.R., Cavaco, J.A., and Mustafa, V. (2009). "Monitoring the Civil Infrastructure with Acoustic Emission: Bridge Case Studies." *J. Acoustic Emission,* Vol. 27, pp. 1- 10.

Hee T. Y. and Isa, M. M. (2009). “Design of a mini solar power system,” Proceeding of 2009 IEEE Student Conference on Research and Development, UPM Serdang, Malaysia, Nov. 16 – 18.

Huang, M., Jiang, L., Liaw, P.K., Brooks, C.R., Seeley, R., and Klarstrom, D.L. (1998). "Using Acoustic Emission in Fatigue and Fracture Materials Research." *JOM,* vol. 50, no. 11, November 1998.

Hobbacher, A. (2008). Recommendations for Fatigue Design of Welded Joints and Components. International Institute of Welding (IIW), doc. XIII-2151r4-07/XV-1254r4-07. Paris, France.

Hu, Y., Shield, C. K., and Dexter, R. J. (2006). *Use of Adhesives to Retrofit Out-of-Plane Distortion Induced Fatigue Cracks*. MN/RC-2003-04, Report to the Minnesota Department of Transportation, St. Paul, MN 55155

Iadicola, M.A., Zobel, R.S., and Ocel, J.M. (2012). "Quantitative evaluation of digital image correlation as applied to large-scale gusset pate experiments." The 6th International Conference on Bridge Maintenance, Safety and Management*,* Stresa, Lake Maggiore, Italy, July 8-12, 2012.

ICEPak® (2014). http://structuralinsights.com/AI/specification.php (Last accessed: Dec. 02, 2014)

Ju, X., and Tateishi, K. (2012). “Structure on Fatigue Crack Propagation of a Through-thickness Crack Subjected to Out-of-plane bending.” International Journal of Steel Structures, Vol. 12, No. 1, pp. 85-92.

Kaphle, M., Tan, A. C. C., Thambiratnam, D. P., and Chan, T. H. T. (2012). “A Study on the Use of Acoustic Emission Technique as a Structural Health Monitoring Tool.” *Journal of Engineering Asset Management and Infrastructure Sustainability,* pp. 459 - 469.

Kaur, M., Sandhu, M., Mohan, N., and Sandhu, P. S. (2011). “RFID Technology Principles, Advantages, Limitations & Its Applications*.” International Journal of Computer and Electrical Engineering*, Vol. 3, No. 1, pp. 151 – 157.

Kazem, H. A., Chaichan, M. T., Al-Shezawi, I. M., Al-Saidi, H.S., Al-Rubkhi, H. S., Al-Sinani, J. K. and Al-Waeli, A. H. A. (2012). "Effect of Humidity on the PV Performance in Oman," Asian Transactions on Engineering (ATE ISSN: 2221 - 4267), Vol. 02, Issue 04, pp. 29 – 32.

Kosnik, D.E. (2008). "A New Approach to Acoustic Emission Testing of Difficult-to-Reach Steel Bridge Details." Infrastructure Technology Institute / Department of Civil & Environmental Engineering, Northwestern University, Evanston, Illinois 60208, USA.

Kühn, B., Lukić, M., Nussbaumer, A., Günther, H. P., Helmerich, R., Herion, S., Kolstein, M. H., Walbridge, S., Androic, B., Dijkstra, O., and Bucak, Ö. (2008). "Assessment of Existing Steel Structures: Recommendations for Estimation of Remaining Fatigue Life," EUR 23252 EN – 2008, European Commission, Joint Research Centre, Brussels – Belgium.

Kujawski, D., Ghantasala, M.; Gokanakonda, S.; and Hussain, S. (2011). Structural health diagnosis and prognostics using fatigue monitoring. SAE 2011 World Congress and Exhibition, Detroit, MI.

Ledeczi, A., Hay, T., Vogyesi, P., Hay, D.R., Nadas, A. and Jayaraman, S. (2009). "Wireless Acoustic Emission Sensor Network for Structural Monitoring." *IEEE Sensors Journal,* Vol. 9, No. 11, November 2009.

Lee, J. M., Seo, J.K., Kim, M.H., Shin, S.B., Han, M.S., Park, J.S., and Mahendran, M. (2010). "Comparison of Hot Spot Stress Evaluation Methods for Welded Structures." The International Journal of Naval Architecture and Ocean Engineering, Vol. 4 (2), pp. 200-210.

Leander, J., Andersson, A., Karoumi, R. (2010). "Monitoring and enhanced fatigue evaluation of a steel railway bridge." *Engineering Structures*. Vol. 32, pp. 854-863.

Leon, A. (1998). "Benefits of Split Mandrel Coldworking." *International Journal of Fatigue*, v 20, n 1, p 1-8.

Li, Z.X., Chan, T.H.T., Ko, J.M. (2001). "Fatigue damage model for bridge under traffic loading: application made to Tsing Ma Bridge." *Theoretical and Applied Fracture Mechanics*, Vol. 35, pp. 81-91.

Li, H., and Schultz, A. E. (2005). *Analysis of Girder Differential Deflection and Web Gap Stress for Rapid Assessment of Distortional Fatigue in Multi-Girder Steel Bridges*. MN/RC-2008-38, Report to the Minnesota Department of Transportation, St. Paul, MN 55155.

Li, F., Xiang, D., Chiang, S., Tittmann, B. R., and Searfass, C. (2011). "Wireless surface acoustic wave radio frequency identification (SAW-RFID) sensor system for temperature and strain measurements." IEEE International Ultrasonics Symposium 2011 (IUS 2011), October 18-21, 2011, Caribe Royale, Orlando, Florida, USA.

Lovejoy, S.C. (2003). "Determining Appropriate Fatigue Inspection Intervals for Steel Bridge Members." *Journal of Bridge Engineering*. Vol. 8, No .2, pp. 66-72.

McCrea, A., Chamberlain, D., and Navon, R. (2002). "Automated inspection and restoration of steel bridges—a critical review of methods and enabling technologies*." Journal of Automation in Construction*, Vol. 11, pp. 351 – 373

MBE. (2011). The Manual of Bridge Evaluation, 2nd Edition, the American Association of State Highway and Transportation Officials, Washington, DC 20001.

MDOT (2009). "Michigan Bridge Analysis Guide," the Michigan Department of Transportation, Lansing, Michigan, 48909. http://www.michigan.gov/documents/mdot/MDOT_2009__InterimBridgeAnalysisGuide_Part1_274530_7.pdf . (Last accessed: September 2014)

Mentes, Y. (2011). Analytical and experimental analysis of steel truss bridge gusset plate connections. A Dissertation Presented to The Academic Faculty, Georgia Institute of Technology, December 2011.

Metal Fatigue Solutions, Inc. (MFS) (2014). http://www.metal-fatigue-solutions.com/technology/ (Last accessed: October 26, 2014).

Moshier, M. and Berks, W. I. (2009). Electrochemical fatigue sensor systems and methods United States Patent, US 7,572,360 B2.

Moshier, M. A., Miceli, M., Le, H., and Leach, D. (2009). “Inspection of Fatigue Cracks on a CN Bridge Using the Electrochemical Fatigue Sensor." The AREMA 2009 Annual Conference & Exposition, September 20 – 23, 2009, Chicago, IL.

NASA. (2014). NASA Langley Research Center Atmospheric Science Data Center, https://eosweb.larc.nasa.gov/project/sse/sse_table. Accessed July 12, 2014

Nair, A., and Cai, C.S. (2010). “Acoustic emission monitoring of bridges: Review and case studies.” *Engineering Structures,* Vol. 32, No. 6, pp. 1704-1714.

NDT (2014). NDT Resource Center, the Collaboration for NDT Education, Iowa State University. <www.ndt-ed.org> (Last accessed: December 17, 2014).

NREL. (2014). The National Renewable Energy Laboratory. http://www.nrel.gov/gis/solar.html (Last accessed: November 27, 2014).

Nguyen, K. T.., Garbatov, Y., and Soares, C. G. (2012). “Fatigue damage assessment of corroded oil tanker details based on global and local stress approaches,” *International Journal of Fatigue*, Vol. 43, pp. 197–206.

Niemi E (1993). “Stress determination for fatigue analysis of welded components. IIW Doc. IIS/IIW-l221-93”, International Institute of Welding.

Niemi, E., Fricke, W., and Maddox, S.J. (2006). “Fatigue Analysis of Welded Components: Designer’s guide to the structural hot-spot stress approach (IIW-1430-00)”, Cambridge: Woodhead Publishing Limited.

Ozelton, M. W., and Coyle, T. G. (1986). “Fatigue Life Improvement by Cold Working Fastener Holes in 7050 Aluminum*.” Fatigue in Mechanically Fastened Composite and Metallic Joints, ASTM STP 927*. Ed. John M. Potter. Philadelphia: ASTM, p 53-71.

Parmar, D.S. and Sharp, S.R. (2009). “Acoustic Emission for Non-Destructive Testing of Bridges and Other Transportation Infrastructure." Beyond the Crossroads: A National Conference on Transportation Infrastructure & Regulatory Policy. May 27-28, 2009. University of Denver, Denver, CO.

Phares, B.M. (2007). "The electrochemical fatigue sensor: A novel sensor for active fatigue crack detection and characterization." The 3rd Conference on Structural Health Monitoring of Intelligent Infrastructure, Vancouver, British Columbia, Canada, November 13-16, 2007.

Pook, L. (2007). *Metal Fatigue, what it is, why it matters*. Springer, P.O.Box 17, 3300 AA Dordrecht, the Netherlands.

Proto Manufacturing Inc., Universal Drive, Taylor, Michigan, USA. <protoxrd.com> (Last accessed: March 29, 2013).

Ramchandra, P., Boucar, D. (2011). Solar Lighting. Springer-Verlag, New York.

Reijmers, J., (2002). The Extrapolation of Finite Element Result to Hot Spot Stresses. Presentation. IV Nevesbu, Papendrecht, Netherlands. file:///C:/Users/attupul/Downloads/FENET_Glasgow_Oct2004_EDU_Reijmers.pdf (Last Accessed: 09/21/2014).

Rose, J.L., and Royer, R.L. (2008). "A Guide wave Health Monitoring Approach for Civil Structures." 26th IMAC: Conference and Exposition on Structural Dynamics 2008 (IMAC XXVI), February 4-7, 2008, Orlando, Florida. Society for Experimental Mechanics (SEM).

Roy, S., Fisher, J., and Yen, B. (2003). "Fatigue Resistance of welded details enhanced by ultrasonic impact treatment (UIT)." *International Journal of Fatigue*. Vol. 25. pp. 1239-1247.

Schultz, A. and Thompson, D. (2010). *Development of an Advanced Structural Monitoring System.* Minnesota Department of Transportation, Research Services Section, St. Paul, MN 55155.

Shield, C. and McKeefry, J. (1999). *Acoustic Emission Monitoring of Fatigue Cracks in Steel Bridge Girders*. MN/RC – 1999-36, Minnesota Department of Transportation, St. Paul, MN 55155.

Shifferaw, Y., and Fanous, F. S. (2013). “Field Testing and Finite Element Analysis of Steel Bridge Retrofits of Distortion-Induced Fatigue.” Engineering Structures, Vol. 49, 2013, pp. 385-395.

Shirahata, H., Ueda, N., Kishida, A. (2014). Development of monitoring system for bridge collapse detection by energy harvest with solar cell. Bridge Maintenance, Safety, Management and Life Extension, Taylor & Francis Group, London, pp. 1405-1410.

Stefanescu, D., Santisteban, J. R., Edwards, L., and Fitzpatrick, M. E. (2004). "Residual Stress Measurement and Fatigue Crack Growth Prediction after Cold Expansion of Cracked Fastener Holes." *Journal of Aerospace Engineering*, v 17, n 3, p 91-97.

Sunsaver. (2014). Sunsaver MPPT Installation and Operation manual. Morningstar Corp., Washington Crossing, PA. (Last accessed: July 12, 2014).

Tarries, D. J., Phares, B. M., Wipf, T. J., Greimann, L., Wood, D. L. (2002). "Bolt Loosening Retrofit to Inhibit Fatigue Cracking in Steel Girder Bridges." *82nd Annual Meeting, Transportation Research Board*, Washington, D. C.

Tianze, L., Hengwei, L., Chuan, J., Luan, H., Xia, Z. (2011). Application and design of solar photovoltaic system. 3rd International Photonics & OptoElectronics Meetings, Journal of Physics: Conference Series 276.

Vallen (2013). http://www.vallen.de/sites/default/files/sov1212.pdf (Last accessed: 10/25/2013).

Wang, C., Tian, L., Fu, B., and Zhang, Y. (2012). "Fatigue cracking monitoring and evaluation using smart sensors for steel bridge decks." The 6th International Conference on Bridge Maintenance, Safety and Management (IABMAS), Stresa, Lake Maggiore, Italy, July 8-12, 2012.

Wipf, T. J., Greimann, D. L., Wood, B. M., Tarries, D. (2003). *Retrofit methods for distortion cracking problems in plate girder bridges*. TR-436, Report to Iowa Highway Research Board, Ames, IA; 2003.

Yang, C. and Fritzen, C. P. (2011). "A novel piezoelectric paint sensor for nondestructive testing." The International Workshop – Smart Materials, Structures & NDT in Aerospace, Montreal, Quebec, Canada, November 2 - 4.

Yang, L., Smith, L., Gothekar, A., and Chen, X. (2010). *Measurement of Strain Distribution Using Digital Image Correlation (DIC) for Tensile Tests.* Final Report. The Advanced High Strength Steel Stamping Team of the Auto/Steel Partnership (A/SP). Southfield, Michigan.

Yekta, T. R., Ghahremani, K., and Walbridge, S. (2013). "Effect of quality control parameter variations on the fatigue performance of ultrasonic impact treated welds." *International Journal of Fatigue*, 55:245-256.

Yi, X., Ruchi, V., Chunhee, C., Chia-Hung, F., Cooper, J., Wang, Y., Leon, R.T., and Tentzeris, M.M. (2012a). "Thermal effects on a passive wireless antenna sensor for strain and crack sensing." Proceedings of SPIE - The International Society for Optical Engineering, San Diego, CA, United states, March 12 - 15, 2012.

Yi, X., Wang, Y., Leon, R.T., Cooper, J., and Tentzeris, M.M. (2012). "Wireless crack sensing using an RFID-based folded patch antenna." The 6th International Conference on Bridge Maintenance, Safety and Management (IABMAS), Stresa, Lake Maggiore, Italy, July 8-12, 2012.

Yildirim, H. C. and Marquis, G. B. (2011). *Fatigue of welded components and structures: Overview of fatigue data for high frequency treated welded joints.* A report to the COMMISSION XIII, International Welding Institute (IIW).

Yoneyama, S., Kitagawa, A., Iwata, S., Tani, K., and Kikuta, H. (2007). "Bridge Deflection Measurement using Digital Image Correlation." *Experimental Techniques,* Volume 31, Issue 1, January/February 2007, pp. 34-40.

Yu, J., Ziehl, P., Zarate, B., and Caicedo, J. (2011). "Prediction of fatigue crack growth in steel bridge components using acoustic emission." *Journal of Constructional Steel Research,* Vol. 67, pp. 1254 - 1260.

Zhang, Y., Zhou, C., Fu, C.C., and Zhou, Y.E. (2013). "Field Monitoring of Fatigue Crack on Highway Steel I-girder Bridge." 92nd TRB Annual Meeting. Transportation Research Board, Washington DC 20001, January 13-17, 2013.

Zhao, X., Gao, H., Zhang, G., Ayhan, B., Yan, F., Kwan, C., and Rose, J.L. (2007). "Active Health Monitoring of and Aircraft Wing with Embedded Piezoelectric Sensor/actuator network: I. Defect Detection, Localization, and Growth Monitoring." *Smart Materials and Structures*, IOP Publishing, pp 1208-1217.

Zhao, X., Qian, T., Qi, K., Mei, G., Liu, A., Xu, R., and Zane, R. (2013). "A Novel Wireless Multi-sensor Network System for Steel Bridge Fatigue Crack Monitoring." 92nd TRB Annual Meeting. Transportation Research Board, Washington DC 20001, January 13-17, 2013.

Zhou, Y. E. (2005). "Assessment of Bridge Remaining Fatigue Life through Field Strain Measurement," ASCE Structures Congress 2005, New York, April 20-24.

Zhu, X, Rizzo, P., Marzani, A., and Bruck, J. (2010). "Ultrasonic guided waves for nondestructive evaluation/structural health monitoring of trusses." *Measurement Science and Technology,* Vol. 21, No. 4, pp. 1-12.

MDOT RC-1629

Remote Monitoring of Fatigue-sensitive Details on Bridges

(Appendices)

MARCH 2015

Research

Department of Civil & Construction Engineering
College of Engineering and Applied Sciences
Western Michigan University

APPENDIX A

ABBREVIATIONS

A

A	Amperage (Amps)
AASHTO	American Association of State Highway and Transportation Officials
AC	Alternating Current
ADT	Average Daily Traffic
ADTT	Average Daily Truck Traffic
AE	Acoustic Emission
Ah	Amp hours
ASTM	American Society for Testing and Materials

C

CAFT	Constant-Amplitude Fatigue Threshold
CFRP	Carbon Fiber Reinforced Polymer

D

DC	Direct Current
DFT	Department for Transport
DIC	Digital Image Correlation
DMRB	Design Manual for Roads and Bridges
DoD	Depth of Discharge
DOT	Department of Transportation

E

EB	Eastbound
EFS	Electrochemical Fatigue Sensor

F

FCM	Fracture Critical Members
FD	Fatigue damage sensor
FE	Finite Element
FHWA	Federal Highway Administration

FF	Fatigue Fuse
FHC	First-Hit Channel

H

HS	Hot Spot
HSS	Hot Spot Stress

I

IIW	International Institute of Welding
LVD	Low-Voltage Disconnect
LVR	Low-Voltage Reconnect

L

LEFM	Linear Elastic Fracture Mechanics
Ly	Langley

M

MBE	Manual for Bridge Evaluation
MDOT	Michigan Department of Transportation
MPPT	Maximum Power Point Tracking

N

NBI	National Bridge Inventory
NCHRP	National Cooperative Highway Research Program
NDT	Nondestructive Testing
NREL	National Renewable Energy Laboratory
NLM	Non-Linear Mapping

O

ODOT	Oregon Department of Transportation

P

PE	Photoelasticity
PLB	Pencil Lead Break
PV	Photovoltaic

R

RFID	Radio Frequency Identification

S

SG	Strain Gauges
SHM	Structural Health Monitoring

T

TS	Temperature Sensor

U

UIT	Ultrasonic Impact Treatment
USGW	Ultrasonic Guided Wave

V

V	Voltage (Volts)

W

WB	Westbound
WEU	Waveform Extraction Utility
WIM	Weight-In-Motion

X

XRD	X-ray Diffraction

APPENDIX B

NOTATIONS

Δf	Stress range
$(\Delta f)_{eff}$	Effective stress range
Δf_i	Particular stress range
$(\Delta f)_{max}$	Maximum stress range
$(\Delta f)_{TH}$	Threshold stress
ΔK	Stress intensity factor range
ρ	Radius of crack-stop hole
σ	Stress
$\sigma_{hs,\ assess}$	Hot spot stress of the detail to be assessed
$\sigma_{hs,\ ref}$	Hot spot stress of the reference detail
σ_y	Yield strength
γ_i	Percentage of cycles at a particular stress range

A	Present age of a detail; Detail category constant
ADT	Average daily traffic
ADTT	Average daily truck traffic
$(ADTT)_{SL}$	Average daily truck traffic in a single lane averaged over fatigue life
$[(ADTT)_{SL}]_{PRESENT}$	Present average daily truck traffic in a single lane
$CAFT_{assess}$	Constant-amplitude fatigue threshold of the detail to be assessed
$CAFT_{ref}$	Constant-amplitude fatigue threshold of the reference detail
D	Damage sum/index, $0 \leq D \leq 1.0$
E	Modulus of elasticity of the material
f_y	Yield Strength
g	Average yearly increase in traffic
i	Stress range
k	$(\sigma_{hs,ref})/ (\sigma_{hs,assess})$
n	Number of stress-range cycles per truck passage
n_i	Number of cycles at stress range i
N_i	Theoretical fatigue life at stress range i
Q	Fatigue Serviceability Index
R_R	Resistance factor specified for evaluation

R_S	The stress-range estimate partial load factor
S_{YY}	Stress in y-direction
t	Plate thickness
T_{fat}	Remaining fatigue life
V_{mp}	Maximum power point voltage
W	Longitudinal attachment thickness + 2×weld leg length
Y	Finite fatigue life

APPENDIX C

TECHNOLOGY FOR FATIGUE-SENSITIVE DETAIL MONITORING

C OVERVIEW

While a few technologies are successfully implemented in the field, a limited number of technologies are evaluated under laboratory and field conditions for fatigue event detection, crack growth monitoring, and for capturing strain profile at or around sensitive details. A limited number of these studies are documented in this appendix. Further, the working principles of a few technologies are also presented.

C.1 TECHNOLOGIES AND PRACTICE – CASE STUDIES

C.1.1 Low-power wireless sensor network (WSN) for strain data acquisition (Fasl 2013, Fasl et al. 2012).

Fasl et al. studied a 900 ft long bridge with the maximum span of 230 ft and twin trapezoidal 78 in. deep box girders. A monitoring system was implemented to record the strains at fatigue-sensitive details of the bridge. The monitoring system included four strain gauge nodes, two thermocouple nodes, and a real-time low-power wireless senor network (WSN). The system was used for continuous acquisition of temperature and traffic-induced strains. A standard rainflow counting algorithm was implemented, and real-time strain data analysis was performed. The processed data was transmitted through the WSN gateway, which was connected to a cellular gateway, to transmit the data to a cloud-based service for storing, further analysis, and sharing (Figure C-1). The data acquired from the system was primarily used to calculate the remaining fatigue life.

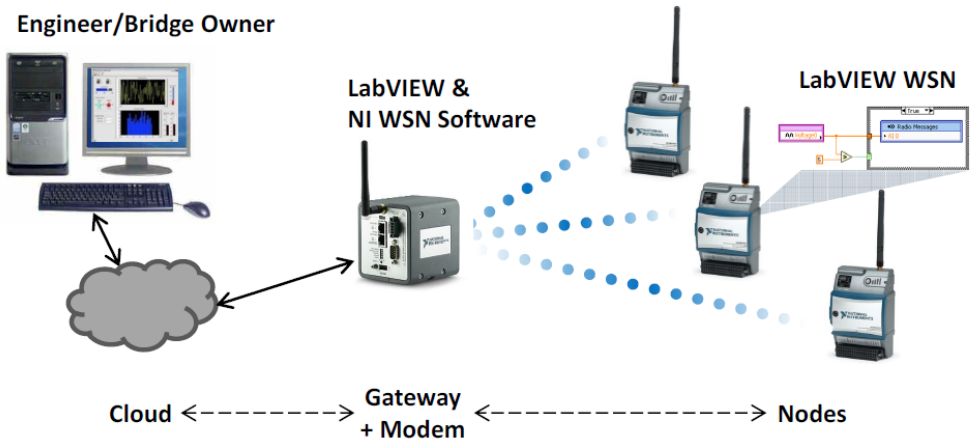

Figure C-1. Schematic of the monitoring system (Fasl et al. 2012)

The strain gauge nodes were programmed to run in five different modes as described below:

- **Idle:** Node acquisition is inactive; waiting for a command.
- **Streaming:** Periodically acquires and transmits strain waveforms.
- **Rainflow:** Continuously acquires dynamic data, performs real-time rainflow counting, and transmits a histogram of the results at a predefined time interval (typically every 30 minutes).
- **Trigger:** Transmits strains as a time-series when a predefined trigger level is exceeded.
- **Rainflow+Trigger:** Execute rainflow counting algorithm and trigger modes simultaneously.

The key features of this system include the capability of the system to process data before transmission, the flexibility in configuring the system to transmit processed data as well as raw data, and the system activation capability through a predefined trigger level.

C.1.2 Multi-sensor network system for steel bridge fatigue crack monitoring (Zhao et al. 2013)

Fatigue events and crack growth were monitored using a multi-channel and multi-sensor network system with acoustic emission (AE), strain, and ultrasonic guided wave (USGW) sensors. Once a possible damage event is captured by AE and strain sensors, the USGW sensors were triggered to perform in-situ inspection of the damaged location to characterize the cracks. The triggering thresholds were set for AE signal and strain change amplitude. Also, the monitoring system included the capability to trigger the USGW sensors to inspect the area as needed. The sensor data was remotely accessible via a Global System for Mobile (GSM) communication network. The monitoring system included the capability to send a Short Message Service (SMS) after detecting a damage event.

The system was implemented on a four-span, multi-girder bridge built in 1966. The primary objective of technology implementation was to monitor the growth of existing fatigue cracks at a diaphragm and girder web connection. The AE sensor was mounted on the girder web near a web gap, a fatigue-sensitive detail (Figure C-2a). The USGW sensors were mounted as a rectangular array, enclosing an existing crack, to monitor growth (Figure C-2b). The arrows in

the USGW sensor array (Figure C-2b) indicate the wave propagation path between the pulsers, located on the left, and the receivers, located on the right. Both the AE and USGW sensors were calibrated after being mounted near the crack.

(a) (b)

Figure C-2. Sensor locations of (a) AE sensor and (b) USGW sensor array (Zhao et al. 2013)

The USGW sensor array included 4 sensors mounted to capture an activity of a crack located within the array (Figure C-3a). The signals from the USGW sensors were categorized based on the sensor location, wave propagation path, and crack tip location (Figure C-3b). As an example, (i) the pair-wise data between sensors 1 and 2 is named as 'crack' when the direct transmission of signals from sensor 2 to 1 is disturbed by a crack; (ii) the pair-wise data between sensors 2 and 3 and 4 and 1 are named as 'crack tip' when the pairwise data between sensors 2 and 3, and 4 and 1 represent a specific signal pattern demonstrating the reach of crack tip closer to the direct signal transmission between these sensors; and (iii) the pairwise data between sensors 3 and 4 was named as 'normal' when the direct signal transmission between those two sensors is not interrupted.

(a) (b)

Figure C-3. Field implementation of the system for fatigue crack monitoring (a) sensor system mounted on the bridge and (b) schematic of the USGW sensor array (Zhao et al. 2013)

A GSM cellular network was used for wireless data transmission to a remote computer. The field data from the AE and USGW sensors was used to characterize the crack and also to evaluate the impact of loads on the structure and traffic noises. The traffic noises rarely triggered the AE sensors due to low energy levels generated by the loads (Figure C-4).

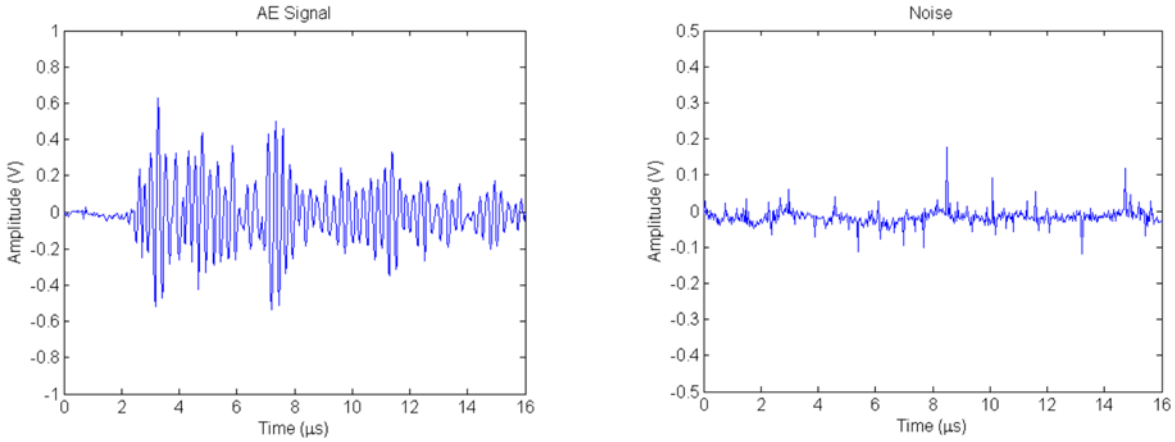

(a) (b)

Figure C-4. Difference in wave pattern from AE signal for (a) simulated crack and (b) external noise (Zhao et al. 2013)

The major improvement of this monitoring system compared to a traditional AE sensor system is the use of automated triggering of USGW sensors to monitor status and growth of cracks once a fatigue event is captured by the AE sensors. Also, the USGW sensors can be triggered to inspect the details, as needed. However, the effectiveness of the system depends on the USGW sensor arrangement and the proximity to the crack location. The drawback of the wireless system compared to the wired system is the delay in triggering USGW sensors for data collection.

C.1.3 Fatigue testing and SHM of retrofitted steel highway bridge web stiffeners (Ghahremani et al. 2013)

Ghahremani et al. (2013) evaluated a retrofitted detail using strain gauges, an alternating current potential drop technique (which is commonly known as eddy current method for crack depth measurement) and direct current differential transducers for displacement measurement. The approach was to predict fatigue crack depth using local strain data supported with 2D and 3D finite element analysis results. The eddy current method was used to calibrate and validate the methodology.

One of the major challenges of this study was to accurately measure the strain near the crack location. This challenge was overcome with the help of detailed FE analysis. The other challenge was to eliminate the effect of environmental and experimental conditions. This challenge was overcome by having additional sensors (guard sensors) mounted away from the critical area to record the effects due to ambient and experimental conditions, and eliminating them from the data recorded from the sensors mounted in the vicinity of the crack locations.

C.1.4 Field monitoring of a fatigue crack on a highway steel I-girder bridge (Zhang et al. 2013)

The piezoelectric film sensors, also referred as the piezoelectric paint sensors, are used in AE sensors (Barut 2006; Yang and Fritzen 2011). These piezoelectric film sensors are made using a composite piezoelectric material that is developed by mixing small piezoelectric particles in a polymer matrix. The piezoelectric powder used in developing these sensors is mainly composed of Lead Zirconate Titanate, with the chemical formula $Pb[Zr_xTi_{1-x}]O_3$, of which x varies between 0 to 1 (i.e., $0 \leq x \leq 1$). The sensors with Lead Zirconate Titanate are called PZT (Yang and Fritzen 2011). The PZT sensors have several advantages when compared to the traditional sensors made of brittle piezoelectric ceramic material. The flexibility of PZT composite material allows mounting these sensors on curved surfaces (Figure C-5). In addition, light weight, small size, and wide bandwidth are the other advantages of these sensors.

(a) (b)

Figure C-5. (a) PZT sensor sample and (b) PZT sensor sample on a curved surface

Zhang et al. (2013) used a health monitoring system with PZT AE wideband low profile (i.e., small and lightweight) sensors to monitor an existing fatigue crack on a weld at the diaphragm connection plate of a 140 ft single span multi-girder steel bridge. The fatigue crack initiated due to live load induced stresses in the welds resulting from differential deflections of adjacent

girders. The monitoring system was comprised of three PZT AE sensors, wireless accelerometers, laser distance sensors, and strain transducers (Figure C-6 and Figure C-7). The growth of the crack was monitored using AE sensors while the wireless accelerometers and laser distance sensors measured the vibration responses and differential deflection of adjacent girders (expected cause of the fatigue cracking).

Average frequency spectrums of triggered signals from the three AE sensors were used to cancel out ambient noise effect instead of using a guard sensor. In addition, a band-pass filter was used to filter out low frequency noises induced by bridge vibration.

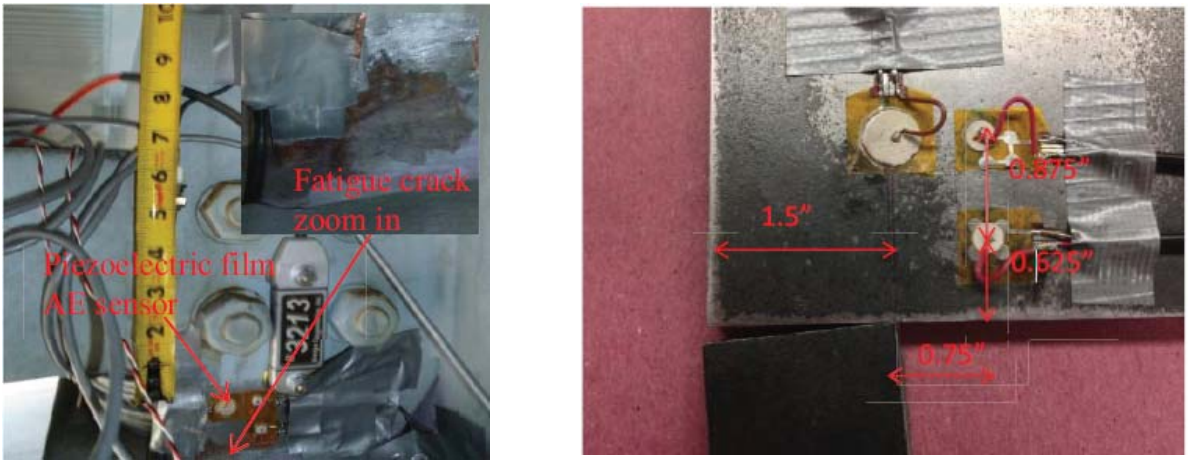

(a) (b)

Figure C-6. (a) PZT film AE sensor on the bridge and (b) a close up of PZT AE sensor on a steel specimen (Zhang et al. 2013)

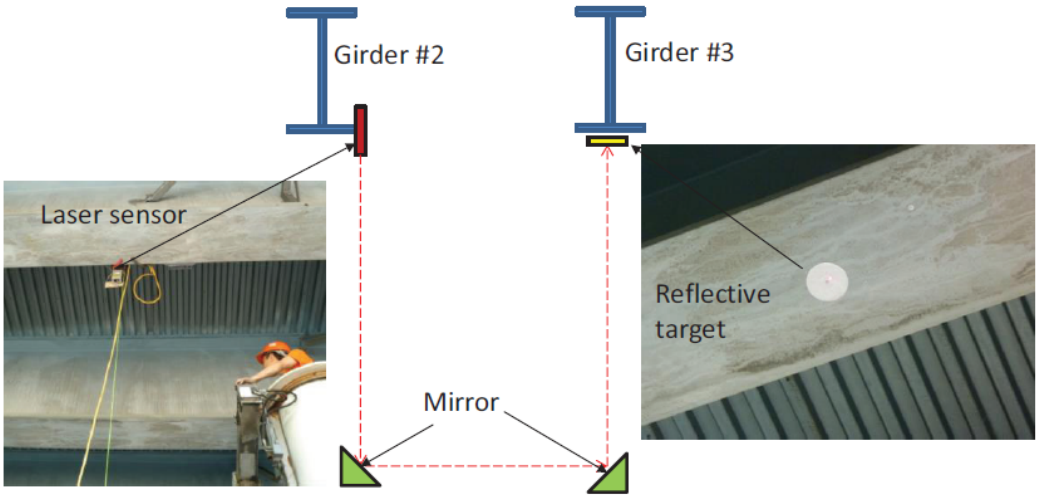

Figure C-7. Test setup of laser distance sensor (Zhang et al. 2013)

C.1.5 Acoustic emission monitoring of a cantilever through truss bridge (Kosnik 2008)

An AE sensor array was used to monitor a 5 in. long, full depth, fatigue crack in a cantilever through truss bridge. As a maintenance activity, an inch diameter crack-stop hole was drilled at the tip of the crack. The objective of the instrumentation was to monitor the effectiveness of the crack-stop hole in preventing crack growth. Four sensors were mounted in a rectangular array around the crack-stop hole while one of them mounted opposite the crack tip (Figure C-8). The system continuously collected and transmitted data to monitor crack growth beyond the crack-stop hole. Even though a threshold value of 40 dB was set to eliminate the noises, the noise levels generated from the bolted connection near the crack were greater than the threshold. Hence, the first-hit channel (FHC) analysis approach was used to filter out the noises from the bolted connection near the crack. Also, the AE hardware was mounted on rubber to avoid noises from the enclosure itself.

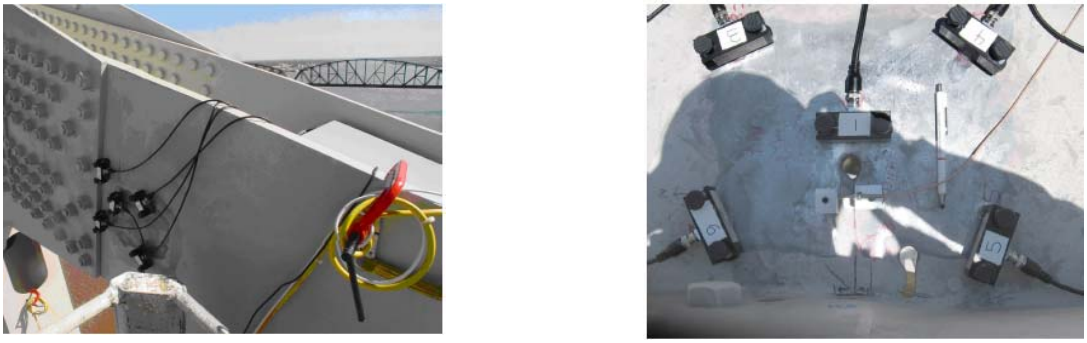

Figure C-8. Field monitoring of a fatigue crack using an AE sensor array (Kosnik 2008)

Few AE activities were identified near the crack-stop hole using the FHC analysis technique. These events were identified using signals with amplitude lower than the threshold. Further investigations revealed that the signals originated due to fretting of the existing crack.

Even though the monitoring system was designed to locate and characterize damage events, complicated geometry and low strength signals made the tasks unattainable. Hence, effective use of AE sensors at a particular structure requires having adequate signal strength to negate the noises or implementation of advanced signal enhancing and processing techniques to minimize the noise effects. Further, a long-term implementation of a monitoring system on a particular structure is required to identify the noise sources and establish thresholds to capture fatigue events.

C.1.6 Fatigue crack detection and monitoring techniques for steel bridges (FHWA 2009, FHWA 2012)

The Federal Highway Administration (FHWA) conducted a multi-year project to evaluate currently available NDE technologies for crack detection and crack growth monitoring in steel bridges, including subsurface flaws as small as 0.01 in. in length or depth. The laboratory studies used plate specimens with surface and subsurface cracks. Field evaluation included monitoring a crack at a web gap of a 3-span, continuous, multi-girder bridge.

Phased array ultrasonic testing (PAUT) and eddy current (EC) capabilities were evaluated for detecting existing cracks or flaws. The parameters considered for the evaluation are crack length, depth, and orientation. The PAUT system was able to detect and characterize subsurface and internal crack length and depth more effectively than an EC system that could only measure the length. Even though the geometry of the crack posed difficulties in sizing the cracks, the PAUT system could locate the crack tip with sectorial scan images. These technologies are not suitable for remote monitoring purposes because both techniques require access to the specific bridge details to perform inspection. Hence, no further information on these technologies is presented.

AE and electrochemical fatigue sensors (EFS) were evaluated for detecting crack growth or the status of a crack (i.e., an active or a dormant crack). A comparative study was carried out using EFS and AE systems using a cruciform specimen test. The conclusions of the study are as follows:

- AE takes almost twice the time of EFS to detect major crack activity. Hence, the EFS has a greater sensitivity in detecting low energy cracking events.
- AE sensors can continuously record crack growth activity.
- AE is suitable for local as well as global structural monitoring whereas the EFS is suitable for local monitoring.
- Frequent refill of chemicals (i.e., every 1-3 days) is needed for proper operation of EFS under hot weather conditions. Hence, an AE system is suitable for long-term monitoring since it does not require direct access to a crack or the sensors once the sensors are installed.

- Even though AE can only detect crack growth activity, it can be used with other NDE methods to characterize the crack.
- The detection of smaller cracks, less than 0.04 in. in length, with AE and EFS can be severely affected by the bridge coating.

C.1.7 Acoustic emission for non-destructive testing of bridges (Parmar and Sharp 2009)

Bridge cables were monitored during low and high traffic volumes as well as during winter and summer (Figure C-9) to evaluate potential use of an AE system to ensure the integrity of the bridge cables. The objective was to detect active cracks and flaws located in hidden areas where visual inspection is difficult.

Figure C-9. Mounting of an AE sensor on a bridge cable (Parmer and Sharp 2009)

The field implementation results show that the AE technique can be used to monitor, record, and analyze real time data remotely from the bridge for structural health monitoring of the cables. AE data was used to identify damage activities of the bridge cable once the noises arising from sources such as rain and wind are eliminated through signal analysis techniques or using data from guard sensors.

C.1.8 AE system development and field implementation plan for a tied arch bridge (Schultz and Thompson 2010)

Schultz and Thompson (2010) presented a system development and field implementation plan of an AE monitoring system for the Cedar Avenue/MN 77 tied arch bridge in Minnesota. The bridge is classified as fracture-critical due to lack of redundancy. The instrumentation plan was

developed for monitoring fatigue crack initiation and crack growth at critical locations such as the steel connections, box ties, floor beams, and the cables. The AE system was chosen as the most applicable monitoring system for the particular bridge after reviewing technical literature for commercially available technologies. The implementation plan recommended following up with visual inspection when an event is detected by the monitoring system.

The FE model was used to identify critical or high stress concentration areas (hot spots) for sensor array design. The hanger plate and diaphragm connection to the box girder web developed high stresses. For this particular detail, three different sensor arrays with two, three, and four sensors were suggested (Figure C-10). The capabilities of three sensor arrays were evaluated with respect to the detail to be monitored. The two sensor array provides linear source location detection capability. The three sensor array is capable of detecting the source location in two-dimension. The advanced four sensor array is capable of detecting the 3D location of a source. After considering the specific detail of the Cedar Avenue bridge and the monitoring system cost, Schultz and Thompson (2010) recommended using a two sensor linear array system.

The signal attenuation rate was calculated by performing several pencil lead break tests while changing the distance between a hand-held AE sensor and the pencil lead break point. This specific process was needed to place the sensors at optimum locations from the expected source location to capture adequate signal strength for source location detection and event characterization.

The noise generated from fretting of bolted connections can be filtered by selecting a lower bound threshold value. Instead, a guard sensor can be placed just outside the sensor array for fatigue monitoring (or close to the noise source), and the signals recorded by the guard sensor can be filtered out of the signals from the sensor array during analysis. The wave form parameters such as amplitude, energy, signal count, signal rise time, and signal duration are used for location detection and event characterization. In addition to the AE sensors, strain data is needed to correlate AE sensor data for crack growth monitoring.

Even though the bridge selected by Schultz and Thompson (2010) for the technology implementation has shown no evidence of cracking during its life time, the AE system has been continuously collecting AE counts which are below the threshold values set in the system.

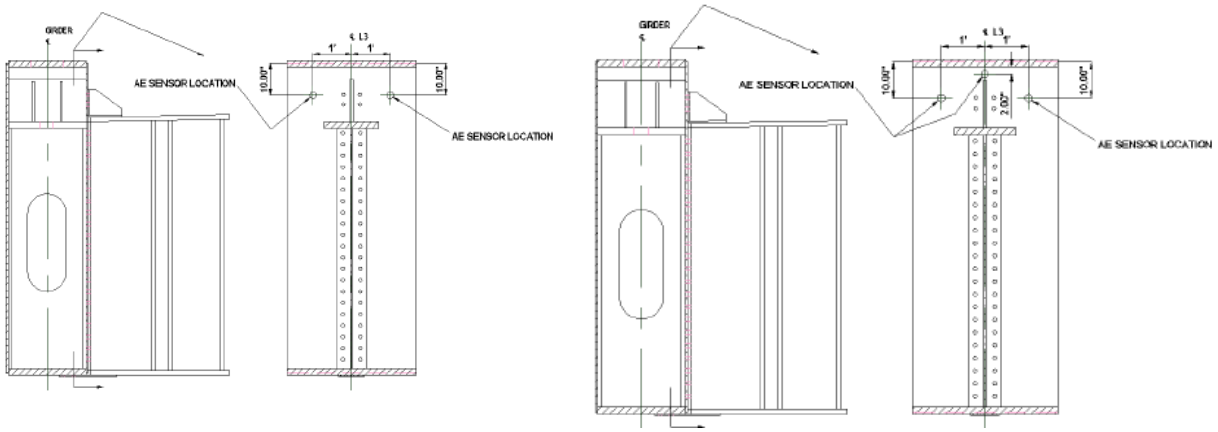

(a) AE sensor array with 2 sensors (b) AE sensor array with 3 sensors

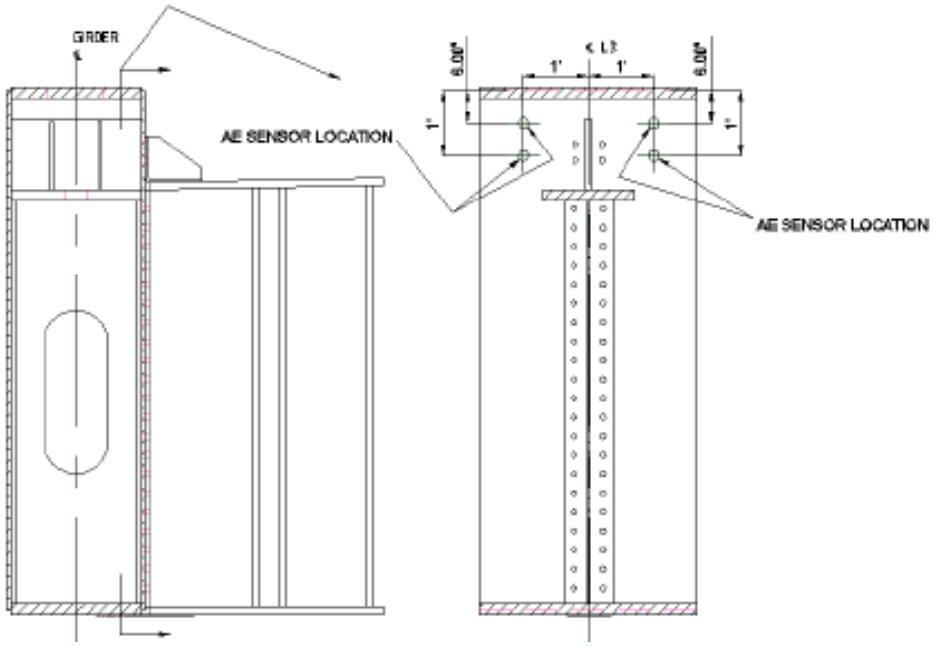

(c) AE sensor array with 4 sensors

Figure C-10. Alternative AE sensor arrays for Cedar Avenue bridge detail (Schultz and Thompson 2010)

C.1.9 Field implementation of acoustic emission (AE) sensors on railway steel bridges (Hay et al. 2009; Ledeczi et al. 2009)

The AE method has been successfully implemented by Hay et al. (2009) for over 20 years to monitor fatigue sensitive details in railway bridges (Figure C-11). An AE monitoring system with strain correlation was implemented to monitor the growth of existing cracks at the bottom of intermediate stiffeners on a 1,233 ft (376 m) open deck bridge with welded girders built in 1910. A similar system was implemented to monitor a link-pin connection of a 320 ft (97.5 m) long open deck bridge built in 1913. The link-pin connection is subjected to out-of-plane bending stresses caused by lateral sway from wind and train motion. The AE system was used

for timely scheduling of the retrofit of the link-pin connection when a crack initiates behind the pin nut that would not be detected by visual inspection. Another example of an AE system installation by Hay et al. (2009) is the monitoring of a 107 spans, 3,444 ft (1050 m) long bridge with various structural configurations such as through trusses and timber pile trestles. The primary objective of monitoring was to help bridge managers make risk-informed decisions to schedule retrofit activities.

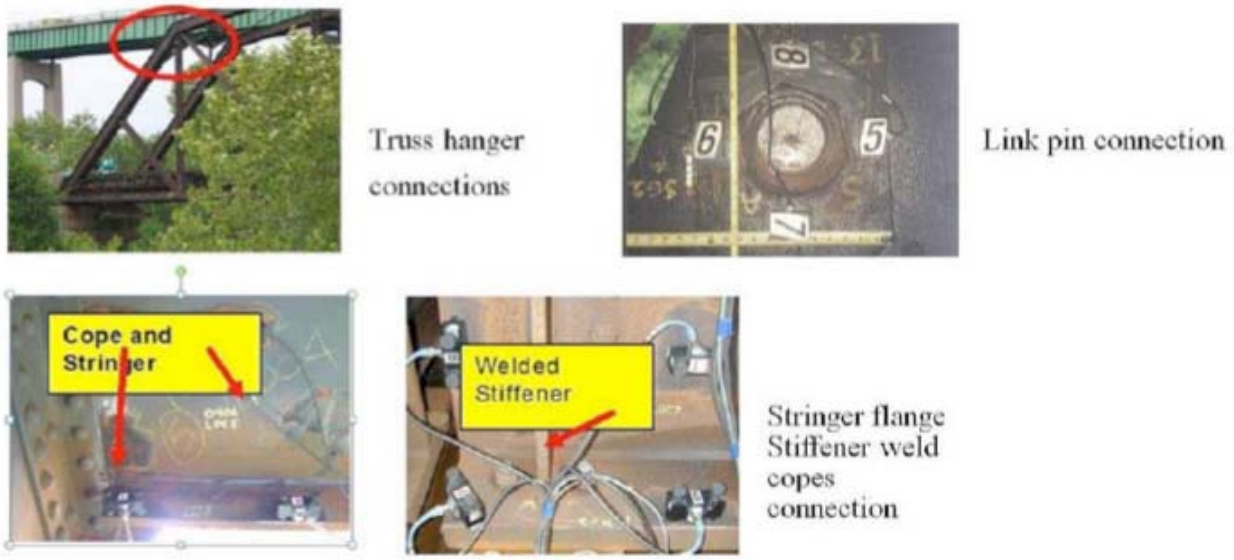

Figure C-11. Fatigue sensitive details on railway bridges (Hay et al. 2009)

Ledeczi et al. (2009) implemented a wireless monitoring system with AE and strain sensors on a railway bridge for fatigue event and location detection. The objective of the field implementation was to benchmark the wireless system against a wired system (Figure C-12). The system consists of 4 AE channels and one strain gauge. A strain sensor was used to trigger AE sensors when traffic is detected on the bridge. This approach makes the system capture only the AE and strain data at the time of traffic passing the bridge, so that the stresses on the monitored component can be correlated to the active fatigue cracks.

Both a wired and wireless system had some sensitivity issues related to fatigue event detection due to sensor location, surface preparation, and sensor coupling to the structure. The accuracy of the fatigue event source location detection had 1-3 in. error due to the complexity of the detail. The detail had multiple fasteners that affected the line-of-sight between the sensors and the

source. However, all the events detected were clustered around the crack tip area within the margin of the location error.

Figure C-12. The monitoring systems wired and wireless (marked in circles) AE sensors (Ledeczi et al. 2009)

C.1.10 Electrochemical fatigue sensors (EFS)

Electrochemical fatigue sensors (EFS) are developed in response to limitations of other fatigue monitoring technologies. As an example, AE technology has widely been used to detect fatigue events by monitoring the stress waves generated due to rapid release of energy. Stress wave propagation is affected by several factors as discussed in section C.2.1.7. Further, the threshold levels established after evaluating the noise levels limit the AE sensor system sensitivity. Above all, the AE sensors cannot predict the potential for future crack growth. This limitation is generally addressed by placing strain gauges at critical locations and monitoring strain profile (or load history). However, this approach may be limited by the sensitivity of the strain gauges.

Two major applications of EFS are (i) monitoring fatigue crack growth by mounting the sensor over a crack tip and (ii) monitoring strain localization and/or micro plasticity to evaluate the potential for crack growth. Monitoring strain localization or micro plasticity is important for evaluating the effectiveness of a retrofit (e.g., crack-stop hole) or for prioritizing or scheduling repair activities (Moshier et al. 2009).

EFS were deployed in the field to monitor growth or growth potential of existing cracks, effectiveness of crack-stop holes in arresting crack growth, and potential for crack initiation or

growth of unidentified cracks at sensitive locations identified through previous experience with similar details (MFS 2013).

The Pennsylvania Department of Transportation implemented an EFS system to monitor three steel girder bridges with cracks at fatigue-sensitive details (Phares 2007). Fatigue cracks were located at the weld toe of the girder above the floorbeam as well as on the floorbeam web. These cracks were initiated due to out-of-plane distortion in the girders and high stresses developed at the floorbeam-girder connection. The objectives of EFS system implementation was to monitor the state of the existing cracks and to determine the effectiveness of crack-stop holes that were installed to arrest further growth. The inspection results from the EFS system indicated continuous growth of weld toe cracks and the effectiveness of the large crack-stop holes in arresting the growth. The system also revealed microplasticity in some potential future crack growth locations.

Several other successful field implementations on highway and railway bridges are documented (MFS 2013). These implementations include three bridges in Australia, the Manahawkin Bay Bridge and George Washington Bridge in New Jersey, and Steven's Point Rail Bridge owned by the Canadian National (CN) Railway. The results of these implementations demonstrated the capability of the technology in detecting actively growing cracks, evaluating the effectiveness of crack-stop holes, and identifying early signs of crack growth.

C.1.11 Fatigue crack monitoring of orthotropic steel bridge deck using piezoelectric (PZT) paint sensors and commercial acoustic emission (AE) sensors (Yi et al. 2012)

Yi et al (2012) evaluated PZT paint AE sensors by comparing the results with commercially available AE sensors. Please refer to section C.1.4 for more information on PZT paint sensors. The fatigue-sensitive details used for the evaluation included orthotropic steel bridge deck details such as longitudinal stiffener to deck plate weld connections, longitudinal stiffener to diaphragm weld connections, through splice butt welds and diaphragm cutout. The full-scale test structure was subjected to static and cyclic loading by using a servo-hydraulic actuator fixed to a load frame (Figure C-13).

Figure C-13. Experimental set up of the orthotropic steel bridge deck (Yi et al. 2012)

The PZT paint and commercial AE sensor array used for the experimental set up is shown in Figure C-14. A 45 dB threshold level was set to the AE system to minimize the effect of external noise. The PZT paint sensors were connected to a signal conditioning circuit containing a preamplifier and a low and high pass filter. The voltage gain of the preamplifier was set to be at 40 dB. A pencil lead break (PLB) test was performed to calibrate the sensors. In addition, the waveform from the PLB test was used as a reference for identifying the other AE data acquired from the experiment. The experimental test results demonstrated the capability of PZT paint sensors to detect AE events associated with fatigue cracks compared to commercial AE sensors.

(a) (b)

Figure C-14. Sensors mounted near the weld joint of the structure (a) strain gauges and PZT paint sensors and (b) commercial AE sensors (Yi et al. 2012)

C.1.12 Strain and crack monitoring using radio frequency identification (RFID) based antenna sensor (Yi et al. 2012b)

Yi et al. (2012b) developed and evaluated a wireless crack sensing system under laboratory conditions. The system is designed as a folded patch antenna that consists of a radiofrequency identification (RFID) chip for signal modulation and collision avoidance (i.e., to prevent potential for reading multiple sensors at the same time which will eventually leads to data loss). The system is capable of detecting change in strain or deformation based on the electrical length change and its electromagnetic resonance frequency. This system can also be used for crack detection using the radiofrequency (RF) that will be described later. The schematic of the system is shown in Figure C-15. The system is passive; it obtains power from RF signals emitted by the wireless reader by means of interrogation. The passive RFID tags are smaller and lighter compared to the active RFID sensors, but the range is limited to several feet. The system has been tested for measuring strain in the range of 20 με - 10,000 με. In addition, the system working principles and capabilities were evaluated by Yi et al. (2012b) through simulations by using an electromagnetic software package.

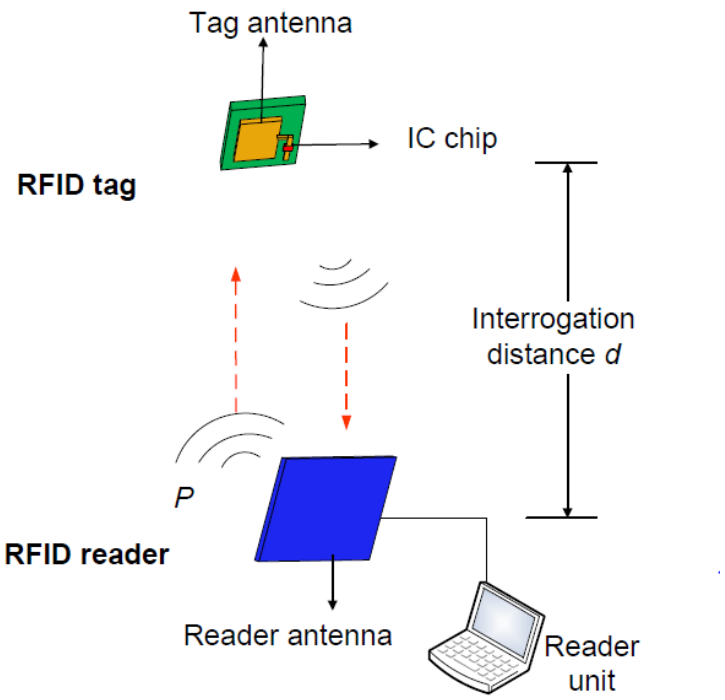

Figure C-15. Schematic of the RFID system (Yi et al. 2012b)

The RFID tag has an electromagnetic antenna and an RFID chip that reflects the RF signal emitted by the RFID reader. The signals received by the RFID tags are amplitude-modulated and reflected back to the RFID reader. The signals captured by the RFID reader are demodulated by the reader to distinguish between other reflected signals from the surrounding environment. The folded patch antenna in the RFID tag is designed to function as a wireless strain sensor. The antenna is folded to reduce the sensor size which is typically 0.04 in × 0.04 in (1 mm x 1 mm). When the electrical current flow in the RFID tag antenna that is induced by the RFID reader is cut off due to cracked folded antenna, the current flow takes a different route around the crack. This new elongated electrical passage causes a shift in the resonance frequency of the sensor indicating the presence of a crack. Figure C-16 shows the variation of interrogation power (P) and the resonance frequency of cracked and uncracked specimens.

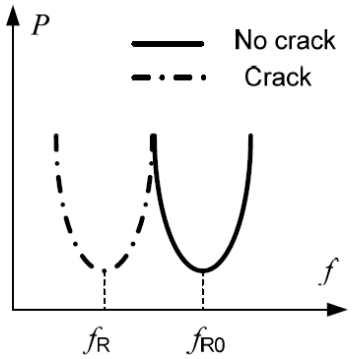

Figure C-16. Resonance frequency shift due to cracking at the folded patch antenna (Yi et al. 2012)

An experimental set up used by Yi et al. (2012b) is shown in Figure C-17. The crack was simulated on an aluminum plate (8 in. × 4 in. × 0.5 in.) by tightening a screw to open the crack. The sensor was mounted right on top of the expected crack location. The RFID reader was located at 12 in. away from the RFID tag. The reader is capable of automatically recognizing the interrogation power threshold and the resonance frequency of the RFID tag by analyzing different frequencies. This is performed five times for each crack opening size to eliminate external noise effects.

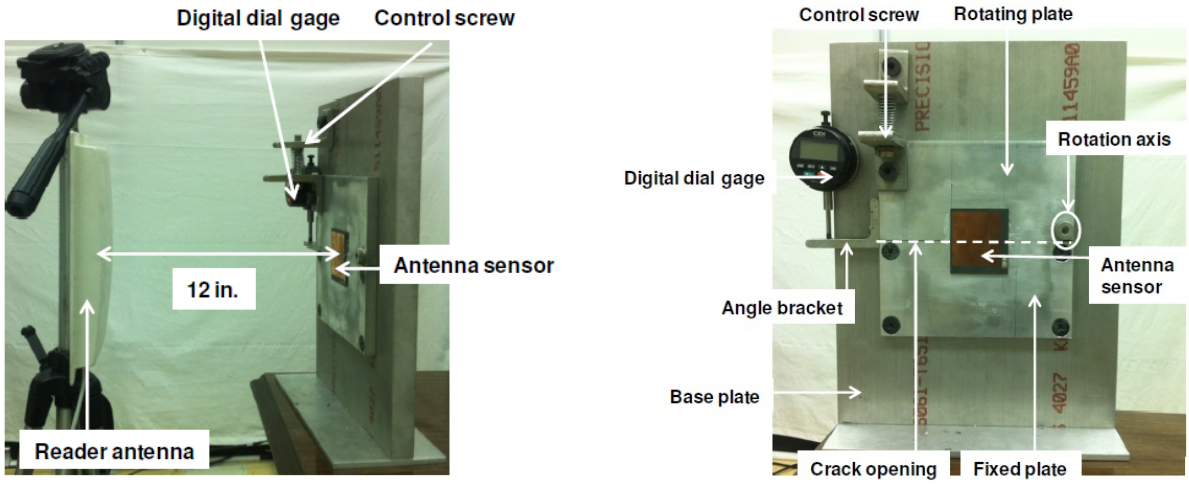

Figure C-17. Experimental set up of the RFID sensor system (Yi et al. 2012)

As shown in Figure C-18, the resonance frequency gradually reduces as the crack size increases. Further, resonance frequency vs. the crack size and resonance frequency vs. equivalent strain show linear relationships (Figure C-19).

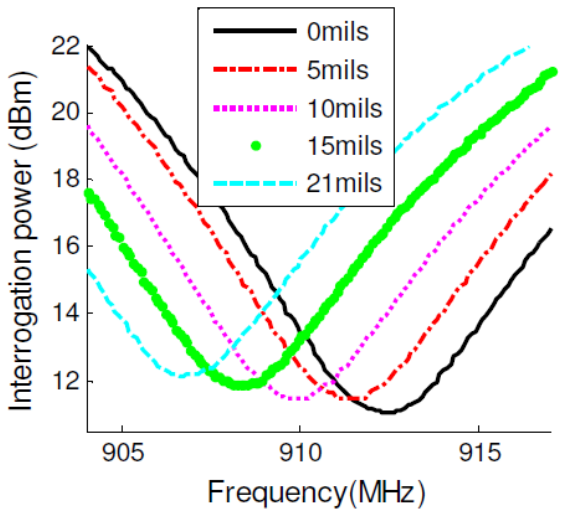

Figure C-18. Interrogation power threshold values at different crack opening size (Yi et al. 2012b)

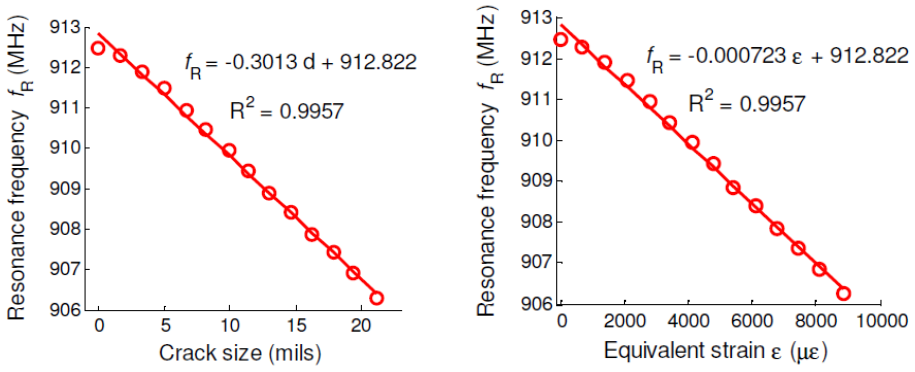

(a) (b)

Figure C-19. Relationship between the resonance frequency and (a) crack size and (b) equivalent strain (Yi et al. 2012b)

One drawback of the system is that the frequency shift can be recorded even when the sensor is not cracked. The electromagnetic disturbance developed by the presence of conductive material such as steel near the sensors is another challenge for implementation of this technology (Kaur et al. 2011). However, Li et al. (2011) used steel specimens to evaluate an RFID sensor that they developed, but they do not discuss any impact of steel on the data. The thermal sensitivity of the material used for fabrication of the antenna component in the RFID system has an impact on the measurements. For example, glass microfiber-reinforced PTFE substrate shows a relatively high temperature sensitivity when compared with ceramic-filled PTFE substrate material. This aspect has been investigated by Yi et al. (2012b). Also, the transmission efficiency, crack pattern, location of the crack with respect to the sensor, growth of multiple simultaneous cracks, and impact of exposure conditions need to be investigated for this system to be practically ready for field implementation.

C.1.13 Structural health monitoring using digital image correlation (DIC) (Iadicola et al. 2012)

As part of the NCHRP 12-84 project, FHWA used digital image correlation (DIC) technique for measuring displacements and strains of a large gusset plate. The experimental setup consisted of 5 members that were connected by two gusset plates and loaded with hydraulic actuators (Figure C-20 and Figure C-21). The gusset plates were labeled as north and south. Moreover, the unloaded structure was used as the reference for all measurements. DIC results were compared with the results from laser point tracking, photoelastic imaging, and traditional foil strain gauges.

The laser tracker was used to compare the measured displacement while the DIC strain profiles were compared with the photoelastic imaging and strain gauge data.

The experimental setup of the DIC is shown in Figure C-20. The system consists of two cameras mounted on an aluminum bar as a rigid support for measuring 3D displacement and surface strain on the north gusset plate. The DIC measurement technique needs a random pattern (speckles) on the surface. The random pattern consisted of approximately 0.2 in. (5 mm) wide black and white areas (Figure C-22). The gusset plate surface was illuminated, and the shadowing was reduced by using two photographic lights mounted behind the cameras.

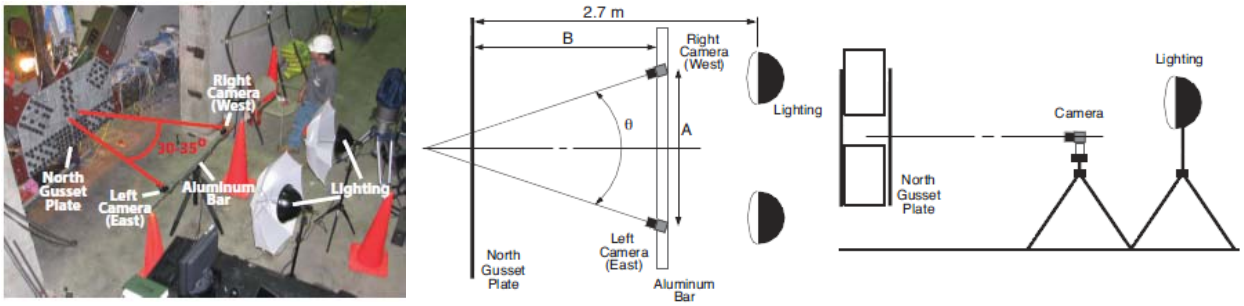

(a) (b) (c)

Figure C-20. Digital image correlation experimental setup (a) general view, (b) plan view, and (c) elevation view (Iadicola et al. 2012)

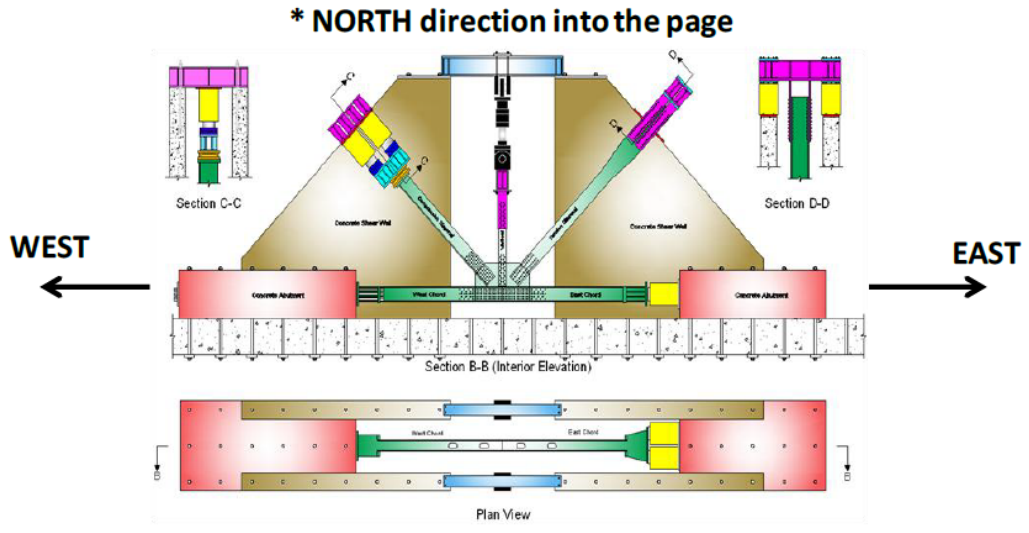

(a)

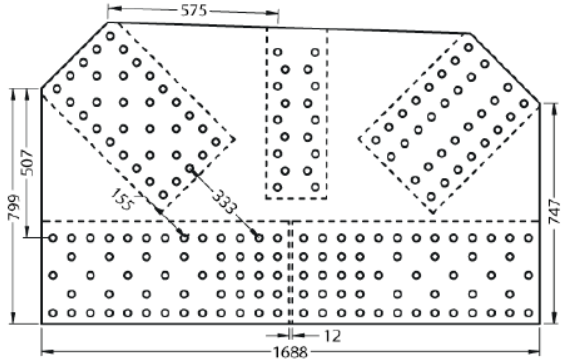

(b)

Figure C-21. Experimental set up of the large-scale test specimen (Iadicola et al. 2012)

(a) (b)

Figure C-22. Speckle pattern used for DIC method (a) full-filed view and (b) close up of the pattern (Iadicola et al. 2012)

As the first step, the unloaded configuration of the plate was measured using DIC and laser tracker systems. The expected accuracies of the laser tracker system are 0.0012 in. (0.03 mm) and 0.0004 in. (0.01 mm) in plane and out-of-plane, respectively. The data points or the measurement locations for both DIC and the laser tracker are shown in Figure C-23. The data from the area covered by the washers and nuts were not considered for the analysis (Figure C-23, Figure C-24). The comparison of data from these two technologies yielded the following findings.

- DIC can acquire more data points in less than 1s time compared to laser tracker which took more than 300 s to cover a similar area.
- The accuracy of the laser tracker is higher than the DIC.
- As shown in the Figure C-24, the laser tracker system can trace the edge of the plate more accurately than the DIC system. (The grey area along the edges of the DIC contour plot shows the inability of the DIC system to trace the edges accurately.)
- The DIC system tracks specific points on the surface so that the strain measurements can be derived.
- The laser tracker can be used to track the initial shape of the plate. However, it cannot track the same point repeatedly for strain measurements unless specific targets are placed on the surface.
- Both methods are capable of capturing out of plane deformations but with different accuracies.

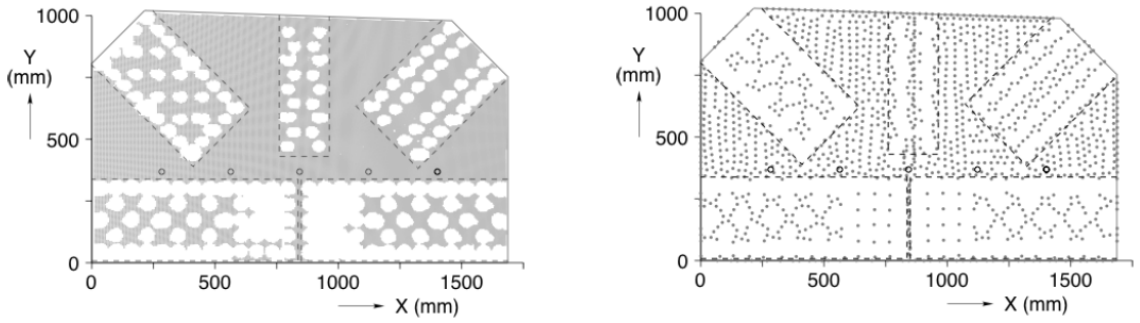

(a) (b)

Figure C-23. Measurement locations for (a) DIC and (b) laser tracker (Iadicola et al. 2012)

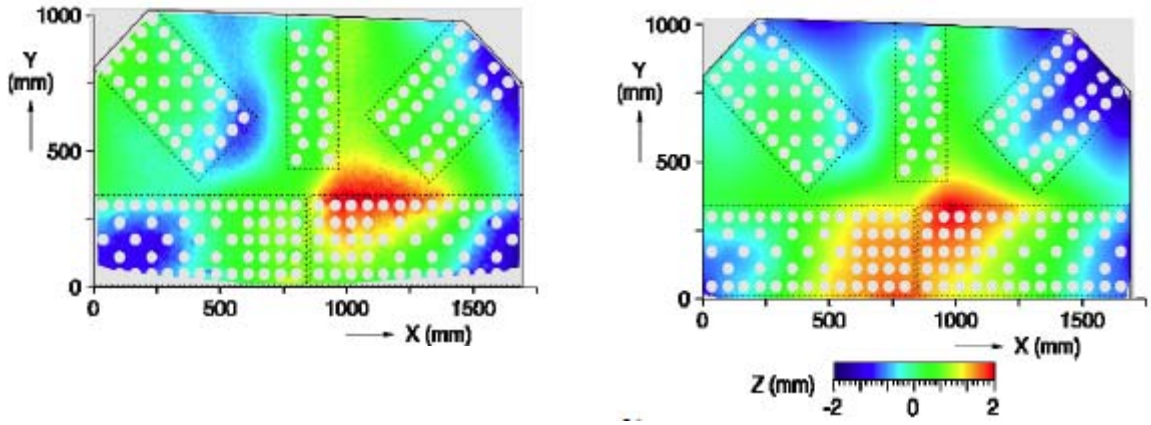

(a) (b)

Figure C-24. Displacement contour plot of the unloaded shape measured by (a) DIC and (b) laser tracker (Iadicola et al. 2012)

The second step was designed to compare the elastic strains calculated using the displacement field measurements of DIC with the results from strain gauges and the photoelastic method. Five strain gauges, with a range of measurement +/- 2 με, were mounted on each plate. They were placed in a horizontal line at 14.8 in. (368 mm) from the bottom of the plate. Small circles on Figure C-26 depict the strain gauge locations. A stress photonics grey-field polariscope photoelastic camera was used for strain measurement on the south plate while the DIC method was implemented on the north plate. The south plate surface was prepared using a special epoxy (photoelastic material) to develop fringe patterns to calculate strains (Figure C-25).

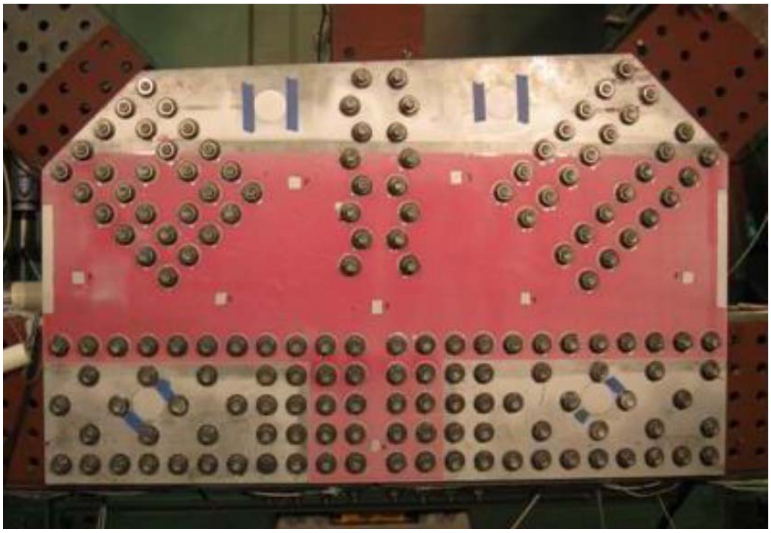

Figure C-25. Epoxy coating (photoelastic material) on the gusset plate for photoelastic measurement (Mentes 2011)

The maximum in-plane shear strain contour plots from DIC and photoelastic methods are shown in Figure C-26. The photoelastic measurement captured only a T shaped region because the photoelastic coating was applied only within that region to view the fringes. In general, both methods were able to capture hot-spot strains and locations. Due to high resolution, the photoelastic method was able to capture the strains between the bolts (Figure C-26).

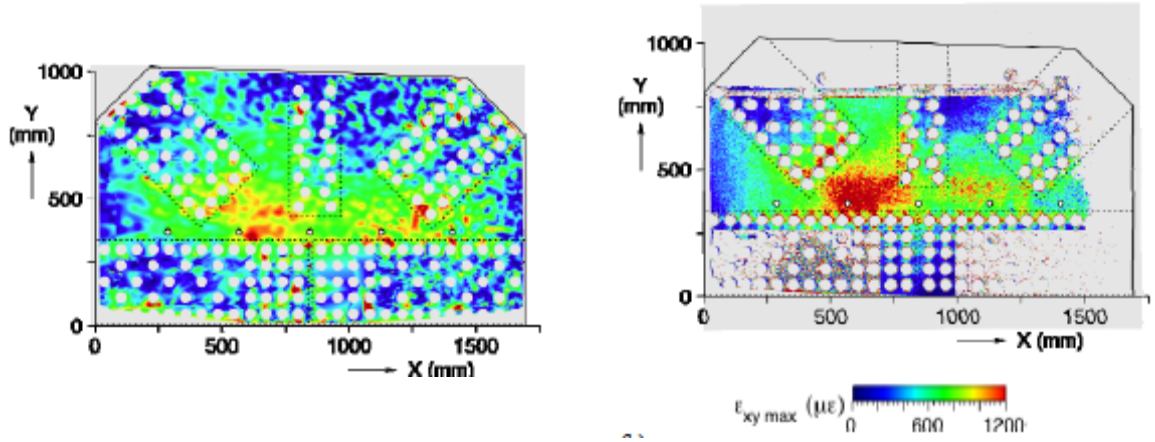

(a) (b)

Figure C-26. Comparison of maximum in-plane shear strain of the elastically loaded connection by (a) DIC and (b) photoelastic method (Iadicola et al. 2012)

Figure C-27a shows the comparison of DIC, photoelastic, and strain gauge results. Since all the strain gauges are located in a horizontal line, DIC and photoelastic results were averaged over a 1 in. (25.4 mm) wide strip (Figure C-27b and c) for the comparison. Further, the upper and lower bounds of DIC and photoelastic results were also calculated. Two of the north rosettes failed during the experiment and recorded almost zero strains. Figure C-27a shows that the measurement of elastic strains from all three methods can be closely related within their noise levels. For an example, the noise level of DIC and photoelastic methods are around +/-150 με and +/- 50 με, respectively. Another preliminary finding from this study is the capability of the DIC system to measure a plastic strain that the photoelastic method cannot measure. However, this conclusion needs to be supported by further analysis of plate curvatures and their effect on the measured strain values.

Even though DIC technology has been extensively used for strain and displacement measurement under lab conditions (Cintron and Saouma 2008, Yang et al. 2010), field implementation has been scarcely reported (Bell et al. 2012, Yoneyama et al. 2007).

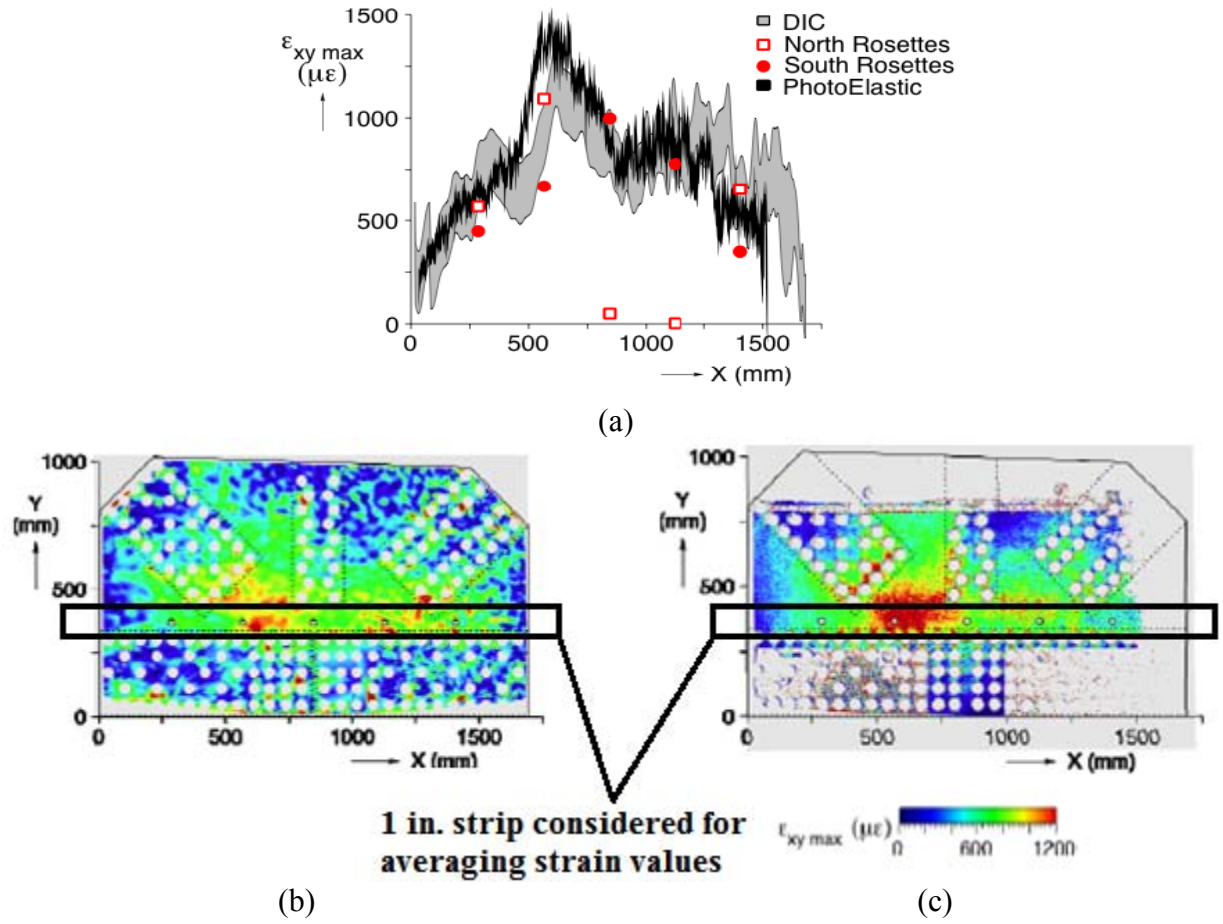

Figure C-27. Comparison of shear strain along the width of the plate (a) shear strain variation, (b) 1 in. strip of DIC results, and (c) 1 in. strip of photoelastic results (Iadicola et al. 2012)

C.1.14 Nondestructive evaluation of structures using stress and strain measurement by x-ray diffraction (www.protoxrd.com)

X-ray diffraction (XRD) technology is generally used for material characterization under laboratory conditions. Recent advances in the technology have allowed measuring strain in crystalline material such as steel. The strain is determined by calculating the atomic lattice spacing (d) using Bragg's law presented by the $n\lambda = 2 \cdot d \cdot Sin\theta$ equation. The XRD equipment measures the wavelength of the incident x-ray (λ) and the angle of diffracted x-ray beam (θ). The variable n represents the order of diffraction, and $n=1$ is used for first order diffraction. The XRD equipment can be equipped with multiple detectors to capture a diffracted signal to enhance the measurement accuracy. Strain is calculated using the change in lattice spacing (d). Then the stress is calculated by multiplying with the material modulus of elasticity. Since the

strain is calculated using the change in lattice spacing, corrections for thermal induced strains are required for accurate calculation of stresses.

Once the stresses are calculated, forces and moments can be calculated using member cross-section properties. As an example, axial force is calculated by multiplying XRD measured strain value, elastic constant of the material, and the cross-section area of the member (i.e., elastic stress multiplied by cross sectional area of the member). The member forces calculated using the XRD measured strain can be compared with the original design values to track the changes due to maintenance, repair, or other damages to the structure that might have caused redistribution of loads or change in load path. Further, this approach can also be used in critical high-stress or fatigue-sensitive areas to measure the stresses due to applied loads, fabrication tolerances, and out-of-plane deformation (distortion). Hence, the capability of the XRD equipment in measuring strain allows performing in-service dead load measurement, load path determination, crack-stop hole validation by checking the stresses around it, baseline stress measurement for enhanced structural monitoring, and residual stress measurement before and after retrofit.

The technology has been implemented in California's Oakland Bay Bridge and New York's Brooklyn Bridge.

C.1.15 Fatigue damage (FD) sensor and the fatigue fuse (FF)

Kujawski et al. (2011) developed the fatigue damage (FD) sensor. MFS (2014) has developed the fatigue fuse (FF). Both the FD sensor and the FF work on the same principle. Both sensors have a series of parallel metal strips (fuses) with different geometric patterns. Each fuse is designed to represent a finite and predictable fatigue life at which the respective fuse is broken. Hence, a sensor can be designed with multiple fuses, each representing a fraction of a component's fatigue life, to detect degradation in fatigue life of a component. The sensor can be mounted at a crack tip to monitor the growth of the crack. Also, the sensor can be mounted at a remote location from the fatigue sensitive detail, and once calibrated, it can calculate the degradation of the fatigue life of the sensitive detail. At present, there is no documentation on field implementation of these sensors for monitoring fatigue life degradation at bridge details.

C.2 FUNDAMENTALS OF THE TECHNOLOGY

Review of the state-of-the-art technology and practice shows that acoustic emission (AE) is the most promising technology for development and field implementation of a remote monitoring system. In addition to AE, the electrochemical fatigue sensor has been used at experimental level as well as in limited field applications for fatigue event detection and detection of early signs of crack growth. Also, the ultrasonic guided wave technique has been used at the experimental level in remote monitoring systems to characterize fatigue cracks. Hence, the fundamentals of these three technologies, AE, EFS, and USGW are presented herein.

C.2.1 ACOUSTIC EMISSION TECHNIQUE

The acoustic emission technique is a potential NDE tool for real-time monitoring to detect and locate active fatigue damage events. AE is the development of transient elastic waves by the rapid release of energy from a localized source or sources within a material when subjected to external stress or other stimuli such as load, deformation, pressure, and temperature (Huang et al. 1998; Nair and Cai 2010; NDT 2014; FHWA 2012; Hay and Nyborg 2000). AE sensors detect elastic waves generated by plastic deformation, initiation and growth of cracks (fatigue and fracture), and slip and dislocation movements in the order of picometers (1.0×10^{-12} m) or smaller (Hay and Nyborg 2000; NDT 2014; FHWA 2012). AE sensors are passive and continuously listen to the sounds from active damage events. The data acquisition systems used with AE sensors can be programmed to continuously gather signals from the sensors. Since AE sensors capture stress waves generated from all the sources, it is vital to identify the noise sources and set up appropriate thresholds for the specific application. In general, the signals that exceed the threshold are used for further analysis (Nair and Cai 2010).

C.2.1.1 AE mechanisms and signal sources

Acoustic emission can be classified into two different modes: burst emission or AE event and continuous emission (Figure C-28). The burst mechanism is related to the plastic deformation mechanisms (dislocation, slipping or gliding of portions of the crystal over on another) occurring in materials at or near the yield stress. Internal or external crack growth is a phenomenon based on the separation of interatomoic bonding between the materials along the crack growth path due to the externally applied loads. This may occur even before complete failure/fracture; hence, AE

emission will be an indication of an active damage event. The continuous emission may occur from external noises such as mechanical and electromagnetic interference. The mechanical noises can occur due to the rubbing or fretting of structural components. The electromagnetic interference may arise due to electrical equipment near the AE sensors. Hence, these noises need to be well understood for a particular monitoring environment and conditioning; furthermore, proper filtering techniques need to be incorporated into the system to gather useful data.

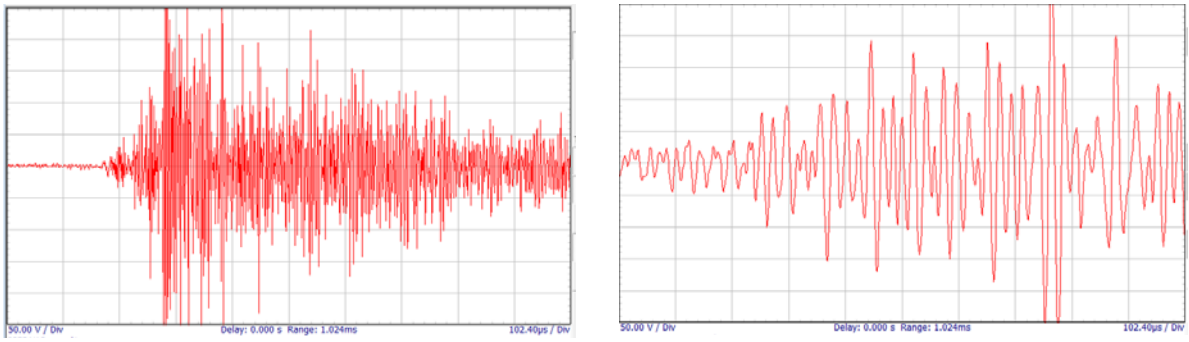

(a) Burst or event (b) Continuous or noise

Figure C-28. Temporal AE modes (Hay and Nyborg 2000)

C.2.1.2 Wave propagation basics for AE detection

An AE event generates three types of elastic waves: dilatational (longitudinal waves), distortional (shear waves), and Rayleigh or surface waves (Figure C-29). In an ideal scenario, a transducer mounted on the surface typically captures these waves at different times due to difference in speed. As an example, longitudinal, shear, and surface wave speeds in steel are 19,422 ft/s (5,920 m/s), 10,663 ft/s (3,250 m/s), and 9,711 ft/s (2,960 m/s), respectively. However, during field applications, the signal detection and analysis becomes complicated due to presence of multiple AE sources, complexity of the details, and signal attenuation. The attenuation is a phenomenon that is described as the gradual reduction in signal amplitude (strength) with the distance from the source to the transducer. Signal strength may be reduced due to geometric attenuation, energy dissipation, dispersion, scattering, and diffraction. As an example, geometric attenuation can occur when the source is located near an edge or a surface. Therefore, an attenuation survey needs to be conducted to determine the optimal placement of AE sensor for monitoring a specific detail (DFT UK 2006).

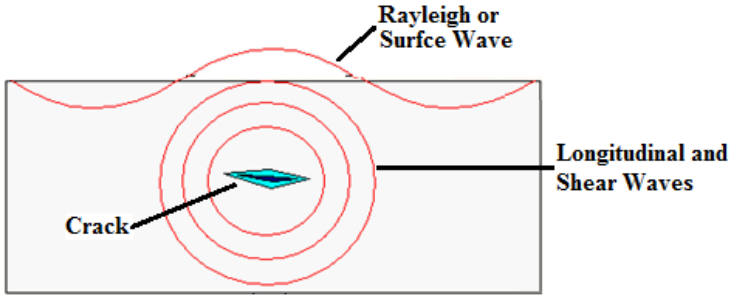

Figure C-29. Wave propagation in solids (Hay and Nyborg 2000)

C.2.1.3 AE event detection and monitoring

AE sensors are commonly made of piezoelectric material that generates electrical current due to deformations. Stress waves, which are generated within the material due to sudden energy release from a crack, generate surface deformations. These deformations are detected by the surface mounted piezoelectric sensors and converted into electrical signals (voltage) (FHWA 2012). These signals are conditioned, filtered, and recorded for further analysis. Depending on the monitoring system features, signal analysis results are presented in various formats to be useful to the intended user (Figure C-30). The AE signal parameters such as amplitude, counts, decay time, duration, energy, and rise time are extracted from a recorded signal to evaluate damage events such as the location and growth rate (Nair and Cai 2010; Parmer and Sharp 2009; Huang et al 1998).

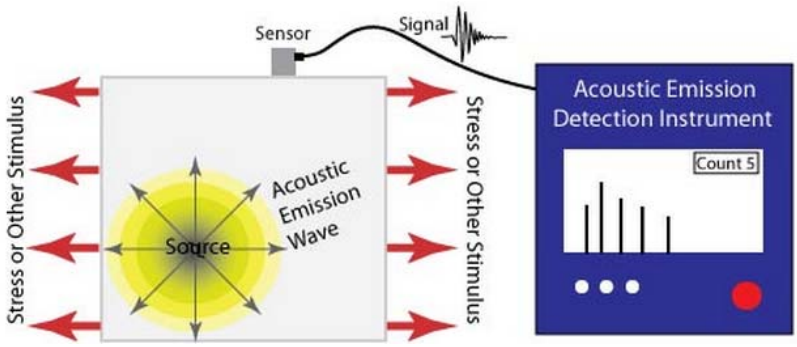

Figure C-30. Acoustic Emission working principle (NDT 2014)

C.2.1.4 AE source location identification and sensor layout

The location of an AE signal source can be calculated using a pre-defined sensor array network. The time difference of arrival between the received signals from two or more sensors mounted near the area of concern can be used to locate the source. The planer location can be precisely

detected using three or more sensors. However, when there is a source with continuous emission of acoustics, the time difference method cannot be adopted. In such cases, use of advanced signal analysis techniques, such as time series analysis using cross correlation, is required. The time difference of arrival can be defined based on the first threshold crossing (FTC) time and peak time (PT) depending on the material and the damage/source being monitored. For accurate location identification in complex situations, the sensor array network should be designed accordingly by combining other sensors such as strain gauges to correlate with the load matrix. The sensors can be arranged in rectangular, triangular, open-ended, and close circular arrangement depending on the complexity of the component being monitored and the sensitivity of the sensors. AE detection sensitivity is discussed in section C.2.1.7.

C.2.1.5 AE monitoring systems

AE monitoring systems can be classified as single channel systems and multi-channel systems. The basic components of these systems are shown in Figure C-31. A single channel system is preferred when a portable system is required to monitor if acoustic events are generated. The multi-channel system is used when source location measurement and data processing are required. AE sensors and instruments typically consist of integrated or external preamplifiers and external noise cancelation or filtration components to improve the signal-to-noise ratio or to filter out unwanted signals from other sources close to the damage location (Nair and Cai 2010; FHWA 2012). However, the amplification needs to be optimized to filter out the noises that are amplified simultaneously with the AE signals. The use of guard sensors just outside the area of concern can also be used for filtering emissions from outside the monitoring area. In addition to the data acquired from the AE transducers, parametric data such as strain, displacement, and temperature can also be measured with the use of other techniques. This parametric data is used for correlation with AE activities. Once the data is stored and transmitted from the job site, the signals can be further analyzed for identifying damage events such as crack initiation and growth precisely by extracting key features of the waveform or pattern.

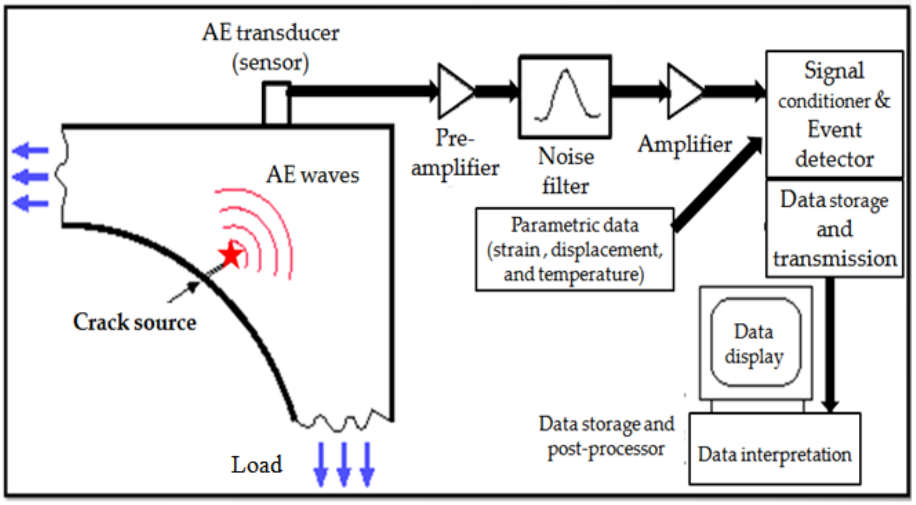

Figure C-31. Schematic of an AE monitoring system (Kosnik 2008, Hay and Nyborg 2000, Huang 1998)

C.2.1.6 AE transducers

The transducers or sensors are the most important elements of an AE monitoring system as they convert the mechanical energy into electrical energy (signals). The sensitivity of the monitoring system and the availability of quality data for post-processing heavily depend on the transducer. The sensing element of these transducers is made of piezoelectric material mainly composed of Lead Zirconate Titanate; hence these sensors are called piezoelectric PZT transducers or simply PZT transducers. Sensor technology is evolving, and the latest sensors are made of flexible piezoelectric sensing elements instead of the commonly used brittle ceramic sensors (Barut 2006; Yang and Fritzen 2011).

The transducer can be connected to the detail to be monitored using a couplant such as silicone, glycerin, stopcock grease, and oil to create a uniform acoustic path between the transducers and the testing material. Silicone provides temperature stability and adequate ductility to tolerate a certain degree of deformation (Hay and Nyborg 2000).

C.2.1.7 Parameters affecting AE detection sensitivity

Currently available transducers can detect AE events in the order of picometers (1.0×10^{-12} m) or smaller. The factors affecting the transducer sensitivity are frequency, size, material, and QA/QC of the manufacturing process. The damage detection from an AE source depends on the type of transducers/sensors, number of sensors, and the sensor arrangement around the damage event source. Two types of sensors are used in AE monitoring systems: resonant or narrow-band

and broadband (Hay and Nyborg 2000). Resonant AE sensors are commonly used due to their greater sensitivity to sources at a particular frequency. Among the other benefits of narrow-band sensors, larger spacing of sensors and minimized background noise capturing by filtration are significant. Contrarily, the broadband AE sensors have reduced sensitivity and require closer sensor spacing (DFT UK 2006). Location sensitivity can also be increased by using higher frequency sensors (DFT UK 2006). Depending on the monitoring objectives, a narrow-band and wide-band sensor integrated system may be required.

The damage event detection sensitivity also depends on the magnitude of the energy released from the damage source as well as the signal strength at the sensor location. Hence, the factors that affect signal strength are the component dimensions, exposure conditions, the path between the sources and the transducer, load or stress levels that generated the elastic waves, and the noise level that establishes the signal thresholds.

C.2.2 ELECTROCHEMICAL FATIGUE SENSORS

The Electrochemical Fatigue Sensor (EFS) was developed by Moshier and Berks (2009) based on the electrochemical working principle. Once the sensor containers are filled with the electrolyte through the fill tube and sealed, a constant voltage is applied by a Potentiostat Data Link (PDL) unit to form an electrochemical film over the monitored steel surface area by anodically polarizing the sensor to produce a DC base current in the sensor (Figure C-32). When the sensor is mounted on the tip of an actively growing crack, the DC current within the cell fluctuates, and an AC current is superimposed on the base DC current. The transient current within the cell provides information on crack growth depending on the structural material, the loading conditions, as well as the state of the fatigue damage in the structure (Phares 2007).

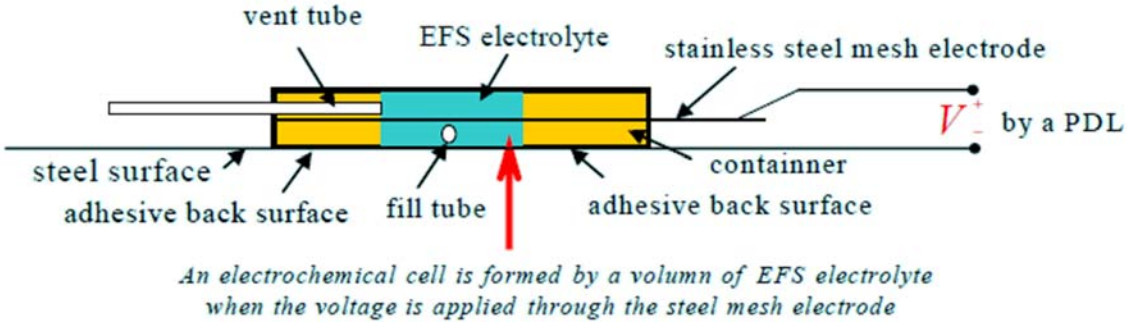

Figure C-32. Electrochemical fatigue sensor configuration (FHWA 2012)

It is necessary to mount two sensors to monitor a specific area or a crack. These two sensors, named crack measurement (CM) sensor and reference (R) sensor, are connected to a portable data logger (PDL unit) (Figure C-33). When the system is used to monitor the growth of an existing crack, the CM sensor is mounted on the crack tip while the R sensor is mounted close to the CM sensor within same stress zone. The crack growth monitoring is calculated based on the energy ratio (ER) (FHWA 2012). This ratio is calculated taking the ratio of the areas under the frequency domain spectrum curves of the CM sensor and the R sensor. As per the manufacturer's information, an actively growing crack is predicted by the system when the energy ratio is greater than 2.0.

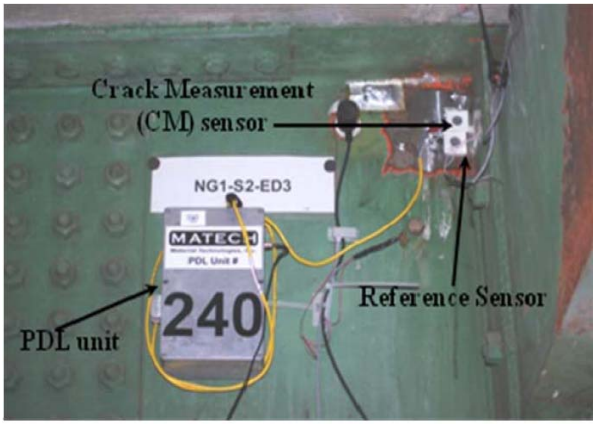

Figure C-33. Configuration of a monitoring system with electrochemical fatigue sensors (FHWA 2012)

C.2.3 ULTRASONIC GUIDED WAVE ACTUATOR-SENSOR SYSTEM

Ultrasonic guided wave (USGW) technology has been experimented and implemented for damage detection in sign support structures (Zhu et al. 2010), fatigue crack monitoring of a steel bridge (Zhao et al. 2013), health monitoring of an aircraft wing (Zhao et al. 2007), and defect growth monitoring in a welded plate (Rose et al. 2008).

Ultrasonic guided waves are based on the principle of elastic wave propagation in solids. The waves are guided by the component surface boundaries or advanced algorithms. The USGW sensors come in two different configurations: (i) a packaged sensor, which consists of the pulser and receiver in the same transducer and (ii) individual transducers that work as either a pulser or receiver. When a packaged sensor is used, the emitting and receiving signals can be captured from the same surface. Otherwise, a receiver can be located at another location to capture the signal. The energy is generated by applying an AC voltage to the transducers in different

frequencies. This pulser-receiver system can be mounted on the surface of the area of concern, such as one with fatigue-sensitive details, in a pre-defined array (Figure C-34). Consequently, the data acquired from the system can be used to develop topographic images by combining every possible data acquired from the sensor combination (i.e., pair-wise comparison) of the array (Figure C-35) for fatigue event detection and damage characterization (Rose et al. 2008).

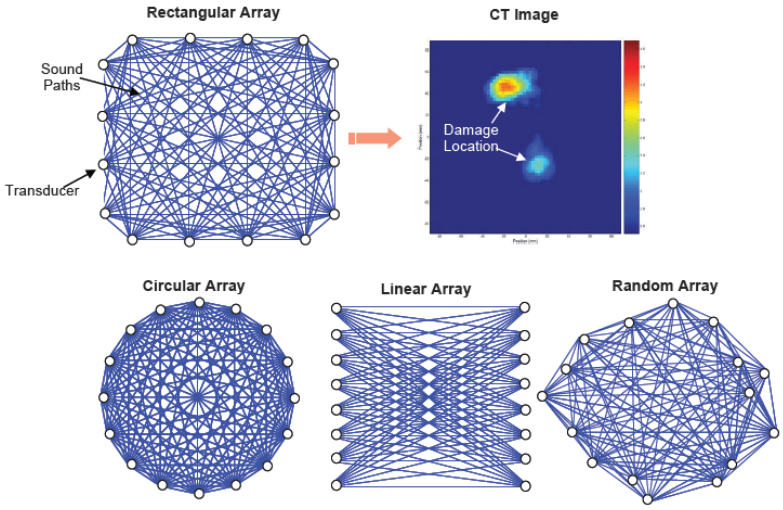

Figure C-34. USGW sensor array configurations and computed tomography (Rose et al. 2008)

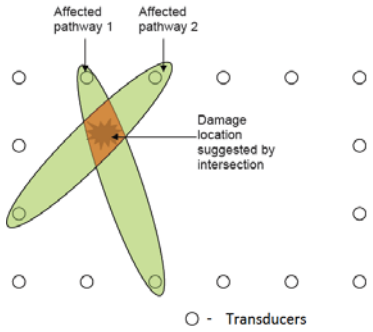

Figure C-35. Damage location detection using a combination of senor data inside a rectangular transducer array (Rose et al. 2008)

The tomography approach for damage detection, growth monitoring, and location mapping can be performed by using wave speed, attenuation, and/or energy from the acquired data (Zhao et al. 2007). As an example, tomography mapping for damage location of a crack (shown in Figure C-36) was calculated from the linear summation of the signal changes of pair-wise data between sensors and the relative position of the damage to those sensors (Zhao et al 2007). In this approach, the wave propagation pattern was assumed to have an elliptical distribution function, in which the most significant pair-wise signal change is assumed to be occurring when the

damage is located along the direct path (Figure C-37). The indirect path of the signal can occur due to reflection of the wave from discontinuities (e.g., edges and corners) in the component being monitored.

The USGW technique requires additional research in data analysis and interpretation for effective damage location detection and characterization in field applications due to complex geometries of fatigue sensitive details that lead to wave propagation in multipath, reflection or echo from the edges, wave scattering, and attenuation (Zhao et al. 2007).

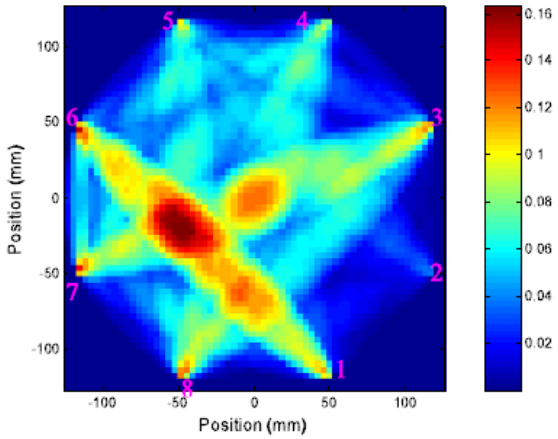

Figure C-36. Damage location mapping using tomography approach with circular array of 8 USGW sensors (Zhao et al. 2007)

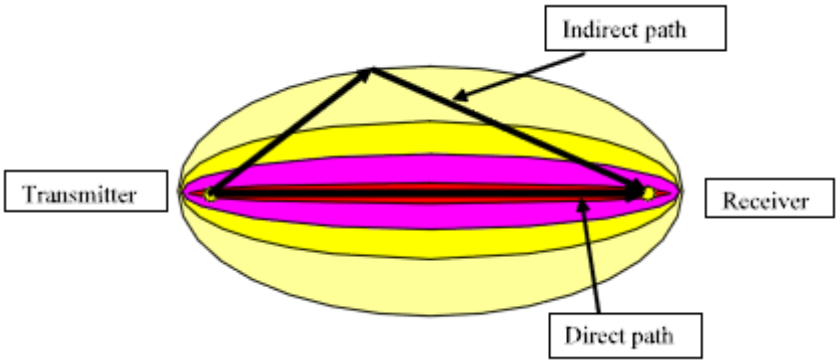

Figure C-37. Wave propagation distribution function (Zhao et al. 2007)